PhD Dissertation

INTEGRATION OF THERMOCHEMICAL MATERIAL (TCM) AND PHASE CHANGE MATERIAL (PCM): HYBRID 3 in 1 SYSTEM FOR ADVANCED THERMAL ENERGY STORAGE APPLICATIONS

A thesis presented to the School of chemical engineering at the University of Birmingham

September 2020

Anabel Palacios Trujillo

Supervisors:

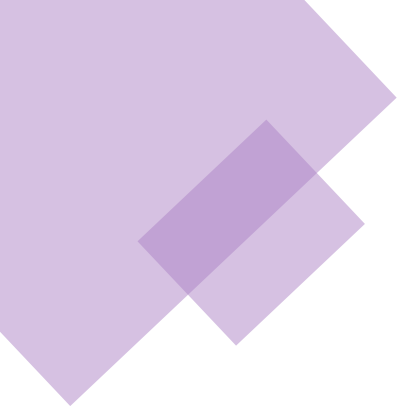 Prof. Yulong Ding and

Dr. Zhenyu Jason Zhang

UNIVERSITY OF BIRMINGHAM

University of Birmingham Research Archive
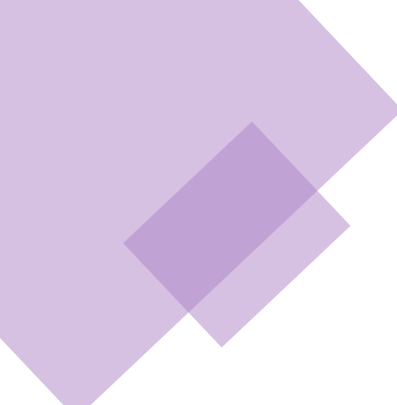
e-theses repository

ABSTRACT

Energy has become the most valuable good in our modern society, dictating our living conditions and social status. In this energy scenario with increasing demand, energy storage has the potential to change the way we live by bringing flexibility into the energy systems and decentralising the network. Thermal Energy Storage (TES) is seen as one of the main key players, but TES needs significant research efforts to address some fundamental challenges to reach its full potential. System hybridisation, which integrates different energy storage sources such as TES technologies, can significantly boost the system efficiency and drive TES deployment offering a highly effective solution to these challenges. This thesis aims to firstly look beyond the three traditional Thermal Energy Storage technologies proposing a novel co-working storage concept where the materials' components are not acting individually but synergistically to maximise the outputs: the 3 in 1 TES system. This has never been attempted before and constitutes the paving way of a new paradigm in Thermal Energy Storage.

The 3 in 1 system integrates the three known thermal storage methods of sensible heat, latent heat and thermochemical based TES into one system, providing three different operational configurations with cascading, charging integrated and discharging integrated working conditions. These different configurations offer controllability of TES charge/discharge processes while enhancing system-level efficiency. The TES materials are theoretically selected through a comprehensive literature review on the area. The candidates are then experimentally validated, and relevant properties not measured in the literature are taken into account. The candidates are narrowed down to five TCMs ($MgSO_4·7H_2O$, $MgCl_2·6H_2O$, $CaCl_2·6H_2O$, $SrBr_2·6H_2O$ and $K_2CO_3·1.5H_2O$), seven PCMs (6 polymers: high-density polyethylene (HDPE), 4,40-diphenylmethane diisocyanate (MDI), polyethylene oxide (PEO), polyethylene glycols (PEG) 1,000, 600 and 35,000 MW) and one sugar alcohol: erythritol (E)), one matrix cellulose (CLU) and two gels as additives (polyacrylamide (PA) and guar gum (GG)). These materials will be combined

to form working pairs according to the three different operational conditions. The working pairs are then studied in two main blocks; SSPCM and SLPCM-gel. The energy stored and the chemical stability of SSPCM/TCM being studied, while the compatibility/synergies between TCM/PCM-gel working pairs are investigated for the SLPCM. The use of gels in the formulation process proofs its potential for thermochemical synthesis as it reduces the leakage and enhances the cycling stability even of pure TCMs. The final working pairs selected for the proof of concept and scale-up study are $MgSO_4$/E/PA and $MgSO_4$/HDPE for charging integrated, $MgSO_4$/MDI for cascade system and $MgSO_4$/CLU, $MgCl_2$/PEO and $MgCl_2$/MDI and $MgCl_2$/HDPE for discharging integrated. The reliability of the $MgSO_4$/HDPE composites containing 75–90 wt.% of TCM was studied after 40 cycles tests; mechanical integrity, stability, energy stored and reaction kinetics was monitored. The results show that the new composite has a great potential for storing heat, up to 2 GJ·m^{-3} and offers a wide working temperature range, from 30 °C to ~150 °C. The PCM/TCM combination give the composites mechanical integrity while accommodating the volume change and maintaining the structural stability during the thermal cycles.
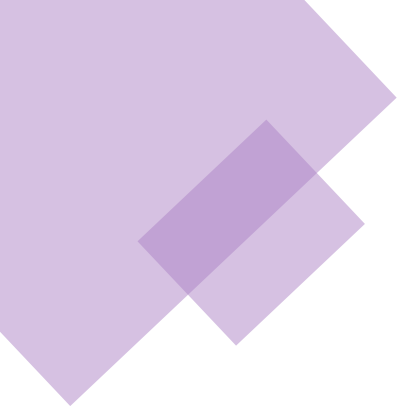
This novel idea addresses some key technology gaps in TES technologies, particularly TCM degradation (increases life-span), cost-effectiveness and TCM flexibility of the based technology. Thus, it offers a paradigm shift to thermal energy storage technology.
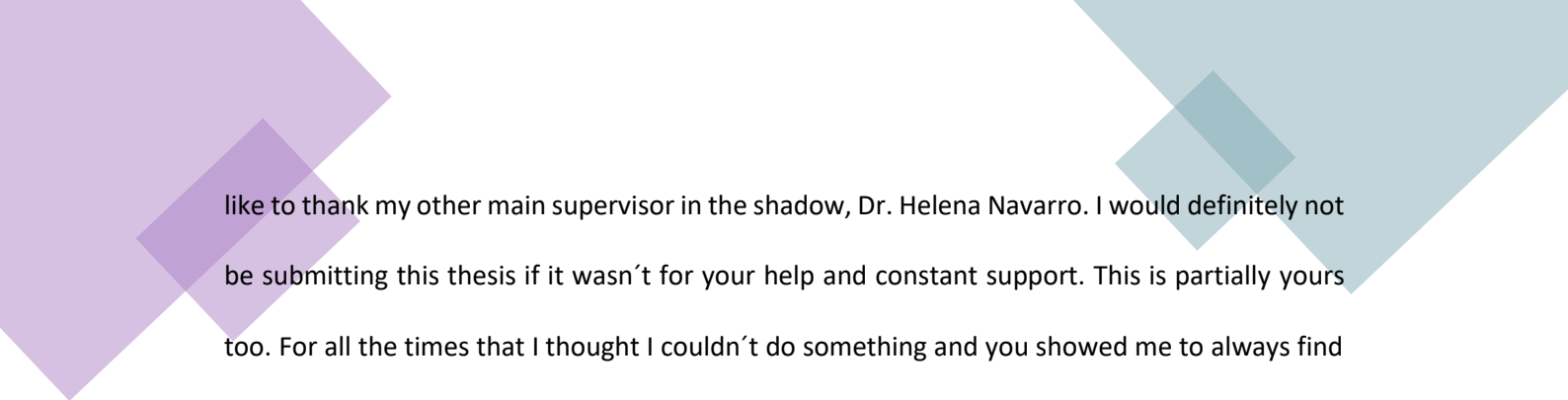
A 'Hic et nunc'.

ACKNOWLEDGEMENTS

This PhD dissertation would not have been possible without the help and support of many people throughout these four intense years. Herein, I would like to express my gratitude to all of them, my heart is filled with small pieces of all of them.

This thesis comes a long way, and I do not think I´ll be writing these words if it wasn´t for the very first people that I encountered during my bachelor´s and who encourage me to do a PhD. To Prof. Luisa Cabeza, who will be also part of my panel closing the cycle, I would like to thank her for the guidance during my baby steps in thermal energy storage research. To Prof. Ana Inés Fernández who also supported me during my very first years as a researcher. To Dr. Camila Barreneche who is my mother in science, my mentor and has been my rock during these years. I believe I would not be here if I had not run into you in materials engineer, I am wonderfully grateful for that. You showed me something that cannot be taught, without passion in our work we are nothing. You believed in me when I did not believe in myself, and you brought me to my limits when needed and also gave me space/freedom when required. Everything that I have achieved it is also yours. You are an amazing mentor Camila, beyond what I had never imagined. Always keep pushing amore, because that´s what we do and what we are.

I would also like to thank my main supervisor, Prof. Yulong Ding for his guidance during the last four years of the PhD degree and for allowing me to work and grow as a researcher at the level that I did here. Although I can be a worrying person sometimes, you have always been kind to me and a stable hand to seek help when needed. I am very glad I decided to come to the BCES for a PhD and that life has guided me for a postdoc here too. I believe you are not where you are professionally just because of your intellect, but also because you are always nice and kind to everyone, regardless of their position. Thanks for the freedom given during these last years, I am very glad to be on board for the next couple of years. Along with my supervisor, I would

like to thank my other main supervisor in the shadow, Dr. Helena Navarro. I would definitely not be submitting this thesis if it wasn´t for your help and constant support. This is partially yours too. For all the times that I thought I couldn´t do something and you showed me to always find the way and nev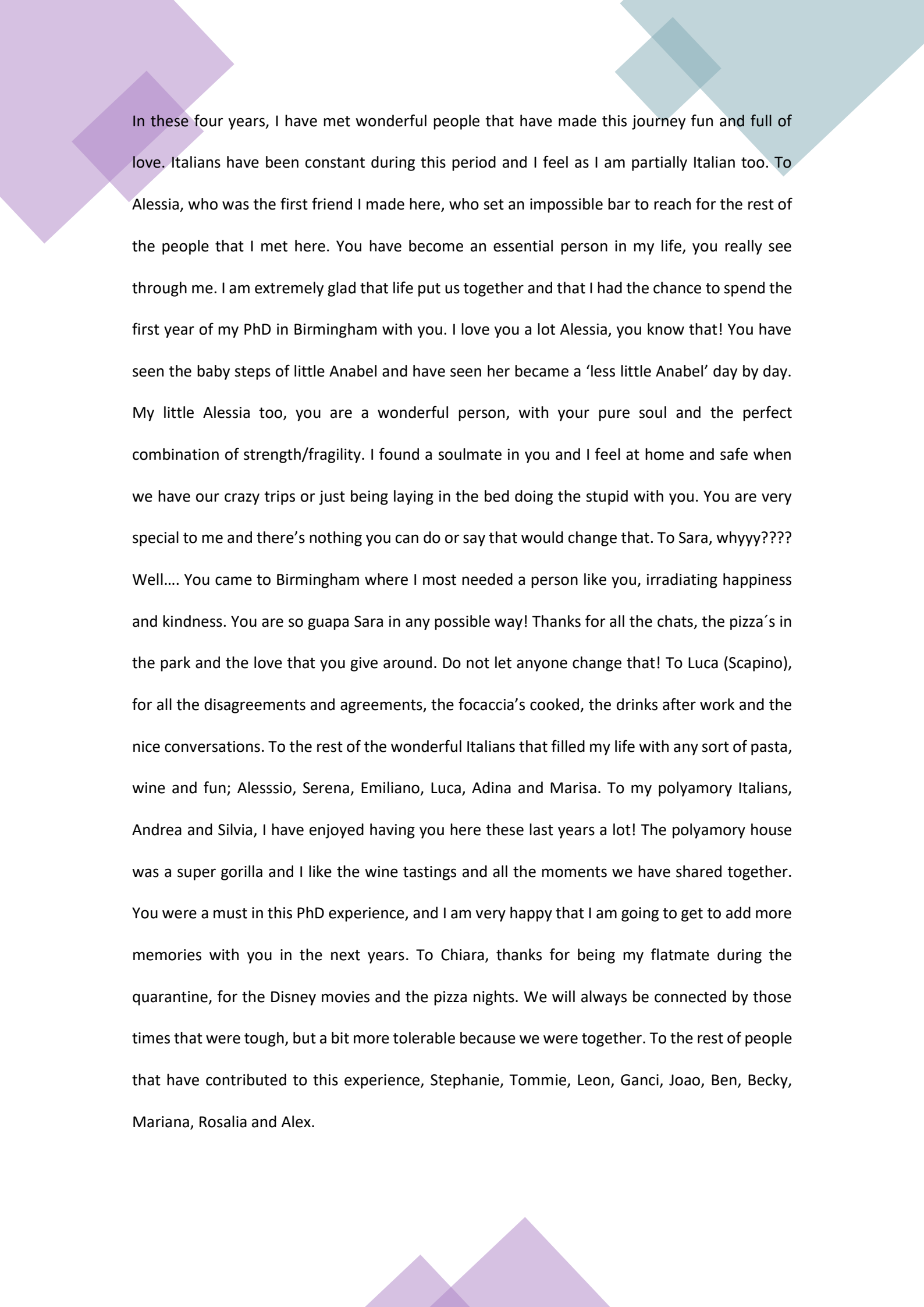er give up. Your strength is something to admire Helena and it´s something that it is part of myself now. Thanks for your dedication to our work, for your patience through grumpy Anabel and for the long list of good moments that I take with me. I am very sure that we are going to be working together for a long time, the BCN-BHAM connection is beating stronger than ever. Ens coneixem bé Helena i ens estimem molt (jo ho se), has estat una persona molt important per mi aquí, sempre he considerat que hi tenia una pseudofamilia amb tu al meu costat. Desitjo que la vida et porti molta tranquilitat i persones a la teva vida que et valorin i t'estimin, jo he gaudit molt d'aquest camí amb tu.
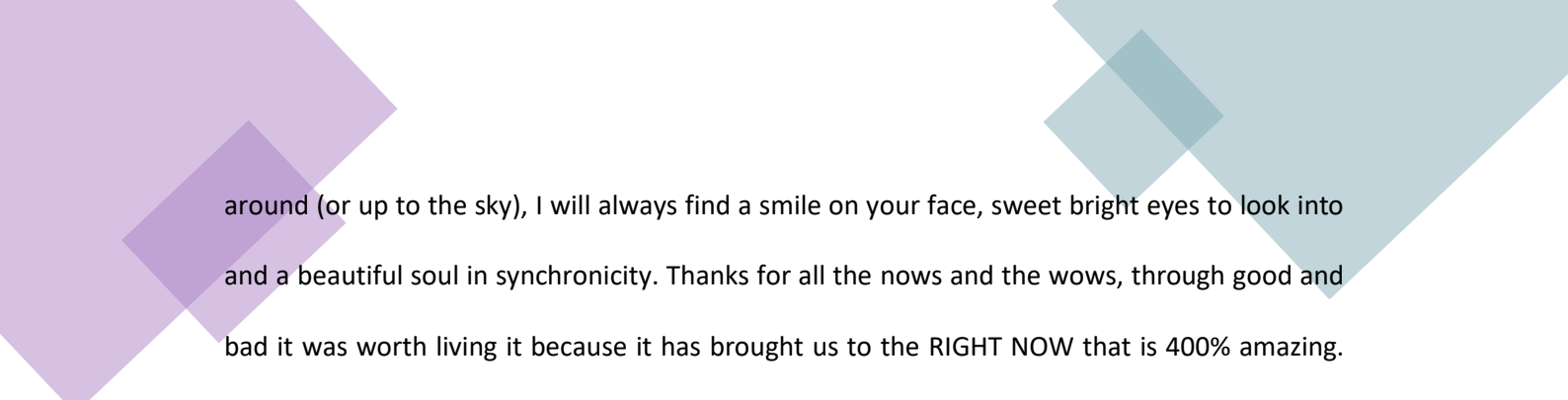
I would like to mention all my colleagues at the BCES, through cultural differences and hard work you have taught me so much and put me completely out of my comfort zone. I feel I have grown a lot in these years because of that and I am glad that I have been part of this process. To Boyang for being the best desk mate that one could have, always bringing sweets and with a smile in her face. You are very guapa, not just in the outside. I am very glad that I can keep working and organising events with you, it is always fun to do. To Jiang, the key technologies project brought us together and I have been very glad to work with you since then. You are a strong and perseverant person and I admire you for that. I liked working with you all along these years. To Gan, who is so special and has taught me so much without knowing. Thanks for all the fun even crazy moments that you have granted me these years, you were such a good mate during the PhD, we made it Ganito. To Shivangi, who has always been nice to me, complimenting me (even though I say I don't like it.. hehe) and telling me all sort of nice things that made my days. It´s nice to have around someone pure and full of light like you Shivangi. I would like to extend my gratitude to Lin, Jie, Daniel, Aris, Binjian, Yunren, Yanqi, Robin, Marco and anyone else that has worked in the BCES during these past four years.

In these four years, I have met wonderful people that have made this journey fun and full of love. Italians have been constant during this period and I feel as I am partially Italian too. To Alessia, who was the first friend I made here, who set an impossible bar to reach for the rest of the people that I met here. You have become an essential person in my life, you really see through me. I am extremely glad that life put us together and that I had the chance to spend the first year of my PhD in Birmingham with you. I love you a lot Alessia, you know that! You have seen the baby steps of little Anabel and have seen her became a 'less little Anabel' day by day. My little Alessia too, you are a wonderful person, with your pure soul and the perfect combination of strength/fragility. I found a soulmate in you and I feel at home and safe when we have our crazy trips or just being laying in the bed doing the stupid with you. You are very special to me and there's nothing you can do or say that would change that. To Sara, whyyy???? Well…. You came to Birmingham where I most needed a person like you, irradiating happiness and kindness. You are so guapa Sara in any possible way! Thanks for all the chats, the pizza´s in the park and the love that you give around. Do not let anyone change that! To Luca (Scapino), for all the disagreements and agreements, the focaccia's cooked, the drinks after work and the nice conversations. To the rest of the wonderful Italians that filled my life with any sort of pasta, wine and fun; Alesssio, Serena, Emiliano, Luca, Adina and Marisa. To my polyamory Italians, Andrea and Silvia, I have enjoyed having you here these last years a lot! The polyamory house was a super gorilla and I like the wine tastings and all the moments we have shared together. You were a must in this PhD experience, and I am very happy that I am going to get to add more memories with you in the next years. To Chiara, thanks for being my flatmate during the quarantine, for the Disney movies and the pizza nights. We will always be connected by those times that were tough, but a bit more tolerable because we were together. To the rest of people that have contributed to this experience, Stephanie, Tommie, Leon, Ganci, Joao, Ben, Becky, Mariana, Rosalia and Alex.
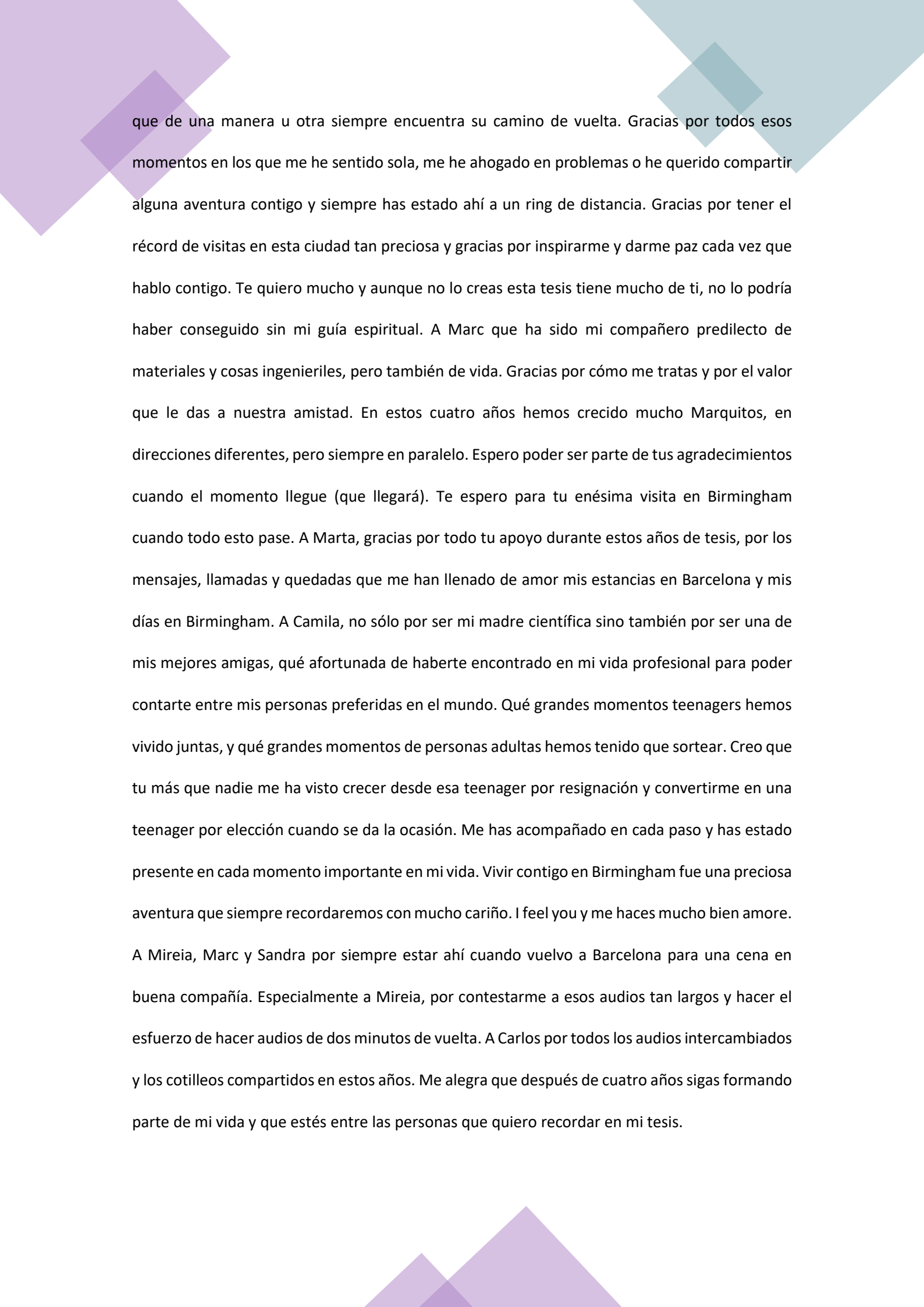
A Noelia, que m´ha acompanyat en visites culturals, cafès i xerrades sobre la vida, ens vam conèixer de forma molt random però el wine tasting ens va unir i estic molt conenta de que hagis format part de la meva expèriencia a UK. To Gilmore, thanks for all your nice words and for sharing with me your PhD related issues/anxiety. Thanks for all the nice moments shared Gilmore, it was very nice having you taking part of this journey. A Afif, porque es el guapi más guapi de todos por dentro y por fuera. Por todos los brownies compartidos en la library, y los paseos por el Green heart. Lo hemos conseguido guapi, estoy infinitamente feliz, seguro nos esperan grandes aventuras, me alegra saber que las compartiré contigo. A Iria, que ha sido mi constante en este último año, sólo ella y yo sabemos lo que hemos pasado juntas y sólo yo sé lo especial que eres para mí. A tu fortaleza y determinación que inspira a cualquiera que tenga la oportunidad de acompañarla en su día a día. Me has enseñado tanta amiga, no tienes ni idea, eres la mujer de verde fosforito. Por todas las cenas, pelis, tardes de compras, charlas intensas y menos intensas, capítulos de libros abiertos y cerrados, autistas y gorilas, doctorados, cumpleaños, Chung Ying's, dolores de tripa, mudanzas, caminatas, miércoles y sábados, todas esas cosas han hecho que este año tenga una lista inmensa de momentos especiales contigo que me han dado la vida. Sigue tiñendo mi vida de verde, todo el mundo necesita una super heroína como tú en su vida. Ya sabes que, aunque no lo decimos mucho te quiero, y sé que esta unión en el espectro verde va a ser muy duradera. A Patricia, gracias por regalarme tantos momentos, has estado desde el principio conmigo aquí. Desde que cogí ese vuelo asustada desde Barcelona a Birmingham y tu estabas ahí esperándome en el aeropuerto sin apenas conocerme con una sonrisa en la cara dispuesta a acompañarme. Y eso has hecho desde entonces, me has acompañado y has estado ahí con tu puro y precioso corazón. He disfrutado muchísimo de ti estos y me alegro de que por cosas del destino podamos seguir viviendo en el mismo país para poder seguir añadiendo momentos contigo. Te considero mi familia en UK. To Lele, thanks for bringing so many genuine feelings to my life, without even realising you have taught me so many things about myself mountain guy. It is nice to know that if I turn my head
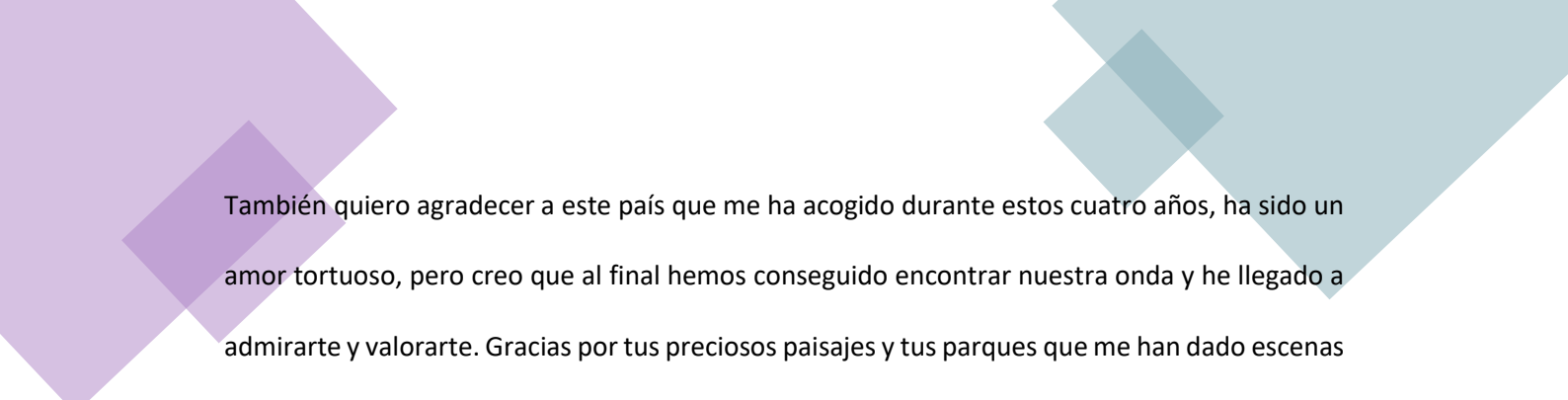
around (or up to the sky), I will always find a smile on your face, sweet bright eyes to look into and a beautiful soul in synchronicity. Thanks for all the nows and the wows, through good and bad it was worth living it because it has brought us to the RIGHT NOW that is 400% amazing. Who knows what nows are yet to come, it is scary to explore, but I am in the 27B seat looking forward to figuring it out.

A mis amigos de siempre, que me ayudan a seguir cuando las cosas se ponen feas y saben siempre cuando aparecer para darme un empujoncito. No podría haber hecho esto sin vosotras, llenáis mi vida de amor y paz. A Ariadna, por ser constante en mi vida siempre, por darme un hombro en el que llorar y unos ojos en los que encontrarme en casa cuando estoy asustada. Por enseñarme quien soy cada vez que pierdo el foco y por intentar entenderme siempre, aunque pensemos de forma diferente. Te quiero mucho, después de 26 años sigues acompañándome de la mano (como cuando éramos niñas disfrazadas de chinitas) y esperando para aparecer cuando más te necesito. Y who knows why, siempre sabes cuándo hacerlo. A Paula, en estos cuatro años en la distancia creo que hemos encontrado nuestro camino a una nueva versión de nuestra amistad. Es curioso que haya ocurrido en la distancia, pero me alegra mucho que haya sido así (¿quizás uno no sabe lo que tiene hasta que se va al quinto pino?). Gracias por estar siempre ahí estoicamente y como una roca, por todas las llamadas y audios largos, por todas las veces que me recibes en Barcelona como si fuera la primera vez que vuelvo a casa y por las veces que has hecho un gran esfuerzo para venir a visitarme. ¡Gracias por no perder la fe en nosotras cuando yo si lo hice, seguimos aprendiendo juntas! A Laura, por esos audios infinitos compartiendo nuestras respectivas vidas en el extranjero. Porque tú más que nadie sabe lo que es hacer un doctorado y por lo menos lo hemos pasado juntas, cada una a su manera, pero siempre compartiendo nuestras vivencias la una con la otra. Dentro de unos años leeremos nuestros respectivos agradecimientos y reiremos y pensaremos que no fue para tanto. A Gerard, a mi Gerfi, estos cuatro años me han demostrado que tenemos algo muy especial que ni la distancia ni la falta de comunicación ni el tiempo puede marchitar. Es tan puro y tan profundo
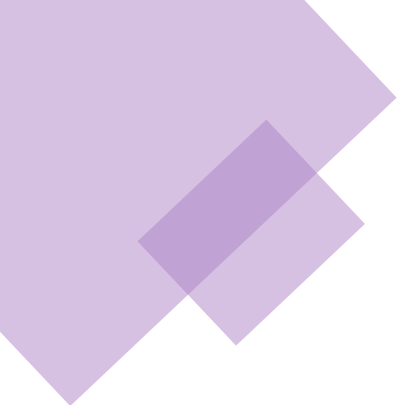
que de una manera u otra siempre encuentra su camino de vuelta. Gracias por todos esos momentos en los que me he sentido sola, me he ahogado en problemas o he querido compartir alguna aventura contigo y siempre has estado ahí a un ring de distancia. Gracias por tener el récord de visitas en esta ciudad tan preciosa y gracias por inspirarme y darme paz cada vez que hablo contigo. Te quiero mucho y aunque no lo creas esta tesis tiene mucho de ti, no lo podría haber conseguido sin mi guía espiritual. A Marc que ha sido mi compañero predilecto de materiales y cosas ingenieriles, pero también de vida. Gracias por cómo me tratas y por el valor que le das a nuestra amistad. En estos cuatro años hemos crecido mucho Marquitos, en direcciones diferentes, pero siempre en paralelo. Espero poder ser parte de tus agradecimientos cuando el momento llegue (que llegará). Te espero para tu enésima visita en Birmingham cuando todo esto pase. A Marta, gracias por todo tu apoyo durante estos años de tesis, por los mensajes, llamadas y quedadas que me han llenado de amor mis estancias en Barcelona y mis días en Birmingham. A Camila, no sólo por ser mi madre científica sino también por ser una de mis mejores amigas, qué afortunada de haberte encontrado en mi vida profesional para poder contarte entre mis personas preferidas en el mundo. Qué grandes momentos teenagers hemos vivido juntas, y qué grandes momentos de personas adultas hemos tenido que sortear. Creo que tu más que nadie me ha visto crecer desde esa teenager por resignación y convertirme en una teenager por elección cuando se da la ocasión. Me has acompañado en cada paso y has estado presente en cada momento importante en mi vida. Vivir contigo en Birmingham fue una preciosa aventura que siempre recordaremos con mucho cariño. I feel you y me haces mucho bien amore. A Mireia, Marc y Sandra por siempre estar ahí cuando vuelvo a Barcelona para una cena en buena compañía. Especialmente a Mireia, por contestarme a esos audios tan largos y hacer el esfuerzo de hacer audios de dos minutos de vuelta. A Carlos por todos los audios intercambiados y los cotilleos compartidos en estos años. Me alegra que después de cuatro años sigas formando parte de mi vida y que estés entre las personas que quiero recordar en mi tesis.

También quiero agradecer a este país que me ha acogido durante estos cuatro años, ha sido un amor tortuoso, pero creo que al final hemos conseguido encontrar nuestra onda y he llegado a admirarte y valorarte. Gracias por tus preciosos paisajes y tus parques que me han dado escenas tan icónicas y mágicas. Gracias por tus bares y restaurantes que me han hecho valorar la gastronomía española y también descubrir mi restaurante preferido en el mundo mundial (Kimchi). Gracias por hacerme apreciar los días de sol, la brisa en mi piel y las gotas de lluvia. Gracias por enseñarme que casa esta dónde uno está y que las zonas de confort pueden estar distribuidas por todo el mundo en forma de personitas con corazones que no les caben en el pecho. Gracias por hacerme sufrir, llorar y reír, de forma genuina y pura, gracias por haber sido el contexto de mi tesis y por proporcionarme mi siguiente gran aventura.

A mi familia, mis padres y mi hermano, que han creído siempre en mí y aunque no siempre estén de acuerdo con mis decisiones, siempre encuentran la manera de apoyarme y estar ahí para mí. Gracias por quererme siempre y sin condiciones, por dejarme ser quien soy y quien quiera ser. Hacer el doctorado ha significado estar lejos de vosotros estos últimos cuatro años, lo cual ha sido duro, pero también me ha brindado la oportunidad de sentir inmensa felicidad multiplicada al volver a casa y de valorar lo que tengo más si cabe. A mi hermano, que es una de las personas más talentosas que conozco, gracias por inspirarme y apoyarme durante este camino. A mi madre, porque la unión que tenemos es muy especial y puede con kilómetros de distancia e indiferencias, este año ha sido complicado, pero después de todo, me ayuda sentirme muy cerca de ti. A mi padre, que es un guerrero y ha demostrado poder con todo lo que se le pone por delante. Gracias por cuidarme siempre como lo haces. Me encanta reconocer cosas de vosotras en mí y os llevo conmigo a donde sea que vaya, hay mucho de vosotros en este doctorado.

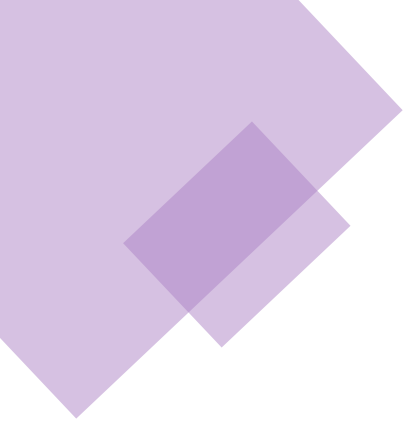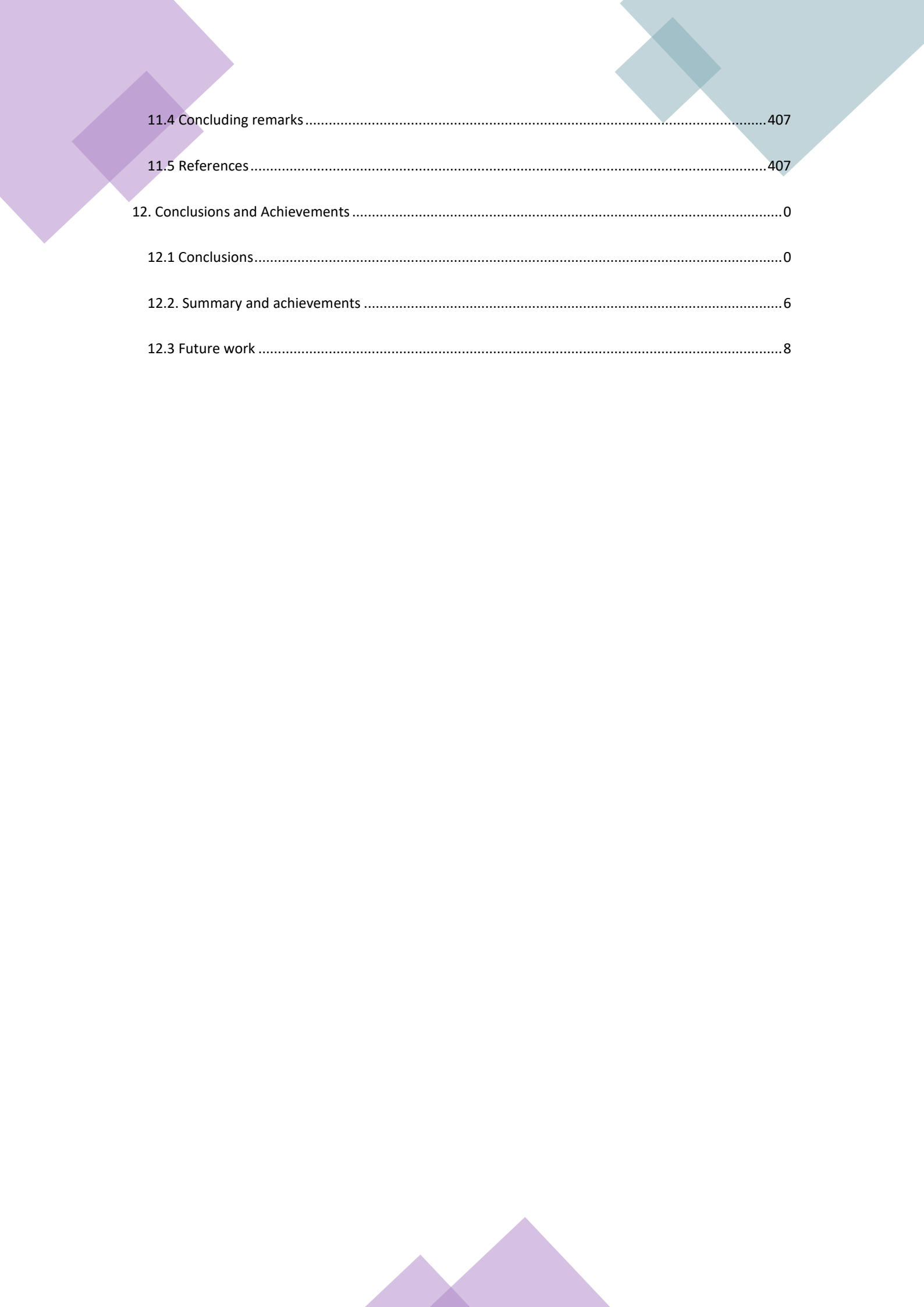*Winners are not those who never fail, but those who never quit.*

Banksy.-

TABLE OF CONTENT

LIST OF FIGURES

LIST OF TABLES

LIST OF ABBREVIATIONS AND ACRONIMS

347, 351, 352, 355, 357, 358, 361, 362, 368, 369, 370, 374, 375, 381, 383, 384, 385, 407, 408, 409, 410, 1, 3, 4, 6

E_d

Energy density, 182, 183, 184, 185, 186, 225, 226, 227, 288

G

GG

Guar gum, 3, 266, 271, 321, 326, 329, 330, 1, 6

H

HDPE

High density polyethylene, 3, 4, 23, 24, 25, 26, 29, 163, 164, 238, 239, 240, 246, 249, 250, 251, 253, 271, 293, 296, 302, 308, 309, 310, 311, 313, 316, 318, 319, 331, 333, 337, 339, 341, 344, 346, 347, 348, 349, 350, 353, 355, 356, 357, 358, 360, 361, 363, 364, 365, 366, 367, 374, 375, 380, 381, 382, 384, 396, 1, 3, 4, 6

K

K

Thermal conductivity, 59, 62, 63, 64, 103, 106, 107, 108, 110, 112, 113, 114, 117, 160, 171, 182, 183, 184, 185, 186, 193, 205, 239, 246, 272, 273, 274, 276, 278, 280, 281, 282, 286, 288, 290, 291, 292, 293, 296, 297, 298, 333, 351, 362, 385, 386, 408, 410

L

LFA

Laser flash analysis, 21, 156, 159, 168, 169, 170

LTES

Latent heat storage, 56

M

MDI

4,40-diphenylmethane.diisocyanate, 3, 4, 23, 24, 29, 237, 238, 246, 249, 250, 253, 271, 290, 291, 295, 296, 302, 307, 308, 309, 310, 311, 313, 314, 315, 316, 317, 318, 319, 331, 346, 347, 348, 349, 351, 354, 384, 1, 3, 6

N

NPG

Neopentyl glycol, 22, 145, 234, 235, 236, 246, 248, 249, 250, 253, 289, 290

P

PA

Polyamides, 3, 4, 25, 26, 29, 44, 117, 237, 271, 321, 326, 329, 330, 331, 347, 349, 352, 355, 358, 361, 362, 368, 369, 370, 371, 374, 375, 381, 383, 408, 1, 3, 6

PCM

Phase change materials, 4, 18, 20, 22, 23, 24, 25, 38, 58, 64, 65, 71, 121, 122, 123, 124, 130, 131, 132, 133, 134, 135, 137, 138, 140, 141, 142, 143, 144, 145, 146, 147, 154, 157, 158, 159,

X

1

THESIS TIMELINE

1. Thesis timeline
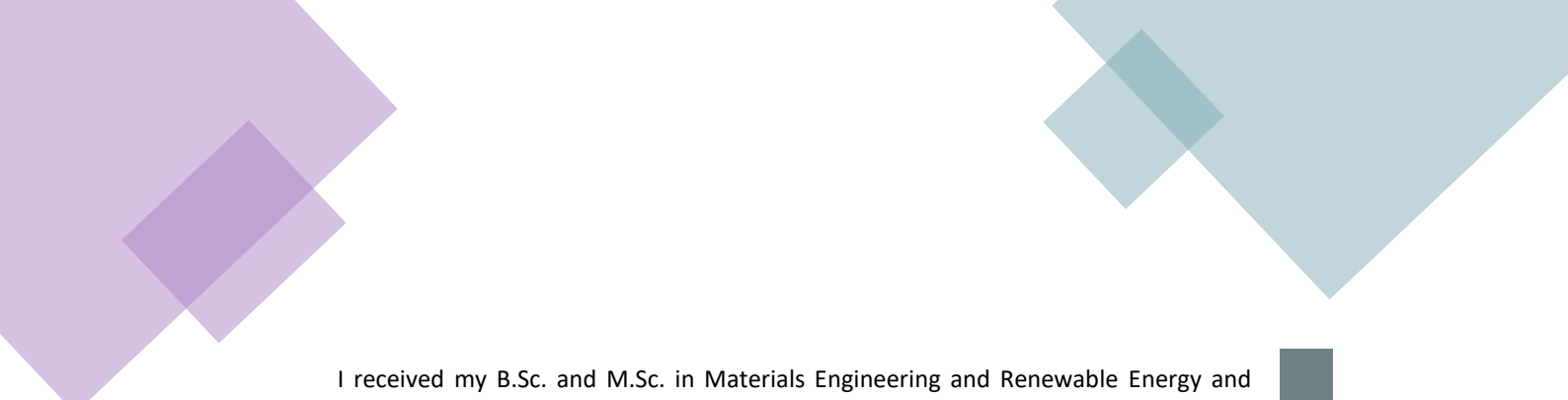
2. Scientific contributions

3. Introduction

4. TCS Outlook

5. Targets and structure of the thesis

6. Hybrid TES system:

3 in 1 concept

I received my B.Sc. and M.Sc. in Materials Engineering and Renewable Energy and Sustainability in 2015 and 2016, respectively, both at the University of Barcelona, Spain. My master's thesis was on the use of solid particle materials as solar energy absorption as well as thermal energy storage (TES) at high temperatures on different aging stages for concentrating solar applications. I was granted with various fellowships at GREA research center (two years) and DIOPMA research center (six months), working with Prof. Luisa F. Cabeza, Dr. Ana Inés Fernández and Dr. Camila Barreneche. This section presents the timeline of this thesis from when I finished my master thesis in Barcelona until the conceptualisation and finalisation of the 3 in 1 concept.

7. Bench study specifications

8. Material screening and selection

9. Working pairs

10. Proof of concept and scale-up

11. Potential applications and prospective

12. Conclusions and achievements

1. THESIS TIMELINE

The thesis timeline presented in this section aims to illustrate various industrial and university-related projects that I have been involved and the time-flow leading to the 3 in 1 system conceptualisation. Figure 1 shows the thesis timeline chart with each block to be briefly described below.

Note that these projects and studies are related and coherent, aimed for a fundamental understanding of TES; and also there are a number of novelties in the work.
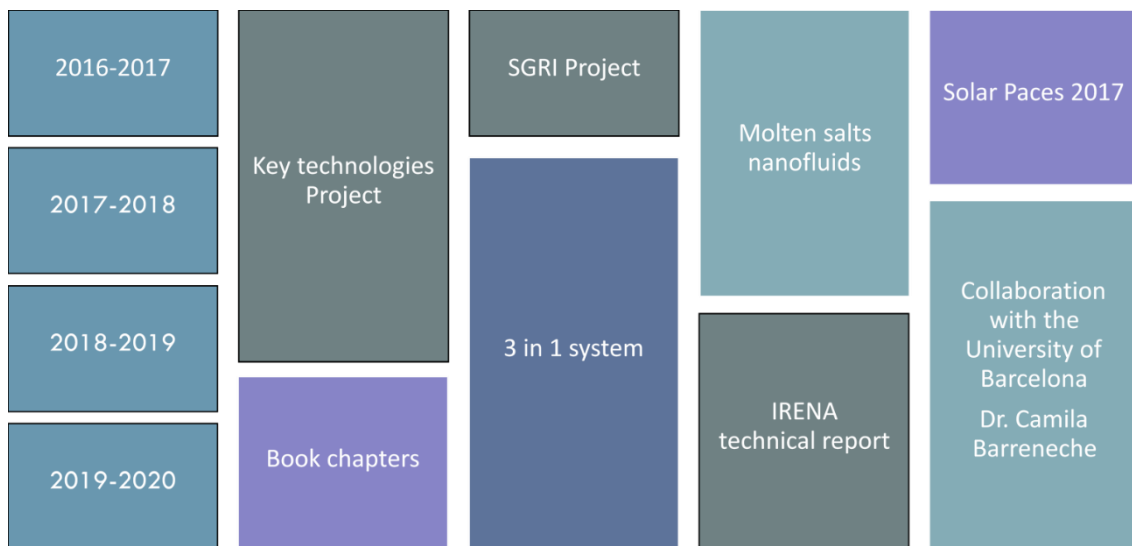
Figure 1. Thesis timeline chart

(1) SGRI project (2016-2017)

This project was mainly focused on the thermal stability of low, medium and high TES materials. A selection of PCM composites was studied for latent heat storage (LTHS). Among the properties measured in the evaluation of these PCM composites, thermal stability after a large number of thermal cycles was a key parameter. Thereby, the thermophysical, mechanical and chemical properties of these PCMs were characterized after different melting/freezing thermal cycles. This work was also presented on the Solar Paces 2019 conference held in Morocco.

(2) Collaboration with the University of Barcelona (2018-2020)

A collaboration with the University of Barcelona was started in 2018 when Dr Camila Barrenche visited our research group. Apart from being involved in the 3 in 1 concept, this collaboration also brought some publications, a Review of thermal conductivity techniques for TES materials and a Thermal energy storage technologies for concentrated solar power – A review from a materials perspective. See publications in the next section.

Thermal conductivity is a key selection and design parameter that must be accurately determined to properly predict the charge, storage and discharge time for any TES application. This study aimed to review the main techniques available to measure the thermal conductivity of TES materials. A complete and detailed literature review was done across the thermal conductivity data and theoretical methods. The paper on concentrated solar power (CSP) reviewed different TES technologies that had been investigated and deployed over the past two decades. It gives a comprehensive overview of TES technologies investigated, demonstrated and/or deployed in CSP plants with a specific emphasis on TES materials. A thorough analysis is also given on the state-of-the-art of the CSP technologies including commercial development and research innovation.

(3) Key technologies project (2017-2018)

The effect of the nanoparticles dispersion on the base fluid was studied by measuring the specific heat capacity, the thermal conductivity, the rheological behaviour and the thermal stability at high temperatures. This work was within a project aimed to formulate and characterise salts with low melting point and high decomposition temperature for high-temperature sensible heat storage. A corrosion test was also performed to determine the most suitable construction materials for Concentrated Solar Power (CSP) systems; the compatibility of low carbon steel A1045, two stainless steel 304H and 316L, and nickel alloys Inconel 600 with $NaNO_3$-KNO_3 (60–40 wt.%) pure and $NaNO_3$-KNO_3 (60–40 wt.%) based nanofluids. The non-confidential data were analysed and presented to four conferences: UK Particle technology Forum 2017, 10th World Congress of Chemical Engineering and 1st Nanofluids Symposium 2017. Besides, two journal papers were published from this project: Novel key parameters for eutectic nitrates based

nanofluids selection for concentrating solar power (CSP) system, and High-temperature corrosion behaviour of metal alloys in commercial molten salts (see next section).

(4) Molten salt nanofluids (2017-2019)

Collaborations with other researchers of the Birmingham Centre for Energy Storage (BCES) has led to some interesting work on molten salt nanofluids; mainly on the effect of shape/particle size on nanofluids properties particularly viscosity, thermal conductivity, specific heat and wettability. From this block, two papers were published: Effect of SiO_2 nanoparticle addition on the wetting and rheological properties of solar salt and Thermal and Rheological Behaviour of Solar Salt Containing Highly Thermally Conductive Particles. The work was also presented in the Solar Paces Conferences 2018 and 2019, as described in the following section.

(5) Book chapters (2019-2020)

Two book chapters on thermal energy storage manufacturing and thermochemical materials were also produced during the thesis work, which also contributes to the introduction and TCS Outlook section of this thesis.

(6) IRENA technical report (2018-2019)

I actively contributed to this technical report during two years of my thesis work as a technical expert, mainly on thermochemical materials. This report provides an overview of current TES technologies for renewable energy utilisation and future developments. It is targeted to a technical audience and policymakers, expected to be published in late 2020.

(7) 3 in 1 system (2017-2020)

I started working on the 3 in 1 concept at the beginning of the second year of my PhD. After all the knowledge acquired on the molten salt/nanofluids area, this concept was conceptualised, and I focused most of my lab work on thermochemical materials. From this research, apart from the papers introducing the concept and outputs, two more studied were performed; screening of water-sorption thermochemical materials and Thermal conductivity enhancement of Thermochemical Energy Storage materials: study of different supporting matrixes. Both presented in the Eurotherm Conference 2019, the first one is part of the material screening from the 3 in 1 system and the second one was the result of the first steps taken on the

thermochemical field. Different thermochemical composites already studied in the literature (e.g. $CaCl_2$ and vermiculite) were mixed with highly thermally conductive particles. These studies are expected to be published in high impact journals in the coming months.

2

SCIENTIFIC CONTRIBUTIONS
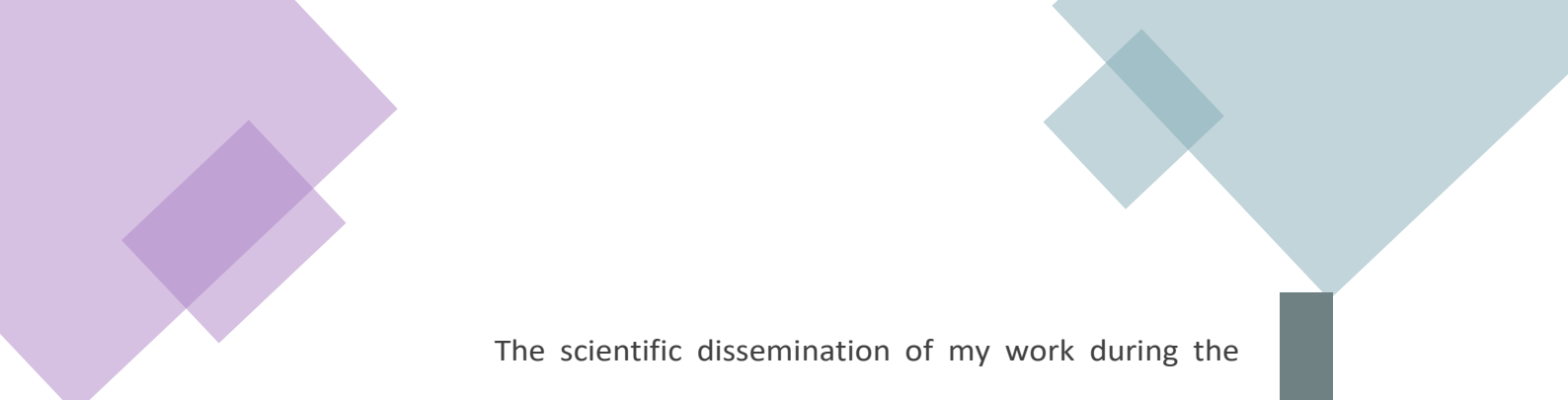
6. **Hybrid TES system:**

3 in 1 concept

5. **Targets and structure of the thesis**

4. **TCS Outlook**

3. **Introduction**

2. **Scientific contributions**

1. **Thesis timeline**

The scientific dissemination of my work during the thesis is summarised in this section for an easy reference. Publications related and partially related to the thesis work are provided as they are all part of my scientific contributions during my PhD study. I have published 11 papers in high impact journals, presented 25 conference papers, and co-authored three book chapters and 1 technical report for IRENA.

7. Bench study specifications

8. Material screening and selection

9. Working pairs

10. Proof of concept and scale-up

11. Potential applications and prospective

12. Conclusions and achievements

2. SCIENTIFIC CONTRIBUTIONS

11 x Publications

2 x Book Chapter

1 x Patent – Key technologies

1 x IRENA TES Report

6 x Conferences – Attendance

3 x Workshops and Conference - Management

Figure 2. Summary of scientific dissemination during the thesis.

All the contributions of this thesis have been published in top-level international conferences, high ranked journals and high impact book editorials, a summary is shown in Figure 2. The list of publications is presented as follows:

- A. Palacios, H. Navarro, C. Barreneche, Yulong Ding, "3 in 1: Outlook to a novel storage strategy". Applied Energy, 2020.

- A.Palacios, M.E. Navarro YD. Integrated Thermal-Chemical-Electrochemical-Electrical Energy Conversion and Storage. Mater. Clean Energy Convers. Util., 2021, p. 41.

- Navarro, M.E, Jiang, Zhu PA. Manufacturing. In: Ding Y, editor. Therm. energy storage Mater. devices, Syst. Appl., Energy and environmental series; 2020

- Attendance to Eurotherm Seminar #112 Advanced in thermal energy storage 2019 in Lleida. Poster presentation: A. Palacios, M.E. Navarro, C. Barreneche, Yulong Ding, "Thermochemical Water-sorption materials screening for Thermal Energy Storage: building application",

Eurotherm proceedings, 2019. Oral presentation: M.E. Navarro, A Palacios, C. Barreneche, Yulong Ding "Thermal conductivity enhancement of Thermochemical Energy Storage materials: study of different supporting matrixes", Eurotherm proceedings, 2019.

Besides the main contributions of this thesis, a number of other research works have been carried out in collaboration with other researchers while this thesis was being written. These works have been focused on nanofluids-molten salt properties, concentrated solar power materials and specific characterisation techniques relevant to TES field. They have been published in top-level international conferences and journals. A list of these publications and attendance at conferences are given in the following:

- M.E. Navarro, Anabel Palacios, Thomos Hughes, Chloe Connolly, Harkiran Uppal, Lin Cong, Xianzhang Lej, Geng Qiao, Guanghui Leng, Yulong Ding. Ceramic-salt based composites for thermal energy storage, energy storage science and technology (2017), 6 (4).

- Z. Jiang, Anabel Palacios, Xianzhang Lei, Helena Navarro, Geng Qiao, Ernesto Mura, GuizhiXu, Yulong Ding. Novel key parameter for eutectic nitrates based nanofluids selection for concentrating solar power (CSP) system, Appl. Energy, vol. 235, pp. 529–542, 2019.

- A. Palacios, L. Cong, M. E. Navarro, Y. Ding, and C. Barreneche, "Thermal conductivity measurement techniques for characterizing thermal energy storage materials – A review," Renew. Sustain. Energy Rev., vol. 108, no. November 2018, pp. 32–52, 2019.

- A. Palacios, Barreneche C, Navarro ME, Ding Y. Thermal energy storage technologies for concentrated solar power – A review from a materials perspective. Renew Energy 2019, 156, pp 1244-1265. doi:10.1016/j.renene.2019.10.127.

- A. Anagnostopoulos, A. Palacios, M.H. Navarro, Sonia Fereres, Yulong Ding, "Effect of SiO2 nanoparticle addition on the wetting and rheological properties of Solar Salt". Solar Energy Materials and Solar Cells, 210, 2020.

- Patent number 201810483268.3, Molten salt-based nanofluid preparation system, 2018, China.

- Palacios A, Navarro ME, Ding Y. Thermal and rheological behaviour of solar salt-containing highly thermally conductive particles. AIP Conf. Proc., 2018. doi:10.1063/1.5067092.

- Attendance to UKES conference in University of Birmingham, Birmingham, United Kingdom (30 November – 2 December).

- Attendance to UK Particle Technology Forum 2017 in the University of Birmingham, Birmingham, United Kingdom (29th March 2017). Participation in the poster session: "In-situ dispersion of highly thermally conductive nanoparticles in a binary molten salt for its property enhancement for thermal energy storage

- Attendance to SolarPaces 24th -29th September (2017) in Chile. Oral presentation: A. Palacios, M.E. Navarro, Yulong Ding, "Thermal and Rheological behaviour of Solar Salt containing highly thermally conductive particles"

- Attendance to World Chemical Engineering Congress (WCECC) 1st -6th of October (2017) in Barcelona. Oral presentation: "Thermophysical properties enhancement of binary molten salt via (in-situ) by dispersion of high thermal conductive nanoparticles for Thermal energy storage applications

- Attendance to 1st Symposium nanofluids 9th -11th of October (2017) in Lisbon. Oral presentation: "Molten salt-based nanofluids with ceramic nanoparticles for concentrated solar power application

- Abstract submitted to SolarPaces 2nd – 5th of October (2018) in Morocco. Oral presentation: A.

Palacios, Ling Cong, Zhu Jiang, M.E. Navarro, Yulong Ding, "Experimental evaluation of a cascaded latent heat storage system from low to high-temperature application" and Argyrios Anagnostopoulos, Anabel Palacios, Nuria Navarrete, M. Elena Navarro, Leonor Hernandez, and Yulong Ding, "Effect of Temperature on the Internal Structure of Solar Salt-SiO2".

- Part of the organising committee of the 2nd UK-China Clean Energy Utilisation / Energy Storage conference, 7th to 9th of August (2019) in Birmingham.

- Part of the technical report on TES commercial technologies for IRENA as a technical expert, this has not been published yet.

3

INTRODUCTION
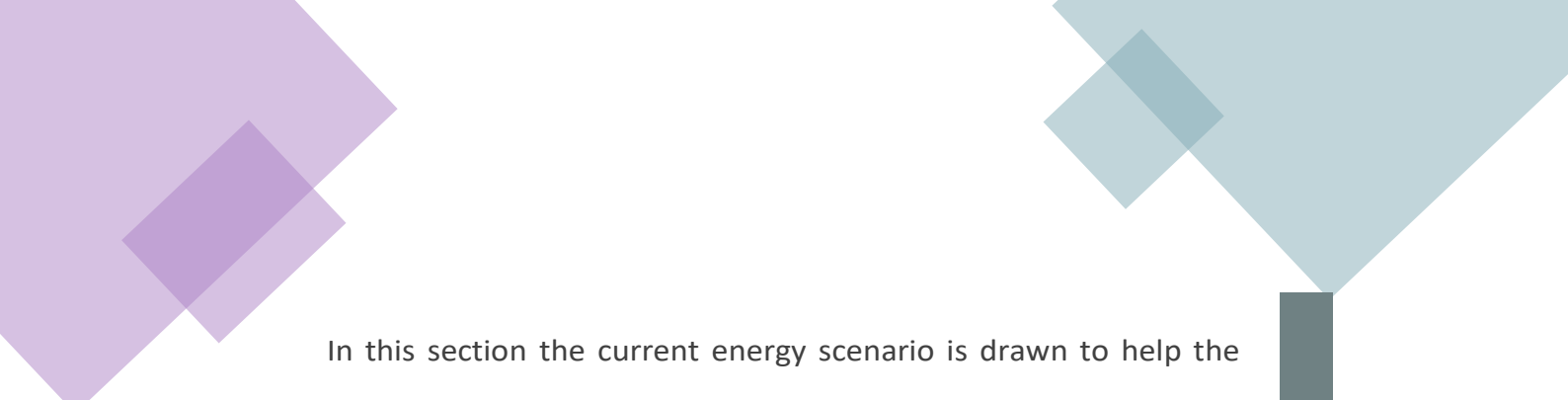
6. Hybrid TES system:

3 in 1 concept

5. Targets and structure of the thesis

4. TCS Outlook

3. Introduction

2. Scientific contributions

1. Thesis timeline

In this section the current energy scenario is drawn to help the reader understand the importance of energy storage in this era. All energy storage technologies are briefly listed and defined to then focused on thermal energy storage, their classification, limitations/challenges and future pathways such as hybrid systems. This is where this thesis finds its way to a hybrid 3 in 1 system that combines the three conventional TES technologies in one.

7. Bench study specifications

8. Material screening and selection

9. Working pairs

10. Proof of concept and scale-up

11. Potential applications and prospective

12. Conclusions and achievements

3. INTRODUCTION

3.1 CURRENT ENERGY SCENARIO

Energy has become one of the most valuable commodities in our modern society, dictating our living conditions and social status. The lack of accessibility to clean and affordable energy in emerging countries currently undergoing urbanization represents a key barrier to their economic development and living standard improvement. While the more developed world is acting on mitigating the effects of climate change, as recently reaffirmed by the Paris Agreement. The global energy demand is expected to increase by 30% in 2040 given the projected economic growth of 3.4% per year and the population growth to 9 billion in 2040 [1]. In such a scenario, the transition to a low or even zero-carbon represents a colossal challenge to the energy sector. Energy is used in a wide range of sectors and areas of human activity, including heating, cooling, industry, transport and buildings. The global share of these sectors in end energy use, and the source of the energy used in 2016, is summarised in Figure 3. According to IRENA's REMap 2050 [2], the total share of renewable energy must rise to 65% by 2050, with 40% of the energy consumption electrified and 85% coming from renewable sources. Renewable energy is, therefore, crucial for future energy supply, emissions reduction and minimisation of the dependence on fossil fuels. However, renewable energy sources, particularly wind and solar, suffer from an inherently variable and non-dispatchable nature. A deep renewable energy penetration will require a flexible energy system that can deal with rapid and large swings in unbalanced supply/demand.
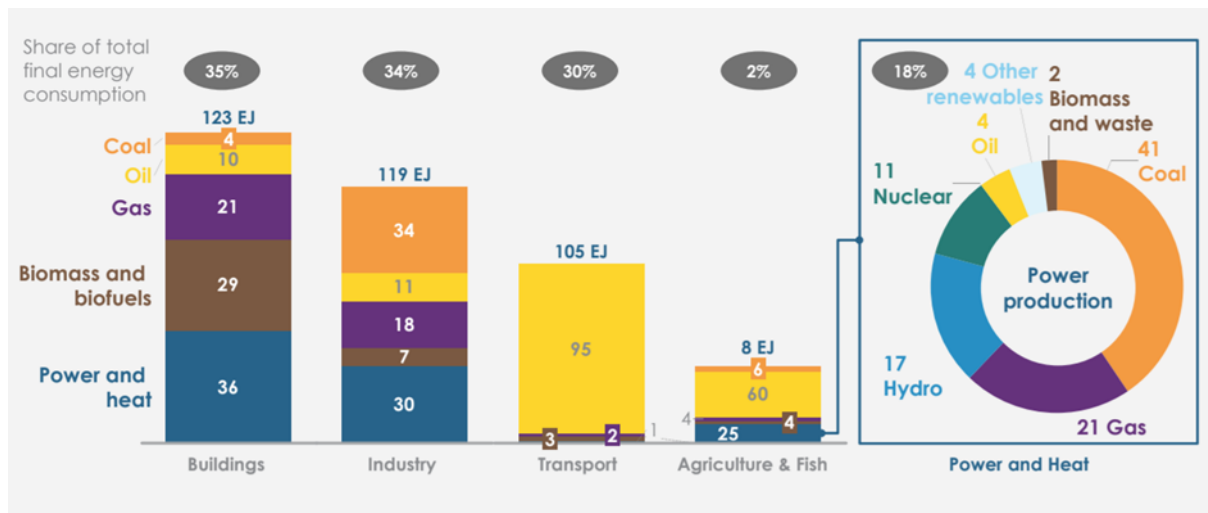
Figure 3. Final energy uses globally by end-use sector and source of energy (2016) [3].

3.2 ENERGY STORAGE

Energy storage has gained global attention recently as a key enabling technology for an energy system to integrate a higher share of variable renewable energy and minimise curtailment. The most important functional characteristic of storage technology is the combination of power and capacity. Together these establish the potential set of suitable applications for specific storage technology. Besides, the speed of reaction (response time) of storage technology is an increasingly important factor for the electricity system [4]. Energy storage technologies can be broadly split into mechanical e.g. pumped hydro storage, Compressed Air Energy Storage (CAES), Liquid Air Energy Storage (LAES) and flywheels; chemical e.g hydrogen storage and synthetic natural gas (SNG); electrochemical e.g. Lithium-Ion and lead-acid batteries; electrical e.g. supercapacitors; and thermal e.g. thermochemical, sensible and latent heat storage [5].
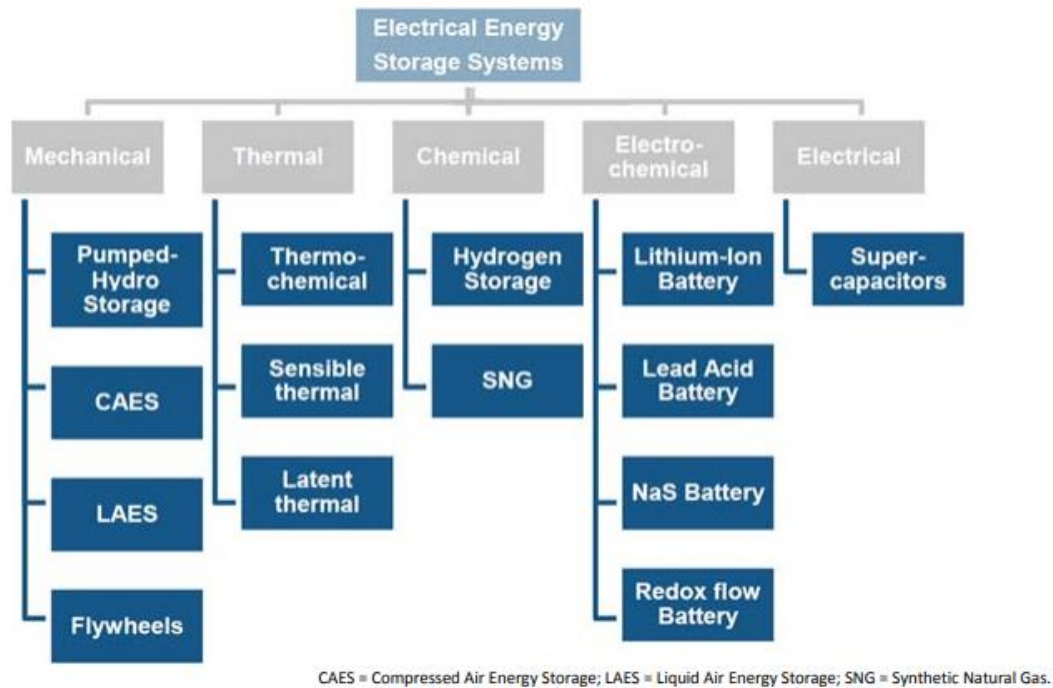
Figure 4. Energy storage types classification [4].

Currently, global energy storage installations are around 210 GW with Pumped Hydro taking ~185 GW and the rest being mechanical ~2.6 GW, batteries ~2.6 GW, and thermal estimated at ~14 GW. Up to date, batteries dominate the energy storage research & development, although their installations account for a small portion compared with thermal and mechanical storage technologies [6]. Whilst batteries have been used for energy storage since the 19th century, mostly in the automotive industry. TES, particularly sensible heat storage, is a much older technology that has found large scale applications for over 200 years e.g. hot stove in blast furnace/ironmaking processes (well before the industrial revolution), for space heating and hot water supply. Battery research, as a hot topic, has been driven mainly by consumer electronics and, more recently, by electric vehicles. A survey of the recent publications on Scopus shows [7] around sixty thousand on batteries over the last fifty years with most of them published before 2017, but some eleven thousand documents on thermal energy storage [8] over the last thirty years with 70% of them from the last 5 years. There is a clear surge in the

thermal energy storage publications over the last few years. While electric batteries are gradually dropping their publications rate per year (9,596 in 2017, 4545 in 2018 and 2,129 in 2019), thermal energy storage is riding the high accounting with their highest publication rate ever.

3.2.1 THERMAL ENERGY STORAGE

Thermal energy (heat) accounts for more than 50% of total energy consumption in terms of end-use with half-consumed in industry, 46% for space/water heating and cooking, and the remainder in agriculture [9]. More than 50% of the overall heat demand can be classified as low-grade (30 °C to 250 °C). Clearly, heating is one of the greatest challenges for decarbonising our energy systems; it is high time for the TES to be seriously considered as an option for increasing dispatchability (peak load shifting), and for inter-seasonal storage, which is likely to play a key role in the future full renewable scenarios.

The benefits that TES can provide vary between energy systems, and likely future evolutions in those systems, particularly concerning variable renewable deployment and the electrification of heat and transport demand (see Figure 5). (1) Variable supply integration; Thermal storage can be used to regulate the outputs from variable energy sources. This is sometimes referred to as capacity firming. Thermal storage is best suited to deliver energy balancing and demand shifting across minutes and hours both from technical and commercial perspectives. (2) Sector coupling; TES can help reduce curtailment and improve renewable utilisation through enabling sector coupling. This refers to linking power generation to demands in other sectors such as heat by converting excess power to heat, significantly increasing the flexibility of the energy system, which helps to improve the potential of strategies such as the power to heat (which already improves renewable integration) and so facilitate whole systems approaches. (3) Demand shifting; Energy demand can be shifted in time using thermal storage

to better match variable energy supply and reduce system strain. This is also a critical enabler to efficient sector coupling which otherwise would require a significantly increased overall capacity to meet the same demand. (4) Load shifting not only helps to improve the utilisation of renewables and allows renewables to meet a higher share of demand but also helps defer or avoid the need for costly electricity network reinforcement. (5) Seasonal storage; Thermal storage can store energy for days or even months to help address seasonal variability in supply and demand. This is of particular benefit to energy systems in regions that have a significant difference in thermal loads between seasons. Surplus heat produced with renewables in the summer can be stored in TES, and then be used to meet winter heating demand.
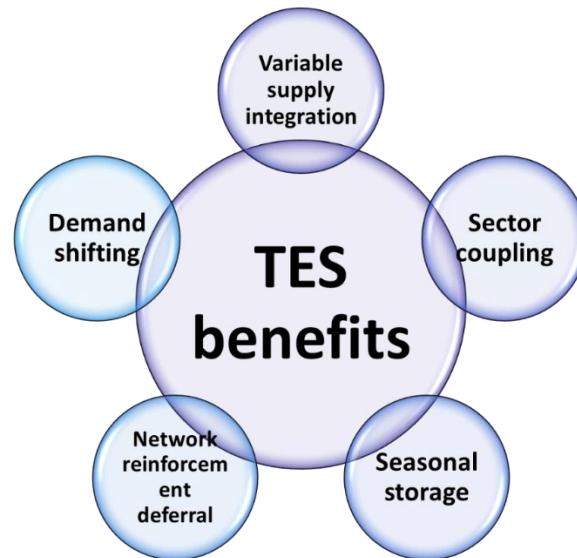
Figure 5. Key system benefits of integrating TES solutions.

TES has been commonly classified into three technology categories of sensible, latent and thermochemical storage (see Table 1). While sensible heat storage has been in large-scale industrial applications; latent heat-based TES has just started to be implemented in industry, whereas thermochemical based is currently at a very low technology readiness level (TRL) [10]. Significant research efforts are needed to address some fundamental challenges such as heat and mass transfer limitations, difficulties in the temperature control during the

charge/discharge processes, life span and cost-effectiveness. These fundamental challenges are holding back and slowing down TES deployment, which is translated on the stagnation of the technology. A clear example of this is the thermochemical storage, which even though having the highest storage capacity within the TES systems (see Table 1), has been under research for 40 years being unable to move the technology readiness level further than "proof of concept" (TRL 3). Research has been carried out but with not enough innovation to unblock the situation and reach the market demands.

Table 1. Thermal energy storage conventional technologies [11–13]

SENSIBLE HEAT

$$E = m \cdot C_p \cdot \Delta T$$

(Graph: Temperature (°C) vs Energy stored (J); T_f, T_{in}, E_{in}, E_f, SENSIBLE region)

Sensible heat storage (STES)

Mechanism: energy is stored by changing the temperature of the storage medium (heating/cooling). The storage material stores/releases heat proportional to its specific heat capacity and density within the working temperature range.

Classification: sensible materials can be classified depending on their phase state into liquids (water, oil, molten salts) or solids (pebbles, concrete, sand, etc.).

Key attributes: low-cost, low complexity system, commercially available, long lifetime, large storage volume and reliability.

LATENT HEAT

$$E = m \cdot \Delta H_L$$

(Graph: Temperature (°C) vs Energy stored (J); T_f, T_L, T_{in}, E_{in}, E_{L_1}, E_{L_2}, E_f; SENSIBLE, LATENT Phase 1 – Phase 2 regions)

Latent heat storage (LTES)

Mechanism: the material stores energy and releases/absorbs the stored energy when the phase change occurs at a fixed temperature (latent heat). The phase change can be solid-solid, solid-viscous, solid-liquid, liquid-gas and solid-gas. Being the first three the most studied.

(Charging)

Phase 1 ⟶ Phase 2 (storing)

(Discharging)
⟵

Key attributes: moderate cost, medium storage density, narrow temperature application, commercially available, corrosion problems, low thermal conductivity, subcooling and limited lifetime.

Classification: These materials are classified as organics (1), inorganics (2) and eutectics (3), which are mixtures of the abovementioned.

THERMOCHEMICAL HEAT

$$E = n \cdot \Delta H_R$$

(Graph: Temperature (°C) vs Energy stored (J); T_f, T_{R_2}, T_{R_1}, T_{in}, E_{in}, E_{R_1}, E_{R_2}, E_f; SENSIBLE, THERMOCHEMICAL Sorption/Forward reaction, Desorption/Backward reaction regions)

Thermochemical energy storage (TCS)

Mechanism: thermochemical TES materials are based on a reversible process that absorbs and releases energy by means of a chemical reaction exothermic/endothermic.

Charging: $C + heat \rightleftharpoons A + B$

Storing: A and B stored separately (no heat losses)

Discharging: $A + B \rightleftharpoons C + heat$

Substance A can be a hydroxide, hydrate, carbonate or ammoniate, etc. B can be water, CO, ammonia, hydrogen, etc. Usually, C is a solid or a liquid and A and B can be any phase.

Key attributes: high-cost, high complexity, high storage density, chemical stability, low commercial availability, long storage periods and highly compact storage.

Classification: The TCM are classified into two main groups: (1) thermochemical without sorption; (2) sorption energy storage. The sorption energy storage group has four sub-groups: (a) chemical reaction; (b) solid adsorption; (c) liquid absorption; (d) composite materials.

3.2.1.1 LIMITATIONS OF CURRENT TES TECHNOLOGIES

The current limitations for TES technologies are described in this section, the key attributes for the most deployed technologies are shown in Table 2. This section aims to offer an overview of each technology for later understanding the novel system presented in this thesis.

Thermochemical TES has been reported as the highest thermal energy storage density media (typically 0.5-3 $GJ \cdot m^{-3}$) [11] with a process involving almost no energy losses during the storage period, which is suitable for short and long-term storage. When it comes to practical application, the challenges of thermochemical storage mainly involve its structure stability at material and device level to achieve optimal heat and mass transfer as well as high reactions conversion rate. Materialwise, this technology is very dependent on any change in the storage media such as agglomeration, volume expansion, deliquescence (formation of a saturated solution), chemical and physical degradation. Researchers have tackled these challenges by introducing a porous (from nano- to micro-sized) solid matrix, which can contain the TCM ensuring a stable structure over cycles [14–16], 'salt inside porous matrix' (CSPM). The composite materials mainly consist of active storage material (e.g. MgSO4/CaCl2/LiBr) and a supporting matrix, which can either provide sorption heat (e.g. Silica gel/zeolites) or can retain larger amounts of salt but does not participate in the sorption process (e.g. graphite, magnesium oxide) [17]. These composites have been reported to improve thermal stability and heat and mass transfer, allowing to withstand larger thermal cycles. However, the utilization of a matrix also brings in new dilemmas: the compromise between large and pore size, the improved thermal stability at the expenses of the energy density decrease and the increase of the production cost [18]. Even though impregnation is the most reported method, researchers have also approached other methods such as microencapsulation with different polymeric shell [19,20], which showed good thermal behaviour and reliable cycling properties although

increasing the complexity of the manufacturing process. Other commercialised alternatives are nanocoating of the TCM with hydrophobic nanoparticles to improve material compatibility and provides a long-term service [21].

Latent heat TES has a moderate energy density among the TES technologies (typically 0.3-0.5 GJ·m^{-3}) [11], allowing relatively small and cost-effective storage systems. The main limitations are related to low thermal conductivity, volume expansion of the storage media (when phase change takes place), corrosion compatibility issues, material reliability in working conditions (subcooling, phase segregation, material stability). These problems led to heat transfer enhancement strategies and the need for finding compatible material containers to hold the phase change [22]. To solve those handicaps, researchers have followed different approaches such as encapsulating the PCM into a polymeric or ceramic shell [23–25], embedding the PCM into a metallic foam [26–28], ceramic or polymeric supporting structures [29–33] and the addition of high thermal conductivity particles with different configurations and particle sizes [34–37]. Despite these solutions provided an enhanced heat transfer capacity while containing the material during the phase change, sometimes they also increased the new material's cost and, in some cases, the material compatibility was still a problem.

Sensible heat TES is the technology that requires the highest storage volume because of its low energy density (0.2 GJ·m^{-3}), which also faces significant heat losses when working at wide temperature ranges [11]. Despite that, its system simplicity, low cost and reliability made it the more deployed TES technology for years. The most popular and commercial heat storage medium is water and has been widely used in residential and industrial applications [11]. Sensible heat maturity led to little innovations in the sector, given it covered the demand requirements. The main appeal of this technology is the low maintenance and installation; if innovating means increasing the cost then other options might appear to be more attractive.

Table 2. Typical parameters of TES systems [38–40]

Type of TES	TES technology	Range of capacities	Range of power	Operating temperature	Round-trip efficiency	Storage period	Energy density (kWh/m³)	Lifetime (years or # of cycles)
Sensible	Water Tank thermal energy storage	kWh to 100 MWh	kW to 10 MW	10 to 90 °C	50 to 90%	Hours to months	15-80	15-40 years
	Underground thermal energy storage	1 to GWh	MW to 100MW	5 to 95 °C	up to 90%	Weeks to months	25-85	50 years
	Solid-state	10 kWh to GWh	kW to 100MW	-160 to 1300 °C	>90%	Hours to months	0.4-0.9 kWh/m³.K (heat capacity)	>5000 cycles
	Molten salts	MWh to 5GWh	100kW to 300MW	265 to 565 °C[c]	>98%	Hours to days	70-200	>20 years
Latent	Ice thermal energy storage	kWh to 100 MWh	kW to 10MW	-3 to 3 °C	>95%	Hours to days	92	>20 years
	Sub-zero temperature PCMs	kWh to 100 kWh	kW to 10kW	down to -114 °C	>90%	Hours	30-85	>20 years
	Low temperature PCMs	kWh to 100 kWh	kW to 10kW	up to 120 °C	>90%	Hours	56-60	300-3000 cycles
	High temperature cPCMs	10 kWh to GWh	10 kW to 100 MW	up to 1000 °C	>90%	Hours to days	30-85	>5000 cycles
Thermo-chemical	Chemical looping (calcium looping)	MWh to 100 MWh	10 kW to 1 MW	500 to 900 °C	45-63%	Months	800-1200	>30 years
	Salt hidrates (solid adsorption)	10 kWh to 100 kWh	n/a	30 to 200 °C	50% (open systems) 60% (closed systems)	Months	200-350	20 years
	Absorption Systems	10 kWh to 100 kWh	10 kW to 1 MW	5 to 165 °C	COP: 0.7-1.7	Hours to days	180-310	50 years

3.2.1.2 PERSPECTIVE OF THERMAL ENERGY STORAGE

In this section, a brief perspective of TES potential pathways is presented. Looking into the future, hybrid systems stand up as a bright alternative allowing to mismatch challenges and benefits of each technology to push TES systems forward. Until now, hybrid systems have been based on the combination of sensible heat storage/latent heat storage, sensible heat storage/ thermochemical storage, and cascade systems. Latent and sensible heat-based systems [41–44] aim to decrease the volume of the sensible heat by adding a percentage of energy stored in latent heat form. In that manner, the capacity of the system is increased, and a stable output

temperature can be achieved. Cascade system has been integrated for latent heat storage [45–47] and thermochemical storage [48–50] using different materials to store heat at different energy levels. The bright side of those systems is a wider operational range and the ability to deliver energy at different output temperatures. Thermochemical is summed up to sensible heat-based systems [51] to enhance sensible heat performance by reducing its volume and allowing a constant discharging temperature.

In the search for a thermal energy storage technology that could cover the actual gap between TES technology and industry, this thesis introduces a novel concept based on the combination of sensible heat, latent heat and thermochemical based TES. This combination has the potential to integrate the three known thermal storage methods in one system maximising the operational energy density while maintaining the controllability of the charge/discharge processes and enhancing the efficiency at the system level. This will be explained and proposed in detail in this thesis.

3.3 REFERENCES

[1]   International Energy Agency. WEO 2017. IEA World Energy Outlook 2017. doi:10.1787/weo-2017-en.

[2]   IRENA. Global Energy Transformation: A roadmap to 2050. Abu Dhabi: 2018.

[3]   European Comission. EU Reference Scenario 2016. 2016. doi:10.2833/9127.

[4]   European Commission. Energy storage-the role of electricity. Brussels: 2017.

[5]   Guney MS, Tepe Y. Classification and assessment of energy storage systems 2017;75:1187–97. doi:10.1016/j.rser.2016.11.102.

[6]   Dunn B, Kamath H, Tarascon JM. Electrical energy storage for the grid: A battery of choices. Science (80-) 2011;334:928–35. doi:10.1126/science.1212741.

[7]   Scopus   data   based   n.d.
        https://www.scopus.com/term/analyzer.uri?sid=481cd47e95109f8ff702d116971b405d
        &origin=resultslist&src=s&s=TITLE-ABS-KEY%28%22electric+batteries%22%29&sort=plf-
        f&sdt=b&sot=b&sl=35&count=60654&analyzeResults=Analyze+results&txGid=950fcd83
        cc0c9d84bd58735e62fb (accessed February 14, 2020).

[8]   Scopus   data   based   n.d.
        https://www.scopus.com/results/results.uri?numberOfFields=0&src=s&clickedLink=&e
        dit=t&editSaveSearch=&origin=searchbasic&authorTab=&affiliationTab=&advancedTab
        =&scint=1&menu=search&tablin=&searchterm1=%22Thermal+energy+storage%22&fiel
        d1=TITLE_ABS_KEY&date (accessed February 14, 2020).

[9]   IEA. Renewables 2019 – Analysis - IEA. Int Energy Agency 2019.

[10]   EASE/EERA. European Energy Storage Technology Development Roadmap 2017 Update.
        2017.

[11]   Abedin A, Rosen M, Choi JC, Kim SD, Eindhoven TU, Habashy GM, et al. A Critical Review
        of Thermochemical Energy Storage Systems. Open Renew Energy J 2011;4:42–6.
        doi:10.2174/1876387101004010042.

[12]   Abhat A. Low temperature latent heat thermal energy storage: Heat storage materials.
        Sol Energy 1983;30:313–32. doi:10.1016/0038-092X(83)90186-X.

[13]   Avghad SN, Keche AJ, Kousal A. Thermal Energy Storage : A Review. IOSR- J Mech Civ Eng
        2016;13:72–7. doi:10.9790/1684-1303027277.

[14]   Casey SP, Aydin D, Elvins J, Riffat S. Salt impregnated desiccant matrices for "open"
        thermochemical energy conversion and storage – Improving energy density utilisation
        through hygrodynamic & thermodynamic reactor design. Energy Convers Manag
        2017;142:426–40. doi:10.1016/j.enconman.2017.03.066.

[15] Korhammer K, Druske MM, Fopah-Lele A, Rammelberg HU, Wegscheider N, Opel O, et al. Sorption and thermal characterization of composite materials based on chlorides for thermal energy storage. Appl Energy 2016;162:1462–72. doi:10.1016/j.apenergy.2015.08.037.

[16] Courbon E, D'Ans P, Permyakova A, Skrylnyk O, Steunou N, Degrez M, et al. A new composite sorbent based on SrBr2and silica gel for solar energy storage application with high energy storage density and stability. Appl Energy 2017;190:1184–94. doi:10.1016/j.apenergy.2017.01.041.

[17] Scapino L, Zondag HA, Van Bael J, Diriken J, Rindt CCM. Sorption heat storage for long-term low-temperature applications: A review on the advancements at material and prototype scale. Appl Energy 2017;190:920–48. doi:10.1016/j.apenergy.2016.12.148.

[18] Scapino L, Zondag HA, Van Bael J, Diriken J, Rindt CCM. Energy density and storage capacity cost comparison of conceptual solid and liquid sorption seasonal heat storage systems for low-temperature space heating. Renew Sustain Energy Rev 2017;76:1314–31. doi:10.1016/j.rser.2017.03.101.

[19] Gaeini M, Rouws AL, Salari JWO, Zondag HA, Rindt CCM. Characterization of microencapsulated and impregnated porous host materials based on calcium chloride for thermochemical energy storage. Appl Energy 2018;212:1165–77. doi:10.1016/j.apenergy.2017.12.131.

[20] Cuypers R, de Jong AJ, Eversdijk J, Van 't Spijker H, Oversloot H, Ingenhut BLJ, et al. Microencapsulation of Salts for Enhanced Thermochemical Storage Materials n.d.:2–3.

[21] Göran Bolin T (SE); D, Glebov K (SE). Salt coated with nanoparticles. US 9.459,026 B2, 2016.

[22] Pielichowska K, Pielichowski K. Phase change materials for thermal energy storage. Prog

Mater Sci 2014;65. doi:10.1016/j.pmatsci.2014.03.005.

[23]   Gondora W, Doudin K, Nowakowski DJ, Xiao B, Ding Y, Bridgwater T, et al. Encapsulation of phase change materials using rice-husk-char. Appl Energy 2016;182:274–81. doi:10.1016/j.apenergy.2016.08.102.

[24]   Zhang H, Wang X, Wu D. Silica encapsulation of n-octadecane via sol-gel process: A novel microencapsulated phase-change material with enhanced thermal conductivity and performance. J Colloid Interface Sci 2010;343. doi:10.1016/j.jcis.2009.11.036.

[25]   Schossig P, Henning HM, Gschwander S, Haussmann T. Micro-encapsulated phase-change materials integrated into construction materials. Sol Energy Mater Sol Cells 2005;89:297–306. doi:10.1016/j.solmat.2005.01.017.

[26]   Zhang G, Li J, Chen Y, Xiang H, Ma B, Xu Z, et al. Encapsulation of copper-based phase change materials for high temperature thermal energy storage. Sol Energy Mater Sol Cells 2014;128:131–7. doi:10.1016/j.solmat.2014.05.012.

[27]   Du Y, Ding Y. Towards improving charge/discharge rate of latent heat thermal energy storage (LHTES) by embedding metal foams in phase change materials (PCMs) 2016;108:181–8. doi:10.1016/j.cep.2016.08.003.

[28]   Zheng H, Wang C, Liu Q, Tian Z, Fan X. Thermal performance of copper foam/paraffin composite phase change material. Energy Convers Manag 2018;157:372–81. doi:10.1016/j.enconman.2017.12.023.

[29]   Zhou M, Lin T, Huang F, Zhong Y, Wang Z, Tang Y, et al. Highly conductive porous graphene/ceramic composites for heat transfer and thermal energy storage. Adv Funct Mater 2013. doi:10.1002/adfm.201202638.

[30]   Zhang P, Hu Y, Song L, Ni J, Xing W, Wang J. Effect of expanded graphite on properties of high-density polyethylene/paraffin composite with intumescent flame retardant as a

shape-stabilized phase change material. Sol Energy Mater Sol Cells 2010;94:360–5. doi:10.1016/j.solmat.2009.10.014.

[31]   Zhang Y, Ding J, Wang X, Yang R, Lin K. Influence of additives on thermal conductivity of shape-stabilized phase change material. Sol Energy Mater Sol Cells 2006;90:1692–702. doi:10.1016/j.solmat.2005.09.007.

[32]   Li R, Zhou Y, Duan X. A novel composite phase change material with paraffin wax in tailings porous ceramics. Appl Therm Eng 2019;151:115–23. doi:10.1016/j.applthermaleng.2019.01.104.

[33]   Ruiping L, Fang Z, Weiming S, Huiyou Z, Wang C. Impregnation of porous mullite with Na2SO4 phase change material for thermal energy storage. Sol Energy Mater Sol Cells 2015;134:268–74. doi:10.1016/j.matchemphys.2009.02.045.

[34]   Shin D, Banerjee D. Enhancement of specific heat capacity of high-temperature silica-nanofluids synthesized in alkali chloride salt eutectics for solar thermal-energy storage applications. Int J Heat Mass Transf 2011;54:1064–70. doi:10.1016/j.ijheatmasstransfer.2010.11.017.

[35]   Xiao X, Zhang P, Li M. Thermal characterization of nitrates and nitrates/expanded graphite mixture phase change materials for solar energy storage. Energy Convers Manag 2013. doi:10.1016/j.enconman.2013.04.007.

[36]   Kean TH, Sidik NAC, Kaur J. Numerical investigation on melting of Phase Change Material (PCM) dispersed with various nanoparticles inside a square enclosure. IOP Conf. Ser. Mater. Sci. Eng., vol. 469, 2019. doi:10.1088/1757-899X/469/1/012034.

[37]   Kant K, Shukla A, Sharma A, Henry Biwole P. Heat transfer study of phase change materials with graphene nano particle for thermal energy storage. Sol Energy 2017;146:453–63. doi:10.1016/j.solener.2017.03.013.

[38]   Abedin A, Rosen M. A Critical Review of Thermochemical Energy Storage Systems. Open Renew Energy J 2011;4:42–6. doi:10.2174/1876387101004010042.

[39]   Sarbu I, Sebarchievici C. A comprehensive review of thermal energy storage. Sustain 2018;10. doi:10.3390/su10010191.

[40]   Pelay U, Luo L, Fan Y, Stitou D, Rood M. Thermal energy storage systems for concentrated solar power plants. Renew Sustain Energy Rev 2017;79:82–100. doi:10.1016/j.rser.2017.03.139.

[41]   Walter H, Mörzinger B, Hofmann R, Hengstberger F, Zauner C. Experimental characterization and simulation of a hybrid sensible-latent heat storage. Appl Energy 2016;189:506–19. doi:10.1016/j.apenergy.2016.12.079.

[42]   Frazzica A, Manzan M, Sapienza A, Freni A, Toniato G, Restuccia G. Experimental testing of a hybrid sensible-latent heat storage system for domestic hot water applications. Appl Energy 2016;183:1157–67. doi:10.1016/j.apenergy.2016.09.076.

[43]   Dabiri S, Mehrpooya M, Nezhad EG. Latent and sensible heat analysis of PCM incorporated in a brick for cold and hot climatic conditions, utilizing computational fluid dynamics. Energy 2018;159:160–71. doi:10.1016/j.energy.2018.06.074.

[44]   Ahmed N, Elfeky KE, Qaisrani MA, Wang QW. Numerical characterization of thermocline behaviour of combined sensible-latent heat storage tank using brick manganese rod structure impregnated with PCM capsules. Sol Energy 2019;180:243–56. doi:10.1016/j.solener.2019.01.001.

[45]   Sergeev D, Bruno F, Bayon A, Müller M, Grigore M, Liu M. Novel solid–solid phase-change cascade systems for high-temperature thermal energy storage. Sol Energy 2018;177:274–83. doi:10.1016/j.solener.2018.10.085.

[46]   Chirino H, Xu B, Xu X. Parametric study of cascade latent heat thermal energy storage

(CLHTES) system in Concentrated Solar Power (CSP) plants. J Energy Inst 2018. doi:10.1016/j.joei.2018.03.007.

[47]   Michels H, Pitz-Paal R. Cascaded latent heat storage for parabolic trough solar power plants. Sol Energy 2007;81:829–37. doi:10.1016/j.solener.2006.09.008.

[48]   Cabeza LF, Solé A, Fontanet X, Barreneche C, Jové A, Gallas M, et al. Thermochemical energy storage by consecutive reactions for higher efficient concentrated solar power plants (CSP): Proof of concept. Appl Energy 2017;185:836–45. doi:10.1016/j.apenergy.2016.10.093.

[49]   N'Tsoukpoe KE, Mazet N, Neveu P. The concept of cascade thermochemical storage based on multimaterial system for household applications. Energy Build 2016;129:138–49. doi:10.1016/j.enbuild.2016.07.047.

[50]   N'Tsoukpoe KE, Osterland T, Opel O, Ruck WKL. Cascade thermochemical storage with internal condensation heat recovery for better energy and exergy efficiencies. Appl Energy 2016;181:562–74. doi:10.1016/j.apenergy.2016.08.089.

[51]   Ströhle S, Haselbacher A, Jovanovic ZR, Steinfeld A. Upgrading sensible-heat storage with a thermochemical storage section operated at variable pressure: An effective way toward active control of the heat-transfer fluid outflow temperature. Appl Energy 2017;196:51–61. doi:10.1016/j.apenergy.2017.03.125.

4

TCS OUTLOOK: STATE-OF-THE-ART
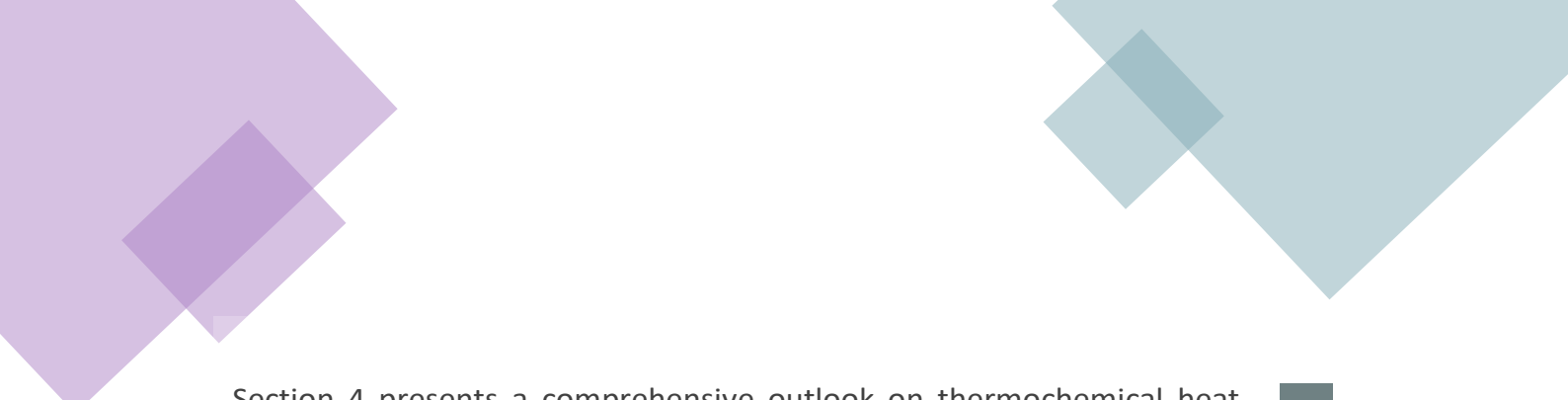
6. Hybrid TES system:

3 in 1 concept

5. Targets and structure of the thesis

4. TCS Outlook

3. Introduction

2. Scientific contributions

1. Thesis timeline

Section 4 presents a comprehensive outlook on thermochemical heat technology, where the basis of the technology are defined, a classification of reversible reactions and sorption system is described and the relevant storage media are reviewed from a material perspective. To understand the key attributes of this store, the main properties of the thermochemical storage are defined at different development levels. To wrap up, the manufacturing routes are also reported by highlighting the current commercial state and the future trends to manufacture thermochemical storage media.

12. Conclusions and achievements

11. Potential applications and prospective

10. Proof of concept and scale-up

9. Working pairs

8. Material screening and selection

7. Bench study specifications

4. TCS OUTLOOK: STATE-OF-THE-ART

4.1 THERMOCHEMICAL STORAGE PRINCIPLE AND CLASSIFICATION

Thermochemical storage (TCS) materials store thermal energy through the heat effect of reversible chemical reactions and/or sorption/desorption processes. The principle of TCS is illustrated by the following processes:

(1) Charging: With heat supply, the TCM (C) can be dissociated into components A and B, which is an endothermic process.

$$C + heat \rightleftharpoons A + B$$
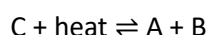
(2) Storing: A and B are then stored separately after charging with no energy loss.

(3) Discharging: energy is released through an exothermic reaction, where material A and B are combined. C is regenerated and can be reused during cycling.

$$A + B \rightleftharpoons C + heat$$
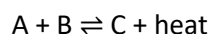
where A, B and C are reactants or products depending on the charge or discharge processes. Examples of A include hydroxide, hydrate, carbonate and ammoniated; and examples of B include water, CO, ammonia, and hydrogen. C can be in solid or a liquid form and A and B can be any phase.

Besides, thermochemical energy storage materials also undergo a phase change (melting) when conversing from low to high hydrates (discharging), if this is high enough to enable storage, the latent heat from the melting can be also used as phase change material. Both mechanisms are illustrated in Figure 6. At the same time, thermochemical materials store heat in the sensible heat form.
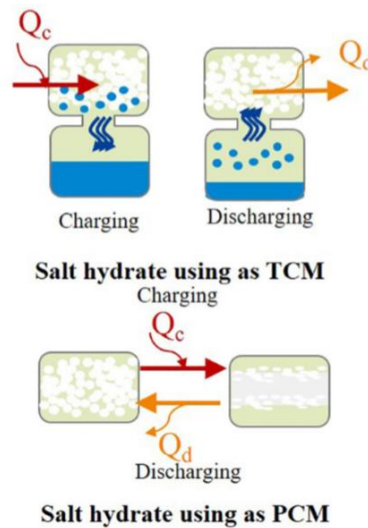
Figure 6. The working temperature of salt hydrate as PCM or TCM [1].

TCS fall broadly into two main groups of a reversible chemical reaction (strictly thermochemical storage without sorption) and sorption energy storage [2], see Figure 7. This thesis classifies thermochemical storage systems into reversible reactions and sorption-based TCS. The two categories are further discussed in the following sections.
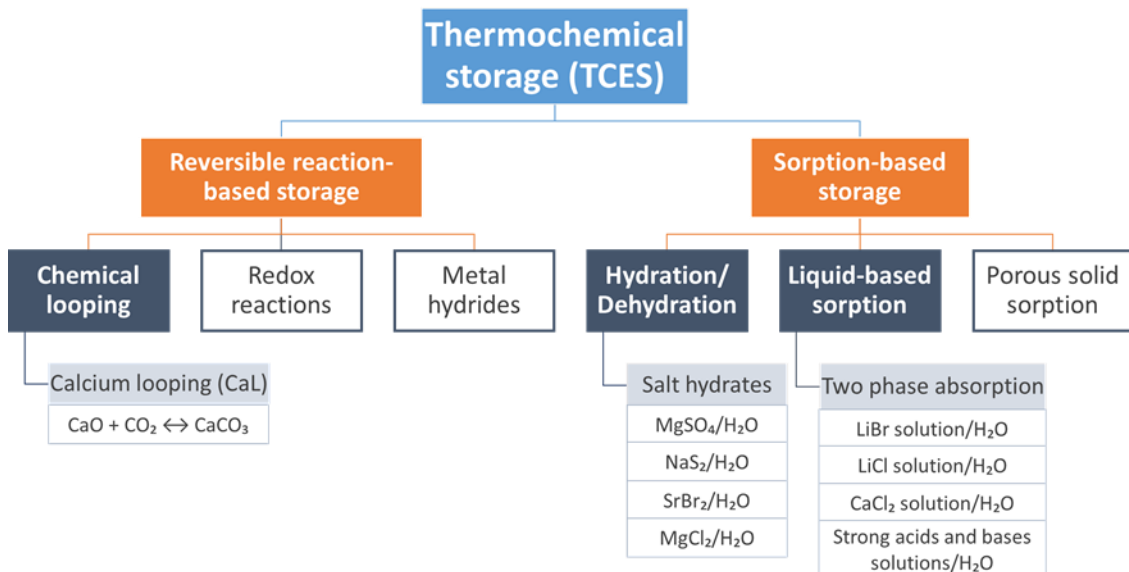
Figure 7. Thermochemical storage methods and materials adapted from [3–5].

<div style="border:1px solid;">

4.1.1 SORPTION-BASED TCS

</div>

Sorption-based TCS store heat by breaking the binding forces such as Van der Waals forces or covalent forces, between a sorbent and a sorbate [6]. The heat required to break the binding forces can be higher than that associated with the evaporation heat of a pure sorbate (e.g. water). Sorption based systems are classified in for sub-groups: (1) solid adsorption, (2) liquid absorption, (3) chemical reactions and (4) composites [7].

(1) Solid adsorption

Adsorption systems commonly involve either solid/liquid or solid/gas, storing energy by the adsorption of a sorbent (normally water) on the surface of a porous material. Zeolites, silica gel and Metal-organic frameworks (MOF's) are the most common solid adsorbents. Silica gel/H_2O offers a wide range of specific surface typically from 750 to 850 (m^2/g) [8]. Silica gel is also widely used due to its hydrophilic properties. However, experiments have shown that when the materials were mixed with water as salt solutions, after several cycles the silica gel particles would turn into powders [9]. Zeolite is also a well-known solid sorption material investigated by previous researchers [10–12]. The most common types being researched are faujasite (FAU framework type), zeolite A (LTA framework type) and Zeolite 13X for both heating and cooling application. In general, zeolites are more hydrophilic than silica with the rate of water uptake of 0.3 kg per kg of materials. Due to porosity of the adsorption materials, common materials such as clays (vermiculite, pillar layered silica), silica gels, zeolites, carbon fibre, etc., are often used as the host matrices to provide the composite structure of chemical reaction material.

(2) Chemical Reaction

The most studied chemical reactions include $MgSO_4 + 7H_2O = MgSO_4 \cdot 7H_2O$; $SrBr_2 + 6H_2O = SrBr_2 \cdot 6H_2O$; $Na_2S + 9H_2O = Na_2S \cdot 9H_2O$; and $MgCl_2 + 6H_2O = MgCl_2 \cdot 6H_2O$. Magnesium sulphate has one of the highest energy densities [13] and hence has been widely studied for seasonal storage [14–16]. However, the use of magnesium sulphate is difficult in a storage reactor

because of the formation of agglomerates during dehydration/hydration cycles, leading to mass transfer, structural stability and reversibility issues [17]. Strontium bromide, on the other another hand, has a lower energy density but experiences less of the reversibility issue [18]. It has therefore been well investigated at both laboratory and prototype scales for various applications including solar cooling and heat storage in a closed process [19] and seasonal storage of solar energy in an open process [20,21]. Calcium chloride and magnesium chloride have a high energy density and work well in a favourable operational temperature range, but thermal decomposition, HCl formation and deliquescence bellow 40 °C make them difficult to use in practical applications. The most outstanding chemical reaction materials will be later reviewed in Section 8.

(3) Liquid absorption

Liquid-gas systems, also called absorption systems, are promising storage options because they can be pumped and used as the working heat transfer fluid. In these systems, the energy is stored by the concentration changes in a solution (strong and weak). Absorption systems are based on the principle of a concentrated solution refrigerant (e.g. aqueous solutions of Calcium Chloride ($CaCl_2$), Lithium Chloride (LiCl), Lithium Bromide (LiBr), Sodium Hydroxide (NaOH), Potassium Hydroxide (KOH) and Ammonia [22]) absorbing water and releasing heat in the process. The energy storage is due to the heat of sorption, which is the energy released when water vapour is sorbed into the volume of a liquid. The system is charged through the addition of heat, causing water molecules to desorb from the refrigerant solution and forming two products: water vapour and a more concentrated solution of refrigerant. These products can then be separated, and when the heat is required they have combined again. Absorption systems are a promising storage option because energy storage densities greatly exceed the storage density provided by water as a sensible storage technology. This is primarily because the

absorption cycle is more suitable for low-grade heat utilization, making them potentially useful for buildings and certain industrial applications.

4.2.1 REVERSIBLE CHEMICAL REACTION BASED TCS

Reversible chemical reaction based TCS relies on endothermic (heat is stored) and exothermic (heat is released) processes of the reaction. Thermochemical systems commonly require higher temperatures to initiate the energy storage, but conversely, provide higher temperatures on the release of that energy. Such reactions are also known as high-temperature TCS reactions and are classified into three categories (see Figure 8); (1) solid-gas, (2) liquid-gas, and (3) gas-gas. The most relevant chemical processes for chemical energy storage are carbonates, redox reactions and metal hydrides [23], this is reviewed in the following.
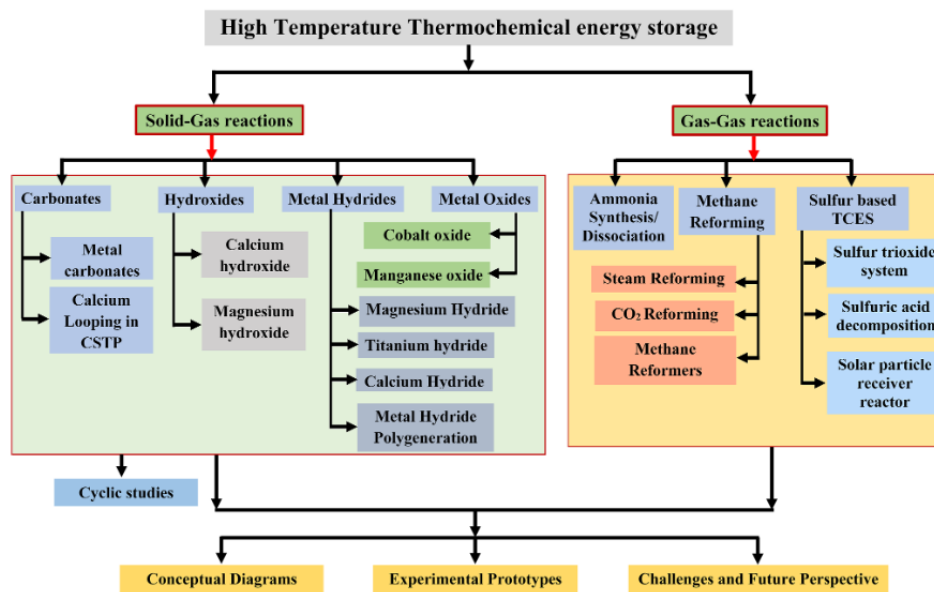
Figure 8. Reversible reaction classification reaction and current research status (below) [24]

(1) Chemical looping

Chemical looping is a technology that has been explored primarily as a potential carbon capture technology. A chemical looping technique which uses the reversible reaction between

carbon oxide (CaO) and calcium dioxide (CO_2) to form calcium carbonate ($CaCO_3$) is known as calcium looping (CaL). In this reaction, $CaCO_3$ is exposed to large amounts of heat, breaking it down into its constituent parts (CaO and CO_2), storing the energy that was provided by the heat in the chemical bonds within the CaO and CO_2 molecules. Both CaO and CO_2 are then stored separately, acting in effect as the energy storage media. Storage of the products could be prolonged to weeks or even months, depending on the conditions and energy demand, with no energy loss. When energy is required, CaO and CO_2 are brought back together again to form $CaCO_3$, releasing heat in the process.

The advantages of such a system is that all materials involved are very low cost, and an extremely high energy density of 3.2 $GJ \cdot m^{-3}$ can be obtained [6]. However, the working temperatures involved are very high (>600 °C). Calcium looping is being explored as a potential technology for storing energy for concentrated solar plants but could also be considered for other high-temperature applications such as in industry or elsewhere in the power sector.

(2) Hydroxides

Reversible hydration/dehydration of metal oxides can be used as a high-temperature ($\sim$500 °C) thermal energy storage option at near atmospheric pressures. Sample reactions associated with charging and discharging processes can be the following, where M represents the concerned metal:

$MO_{(s)} + H_2O_{(v)} \rightarrow M(OH)_2 + \Delta H$

$M(OH)_2 + \Delta H \rightarrow MO_{(s)} + H_2O_{(v)}$
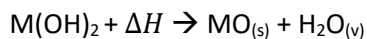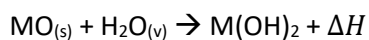
Such a reaction often has an operating temperature of ~250-600 °C. Calcium hydroxide and magnesium hydroxide, among others, are the most commonly studied in the literature, mainly for chemical heat pump, with a high volumetric energy density up to 600 $MJ \cdot m^{-3}$). $Ca(OH)_2$ has been regarded as more attractive than magnesium hydroxide because MgO is inert to hydration

in highly superheated steam and the reaction rate deteriorates with the rise of temperature [24]. $Ca(OH)_2$ based TCS works via $Ca(OH)_2 + 104.4 \text{ kJ/mol} = CaO + H_2O$ and can achieved 290 cycles with a conversion of 95% [25]. Criado et al. [26] found that the performance of the hydration process declined sharply when both hydration and dehydration occurred under a 100% water vapour environment. The feasibility of the $Ca(OH)_2$ - CaO system for TCS applications has also studied by examining the reversibility and cyclic stability [128-130]. Heat transfer can be a limiting factor in a TCS reactor, for that reason, the use of copper fins have been used to enhance heat transfer [29] [30], successfully achieving 20 cycles of operation.

(3) Metal hydride

Metal hydrides are materials containing metal or metalloid bonded to hydrogen. The principle of the use of a metallic hydride for TCS can be illustrated simply by a general expression of $MH_n + \Delta H_r = M + (n/2)H_2$, with M representing a metallic element in the d-block and f-block of the periodic table; H the hydrogen and ΔH_r the reaction enthalpy. A typical device for realising the metallic hydride based TCS consists of a TCS reactor, a hydrogen supply unit and control unit, a hydrogen store and a heat extraction/addition unit. Examples of metallic hydrides include MgH_2, TiH_2, CaH_2, LiH, Mg_2NiH_4, Mg_2FeH_6, Mg_2CoH_5, $NaMgH_3$ and $Ca(BH_4)_2$ [60-69]. Among these metallic hydrides, MgH_2 has attracted considerable attention due to its relatively high theoretical energy density (~2257 kJ/kg) with a hydrogen content of 7.7wt% and a reaction temperature of 250-500 °C [60-67]. More research is necessary to develop new MH materials (like complex hydrides) that can provide higher hydrogen storage capacity, faster reaction kinetics, better reversibility, and cyclic stability. Further, there is still scope for improving the reactor design to minimize the parasitic loss and to facilitate better heat transfer.

(4) Redox reactions

The principle of a redox-based TCS technology can be illustrated by a generalised reaction of $M_xO_y + \Delta H_r = M_xO_{y-z} + (z/2)O_2$, with M_xO_y being a metal oxide [115-116]. There are many potential redox pairs for the TCS, and examples include Co_3O_4/CoO, MnO_2/Mn_2O_3, CuO/Cu_2O,

Fe_2O_3/FeO, Mn_3O_4/MnO and V_2O_5/VO_2. These materials store/release thermal energy by absorbing/releasing oxygen at temperatures be-tween 350 °C and 1100 °C [34]. Among the pure metal oxides, only cobalt oxide, iron oxide, copper oxide, and manganese oxide show suitable reaction temperatures, re-action enthalpies, cycling stabilities, and material costs [35]. The Co_3O_4/CoO pair show feasibility for reducing and oxidizing cobalt oxide at around 900 °C during an on-sun period and lower temperatures during an off-sun period was tested. and has been studied by several groups [71-78]. Research is focused on developing more efficient materials (doped metal oxides, binary composites, and perovskites, etc.) [36] [37] and reactor designs (cordierite honeycomb coated with oxide, cascading of oxide systems, packed bed, fluidized bed, moving bed, etc.) to prove the potential of redox system as an efficient TES for future CSP plants. However, there is still scope for improving the materials performance and reactor design.

In this thesis, the focus is on the salt hydrates chemical reaction system, therefore from now on the TCS part will be mainly oriented to those systems.

4.3 TCS KEY ATTRIBUTES

To bring material from conceptualization to commercialization, relevant properties to the technology at every development stage should be identified. Such properties for sorption-based systems, have been widely detected in the available literature in the last decade [1,38–42]. TCS has found its way through tech feasibility and tech demo but has not been able to overcome the barriers to tech maturation (TRL 4-5). The technology is currently going back and forth from demonstration project and pilot-scale systems to feasibility studies at lab-scale, given there are still important challenges at a material level that must be addressed prior moving forward and parallelly along with system design tasks.

To select a suitable TCM for a certain application, a set of thermodynamic and non-thermodynamic factors should be evaluated to obtain a shortlist of candidates for the

experimental screening process. Those factors have been gathered from the literature and are briefly described in this section, for more information see the following references [38,40,43–46]. Properties related to a bed of salt powder (reactor level) although dependent to material attributes are also included in this section.   In Figure 9 the four technology stages from conceptualization (TRL 1) to commercial level (TRL 8-9) are linked to the relevant key attributes identified in the literature in a way that the properties are grouped by importance in accordance to the tech stage.
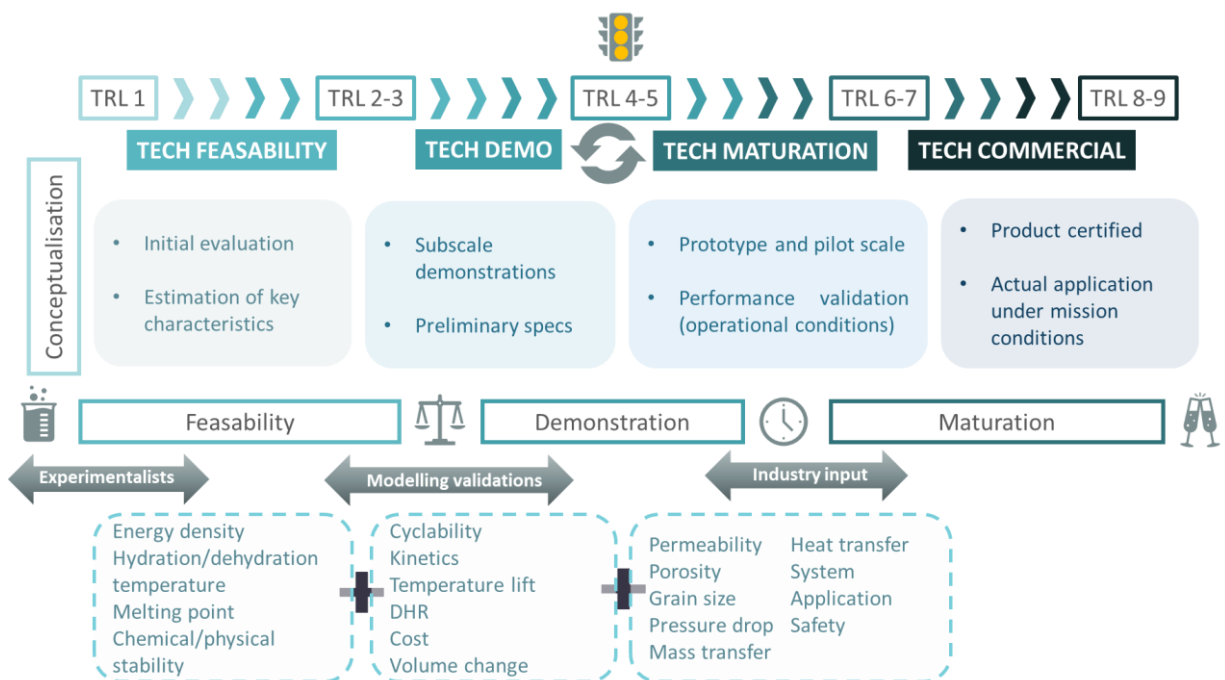
Figure 9. TCS research development chart linked to relevant properties at material and system level.

(1) Application (system): Salt hydrates can be implemented in closed or open systems either whether the system can have separate or integrated reactors. The open system consists of a working fluid (air) and a thermochemical material. Supplied thermal energy is transferred to a transport medium (air) and provides the energy necessary for desorption of the thermochemical material [47]. After a storing period, a discharging period occurs during which the energy stored is released for heating purposes. The closed system consists of a working fluid (e.g. water) and

a TCM (hydrated TCM), where the working fluid is separated from the heat transport fluid. Thermal energy from an external energy source provides the energy necessary for the TCM dissociation, which is transferred to a working fluid. This decision making will be dependent on the storage media selected e.g. materials that release toxic substances through sorption process should be implemented into a closed system. But also dependent on the application (e.g. temperature constraints), desired energy input/output, etc [48].

(2) Hydration/ dehydration temperature (regeneration temperature): hydration temperature is the lowest temperature that can be generated in a sorption reaction at a given vapour pressure and system conditions. While dehydration temperature determines the highest temperature that can be generated under certain conditions (pressure, temperature, etc.). The dehydration temperature can be set below the regeneration temperature that is defined as the temperature the sorbent has desorbed the maximum possible loading of adsorbate without causing degradation of the sorbents. Both hydration and dehydration temperature, are dependent to the material properties and especially crucial from an application point of view, as the hydration temperature limits the output temperature of the system, as it will determine whether the TCM is appropriate for domestic heating and, also for hot water supply, or industrial processes. Dehydration temperature should match the input energy of the system, which can come from solar collectors, waste heat, etc.

(3) Energy density: the heat storage system partially depends on the material energy density as well as on the system selection and reactor configuration (an open system will lead to a higher energy density.) However, the storage material limits the highest energy density achievable by the heat storage system regardless of the system selected (open or closed). Thus, the energy density is desired to be maximized to meet the energy density required at a reactor level.

(4) Melting point: Unlike pure salt or other ionic solids, the water within the hydrated salt crystal leads to the complex performances of melt and dehydration [1], which can limit the performance of the storage media given the solid hydrated salt will melt into molten hydrated salt under phase change temperature. Such melting can follow different melting behaviours: congruent melting (the dehydrated salt is completely soluble in the hydration water), incongruent melting (the salt is partially soluble in the hydration water), and semi-congruent melt (the liquid and solid are in equilibrium with different compositions for the hydrate transformation to a lower hydrated salt). This phenomenon should be carefully studied to understand the interaction between the chemical process (hydration/dehydration) and the physical process (latent heat), see Figure 6. In TCS, the melting point of a salt hydrate should be considered (preferably and when possible) to be higher than the dehydration temperature to ensure proper dehydration. In case the melting point takes place at a lower temperature (between hydration/dehydration), this might reduce the porosity of the system also reducing the vapour transport into the storage media.

(5) Volume change: the volume of the crystal structure varies during hydration/dehydration. Such volume variation is required to be minimal for the sake of the system design and storage media performance. When changing from lower to higher hydrates the crystal structure changes, these changes are not always heterogeneous. This heterogeneity leads to voids formation inside the grains, which changes the entire performance of the reactor changing the permeability, thermal conductivity and mechanical stability. This is an intrinsic attribute from the material but is dependent on particle size, porosity and, also, the shapeable method used. This property has not been extensively studied in the literature, theoretical values between the different density from the low to the high hydrate are normally taken for volume change calculation.

(6) Deliquescence vapour pressure (DHR): this phenomenon takes place above the hydration reaction, where the equilibrium humidity is surpassed and the salt absorbs water forming a higher hydration state (see Figure 10). When the vapour pressure of the system increases above the DHR, the water dissolves until the equilibrium is reached. For that reason, the system must work always under the DHR to avoid the salt to become a solution. If the relative humidity (RH) exceeds the deliquescence relative humidity (DRH), the salt absorbs water and dissolves. While at RH below DRH, the salt picks up water vapor and still in solid state as illustrated in the two following equations; Salt(s) H O(g) hydrated form(s) for RH + ↔ 2 < DRH (4) Salt(s) H O(g) solution(l) for RH DRH +↔ > 2 (5) [49]. The deliquescence is given by the following equation, where pH_2O_{salt} is the vapour pressure of an aqueous solution saturated with the salt or salt mixture of interest, and $pH_2O°$ is the vapour pressure of the pure water:

DHR= $pH_2O_{salt}/pH_2O°$ Equation 1
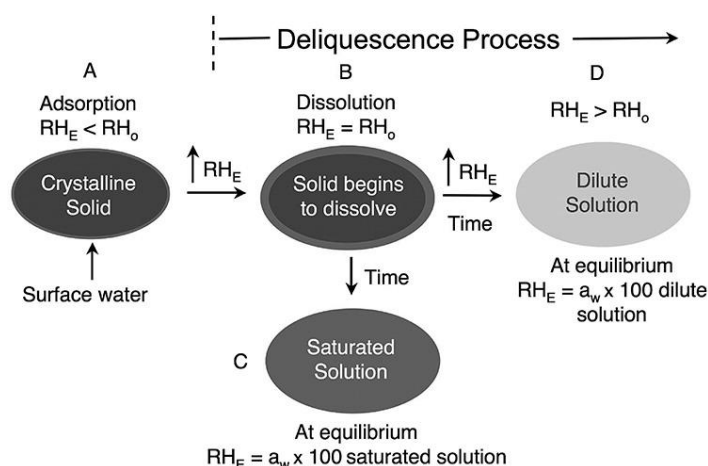
Figure 10. Schematic diagram of the interaction of a crystalline solid, with water vapour in the atmosphere at various relative humidity values, where RH_E = environmental relative humidity and RH_o = critical relative humidity [50].

Several methods have been described in the literature for determining the DHR, they are mainly classified into open and closed methods, dynamic and static methods, vapour and condensed phase methods.

(7) Chemically stability (safety): during the charging/discharging periods the storage material should not decompose into toxic, unstable, explosive or flammable compounds. This is directly linked to safety, which is an important aspect for the TCM selection, especially if the material will be implemented in the domestic sector or open systems. This property is directly related to the material nature, although it can be controlled and mitigated through the atmosphere and conditions used during the storage period.

(8) Cyclability (physical stability): The storage media should also have a service life about 15-20 years, while ideally during service the TCM should not decompose, agglomerates or transform into another specie. For that purpose, the sample must be cycled and the physical/chemical transformation during cycles should be studied to predict the behaviour of the material under operational conditions.

(9) Permeability and porosity: permeability in literature is defined as the ability of the fluid to flow through a material. Permeability is often related to porosity since they are directly related since the permeability of a material depends on the amount of pore-space or porosity of the material. Porosity (void fraction) is a measure of the void spaces in material or another word, a fraction of the volume of voids over the total volume. These two attributes rule one of the major problems of TCS, mass and heat transfer [51].

(10) Particle size: Another parameter, that has a great importance on the reaction time, is the texture of the salt bed, especially the size of the grains [45]. This is an intrinsic attribute of the material (in the commercially available form) and should be considered since it is also related to many other properties here listed (heat transfer, physical stability, etc.). The particle size also influences on the conversion rate, agglomeration issues, pore-plugging effect among others.

(11) Hydration/dehydration kinetics (sorption rate): the sorption rate is defined as the amount of sorbate absorbed over time, this strongly depends on the system (applied temperature,

vapour pressure, etc) but it is also ruled by intrinsic material properties such as grain size, porosity, BET surface area, etc. Sorption rate is desired to be maximized, although it will certainly depend on the storage period (long or short) and the application´s requirements.

(12) Cost: thermochemical storage is already a cost-intensive technology, thus a maximized cost per energy stored is needed for this technology to be feasible.

Other variables that depend on the properties above defined are temperature lift, pressure drop and mass and heat transfer. This is a combination of material properties and system selected and should be adjusted to the application's requirements (e.g. input heat source, open or closed system, etc). Although these attributes will not be studied in this paper since they belong to further development stages and we focus only on initial material selection/screening methodology, briefly described in this section.

(14) Temperature lift: this is defined as the difference in temperature between the heat source a heat pump is connected to (source) and the temperature that is being produced (destination). In compression heat pumps, the inner temperature lift corresponds (with good approximation) to the temperature difference between the condensation temperature and the evaporation temperature [52]. The efficiency of heat pumps and chillers are strongly influenced by the temperature lift, for an efficiently heated low-energy building, the desired temperature lift is in the range of 15 °C to 30 °C [52]. TCS experience a significant temperature lift during discharging, which is a crucial character for long-term and seasonal TES [53].

(15) Pressure drop: pressure drop is defined as a difference in total pressure between two points of a fluid carrying network, which occurs when frictional forces, caused by the resistance to flow, act on a fluid as it flows through the media. This is directly related to mass transfer and has been reported to increase with the operation time during desorption given the decrease in vapour content inside the porous materials (porosity) [54].

(16) Mass and heat transfer: these are important attributes that limit the output energy of the TCS system, both are strongly dependent on the porosity (bed porosity). Thus, a compromise should be found between proper mass and heat transfer within the porous media. While open systems suffer from mass transfer issues of the sorbate through the sorbent leading to pressure drops within the porous material that can highly reduce the system efficiency, closed systems present limitation in heat transfer [48].

4.4 TCS MANUFACTURING ROUTES

Thermochemical-based energy storage is very dependent on any change in the storage media such as agglomeration, volume expansion, deliquescence (formation of a saturated solution), chemical and physical degradation. Suitable modifications could ensure a homogeneous particle distribution by the prevention of agglomeration effects [55]. Ideally, the modifications to the based thermochemical material must minimise the cost production process, step processes should not affect the conversion rate of the thermochemical material, and it should be simple and easily scalable. This is currently a paradigm for the scientific community and it also brings up manufacturing challenge. Unlike other TES systems reported, little has been done on the manufacturing at a large scale of thermochemical materials and this is still at a lab-scale (from grams to kilos). Some of the manufacturing paths that have been considered by researchers are summarized in Figure 11.

Up to now, only a few approaches for particle stabilisation of thermochemical storage materials are described in the literature [55]. The fact is that authors have not agreed on a manufacturing process at the lab scale lessens the potential for large scale manufacturing. The most obvious, simple and convenient way of stabilising TCM materials is by shaping. Such method maximises the energy stored while shaping the pure salt in the form of granulates or pellets. However, given the change in volume and crystal structure over sorption/desorption cycles, the pellets cannot withstand more than one cycle tending to agglomerate after repeated

cycles. To tackle the issues regarding salt stability and agglomeration during the sorption process, THS has been moving towards the combination of salts hydrates and a holding matrix. The most popular method to prepare such 'salt inside porous matrix' (CSPM), is the impregnation of hygroscopic salt into the pores of porous desiccant host matrixes in any of its forms: direct, wet, vacuum, etc. Given that, for now, porous ceramic foams are the most plausible solution to all the stability related problems, impregnation is the simplest and most effective way of introducing the salt into the ceramic foam pores. New concepts have recently emerged such as microencapsulation with different polymeric shell [56,57], which showed good thermal behaviour and reliable cycling properties although increasing the complexity of the manufacturing process. Other commercialised alternatives are nanocoating of the TCM with hydrophobic nanoparticles that improve material compatibility and provides a long-term service [58]. The aforementioned manufacturing routes have been divided into conventional manufacturing routes and emerging manufacturing routes and are explained in the following sections.
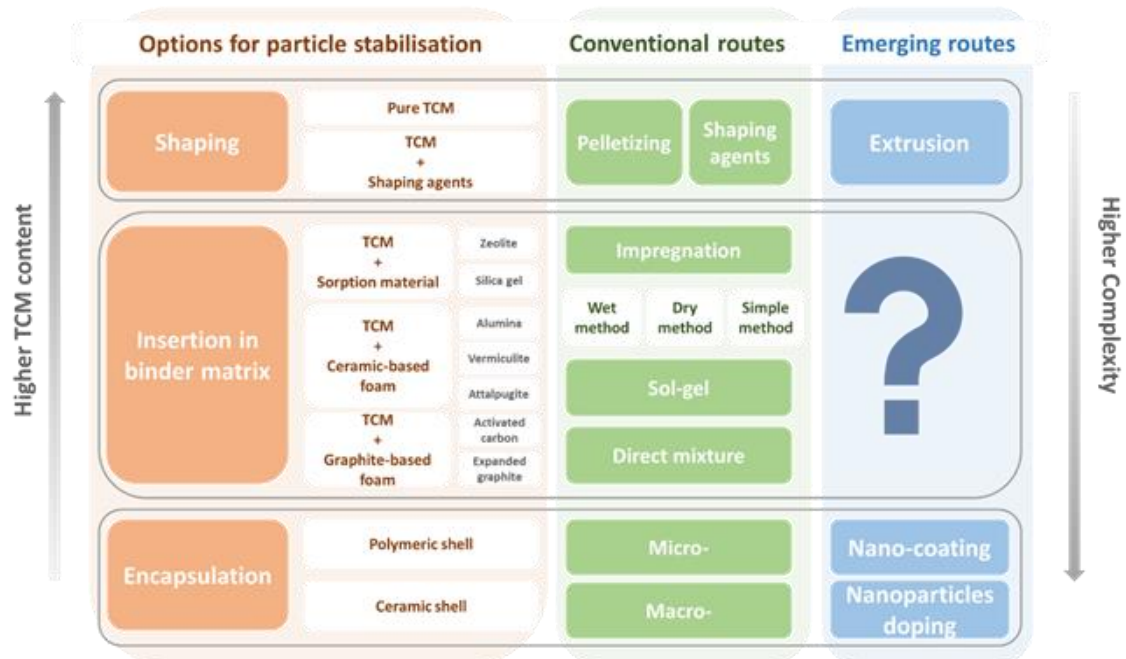
Figure 11. Thermochemical energy storage materials manufacturing routes.

4.3.1 CONVENTIONAL MANUFACTURING ROUTES

Conventional manufacturing routes comprehend those that have been studied for longer and that are currently most commonly used. Even though these routes have almost not been used at a commercial level yet, most of the thermochemical projects and prototype performances use either shaping or insertion in a binder matrix.

4.3.1.1 SHAPING

As stated in the introductory section, to maximise the energy density, the most convenient and obvious manufacturing route for thermochemical materials suggested by researchers is the shaping or pelletizing of pure thermochemical powder. Although this might appear as the cheapest and less complex solution, after one cycle of hydration/dehydration a significant change in molar density and molar volume takes place. This leads to a breakage of the pellets or granules decomposing quickly upon repeated cycles [55,59]. Therefore, shaping does not stand as a containment measure for avoiding agglomeration, deliquescence or poor cyclability.

4.3.1.2 INSERTION IN BINDER MATRIX

Binders are generally necessary for the shaping process influencing the adsorption performance, where problems concerning permeability, pressure drop, mechanical stability and system integration occur (e.g. high contact resistance between the adsorbent and heat exchanger surface) [60]. Potential host matrices are selected primarily on their ability to disperse the salt, prevent deliquescence during hydration, possess a high internal surface area on which to disperse the salt, be highly porous (to both gas and liquid phases), lightweight, durable, inert and be of relatively low cost [61]. The role of the porous matrix is also of importance. The confinement of the salt into the matrix pores can change fundamentally the equilibrium 'sorbent

– sorbate' [62]. Matrices would act as a proper container for the hygroscopic salts that are deliquescent, and it would also allow target-oriented synthesis of a composite adapted to particular climatic conditions. They help to disperse the salt particles, affect the phase composition and the sorption properties of the salt and provide heat and mass transport to the salt particles located inside the matrix grains [62]. First publications on composites 'salt inside porous matrix' (CSPM) are found at the beginning of the twentieth century. Since then, the number of papers has increased exponentially. Besides, some of such composite materials have been implemented at pilot plant level providing promising data for its future development [4].

The most basic method to prepare composites is the so-called "simple method", which is mainly based on the pellet preparation of a mixture of the matrix and the TCM materials varying the porosity and the ratios [63–65]. This method has been most commonly used with expanded graphite, the pros and cons of each matrix used will be described later in the section (see Table 5). Another reported method for composite preparation is the melting-solidifying method [66], where the TCM is melted and the matrix (in the reported case, cellulose) is dispersed in the hot solution. Then, the dispersion is cooled down to room temperature and the composite powder is pressed into pellets. In graphite composites, there is the need of using a vacuum to impregnate into the matrix. This is because the capillary force generated by graphite is not enough to drive the salt solution into the pores of the graphite matrix, so the vacuum force is needed to ensure a proper impregnation of the matrix.

Moving towards a more complex manufacturing route, one can find impregnation, which is the most common method used for thermochemical energy storage materials and also catalysis synthesis [67]. Impregnation is defined as the procedure whereby a certain volume of solution containing the precursor of the active phase is contacted with the solid (support or another active solid phase), which, in a subsequent step, is dried to remove the imbibed solvent [12,68]. As shown in Figure 12, the common steps when impregnating a matrix with an aqueous

salt solution are: (1) drying the matrix to remove absorbed water; (2) impregnate the grains with salt solution; (3) filtration and (4) drying the composite matrix to remove the adsorbed water [69]. Impregnation can be further divided into two methods, depending on the volume of solution and the driving forces to hold the salt inside the matrix: wet impregnation and dry impregnation (see Figure 12).

In the dry impregnation method, capillary action draws the salt solution into the pores while in the wet impregnation method the solution transport changes from a capillary action process to a diffusion process, which is much faster. Regarding the volume of the salt solution versus the pore volume; in wet impregnation, the volume of the salt solution exceeds the volume of the pores, which leads to an excess of solution that has to be removed either by filtration or vacuum desiccator. However, a portion of the salt will remain on the external surface [70]. After drying, such content of salt can partially precipitate on the outside of the grains [69] that can be later removed using a special humidity/temperature camera [71]. When the content of salt on the surface is not excessive, the composites are directly dried to obtain composites without large crystals formed on the surface. Conversely, dry impregnation, also known as "incipient wet impregnation", involves a salt solution equal or slightly lower than the pore volume. Since the process of the salt penetrating the matrix pores is rather slow, after several hours of impregnation, one can assume that the salt is located inside the pores. Therefore, in this case, when drying the salt, precipitates will not be formed/observed on the surface of the composite [69]. However, the maximum loading is limited by the solubility of the precursor in the solution. Besides, the concentration profile of the impregnated compound depends on the mass transfer conditions within the pores during impregnation and drying [72]. Impregnation can be then carried out under vacuum to avoid the crush of the matrix grains due to disjoining actions of capillary forces [62]. The main advantages of the impregnation methods, and why it has become so popular, is that is inexpensive, allows final property and configuration to be

controllable by tailoring the pore size, loading of salt and topology. The role of the porous matrix is also of importance. This matrix not only absorbs an adsorbate but also serves as a dispersion medium, which forms a required salt particle size and a high salt surface area, affects the state and properties of the salt, and provides heat supply through the solid phase and gas transport through the pore system.
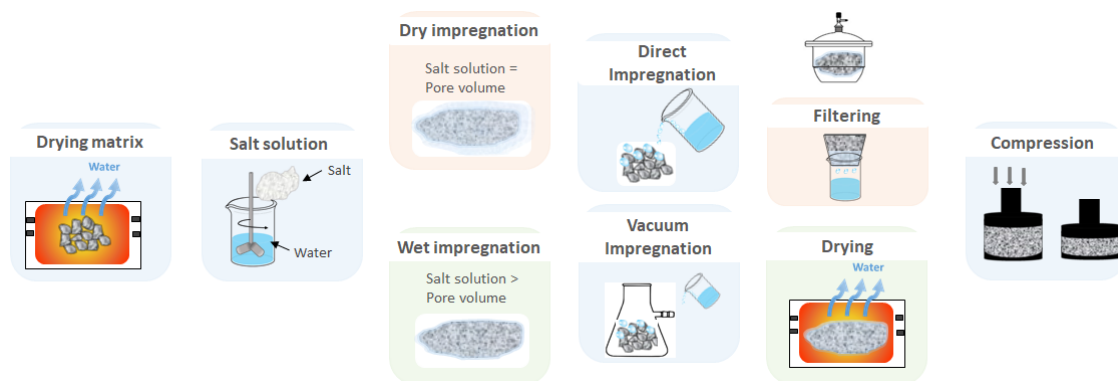
Figure 12. Impregnation methods scheme.

Some authors have also used the sol-gel method to impregnate the TCM into silica gel [73], the hybrid materials prepared by sol-gel route do not dissolve in water vapour and show an enhanced affinity for water vapour and adsorption capacities at higher relative pressures. Although silica-gel can be also impregnated by the conventional impregnation methods with the aqueous solution, such an approach does not ensure a uniform distribution within the sample. Meanwhile, sol-gel offers an alternative that allows synthesizing composites with an aero-gel structure that possesses an extremely large pore volume and sorption capacity [62]. This method consists of the preparation of a colloidal solution by mixing in an aqueous solution of the TCM, silica glass and the precursors by magnetic stirring until the solution is converted into a gel-like shape [74]. At the end of the synthesis, the composite sorbent in the form of a fine precipitate is filtered from the aqueous phase and dried to a constant weight. Although the results are promising sol-gel is

a cost extensive technique given the high cost of the precursors (metal alkoxides) and, for obvious reasons, it is not the preferred technique when preparing large quantities of bulk material.

Aside from a different kind of impregnation, there are different ways of preparing the CSPM regarding: the type of matrix used, the pore size, the microstructure, and so on. A review of the state of the art is listed in Table 3, the thermochemical material used, matrix or additive and the preparation used are thereof detailed. Dry impregnation has been the method preferably chosen by researchers given that since the filtration stage is omitted the dry impregnation method is easier in realization [62]. Nevertheless, when manufacturing large amounts of salt, the main handicap is that special procedure and equipment are required to ensure a uniform distribution of the salt into the solution. Therefore, even though at lab scale dry impregnation might stand as a feasible solution, many challenges must be faced prior bringing it to the next level.

Table 3. State of the art of sorption-based composite preparation at lab-scale with dry impregnation as the preparation method.

Preparation method	TCM	Matrix	Reference
Dry impregnation	$BaCl_2$	Expanded graphite	[75]
	$Ca(NO_3)_2$	Silica gel (micro-porous)	[76]
	$CaCl_2$	Activated carbon fibre and silica gel	[77]
	$CaCl_2$	Expanded natural graphite (ENG)	[78]
	$CaCl_2$	Silica gel (mesoporous)	[79]
	$CaCl_2$	Silica gel (mesoporous)	[80]
	$CaCl_2$, $Ba(OH)_2$, $LiNO_3$	Silica-Alumina	[81]
	$CaCl_2$, $MgCl_2$, LiBr	Alumina and KSK silica gel	[82]
	$CaCl_2$, $MgSO_4$, $Ca(NO_3)_2$, $Li(NO_3)_2$ and LiBr	Activated Carbon, Silica Gel, Zeolite, vermiculite	[83]
	$CaCl_2$ and $SrCl_2$	Expanded natural graphite (ENG)	[84]
	LiCl	Silica gel (mesoporous)	[85]
	$MgCl_2$	Zeolites	[86]
	$MgSO_4$	Zeolites	[87]
	$MgSO_4$	Zeolites	[16]
	$MgSO_4$ and $MgCl_2$	13X, Na-Y and Na-X	[88]
	$MgSO_4$ + $MgCl_2$	Attapulgite	[89]
	MnCl	Expanded Graphite	[90]

Table 4. State of the art of sorption-based composite preparation at lab-scale with dry impregnation as the preparation method.

Preparation method	TCM	Matrix	Reference
Wet impregnation	7 wt.% of $CaCl_2$	Disordered and ordered iron silicate matrix	[91]
	$CaCl_2$	Disordered mesoporous iron silicate	[92]
	$CaCl_2$	Ordered mesoporous iron silicate	[92]
	$CaCl_2$	Mesoporous Silica gel	[93]
	$CaCl_2$	Activated carbon fibre	[94]
	$CaCl_2$	Γ-alumina "IK-02-200"	[95]
	$CaCl_2$	Activated carbon/silica gel	[96]
	$CaCl_2$ and $MgSO_4$	Bentonite and zeolite	[97]
	LiBr and $Mg(OH)_2$	Expanded Graphite	[98]
	$Mg(OH)_2$	Vermiculite	[99]
	$Mg(OH)_2+CaCl_2$	Expanded Graphite	[100]
	$MgO/Mg(OH)_2$	Expanded Graphite	[101]
Sol-gel method	$CaCl_2$	SiO_2 (silica)	[73]
Simple method	$SrBr_2$	Expanded natural graphite ENG	[102]
	$CaCl_2$	Expanded graphite	[103]
	$Na_2S·9H_2O$	Graphite	[104]
Melting/ solidifying method	$Na_2S·9H_2O$	Cellulose fibres	[105]
Impregnation (not specified which one)	LiBr	Carbon sibunit and expanded graphite	[106]

Aiming to compare the most commonly used matrix, the authors have gathered them into Table 5. In broad terms, two different matrixes with different working mechanism can be selected; the first one just acts as a supporting material increasing the thermal conductivity and heat/mass transfer by providing a porous and solid structure, but not being involved in the storage process; the second one, provides similar attributes of the first one, but it also involves a storage process itself (normally solid adsorption) that allows storing much less energy density than the primary storage process, since non-chemical processes are involved. Carbon-based matrixes are normally the ones used for solely matrix purposes. Activated carbon has been used as a matrix given it can increase the surface area, enhance the capillary force of the materials, and ensure it becomes a good carrier to conduct and hold water [77]. Activated carbon has a large internal surface area and high surface reactivity [96]. Moreover, the thermal conductivity of the activated carbon itself is the best among all common adsorbents [107]. Nevertheless, activated carbon is cost-intensive, present leakage problems and its adsorption capacity are very dependent on temperature and pressure [108]. Expanded graphite (EG) has been used as a binding material to enhance the heat transfer properties of the thermochemical reactants [101,109,110]. EG is characterized by a high thermal conductivity, chemical stability, large surface area and does not react with adsorbents reactants [65,103]. Given EG have a wormlike particle shape that can host the TCM particles, this is required to remain unaltered after the binding method. Some authors have experienced some issues when preparing the EG/TCM composites such as breakage or exfoliation [111]. Eventually, the inherent incompatibility between the structure of graphite and the salt results in big salt aggregates, minimising water adsorption kinetics and the heat transfer rate [112]. To avoid this problem, some alternatives have been approached; Salviati et al. [112] added polyelectrolyte binder, PDAC (polydiallyldimethylammonium chloride), to enhance the compatibility between salt and matrix. Although, that increased compatibility it is not a plausible solution given the cost and complexity added to the process.

As stated above, another approach to CSPM matrix selection is the use of a solid adsorption thermochemical media, which can also act as a sorption material while performing as the matrix of the primary storage media (salt hydrate undergoing hydration/dehydration). Among this kind, the most used are silica gel, zeolite and vermiculite. Although aluminosilicates-based matrix has been also explored as seen in Table 2. Mesoporous disordered silicas (silica gels) are widely studied as hydrophilic compounds due to the high affinity to water vapour [113]. Silica gel composite shows a carryover problem at high humidity and temperatures, which depends on the ratio between the concentration of salt/pores [77]. When the salt concentration is too high, the limited pore volume cannot hold all the water absorbed by the compound materials, the salts drop from the pore and the absorption efficiency decreases. Silica gel also adds up complexity to the preparation method since the structure tends to break while preparing the composite. Zeolite is a class of highly porous crystalline aluminosilicates materials that are most commonly used in granular, cylindrical or beaded forms. Zeolite provides high specific surface area and accessible reaction sites to ensure good mass transfer, given the high absorbance capacity the salt can be absorbed into the pores [114]. Li et al. [115] found that adding bentonite to zeolite a honeycomb structure can be produced easing lubrication, preventing cracking and providing sufficient strength while maintaining the thermochemical performance. Researchers have found that when the more zeolite contents, the higher the compressive strength in the composite [116]. Zeolite can be also structurally modified by organic agents that influence the adsorption properties by ion exchange of the matrix [117,118], which allows a tuneable sorption capacity. The main disadvantages are its high affinity towards the water and the related high desorption temperatures (>200 °C) [60] and the fact that it allows low loading of TCM into the structure (80-95%). The macroporous nature of vermiculite offers an ideal host matrix for salt impregnation, overcoming the issue

of the deliquescence of the salts [119]. Vermiculite allows a single layer impregnation of the salt while absorbing large content of TCM than any other matrix used in the literature (see Table 5). As stated by Aydin [120], vermiculite stands as an excellent host matrix due to its low regeneration temperature (50-80 °C) and low cost. Casey et al. [83] prepared different composites by using silica gel, activated carbon, zeolite and vermiculite. The study suggested that following impregnation with the salt a reduction in mesoporous volume occurs with non-vermiculite matrices, reducing accessibility to moisture and that the vermiculite suffered no such performance degradation.

Table 5. Most used matrix for impregnation of thermochemical materials.

Matrix	Most used	Preparation method	Ratio (min-max %)	Advantages	Disadvantages
Silica gel	Mesoporous and microporous	Sol-gel, dry impregnation	60-70	High surface area. Good cyclability. Relatively cheap. Low desorption temperatures. Available. Low price.	Breakage of the structure while preparing the composite. Complex preparation method. Low sorption capacity.
Expanded graphite	3-10 mm	Sol-gel Dry/wet impregnation and simple method	35-80	Higher effective thermal conductivity. Lower porosities (large heat transfer). High gas permeability. Inert material. Large surface area.	High cost. Leakage problems after several cycles. More complex preparation to avoid breakage and exfoliation of the matrix. Need to use a vacuum. Salt aggregates.
Zeolite	13X, 4A, 5A, Na-Y and Na-X.	Dry/wet Impregnation	80-95	Provide high strength. Structure modification and tuneable sorption properties.	High cost. High temperatures of desorption. The low percentage of TCM in the matrix. Sieving effects Microporous range.
Vermiculite	2-8 mm	Dry/wet Impregnation	30-40	Cheap and available. A high percentage of TCM in the matrix.	Partially closed porous. Low water uptake.

| Activated carbon | | | | Macroporous. | The large variance of the pore volume. Low regeneration temperature. |
| | Powder and fibre (1-3 mm) | Dry/wet impregnation | 60-80 | Higher effective thermal conductivity. Great capillary force. Can be shaped without rupture. High adsorption capacity. High surface reactivity | Leakage problems. High cost. Adsorption influenced by temperature, pH and concentration. The low percentage of TCM. |

4.3.2 EMERGING MANUFACTURING ROUTES

In the previous manufacturing routes, we considered the option of artificially increase the size of particles (by pelletizing) or re-structuring the material to prevent further agglomeration problems (impregnation and encapsulation). However, due to volume changes these structures can break, which leads to smaller particle size and (again) tend to agglomerate.

4.3.2.1 NANO-ALTERNATIVES

Another approach to thermochemical materials stabilisation is to decrease the Van-deer-Waals forces, attractive forces between the particles that induce to agglomeration, by increasing the surface roughness (nano-coating) or minimise the contact area between particles to improve flow behaviour, nanoparticles addition (flowing agents). In bulk industries, several flow agents are known to improve the powder flowability mainly for better handling properties. However, the main challenge for thermochemical applications is that the additives have to keep their beneficial effect during several cycles. Silicon dioxide (SiO_2) nanoparticles [121] is used as a doping agent, they can be used either to improve fluidization behaviour or as a host matrix by using its agglomerates. Roßkopf et al. [122] used a dry mixing process to coat calcium hydroxide with silicon dioxide nanoparticles agglomerates. They found some difficulties in the

manufacturing process: the mixing intensity strongly influences the conversion of the reaction; higher intensity leads to higher conversion. Pontiga et al. [121],[123] used nanosilica to contain calcium hydroxide reaction, the authors used the dry mixing technique to prepare the composite aiming to improve the fluidization. The use of nanosilica additive was useful to increase the flowability and enhance the mass transfer. Interestingly, a commercialised nano-alternatives is the nanocoating of the TCM with hydrophobic nanoparticles that improves material compatibility and provides a long-term service [58]. In the patent the authors describe the coating of CaO, lithium bromide, lithium chloride, calcium chloride, calcium bromide and sodium sulphate with silica nanoparticles that are modified by covalently bound hydrophobic compounds. The nanocoating is prepared in a blender with the nanoparticles added to the salt solution and mixed in different intervals. The company (SaltX©) that owns the patent, manufacture and deliver the product at commercial scale.

Nano-composites are a new class of chemical heat storage materials for moderate-temperature storage owing to its comparatively lower decomposition temperatures [124]. Some of the composites considered in the previous section can be also considered as nanocomposites, depending on the particles size of the matrix. However, the authors wanted to stress the importance of nanocomposites in this section as well, especially when it comes to atomic size combination of metal hydroxides. Such nano-composites are generally co-precipitated metallic hydroxides, following a similar manufacturing method as the one reported in "insertion in a binder" section. Researchers have used the co-precipitated method of two metallic hydroxides [125–128], the advantage of this method is that a homogeneous nano-composite can be obtained through the chemical reaction in the solution directly [128]. By using such a method, the decomposition temperature can be substantially reduced (300 °C lower) while improving the cyclability and achieving an optimal storage capacity.

4.3.2.2 ENCAPSULATION

In the last couple of years, encapsulation has been proposed as a promising method to solve CSPMs issues such as the low-temperature lift and the interaction of the matrix with the sorption process. It does not just act as a matrix but aims to offset the energy taken away from the thermochemical utilizing the host matrix. In CSPMs, the matrix can be seen as the main driving force for energy storage given the percentages of TCM in the composite are lower than 40% (in the best of the cases). In encapsulation, researchers aim to provide a holding "matrix" by enabling a structure for the sorption process to happen, although respecting the main precursor of the sorption storage process. In this approach, the salt hydrate particles are enveloped with a second inherently stable material to prevent coalescence and agglomeration. There is a critical point to be considered when encapsulating thermochemical material that is not considered when encapsulating phase change materials. This requirement is that the sorption product (e.g. water vapour) have to scape and penetrate the capsule during sorption and desorption of the storage media. Apart from the challenge of having a semipermeable capsule to allow the steam to diffuse inside the shell, the shell must enable mechanical stability over several cycles. The capsule should be able to bear forces resulting from volume expansion of the core material during charging-discharging. The material must be inert and do not react or interact with the reversible reaction in any way, which can be challenging under hydrothermal conditions and temperature up to 550 °C. Cuypers et al. [57] encapsulated calcium chloride by using a Büchi Spray Dryer. The authors conclude that the encapsulated TCM can store energy at lower temperatures and the material shows a large thermal response on dehydration upon temperature increase. The microencapsulation of calcium chloride has been studied by Gaeni et al. [56], the encapsulated material is produced by spray-drying a solution of calcium chloride and ethyl cellulose in a solvent mixture composed of ethanol and water, which is a procedure used in pharmaceutical applications. Encapsulation showed high multicycles stability and fastest kinetic among all the methods assessed in the study (impregnation of graphite and vermiculite

composite). As the main disadvantages they pointed out for dehydration, is the low energy density in comparison to the pure TCM. Afflerbach et al. [55] encapsulated calcium hydroxide by an oxide ceramic capsule material that is based on a naturally occurring precursor. Such precursor can naturally contain fine-grained in the overall powder homogeneously. The four-step encapsulation process based on the core-shell principle was proposed by the authors: pre-granulated material, adhesion promoting agent, drying of the ceramic precursor and sintering. Although the mechanical stability of the particles was increased by the ceramic encapsulation, the authors encountered some difficulties when synthesizing the capsules such as the homogeneity of the ceramic shell and chemical modifications of the shell to increase the mechanical stability after sintering. Kallenberger et al. [129] synthesized a magnesium sulphate/polymer composite, magnesium sulphate was confined in pristine polymer cavities of around 10 um. When hydrating/dehydration the salt magnesium sulphate 1.25-hydrate, revealing that the dehydration to the monohydrate was not sufficient.

Though it shows great potential at lab-scale, this route brings additional steps that increase the complexity of the manufacturing process. Also, the materials needed to encapsulate the TCM are expensive and not highly available, which will hinder the production of large quantities of encapsulated storage media.

4.3.2.3 EXTRUSION

Extrusion is a widely used method in many commercialised manufacturing routes. When it comes to the thermochemical field, extrusion has been used to shape zeolites to an extruded form (honeycomb). In general, extruded materials are manufactured with the inclusion of a certain amount of binder which is used primarily to help cement zeolite crystals together in the past [115]. Many types of binder exist natural or synthetic, organic or inorganic, colloidal particle type or molecular type and water-soluble or non-polar liquid soluble. Common binders are clays, such as kaolin, attapulgite, boehmite, aluminas and/or silica or a combination of them [130].

Paste extrusion is widely used to manufacture a variety of products for mechanical, electrical and chemical engineering applications, as well as in the field of medicine. Li at al. [115] used paste extrusion to extrude different percentages of bentonite and zeolite using an organic and inorganic binder. The use of less bentonite will enhance the internal particle friction in the paste and cause failure in extrusion whilst the use of more than 35 wt.% bentonite will cause difficulty in handling before and after extrusion. This method has not been scaled up yet, although is the one that has greatest potential as it is a conventional manufacturing routes in many other industries. It could be easily modified according to the thermochemical properties/manufacture requirements.

4.4 OUTCOMES

A comprehensive overview of the material side from conceptualisation to manufacturing level has been described in this section. With this, we aim to position the reader in the current development stage of TCS systems to understand the importance of the 3 in the system proposed in this thesis. TCS materials are still at a low development level, while problems at the material level are still to be faced, novel manufacturing routes must be found to ease the commerciality way of these materials.

4.5 REFERENCES

[1]   Yan TS, Li TX, Xu JX, Chao JW. Understanding the transition process of phase change and dehydration reaction of salt hydrate for thermal energy storage. Appl Therm Eng 2020;166. doi:10.1016/j.applthermaleng.2019.114655.

[2]   Chiu JN. A Review of Thermal Energy Storage Systems with Salt Hydrate Phase Change Materials for Comfort Cooling. Inorg Mater 2009;15:24–46.

[3]   Yu N, Wang RZ, Wang LW. Sorption thermal storage for solar energy. Prog Energy Combust Sci 2013;39:489–514. doi:10.1016/j.pecs.2013.05.004 Review.

[4]   Scapino L, Zondag HA, Van Bael J, Diriken J, Rindt CCM. Sorption heat storage for long-term low-temperature applications: A review on the advancements at material and prototype scale. Appl Energy 2017;190:920–48. doi:10.1016/j.apenergy.2016.12.148.

[5]   Ding Y, Riffat SB. Thermochemical energy storage technologies for building applications: a state-of-the-art review. Int J Low-Carbon Technol 2012;8:106–16. doi:10.1093/ijlct/cts004.

[6]   Chang MH, Huang CM, Liu WH, Chen WC, Cheng JY, Chen W, et al. Design and Experimental Investigation of Calcium Looping Process for 3-kWth and 1.9-MWth Facilities. Chem Eng Technol 2013;36:1525–32. doi:10.1002/ceat.201300081.

[7]   Lele AF. State-of-Art of Thermochemical Heat Storage Systems. 2016. doi:10.1007/978-3-319-41228-3.

[8]   Aydin D, Casey SP, Riffat S. The latest advancements on thermochemical heat storage systems. Renew Sustain Energy Rev 2015;41:356–67. doi:10.1016/j.rser.2014.08.054.

[9]   Yu N, Wang RZ, Lu ZS, Wang LW. Study on consolidated composite sorbents impregnated with LiCl for thermal energy storage. Int J Heat Mass Transf 2015;84:660–70. doi:10.1016/j.ijheatmasstransfer.2015.01.065.

[10]   Hauer A. Evaluation of adsorbent materials for heat pump and thermal energy storage applications in open systems. Adsorption, 2007. doi:10.1007/s10450-007-9054-0.

[11]   Boukhanouf R, Riffat S. Theoretical and experimental investigation of a two-bed adsorption system using a novel adsorber configuration. Int J Green Energy 2007. doi:10.1080/15435070701193167.

[12]   Casey SP, Aydin D, Elvins J, Riffat S. Salt impregnated desiccant matrices for "open"

thermochemical energy conversion and storage – Improving energy density utilisation through hygrodynamic & thermodynamic reactor design. Energy Convers Manag 2017;142:426–40. doi:10.1016/j.enconman.2017.03.066.

[13]   Abedin A, Rosen M, Choi JC, Kim SD, Eindhoven TU, Habashy GM, et al. A Critical Review of Thermochemical Energy Storage Systems. Open Renew Energy J 2011;4:42–6. doi:10.2174/1876387101004010042.

[14]   van Essen VM, Zondag H a., Gores JC, Bleijendaal LPJ, Bakker M, Schuitema R, et al. Characterization of MgSO4 Hydrate for Thermochemical Seasonal Heat Storage. J Sol Energy Eng 2009;131:41014. doi:10.1115/1.4000275.

[15]   van Essen VM, Cot Gores J, Bleijendaal LPJ, Zondag H a., Schuitema R, Bakker M, et al. Characterization of Salt Hydrates for Compact Seasonal Thermochemical Storage. ASME 2009 3rd Int Conf Energy Sustain Vol 2 2009;2:825–30. doi:10.1115/ES2009-90289.

[16]   Hongois S, Kuznik F, Stevens P, Roux JJ. Development and characterisation of a new MgSO4-zeolite composite for long-term thermal energy storage. Sol Energy Mater Sol Cells 2011;95:1831–7. doi:10.1016/j.solmat.2011.01.050.

[17]   Okhrimenko L, Favergeon L, Johannes K, Kuznik F, Pijolat M. Thermodynamic study of MgSO4– H2O system dehydration at low pressure in view of heat storage. Thermochim Acta 2017;656:135–43. doi:10.1016/j.tca.2017.08.015.

[18]   N'Tsoukpoe KE, Schmidt T, Rammelberg HU, Watts BA, Ruck WKL. A systematic multi-step screening of numerous salt hydrates for low temperature thermochemical energy storage. Appl Energy 2014;124:1–16. doi:10.1016/j.apenergy.2014.02.053.

[19]   Lahmidi H, Mauran S, Goetz V. Definition, test and simulation of a thermochemical storage process adapted to solar thermal systems. Sol Energy 2006;80:883–93. doi:10.1016/j.solener.2005.01.014.

[20]   Michel B, Mazet N, Neveu P. Experimental investigation of an innovative thermochemical process operating with a hydrate salt and moist air for thermal storage of solar energy: Global performance. Appl Energy 2014. doi:10.1016/j.apenergy.2014.04.073.

[21]   Marias F, Neveu P, Tanguy G, Papillon P. Thermodynamic analysis and experimental study of solid/gas reactor operating in open mode. Energy 2014. doi:10.1016/j.energy.2014.01.101.

[22]   Lele AF. State-of-Art of Thermochemical Heat Storage Systems. 2016. doi:10.1007/978-3-319-41228-3.

[23]   Gil A, Medrano M, Martorell I, Lázaro A, Dolado P, Zalba BBB, et al. State of the art on high temperature thermal energy storage for power generation. Part 1-Concepts, materials and modellization. Renew Sustain Energy Rev 2010;14:31–55. doi:10.1016/j.rser.2009.07.035.

[24]   Sunku Prasad J, Muthukumar P, Desai F, Basu DN, Rahman MM. A critical review of high-temperature reversible thermochemical energy storage systems. Appl Energy 2019. doi:10.1016/j.apenergy.2019.113733.

[25]   Ervin G. Solar heat storage using chemical reactions. J Solid State Chem 1977;22:51–61. doi:10.1016/0022-4596(77)90188-8.

[26]   Criado YA, Huille A, Rougé S, Abanades JC. Experimental investigation and model validation of a CaO/Ca(OH)2 fluidized bed reactor for thermochemical energy storage applications. Chem Eng J 2017;313:1194–205. doi:10.1016/J.CEJ.2016.11.010.

[27]   Yan J, Zhao CY. Experimental study of CaO/Ca(OH)2in a fixed-bed reactor for thermochemical heat storage. Appl Energy 2016;175:277–84. doi:10.1016/j.apenergy.2016.05.038.

[28]   Yan J, Zhao CY. Thermodynamic and kinetic study of the dehydration process of

CaO/Ca(OH)2 thermochemical heat storage system with Li doping. Chem Eng Sci 2015;138:86–92. doi:10.1016/J.CES.2015.07.053.

[29]   Kanzawa A, Arai Y. Thermal energy storage by the chemical reaction augmentation of heat transfer and thermal decomposition in the CaOCa(OH)2 powder. Sol Energy 1981;27:289–94. doi:10.1016/0038-092X(81)90061-X.

[30]   Azpiazu MN, Morquillas JM, Vazquez A. Heat recovery from a thermal energy storage based on the Ca(OH)2/CaO cycle. Appl Therm Eng 2003;23:733–41. doi:10.1016/S1359-4311(03)00015-2.

[31]   Paskevicius M, Sheppard DA, Buckley CE. Thermodynamic Changes in Mechanochemically Synthesized Magnesium Hydride Nanoparticles. J Am Chem Soc 2010;132:5077–83. doi:10.1021/ja908398u.

[32]   Fahim MA, Ford JD. Energy storage using the BaO2-BaO reaction cycle. Chem Eng J 1983;27:21–8. doi:10.1016/0300-9467(83)80042-2.

[33]   Wong B, Brown L, Schaube F, Tamme R, Sattler C. Oxide Based Thermochemical Heat Storage 2010.

[34]   Pardo P, Deydier A, Anxionnaz-Minvielle Z, Rougé S, Cabassud M, Cognet P. A review on high temperature thermochemical heat energy storage. Renew Sustain Energy Rev 2014;32:591–610. doi:10.1016/j.rser.2013.12.014.

[35]   Block T, Schmücker M. Metal oxides for thermochemical energy storage: A comparison of several metal oxide systems. Sol Energy 2016. doi:10.1016/j.solener.2015.12.032.

[36]   Block T, Knoblauch N, Schmücker M. The cobalt-oxide/iron-oxide binary system for use as high temperature thermochemical energy storage material. Thermochim Acta 2014;577:25–32. doi:10.1016/j.tca.2013.11.025.

[37]   Carrillo AJ, Moya J, Bayón A, Jana P, de la Peña O'Shea VA, Romero M, et al. Thermochemical energy storage at high temperature via redox cycles of Mn and Co oxides: Pure oxides versus mixed ones. Sol Energy Mater Sol Cells 2014;123:47–57. doi:10.1016/J.SOLMAT.2013.12.018.

[38]   Donkers PAJ, Sögütoglu LC, Huinink HP, Fischer HR, Adan OCG. A review of salt hydrates for seasonal heat storage in domestic applications. Appl Energy 2017. doi:10.1016/j.apenergy.2017.04.080.

[39]   Hawwash AA, Hassan H, Ahmed M, Ookawara S, Feky K El. Long-term Thermal Energy Storage Using Thermochemical Materials. Energy Procedia 2017;141:310–4. doi:10.1016/j.egypro.2017.11.111.

[40]   Clark RJ, Mehrabadi A, Farid M. State of the art on salt hydrate thermochemical energy storage systems for use in building applications. J Energy Storage 2020. doi:10.1016/j.est.2019.101145.

[41]   Duhoux B, Mehrani P, Lu DY, Symonds RT, Anthony EJ, Macchi A. Combined Calcium Looping and Chemical Looping Combustion for Post-Combustion Carbon Dioxide Capture: Process Simulation and Sensitivity Analysis. Energy Technol 2016;4:1158–70. doi:10.1002/ente.201600024.

[42]   De Jong AJ, Van Vliet L, Hoegaerts C, Roelands M, Cuypers R. Thermochemical Heat Storage - From Reaction Storage Density to System Storage Density. Energy Procedia 2016;91:128–37. doi:10.1016/j.egypro.2016.06.187.

[43]   Kato Y, Funayama S, Piperopoulos E, Milone C. Experimental Methods for the Characterization of Materials for Thermal Energy Storage with Chemical Reactions. In: Frazzica A. CL, editor. Recent Adv. Mater. Syst. Therm. Energy Storage. Green Energy Technol., Recent Advancements in Materials and Systems for Thermal Energy Storage.

Green Energy and Technology; 2019. doi:https://doi.org/10.1007/978-3-319-96640-3_8.

[44]   Solé A, Martorell I, Cabeza LF. State of the art on gas-solid thermochemical energy storage systems and reactors for building applications. Renew Sustain Energy Rev 2015. doi:10.1016/j.rser.2015.03.077.

[45]   Michel B, Mazet N, Mauran S, Stitou D, Xu J. Thermochemical process for seasonal storage of solar energy: Characterization and modeling of a high density reactive bed. Energy 2012;47:553–63. doi:10.1016/j.energy.2012.09.029.

[46]   Glasser L. Thermodynamics of inorganic hydration and of humidity control, with an extensive database of salt hydrate pairs. J Chem Eng Data 2014;59:526–30. doi:10.1021/je401077x.

[47]   Michel B, Neveu P, Mazet N. Comparison of closed and open thermochemical processes, for long-term thermal energy storage applications. Energy 2014;72:702–16. doi:10.1016/j.energy.2014.05.097.

[48]   Scapino L, Zondag HA, Van Bael J, Diriken J, Rindt CCM. Energy density and storage capacity cost comparison of conceptual solid and liquid sorption seasonal heat storage systems for low-temperature space heating. Renew Sustain Energy Rev 2017;76:1314–31. doi:10.1016/j.rser.2017.03.101.

[49]   Ali ES, Askalany AA, Harby K, Diab MR, Alsaman AS. Adsorption desalination-cooling system employing copper sulfate driven by low grade heat sources. Appl Therm Eng 2018;136:169–76. doi:10.1016/j.applthermaleng.2018.03.014.

[50]   Yao W, Yu X, Lee JW, Yuan X, Schmidt SJ. Measuring the deliquescence point of crystalline sucrose as a function of temperature using a new automatic isotherm generator. Int J Food Prop 2011. doi:10.1080/10942910903474393.

[51]   Fopah Lele A. A Thermochemical Heat Storage System for Households - Combined Investigations of Thermal Transfers Coupled to Chemical Reactions. 2016. doi:10.1007/978-3-319-41228-3.

[52]   Gasser L, Flück S, Kleingries M, Meier C, Bätschmann M, Wellig B. High efficiency heat pumps for low temperature lift applications. 12th IEA Heat Pump Conf 2017.

[53]   Xu SZ, Lemington, Wang RZ, Wang LW, Zhu J. A zeolite 13X/magnesium sulfate–water sorption thermal energy storage device for domestic heating. Energy Convers Manag 2018;171:98–109. doi:10.1016/j.enconman.2018.05.077.

[54]   Michel B, Mazet N, Neveu P. Experimental investigation of an open thermochemical process operating with a hydrate salt for thermal storage of solar energy: Local reactive bed evolution. Appl Energy 2016;180:234–44. doi:10.1016/j.apenergy.2016.07.108.

[55]   Afflerbach S, Kappes M, Gipperich A, Trettin R, Krumm W. Semipermeable encapsulation of calcium hydroxide for thermochemical heat storage solutions. Sol Energy 2017;148:1–11. doi:10.1016/j.solener.2017.03.074.

[56]   Gaeini M, Rouws AL, Salari JWO, Zondag HA, Rindt CCM. Characterization of microencapsulated and impregnated porous host materials based on calcium chloride for thermochemical energy storage. Appl Energy 2018;212:1165–77. doi:10.1016/j.apenergy.2017.12.131.

[57]   Cuypers R, de Jong AJ, Eversdijk J, Van 't Spijker H, Oversloot H, Ingenhut BLJ, et al. Microencapsulation of Salts for Enhanced Thermochemical Storage Materials n.d.:2–3.

[58]   Göran Bolin T (SE); D, Glebov K (SE). Salt coated with nanoparticles. US 9.459,026 B2, 2016.

[59]   Fujii I, Ishino M, Akiyama S, Murthy MS, Rajanandam KS. Behavior of Ca(OH)2/CaO pellet under dehydration and hydration. Sol Energy 1994;53:329–41. doi:10.1016/0038-

092X(94)90036-1.

[60]   Sarkar J, Bhattacharyya S. Application of graphene and graphene-based materials in clean energy-related devices Minghui. Arch Thermodyn 2012;33:23–40. doi:10.1002/er.

[61]   Sutton R, Jewell E, Searle J, Elvins J. Discharge performance of blended salt in matrix materials for low enthalpy thermochemical storage. Appl Therm Eng 2018;145:483–93. doi:10.1016/j.applthermaleng.2018.09.052.

[62]   Gordeeva LG, Aristov YI. Composites "salt inside porous matrix" for adsorption heat transformation: A current state-of-the-art and new trends. Int J Low-Carbon Technol 2012;7:288–302. doi:10.1093/ijlct/cts050.

[63]   Sánchez AR, Klein HP, Groll M. Expanded graphite as heat transfer matrix in metal hydride beds. Int J Hydrogen Energy 2003;28:515–27. doi:10.1016/S0360-3199(02)00057-5.

[64]   Klein HP, Groll M. Heat transfer characteristics of expanded graphite matrices in metal hydride beds. Int J Hydrogen Energy 2004;29:1503–11. doi:10.1016/j.ijhydene.2004.01.017.

[65]   Mauran S, Prades P, L'Haridon F. Heat and mass transfer in consolidated reacting beds for thermochemical systems. Heat Recover Syst CHP 1993;13:315–9. doi:10.1016/0890-4332(93)90055-Z.

[66]   Roelands M, Cuypers R, Kruit KD, Oversloot H, De Jong AJ, Duvalois W, et al. Preparation & Characterization of Sodium Sulfide Hydrates for Application in Thermochemical Storage Systems. Energy Procedia 2015;70:257–66. doi:10.1016/j.egypro.2015.02.122.

[67]   Perego C, Villa P. Catalyst preparation methods. Catal Today 1997;34:281–305. doi:10.1016/S0920-5861(96)00055-7.

[68]   Van Dillen AJ, Terörde RJAM, Lensveld DJ, Geus JW, De Jong KP. Synthesis of supported

catalysts by impregnation and drying using aqueous chelated metal complexes. J Catal 2003;216:257–64. doi:10.1016/S0021-9517(02)00130-6.

[69]   Jarimi H, Aydin D, Yanan Z, Ozankaya G, Chen X, Riffat S. Review on the recent progress of thermochemical materials and processes for solar thermal energy storage and industrial waste heat recovery. Int J Low-Carbon Technol 2019;14:44–69. doi:10.1093/ijlct/cty052.

[70]   Gordeeva LG, Freni A, Krieger TA, Restuccia G, Aristov YI. Composites "lithium halides in silica gel pores": Methanol sorption equilibrium. Microporous Mesoporous Mater 2008;112:254–61. doi:10.1016/j.micromeso.2007.09.040.

[71]   Gong LX, Wang RZ, Xia ZZ, Chen CJ. Adsorption equilibrium of water on a composite adsorbent employing lithium chloride in silica gel. J Chem Eng Data 2010;55:2920–3. doi:10.1021/je900993a.

[72]   Deraz NM. The comparative jurisprudence of catalysts preparation methods: I. precipitation and impregnation methods. J Ind Environ Chem 2018;2:1–3.

[73]   Mrowiec-Białoń J, Jarzębski AB, Lachowski AI, Malinowski JJ, Aristov YI. Effective Inorganic Hybrid Adsorbents of Water Vapor by the Sol-Gel Method. Chem Mater 1997;9:2486–90. doi:10.1021/cm9703280.

[74]   Yeromin O, Belyanovskaya E, Sukhyy K, Kotok V, Gubynskyi M, Kolomiyets O, et al. The study of properties of composite adsorptive materials "silica gel – crystalline hydrate" for heat storage devices. Eastern-European J Enterp Technol 2018;1:52–8. doi:10.15587/1729-4061.2018.123896.

[75]   Li TX, Wang RZ, Wang LW, Kiplagat JK. Study on the heat transfer and sorption characteristics of a consolidated composite sorbent for solar-powered thermochemical cooling systems. Sol Energy 2009;83:1742–55. doi:10.1016/j.solener.2009.06.013.

[76]   Simonova IA, Freni A, Restuccia G, Aristov YI. Water sorption on composite "silica modified by calcium nitrate." Microporous Mesoporous Mater 2009;122:223–8. doi:10.1016/j.micromeso.2009.02.034.

[77]   Wang JY, Wang RZ, Wang LW. Water vapor sorption performance of ACF-CaCl2 and silica gel-CaCl2 composite adsorbents. Appl Therm Eng 2016;100:893–901. doi:10.1016/j.applthermaleng.2016.02.100.

[78]   Tian B, Jin ZQ, Wang LW, Wang RZ. Permeability and thermal conductivity of compact chemical and physical adsorbents with expanded natural graphite as host matrix. Int J Heat Mass Transf 2012;55:4453–9. doi:10.1016/j.ijheatmasstransfer.2012.04.016.

[79]   Aristov Y., Tokarev M., Cacciola G, Restuccia G. SELECTIVE WATER SORBENTS FOR MULTIPLE APPLICATIONS, 1. CaCl2 CONFINED IN MESOPORES OF SILICA GEL: SORPTION 1996;59:325–33.

[80]   Wu H, Wang S, Zhu D. Effects of impregnating variables on dynamic sorption characteristics and storage properties of composite sorbent for solar heat storage. Sol Energy 2007;81:864–71. doi:10.1016/j.solener.2006.11.013.

[81]   Jabbari-Hichri A, Bennici S, Auroux A. Enhancing the heat storage density of silica–alumina by addition of hygroscopic salts (CaCl 2 , Ba(OH) 2 , and LiNO 3). Sol Energy Mater Sol Cells 2015;140:351–60. doi:10.1016/j.solmat.2015.04.032.

[82]   Tanashev YY, Krainov A V., Aristov YI. Thermal conductivity of composite sorbents "salt in porous matrix" for heat storage and transformation. Appl Therm Eng 2013;61:401–7. doi:10.1016/j.applthermaleng.2013.08.022.

[83]   Casey SP, Elvins J, Riffat S, Robinson A. Salt impregnated desiccant matrices for "open" thermochemical energy storage - Selection, synthesis and characterisation of candidate materials. Energy Build 2014;84:412–25. doi:10.1016/j.enbuild.2014.08.028.

[84]   Jiang L, Wang LW, Jin ZQ, Wang RZ, Dai YJ. Effective thermal conductivity and permeability of compact compound ammoniated salts in the adsorption/desorption process. Int J Therm Sci 2013;71:103–10. doi:10.1016/j.ijthermalsci.2013.03.017.

[85]   Freni A, Gordeeva LG, Vasta S, Restuccia G. Composite sorbent of methanol " Lithium Chloride in mesoporous silica gel " for adsorptive cooling machines : performance evaluation. Combustion 2007;V:28–32.

[86]   Whiting GT, Grondin D, Stosic D, Bennici S, Auroux A. Zeolite-MgCl2 composites as potential long-term heat storage materials: Influence of zeolite properties on heats of water sorption. Sol Energy Mater Sol Cells 2014;128:289–95. doi:10.1016/j.solmat.2014.05.016.

[87]   Whiting G, Grondin D, Bennici S, Auroux A. Heats of water sorption studies on zeolite-MgSO 4 composites as potential thermochemical heat storage materials. Sol Energy Mater Sol Cells 2013;112:112–9. doi:10.1016/j.solmat.2013.01.020.

[88]   Shere L, Trivedi S, Roberts S, Sciacovelli A, Ding Y. Synthesis and Characterization of Thermochemical Storage Material Combining Porous Zeolite and Inorganic Salts. Heat Transf Eng 2018:1–6. doi:10.1080/01457632.2018.1457266.

[89]   Posern K, Kaps C. Calorimetric studies of thermochemical heat storage materials based on mixtures of MgSO4 and MgCl2. Thermochim Acta 2010;502:73–6. doi:10.1016/j.tca.2010.02.009.

[90]   Li TX, Wang RZ, Kiplagat JK, Wang LW. Performance study of a consolidated manganese chloride-expanded graphite compound for sorption deep-freezing processes. Appl Energy 2009;86:1201–9. doi:10.1016/j.apenergy.2008.06.004.

[91]   Duan Z, Zhang H, Sun L, Cao Z, Xu F, Zou Y, et al. CaCl2·6H2O/Expanded graphite composite as form-stable phase change materials for thermal energy storage. J Therm

Anal Calorim 2014;115:111–7. doi:10.1007/s10973-013-3311-0.

[92]   Ristić A, Henninger SK. Sorption composite materials for solar thermal energy storage. Energy Procedia, vol. 48, 2014, p. 977–81. doi:10.1016/j.egypro.2014.02.111.

[93]   Zhu D, Wu H, Wang S. Experimental study on composite silica gel supported CaCl2 sorbent for low grade heat storage. Int J Therm Sci 2006;45:804–13. doi:10.1016/j.ijthermalsci.2005.10.009.

[94]   Druske M-M, Fopah-Lele A, Korhammer K, Rammelberg HU, Wegscheider N, Ruck W, et al. Developed Materials for Thermal Energy Storage: Synthesis and Characterization. Energy Procedia 2014;61:96–9. doi:10.1016/j.egypro.2014.11.915.

[95]   Gordeeva LG, Tokarev MM, Parmon VN, Aristov YI. Selective water sorbents for multiple application, 6. Freshwater production from the atmosphere. React Kinet Catal Lett 1998;65:153–9. doi:10.1007/BF02475329.

[96]   Tso CY, Chao CYH. Activated carbon, silica-gel and calcium chloride composite adsorbents for energy efficient solar adsorption cooling and dehumidification systems. Int J Refrig 2012;35:1626–38. doi:10.1016/j.ijrefrig.2012.05.007.

[97]   Kerskes H. Experimental and Numerical Investigations on Thermo Chemical Heat Storage, 2016, p. 1–10. doi:10.18086/eurosun.2010.16.14.

[98]   Myagmarjav O, Ryu J, Kato Y. Lithium bromide-mediated reaction performance enhancement of a chemical heat-storage material for magnesium oxide/water chemical heat pumps. Appl Therm Eng 2014;63:170–6. doi:10.1016/j.applthermaleng.2013.10.045.

[99]   Shkatulov A, Ryu J, Kato Y, Aristov Y. Composite material " Mg(OH)2/vermiculite": A promising new candidate for storage of middle temperature heat. Energy 2012;44:1028–

34. doi:10.1016/j.energy.2012.04.045.

[100]   Kim ST, Ryu J, Kato Y. Optimization of magnesium hydroxide composite material mixed with expanded graphite and calcium chloride for chemical heat pumps. Appl Therm Eng 2013;50:485–90. doi:10.1016/j.applthermaleng.2012.07.005.

[101]   Zamengo M, Ryu J, Kato Y. Thermochemical performance of magnesium hydroxide-expanded graphite pellets for chemical heat pump. Appl Therm Eng 2014;64:339–47. doi:10.1016/j.applthermaleng.2013.12.036.

[102]   Mauran S, Lahmidi H, Goetz V. Solar heating and cooling by a thermochemical process. First experiments of a prototype storing 60 kW h by a solid/gas reaction. Sol Energy 2008;82:623–36. doi:10.1016/J.SOLENER.2008.01.002.

[103]   Fujioka K, Hatanaka K, Hirata Y. Composite reactants of calcium chloride combined with functional carbon materials for chemical heat pumps. Appl Therm Eng 2008;28:304–10. doi:10.1016/j.applthermaleng.2006.02.032.

[104]   Iammak K, Wongsuwan W, Kiatsiriroj T. Investigation of Modular Chemical Energy Storage Performance. Proc Jt Int Conf ''sustainable Energy Environ 2004;22:504–7.

[105]   Roelands M, Cuypers R, Kruit KD, Oversloot H, De Jong AJ, Duvalois W, et al. Preparation & Characterization of Sodium Sulfide Hydrates for Application in Thermochemical Storage Systems. Energy Procedia, vol. 70, 2015, p. 257–66. doi:10.1016/j.egypro.2015.02.122.

[106]   Gordeeva LG, Restuccia G, Freni A, Aristov YI. Water sorption on composites "LiBr in a porous carbon." Fuel Process Technol 2002;79:225–31. doi:10.1016/S0378-3820(02)00186-8.

[107]   Menard D, Py X, Mazet N. Activated carbon monolith of high thermal conductivity for adsorption processes improvement. Part B. Thermal regeneration. Chem Eng Process

Process Intensif 2007;46:565–72. doi:10.1016/j.cep.2006.07.013.

[108] Shigeishi RA, Langford CH, Hollebone BR. Solar energy storage using chemical potential changes associated with drying of zeolites. Sol Energy 1979;23:489–95. doi:10.1016/0038-092X(79)90072-0.

[109] Fopah Lele A, N'Tsoukpoe KE, Osterland T, Kuznik F, Ruck WKL. Thermal conductivity measurement of thermochemical storage materials. Appl Therm Eng 2015;89:916–26. doi:10.1016/j.applthermaleng.2015.06.077.

[110] Cammarata A, Verda V, Sciacovelli A, Ding Y. Hybrid strontium bromide-natural graphite composites for low to medium temperature thermochemical energy storage: Formulation, fabrication and performance investigation. Energy Convers Manag 2018;166:233–40. doi:10.1016/j.enconman.2018.04.031.

[111] Zamengo M, Ryu J, Kato Y. Magnesium hydroxide - Expanded graphite composite pellets for a packed bed reactor chemical heat pump. Appl Therm Eng 2013;61:853–8. doi:10.1016/j.applthermaleng.2013.04.045.

[112] Salviati S, Carosio F, Saracco G, Fina A. Hydrated Salt/Graphite/Polyelectrolyte Organic-Inorganic Hybrids for Efficient Thermochemical Storage. Nanomaterials 2019;9:420. doi:10.3390/nano9030420.

[113] Ristić A, Henninger SK. Sorption composite materials for solar thermal energy storage. Energy Procedia 2014;48:977–81. doi:10.1016/j.egypro.2014.02.111.

[114] Shere L, Trivedi S, Roberts S, Sciacovelli A, Ding Y. Synthesis and Characterization of Thermochemical Storage Material Combining Porous Zeolite and Inorganic Salts. Heat Transf Eng 2018;0:1–6. doi:10.1080/01457632.2018.1457266.

[115] The effect of the binder on the manufacture of a 5A zeolite monolith. Powder Technol

2001;116:85–96. doi:10.1016/S0032-5910(00)00366-1.

[116] Yim T, Kim HS, Lee JY. Cyclic assessment of magnesium oxide with additives as a thermochemical material to improve the mechanical strength and chemical reaction. Energies 2018;11. doi:10.3390/en11092366.

[117] Jänchen J, Ackermann D, Stach H, Brösicke W. Studies of the water adsorption on Zeolites and modified mesoporous materials for seasonal storage of solar heat. Sol Energy 2004;76:339–44. doi:10.1016/j.solener.2003.07.036.

[118] Herzog TH, Jänchen J. Adsorption Properties of Modified Zeolites for Operating Range Enhancement of Adsorption Heat Pumps through the Use of Organic Adsorptive Agents. Energy Procedia 2016;91:155–60. doi:10.1016/j.egypro.2016.06.192.

[119] Jarimi H, Devrim A, Zhang Y, Ding Y, Ramadan O, Chen X, et al. Materials characterization of innovative composite materials for solar-driven thermochemical heat storage (THS) suitable for building application. Int J Low-Carbon Technol 2018;13:30–42. doi:10.1093/ijlct/ctx017.

[120] Aydin D, Casey SP, Riffat S. The latest advancements on thermochemical heat storage systems. Renew Sustain Energy Rev 2015;41:356–67. doi:10.1016/j.rser.2014.08.054.

[121] Pontiga F, Valverde JM, Moreno H, Duran-Olivencia FJ. Dry gas-solid carbonation in fluidized beds of Ca(OH)2 and nanosilica/Ca(OH)2 at ambient temperature and low CO2 pressure. Chem Eng J 2013;222:546–52. doi:10.1016/j.cej.2013.02.067.

[122] Roßkopf C, Afflerbach S, Schmidt M, Görtz B, Kowald T, Linder M, et al. Investigations of nano coated calcium hydroxide cycled in a thermochemical heat storage. Energy Convers Manag 2015;97:94–102. doi:10.1016/j.enconman.2015.03.034.

[123] Roßkopf C, Haas M, Faik A, Linder M, Wörner A. Improving powder bed properties for thermochemical storage by adding nanoparticles. Energy Convers Manag 2014;86:93–8.

doi:10.1016/j.enconman.2014.05.017.

[124]   Cot-Gores J, Castell A, Cabeza LF. Thermochemical energy storage and conversion: A-state-of-the-art review of the experimental research under practical conditions. Renew Sustain Energy Rev 2012;16:5207–24. doi:10.1016/j.rser.2012.04.007.

[125]   Kato Y, Takahashi R, Sekiguchi T, Ryu J. Study on medium-temperature chemical heat storage using mixed hydroxides. Int J Refrig 2009;32:661–6. doi:10.1016/j.ijrefrig.2009.01.032.

[126]   Ryu J, Takahashi R, Hirao N, Kato Y. Effect of transition metal mixing on reactivities of magnesium oxide for chemical heat pump. J Chem Eng Japan 2007;40:1281–6. doi:10.1252/jcej.07WE171.

[127]   Ishitobi H, Uruma K, Takeuchi M, Ryu J, Kato Y. Dehydration and hydration behavior of metal-salt-modified materials for chemical heat pumps. Appl. Therm. Eng., vol. 50, 2013, p. 1639–44. doi:10.1016/j.applthermaleng.2011.07.020.

[128]   Preparation of nano-composite $Ca_2-\alpha Zn\alpha(OH)_4$ with high thermal storage capacity and improved recovery of stored heat energy. Open Eng 2015;5:42–7. doi:10.1515/eng-2015-0002.

[129]   Kallenberger PA, Brieler FJ, Posern K, Fröba M. Magnesium Sulfate/Polymer Composites for Seasonal, Thermochemical Energy Storage. Chemie-Ingenieur-Technik 2016;88:379–84. doi:10.1002/cite.201500095.

[130]   Bingre R, Louis B, Nguyen P. An Overview on Zeolite Shaping Technology and Solutions to Overcome Diffusion Limitations. Catalysts 2018;8:163. doi:10.3390/catal8040163.

5

Targets and structure of the thesis

A guidance for readers is provided in these sections along with the main objectives and targets of this thesis.

7. Bench study specifications

8. Material screening and selection

9. Working pairs

10. Proof of concept and scale-up

11. Potential applications and prospective

12. Conclusions and achievements

5. TARGETS AND STRUCTURE OF THE THESIS

As stressed in the previous section, thermal energy storage (TES) needs a breakthrough concept to enable its rapid deployment and contribute to achieving a net zero-carbon energy system. In this thesis, we propose an alternative storage strategy that looks beyond the three traditional TES technologies and proposes a novel concept where TES is brought to its ultimate level. Instead of thinking on TES based on either sensible, latent or thermochemical processes and tackle each technology challenges independently with incremental improvements, our vision is based on a holistic/synergistic and interdisciplinary approach. The idea goes around a consequent storage strategy utilizing sensible, latent and thermochemical processes in one single unit. Thus, opening a new vision of storing thermal energy, where the components are co-working synergistically to maximise the operational energy density while maintaining the controllability of the charge/ discharge processes; and at the same time enhance the efficiency and lifetime at the system level. In this 3 in 1 system, the main fundamental challenges of traditional TES technologies are surpassed: more compact system (sensible), accommodation of volume change (latent heat), higher energy conversion and life span (thermochemical). The eventual goal is to provide a novel technology that a) conceives a unique and revolutionary way to store thermal energy that can overpass the other TES technologies, b) follows a top-down approach to match the current energy requirements with the technology potential and c) constitutes the vehicle that suppresses the gap between TES technologies and applications that can potentially reuse a surplus of heat energy. This thesis layout proposes the 3 in 1 technology concept, proofs its feasibility through a detailed material study while explores and assesses its potential. **The main purpose is to conceptualise the 3 in 1 system, experimentally validate working pairs framing the candidates to low-medium temperature requirements (25 to 150**

°C), conduct a cycling study to come up with final candidates and explore the main applications/potential pathways of the technology.

The novel system proposed can be mainly studied at three levels: material level, thermodynamic level and reactor level as shown in Figure 13. The three levels are related to themselves and proper comprehension of such interaction is needed to successfully go through all of them. The key properties related to each level and the main burning questions that come up from this novel system are also shown.
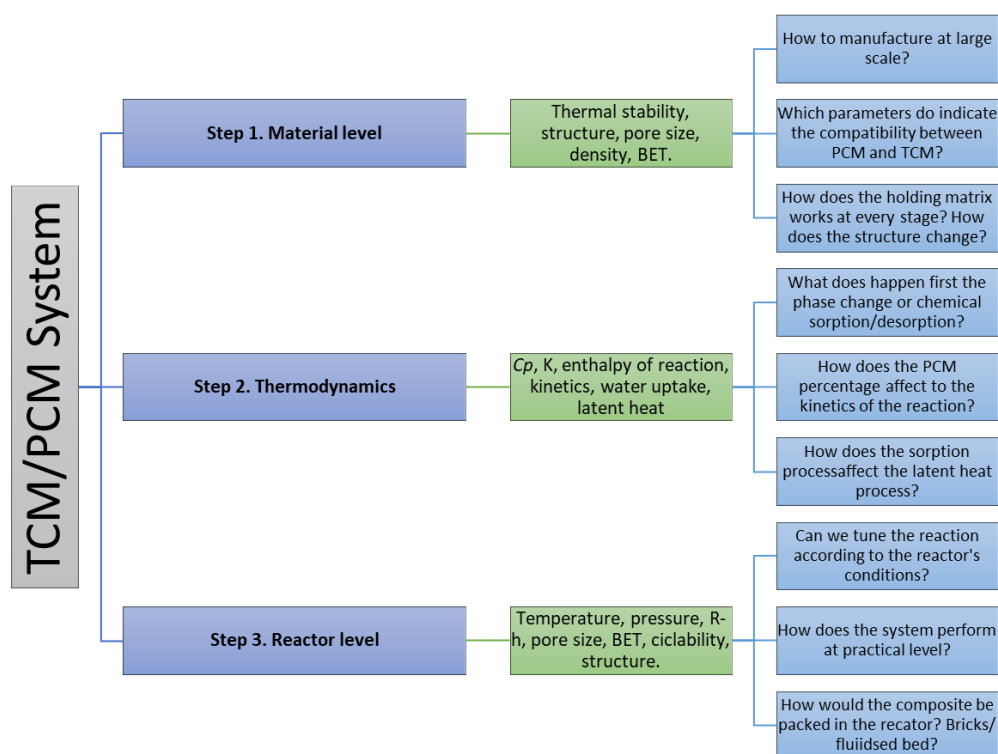
Figure 13. TCM/PCM system levels and main key properties and questions to address.

The first level, material level, is the first one to be approached given that the stability of the structure and physical integrity are key parameters to first develop a novel composite. In other words, in that level, the material is just seen as a combination of two materials where the study of the physical interaction and chemical compatibility of the composite is the main focus.

The thermodynamic level brings the study to the next level. In this case, it is not just about the physical and chemical interaction but how the physical interaction does affect the sorption and phase change process taking place in the composite. The material distribution and microstructure, the pore size and the thermal stability will affect the kinetics of the reaction altering the hydration rate. Thus, both levels must be studied in parallel because even if the formulation might work properly at the material level, it is important to consider also how it works at the thermodynamic level. The reactor level is the ultimate level to consider and it is strongly related to its application and performance within the TES system. Given the time limit during the thesis, the material was brought from conceptualisation to lab-scale and then scale-up material study; the reactor level study is beyond the scope of this thesis although is of high importance to understand all the implications of the TCM/PCM interactions at any level of knowledge. The flow chart to answer the raised questions is shown in Figure 14, from the conceptualisation, where the three systems are envisioned, to the prospectives of the 3 in 1 system, where the potential applications and future pathways are explored.
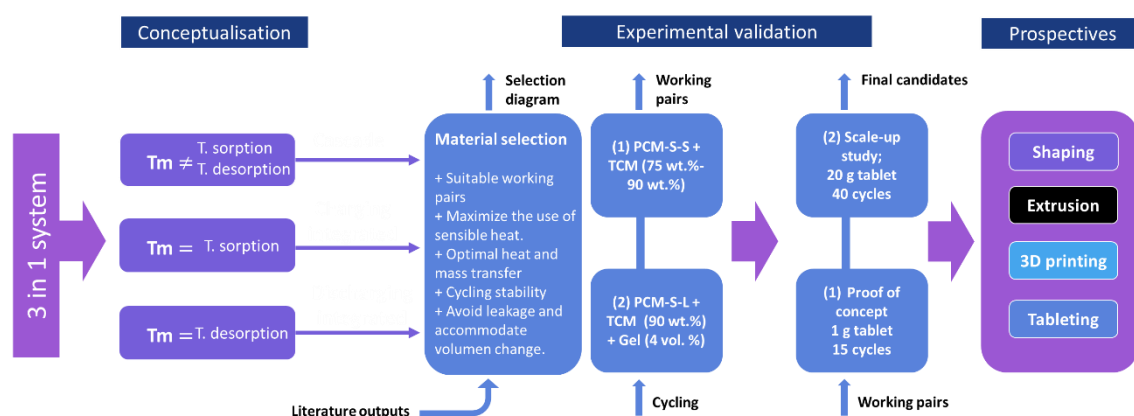
Figure 14. Flow chart of the 3 in 1 concept proposed in this thesis.

To achieve the stations shown in Figure 14, six main objectives have been targeted, which offer a balance of ambition and solid scientific knowledge. The objectives are listed below;

(1)   **OB1: Open a new TES technology pathway, where the new system will change the conventional TES classification.** The 3 in 1 system presents many unique attributes; the tactic combination of thermochemical energy storage materials (TCM) and phase change materials (PCM) that allows a more efficient low-grade waste heat recovery and a controlled charge/discharge process while maintaining a high energy density. This will be achieved by the conceptualisation of three 3 in 1 system according to the combination of TCM/PCM charging/discharging temperatures (cascade system, charging integrated, discharging integrated).

(2)   **OB2: The selection and screening of PCM and TCM candidates as the 3 in 1 working pairs.** Current TCM and PCM candidates are studied as potential candidates to conform the 3 in 1 working pairs experimentally validated in the thesis. A literature review is used to list the candidates and an experimental study with a set of characterisation techniques is conducted to come up with a selection of PCM and TCM candidates. Solid-solid and solid-liquid PCMs are both considered, while just salt hydrates are considered as TCM. The reason behind this is that the 3 in 1 system, for this thesis, is envisioned to work in a low-medium temperature range; salt hydrates have been targeted as high energy storage TCS materials at such temperature range. The selected candidates are then combined according to the three conceptual systems providing a list of potential working pairs.

(3)   **OB3: The optimization and experimental validation of various TCM/PCM pairs for different applications.** The set of working pairs selected from OB2 candidates are cycled (1 g tablet) and after a certain number of cycles, the physical and chemical stability are studied. This approach helps to discard the candidates that cannot initially withstand charging/discharging cycles prior to a deep understanding of the synergies between the three storage technologies combined. SSPCM/TCM in different percentages and SLPCM/TCM working pairs are studied to output an optimal TCM/PCM

ratio working range. In this stage, additional structural enablers materials are considered (e.g. gelling agents) and its compatibility with the 3 in 1 component is also studied. Final candidates, either combining SSPCM and SLPCM/gelling agent with the TCM are output from this process and further study.

(4)   **OB4: The study of proof of concept and validation.**   One of the optimised working pairs from OB3, keeping the same manufacturing specifications (1 g tablet), is experimentally validated to ensure their performance under a larger number of cycles and, therefore, to prove the feasibility of the 3 in 1 system looking not just at the physical integrity but at how the components interact (volume change, energy density, microstructure, crystal phases, etc). The final candidates are assessed following criteria of better performance under cycling conditions.

(5)   **OB5: The study of material scale-up and validation.** This objective is targeted to study the cyclability of the optimised working pairs in OB3. To prove the scalability of the 3 in 1 system in this stage the working pairs are 20 g tablets and are cycled over up to 40 charging/discharging cycles. Same detailed studied as in OB4 is conducted to understand the underlying mechanisms and interactions between TCM/PCM at this level.

(6)   **OB6: Explore how the 3 in 1 system can change the TES portrait by studying its integration into different applications and potential.** The 3 in 1 system is evaluated in terms of potential advantages and disadvantages over the traditional TES store and economically assessed comparing it to current TCS materials. How the system can be integrated at the device level (open or closed) and the added value of the 3 in 1 system is also studied. The integration of the 3 in 1 system into the current TES applications scheme (waste heat, building, solar energy, etc) is also considered, as it also provides multiple discharging/charging (output/input) temperatures, enabling a flexible energy storage system for coupling with renewables (especially solar power).

5.1 STRUCTURE OF THE THESIS

The thesis is structured in two main blocks; (1) Background on TES and (2) 3 in 1 system. Block 1 which includes Chapter 3; Introduction, and Chapter 4; TCS outlook, it is meant to situate the readers in the current energy scenario. Those chapters frame the 3 in 1 system in the current energy scenario and the state-of-the-art, which have been the foundation of the visualisation of the 3 in 1 system.

The second block is then a study, both theoretical and experimental, of the proposed 3 in 1 technology. The layout of the 3 in 1 system conceptualisation and development is shown in Figure 15. From Chapter 5 onwards, this thesis describes the 3 in 1 system in subsequent steps; in Chapter 6 the processes to store energy in the 3 in 1 system are introduced as well as the thermodynamics equations, working diagrams and energy levels. Chapter 7 describes the experimental methodology validation performed in Chapter 8, 9 and 10; it is meant to be a manual of the techniques and test conditions used. In Chapter 8 is presented the screening and selection of the two main components, thermochemical and phase change material, including a literature review and experimental validation under the conditions of interest. The working pairs proposed in Chapter 8 are experimentally studied in Chapter 9, aiming to provide a list of final candidates for the proof of concept and scale-up study (Chapter 10). To sum up, in chapter 11 a prospectives of the 3 in 1 system including potential and applications is provided.

3 in system conceptualization

Co-working matrix of TCM and PCM

System theoretical study

(1) Cascade

(2) Charging integrated

(3) Discharging integrated

Material screening

(1) Selection constrains

(2) Filters

(3) Candidates

PCM:

S-S and S-L

TCM:

Salt hydrates

Working pairs

(1) PCM-S-S + TCM (75wt.%-90wt.%)

(2) PCM-S-L + TCM (90 wt.%) + Gel (4%)

Proof of concept

(1) 20 cycles: 1 g tablets

(2) 40 cycles: 20 g tablets

Potential and Applications

Figure 15. The layout of 3 in 1 concept proposal in this thesis.

6 HIBRID TES SYSTEM: 3 IN 1 CONCEPT

1. Thesis time-line
Guidance

2. Scientific dissemination

3. Introduction

4. TCS Outlook

5. Innovation needs and targets

6. Hybrid TES system:
3 in 1 concept

In this section the 3 in 1 system operability and processes involved are described. Firstly, the three systems obtained from the tactical combination of the thermochemical and phase change material technologies are described: cascade system, charging integrated and discharging integrated. Then, the processes involved, and the thermodynamic equations of the storage are detailed. To wrap up, a section on theoretical potential material selection is provided at the end of this chapter.

7. Bench study specifications

8. Material screening and selection

9. 3 in 1 working pairs

10. Proof of concept

11. Potential applications and prospective

12. Conclusions and achievements

6. HYBRID TES SYSTEM: 3 IN 1 CONCEPT

6.1 SYSTEMS

The 3 in 1 system compiles the strengths of all three TES systems (sensible, latent and thermochemical) by using its components as a synergic matrix that allows structural integrity along with the different storage processes. The 3 in 1 system consists of the combination of both thermochemical materials (TCMs) and phase change materials (PCMs) in one stand-alone system. The unique combination works accommodating the volume change (contraction) of the TCM when dehydrating and holding the structure after several cycles. The 3 in 1 system structure will be constituted by both, PCM and TCM, being in some cases the content of TCM up to nine times higher than the PCM.

To understand how each TES technology behaves within the triple storage media, the fundaments of each solely TES technology are fully explained in Table 1. In the 3 in 1 hybrid system, thermochemical heat storage is added by means of the TCM, while the PCM allows for the latent heat storage. Both materials are at the same time capable of storing a certain amount of heat, proportional to the temperature rise of the medium, as sensible heat. A composite made of different percentages of TCM and PCM material would be placed into a storage unit for charging and discharging trough an external heat source. The output and input temperature of the system will be determined by the charging and discharging processes involved in the storage. The integrated 3 in 1 hybrid system designed will match the output/input temperatures with the charging/discharging temperatures of the storage media. This is given by the TCM attributes to discharge (discharging temperature) and charge (charging temperature) at unequal temperatures, while PCM charges/discharges at the same narrow temperature (melting point). From those singularities, three different systems can be achieved by

selecting the charging/discharging temperature of the PCM and TCM: cascade, charging integrated and discharging integrated, as described below (see Figure 16). The PCM melting point (T_L) dictates the type of system that we would be looking at; as seen in Figure 16, where the same temperatures for sorption/desorption are considered for simplicity purposes. For a better understanding of the system energy absorption/release and working mechanisms, diagrams are provided in the following subsections for each of the 3 in 1 systems proposed.
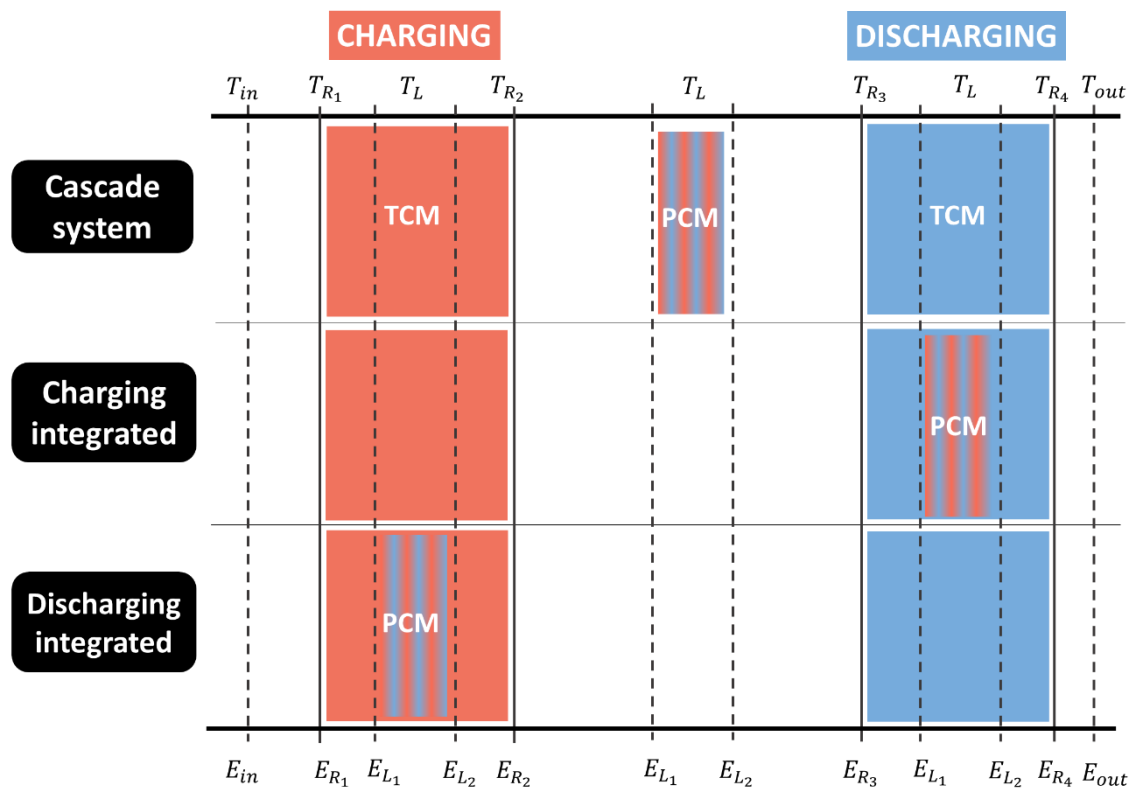
Figure 16. Energy and temperature diagram of the TCM/PCM combination for cascade, charging integrated and discharging integrated system. T_{in} is the initial temperature, T_{out} is the final temperature, T_L is the melting point of the PCM, T_{R1} is the starting desorption/forward temperature, the T_{R2} is the final desorption/forward reaction, T_{R3} is the starting sorption/backward temperature, which is considered at a constant temperature.

6.1.1 CASCADE SYSTEM

The cascade system can be seen in a similar way as a conventional cascade system widely used in the storage sector (see Figure 17 and Figure 18). However, in this case, the charging and discharging temperatures are given by the different PCM's melting point and TCM's reactions temperatures. The melting point of the PCM will lie in between the discharging-charging process of the TCM, the system will be charged and discharged at two different temperatures allowing to have two input/output temperatures. Thereof, the cascade system will be able to store a large amount of energy in a wide temperature range. The PCM will firstly store heat at the melting point, increasing its volume during the phase transition. Once the system will be at the TCM's charging temperature, it will start storing energy, both PCM and TCM will keep this energy within the system. When desired, the temperature of the system will decrease discharging, in the first place the PCM, and eventually, the TCM at its discharging temperature.

Ideally, the structural support would be provided mainly by the PCM, when the PCM changes phase (either solid-solid or solid-liquid) it experiences a volume change that will accommodate the thermochemical reaction to take place. However, this is dependent on the material selection which aims the 3 in 1 composite work as a co-working matrix in a synergistic manner. In the way that both PCM and TCM support each other, forming a countered force system that could work in equilibria.

Since the phase change occurs at a constant temperature, far from the desorption temperature, the processes will not be affected by the TCM reactions, if both material are chemically compatible in the working temperature range. At the desorption temperature ($T = T_{desorp.}$), the latent heat and the sensible heat at that temperature are already stored in the system. Consequently, the thermochemical heat will start its desorption process and at the final desorption temperature the latent heat, the heat of

reaction and the sensible heat, from both TCM and PCM, will be stored. At this point (T> $T_{desorp.}$), the system will be fully charged and could store its energy with almost no heat losses. The inverse process, when discharging the system, will occur following to consequential steps, first PCM and then TCM in the reverse order. At a temperature lower than the sorption temperature, the system will be fully discharged.
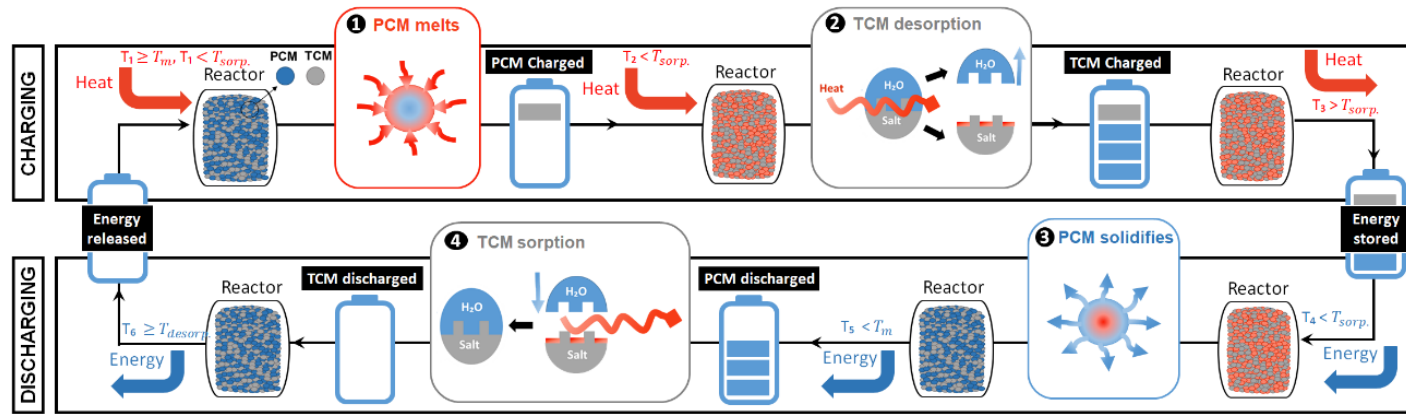
Figure 17. Cascade system working mechanism, where the charging and discharging processes are schematically illustrated. T_n refers to the temperature level (e.g. T_1 is the first temperature level), T_m is the melting point of the phase change material, $T_{sorp.}$ is the sorption temperature of the thermochemical material and $T_{desorp.}$ is the desorption temperature of the thermochemical material.
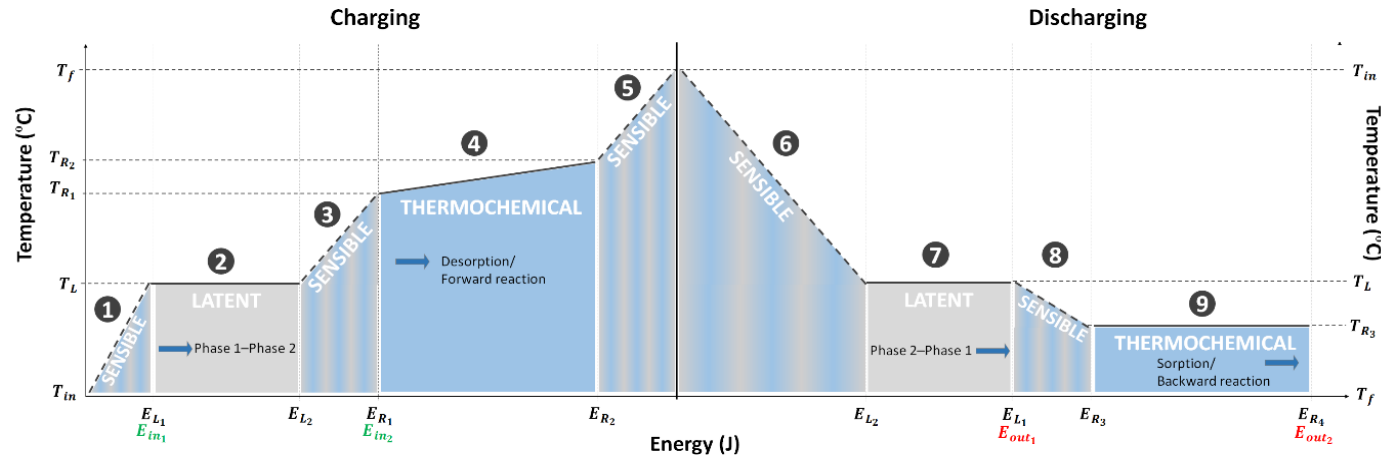
Figure 18. Cascade system energy diagram, where the energy stored/released through the charging/discharging processes is presented. E_{in1} is the first energy input to charge the PCM, E_{L1} and E_{L2} are the energy levels involved in the phase change, E_{in2} is the second energy input to charge the TCM, E_{R1} and E_{R2} are the energy involved in the thermochemical desorption and E_{R3} and E_{R4} are the energy levels involved in the thermochemical sorption; E_{out1} is the first energy output and E_{out2} is the second energy output. T_{in} is the initial temperature, T_f is the final temperature, T_L is the melting point of the PCM, T_{R1} is the starting desorption/forward temperature, the T_{R2} is the final desorption/forward reaction, T_{R3} is the starting sorption/backward temperature, which is considered at a constant temperature. The numbers in the figure are linked to the equations listed in Table 1.

6.1.2 CHARGING INTEGRATED

The charging integrated system is called after the concept of charging at the same temperature (or temperature range) and discharging at two different temperatures (see Figure 19 and Figure 20). Following the same rationale as in the cascade system, the TCM and PCM charges at the same temperature but discharges separately; the phase change temperature of the PCM lays around the charging temperature of the TCM. The system can be charged for both TES media by using a stable input temperature. Once the thermochemical material starts charging the PCM will simultaneously store energy, the system will keep the energy up to the upper operational temperature. The discharging process will happen firstly for the PCM, and secondly for the TCM when reaching the discharging temperature.

When charging, the volume increase of the system will be at its highest value because of the PCM phase change, which will be depending on the PCM selected and the TCM desorption process. To allow a stable TCM structure, avoiding agglomeration and assuring a constant conversion rate during the cycles, solid-solid PCMs will be preferable selected, although optimal working pairs S-L could be found. The synergy between both components is critical since they charge at the same temperature range. The phase change constant temperature might affect the desorption process by changing the kinetics of the reaction. Ideally, the low volume change of these phase change materials will assure the overall composite integrity by 'absorbing' and 'countering' the volume change from low to high hydrates from the thermochemical material.

At the final desorption temperature (T $_{desorp.}$), the system will be completely charged (latent heat, the heat of reaction and sensible heat). The system can store the heat at higher temperatures if the material selected can withstand the operational temperatures. When discharging, the PCM will first discharge by contracting its volume

and lowering the temperature of the reactor, this will allow reaching the sorption temperature for a fully discharged system.
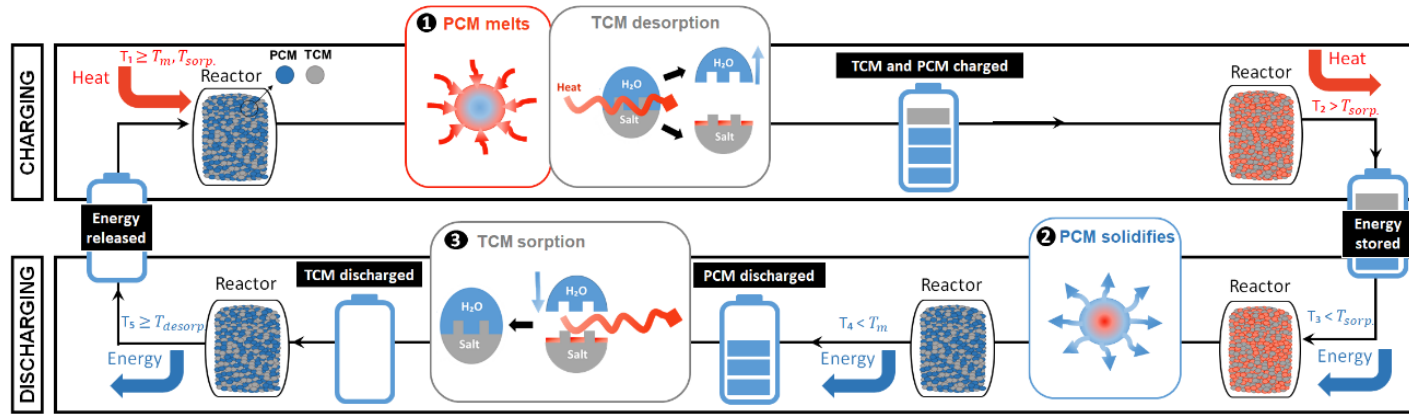
Figure 19. Charging integrated system working mechanism, where the charging and discharging processes are schematically illustrated. T_n refers to the temperature level (e.g. T_1 is the first temperature level), T_m is the melting point of the phase change material, $T_{sorp.}$ is the sorption temperature of the thermochemical material and $T_{desorp.}$ is the desorption temperature of the thermochemical material.
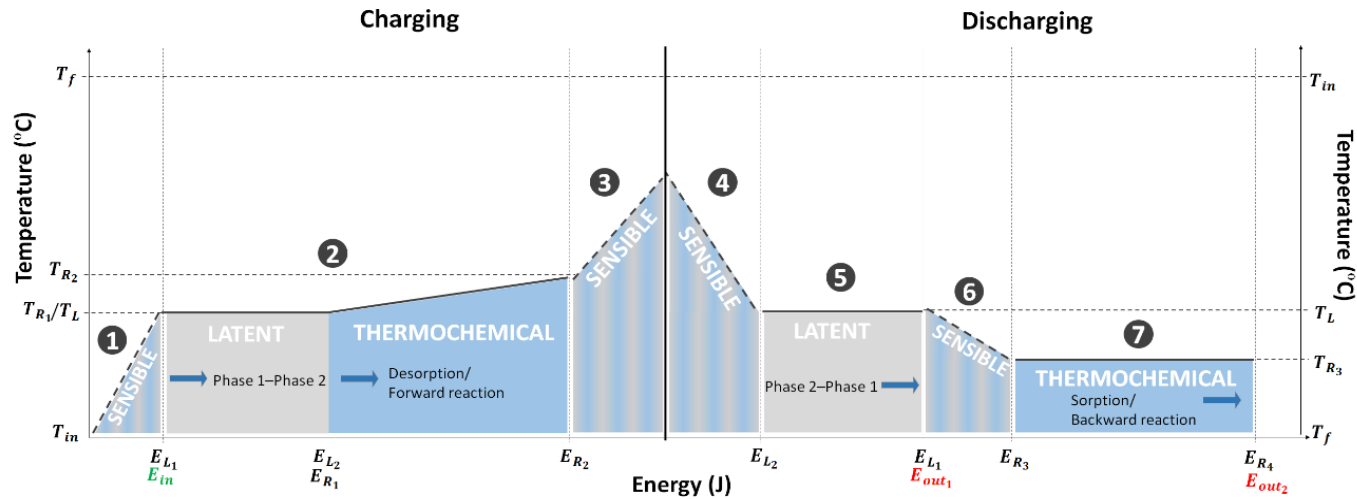
Figure 20. Charging integrated system energy diagram, where the energy stored/released through the charging/discharging processes is presented. E_{in1} is the first energy input to charge the PCM and the TCM; E_{L1} and E_{L2} are the energy levels involved in the phase change; E_{R1} and E_{R2} are the energy involved in the thermochemical desorption and E_{R3} and E_{R4} are the energy levels involved in the thermochemical sorption; E_{out1} is the first energy output and E_{out2} is the second energy output. T_{in} is the initial temperature, T_f is the final temperature, T_L is the melting point of the PCM, T_{R1} is the starting desorption/forward temperature, the T_{R2} is the final desorption/forward reaction, T_{R3} is the starting sorption/backward temperature, which is considered at a constant temperature. The numbers in the figure are linked to the equations listed in Table 1.

6.1.3 DISCHARGING INTEGRATED

The discharging integrated system works mirroring the charging integrated system, TCM and PCM will charge at different temperatures but discharging at the same temperature range (see Figure 21 and Figure 22). The melting point of the PCM and discharging temperature of the TCM lie together, allowing a controlled output temperature and discharging process. In this particular case, during the PCM phase change, the TCM/PCM co-working matrix will act as the supporting structure of the composite. Firstly, the PCM will experience the volume expansion and later the TCM sorption reaction will take place. As for charging integrated a solid-solid phase change material is also preferred, although optimal working pair can be explored. This fact will be discussed in depth over the next sections.

Material selection is also crucial to this system, the synergies between both working pairs must be appropriate to allow the system to charge and discharge (especially for the discharging process). The TCM selected needs to avoid the PCM leakage and the TCM/PCM composite needs to allow the heat and mass transfer. A TCM with low volume change is preferred to assure a reliable composite microstructure. During the discharging process, at the same temperature the PCM will contract and the TCM mass will increase. At this point, the system will be discharged releasing the energy coming from the latent heat, the heat of reaction and the sensible heat at a constant temperature.

For further reference in the thesis, the energy equations for each of the systems are listed in Table 6. The assumptions for the equations are as follows: Open system, constant pressure, constant specific heat, kinetic and potential energy are negligible and there are no energy losses. These equations are linked to Figure 20, Figure 22 and Figure

18 with the numbers in bold, in the way that different energy equations are provided for each storage segment.
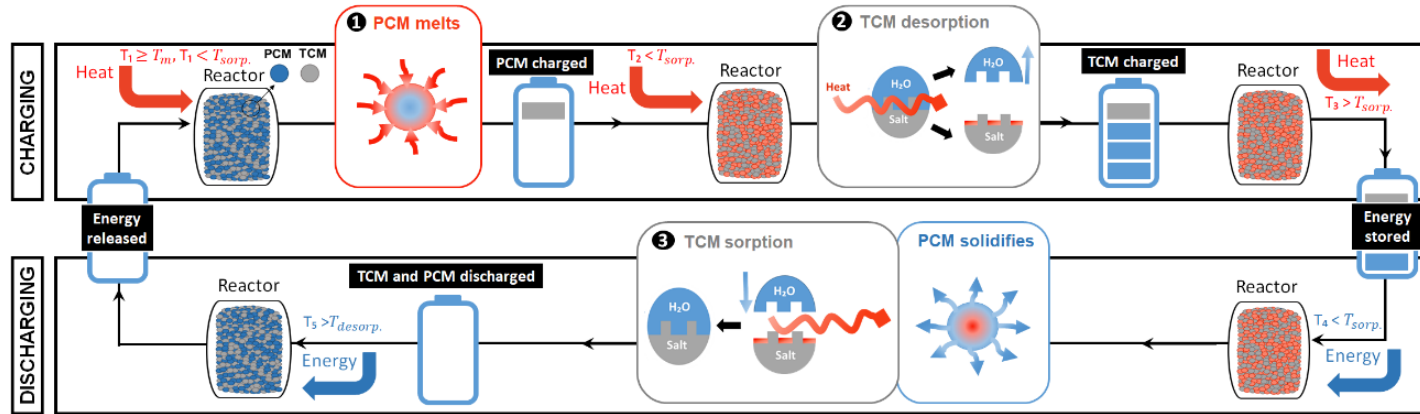
Figure 21. Discharging integrated system working mechanism, where the charging and discharging processes are schematically illustrated. T_n refers to the temperature level (e.g. T_1 is the first temperature level), T_m is the melting point of the phase change material, $T_{sorp.}$ is the sorption temperature of the thermochemical material and $T_{desorp.}$ is the desorption temperature of the thermochemical material.
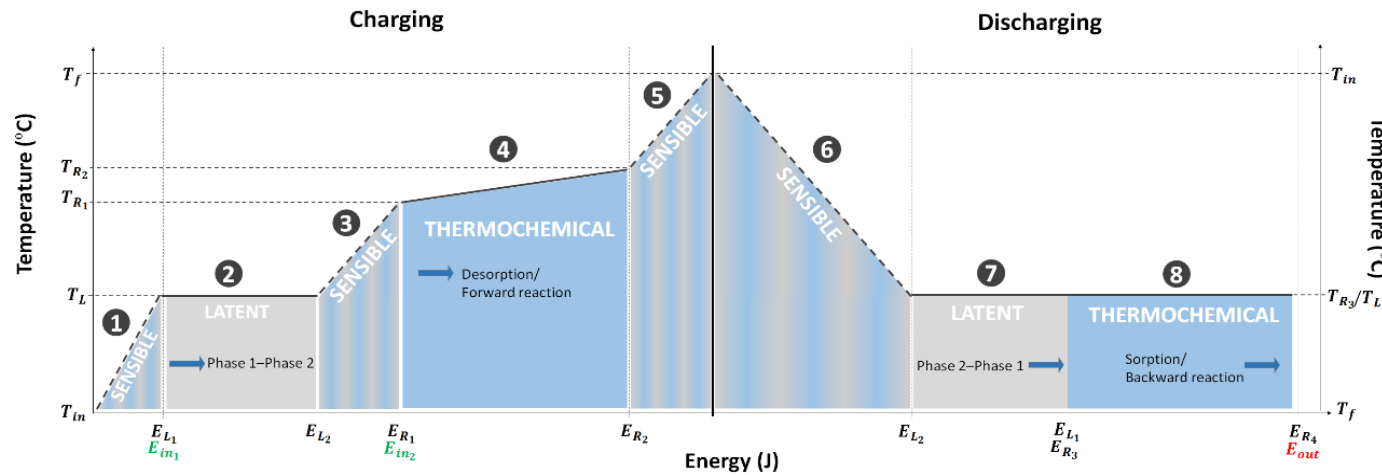
Figure 22. Discharging integrated system energy diagram, where the energy stored/released through the charging/discharging processes is presented. E_{in1} is the first energy input to charge the PCM, E_{L1} and E_{L2} are the energy levels involved in the phase change, E_{in2} is the second energy input to charge the TCM, E_{R1} and E_{R2} are the energy involved in the thermochemical desorption and E_{R3} and E_{R4} are the energy levels involved in the thermochemical sorption; E_{out} is the energy output. T_{in} is the initial temperature, T_f is the final temperature, T_L is the melting point of the PCM, T_{R1} is the starting desorption/forward temperature, the T_{R2} is the final desorption/forward reaction, T_{R3} is the starting sorption/backward temperature, which is considered at a constant temperature. The numbers in the figure are linked to the equations listed in Table 1.

Table 6. Equations for charging and discharging at each energy level described in Figures 20 to 22, the n° in the table refers to the numbers of the process in the Figure. M_R is the mass of the TCM at the reaction time, M_L is the mass of the PCM, Cp_R is the specific heat of the TCM at the reaction time, Cp_L is the specific heat of the PCM at the reaction time, T_{in} is the initial temperature, T_f is the final temperature, T_L is the melting point of the PCM, T_{R1} is the starting desorption/backward temperature, the T_{R2} is the final desorption/backward reaction, T_{R3} is the starting sorption/forward temperature and T_{R4} is the final desorption/forward reaction temperature (in case of not happening at a constant temperature, otherwise just T_{R3} will be considered).

N°	Cascade system	Charging integrated	Discharging integrated
1	$Q_1 = M_R \cdot Cp_R \cdot (T_L - T_{in}) + M_L \cdot Cp_L \cdot (T_L - T_{in})$	$Q_1 = M_R \cdot Cp_R \cdot \left(T_{R_{1/L}} - T_{in}\right) + M_L \cdot Cp_L \cdot \left(T_{R_{1/L}} - T_{in}\right)$	$Q_1 = M_R \cdot Cp_R \cdot (T_L - T_{in}) + M_L \cdot Cp_L \cdot (T_L - T_{in})$
2	$Q_2 = \Delta H_L \cdot M_L$	$Q_2 = \Delta H_R \cdot M_R + \Delta H_L \cdot M_L + M_R \cdot Cp_R \cdot \left(T_{R_2} - T_{R_{1/L}}\right) + M_L \cdot Cp_L \cdot \left(T_{R_2} - T_{R_{1/L}}\right)$	$Q_2 = \Delta H_L \cdot M_L$
3	$Q_3 = M_R \cdot Cp_R \cdot (T_{R_1} - T_L) + M_L \cdot Cp_L \cdot (T_{R_1} - T_L)$	$Q_3 = M_R \cdot Cp_R \cdot (T_f - T_{R_2}) + M_L \cdot Cp_L \cdot (T_f - T_{R_2})$	$Q_3 = M_R \cdot Cp_R \cdot (T_{R_1} - T_L) + M_L \cdot Cp_L \cdot (T_{R_1} - T_L)$
4	$Q_4 = \Delta H_R \cdot M_R + M_R \cdot Cp_R \cdot (T_{R_2} - T_{R_1}) + M_L \cdot Cp_L \cdot (T_{R_2} - T_{R_1})$	$Q_4 = M_R \cdot Cp_R \cdot (T_L - T_{in}) + M_L \cdot Cp_L \cdot (T_L - T_{in})$	$Q_4 = \Delta H_R \cdot M_R + M_R \cdot Cp_R \cdot (T_{R_2} - T_{R_1}) + M_L \cdot Cp_L \cdot (T_{R_2} - T_{R_1})$
5	$Q_5 = M_R \cdot Cp_R \cdot (T_f - T_{R_2}) + M_L \cdot Cp_L \cdot (T_f - T_{R_2})$	$Q_5 = \Delta H_L \cdot M_L$	$Q_5 = M_R \cdot Cp_R \cdot (T_f - T_{R_2}) + M_L \cdot Cp_L \cdot (T_f - T_{R_2})$
6	$Q_6 = M_R \cdot Cp_R \cdot (T_L - T_{in}) + M_L \cdot Cp_L \cdot (T_L - T_{in})$	$Q_6 = M_R \cdot Cp_R \cdot (T_{R_3} - T_L) + M_L \cdot Cp_L \cdot (T_{R_3} - T_L)$	$Q_6 = M_R \cdot Cp_R \cdot \left(T_{R_{3/L}} - T_{in}\right) + M_L \cdot Cp_L \cdot \left(T_{R_{3/L}} - T_{in}\right)$
7	$Q_7 = \Delta H_L \cdot M_L$	$Q_7 = \Delta H_R \cdot M_R + M_R \cdot Cp_R \cdot (T_f - T_{R_3}) + M_L \cdot Cp_L \cdot (T_f - T_{R_3})$	$Q_{7/8} = \Delta H_L \cdot M_L + \Delta H_R \cdot M_R + M_R \cdot Cp_R \cdot \left(T_f - T_{R_{3/L}}\right) + M_L \cdot Cp_L \cdot \left(T_f - T_{R_{3/L}}\right)$
8	$Q_8 = M_R \cdot Cp_R \cdot (T_{R_3} - T_L) + M_L \cdot Cp_L \cdot (T_{R_3} - T_L)$		
9	$Q_9 = \Delta H_R \cdot M_R + M_R \cdot Cp_R \cdot (T_f - T_{R_3}) + M_L \cdot Cp_L \cdot (T_f - T_{R_3})$		

6.2 POTENTIAL MATERIAL AND SYSTEM SELECTION

As presented throughout the previous sections, TCM technology is already seen as a high ranked candidate for compact short and long-term storage applications. However, its full potential is yet to be explored since one of the main challenges when it comes to storage media is the need of stale matrices to hold the charging/discharging reactions and overcome problems such as poor reaction reversibility, lower than anticipated efficiencies and agglomeration over cycles. The uniqueness of the 3 in 1 system relies on the fact that one component can act as the matrix of the other when charging/discharging. To ensure optimal performance, a suitable PCM/TCM selection for each of the above-mentioned systems is needed. The novel system potentially relies on the energy stored due to the specific heat capacity of the composite material, the phase change and the chemical reaction, which properties need to remain unaltered over the thermal cycles. The selection needs to meet the required capacity to store heat in the three forms (energy - the amount of heat stored) and optimal kinetics of the storage/release processes (power - the rate to heat charge and discharge processes). The energy and power requirements should remain unaltered over the thermal cycles. These also means adequate mass and heat transfer during the charging and discharging processes. Also, the new 3 in 1 system performance will be affected by the optimal combination of the three heat storage media. To achieve the above, the selection of materials should consider the following:

- Maximize the use of sensible heat during the working temperature range.

- Accommodate the volume change of the TCM and PCM to avoid leakage and obtain a mechanically reliable structure.

- Achieve optimal heat and mass transfer for a maximum output performance.

-     Maintain chemical and structural stability during cycles.

The selection of the PCM/TCM pair will depend on the system selected: cascade, charging integrated and discharging integrated; as well as the operating temperatures. Some of the TCM and PCM requirements, as well as material level challenges for the 3 in 1 material selection, are listed in Table 7.

Table 7. Material requirements and experimental challenges for 3 in 1 system selection.

System	TCM requirements	PCM requirements	Challenges
Common	* Fairly chemically and physically stable over cycles. * Low agglomeration over cycles. * Melting point TCM higher than charging temperature.	* High viscosity. * High flashpoint. * Structurally stable over the working temperature. * Low volume change. * Compatible with TCM. * Low cost. * Easily available.	* Avoid the use of binders. * Material compatibility. * Structural integrity * Leakage * Heat and mass transfer channels.
Cascade	* Low charging temperature. * Wide charge-discharge temperature difference. * Narrow charging temperature range (if there).	* Solid-solid transition (preferable). * Medium-high melting point.	* Consequential processes (conversion over cycles, subcooling, etc). * Input and output temperature integration.
Charging integrated	* Structurally stable to act as a co-working matrix. * Low charging temperature.	* Match phase change with charging temperature. * Good physical integrity (potential matrix). * High melting point.	* Coexisting phase change and thermochemical reaction. * The use of S-L PCM. * PCM screening.
Discharging integrated	* Structurally stable to act as a holding matrix. * Narrow charge-discharge temperature difference. * Low charging temperature.	* Match phase change with discharging temperature. * Good physical integrity (potential matrix). * Low melting point.	* Coexisting phase change and thermochemical reaction. * The use of S-L PCM. * Find PCM with a low melting point that can withstand temperatures up to 150°C. * PCM screening.

The variety of materials and working temperatures range gives us multiple working pair possibilities for the 3 in 1; see Figure 23. In the following paragraphs, we present the possible PCM and TCM candidates for the 3 in 1 working pairs. Although thermochemical materials can store heat in a wide temperature range, here we just explore the combination considering low to medium temperature applications. TCMs, due to the reaction process, it can be found in different forms, with varying properties (density, thermal conductivity, specific heat capacity, etc.). Depending on the interface between sorbent and sorbate, sorption can be divided into four types: solid/gas, solid/liquid, liquid/liquid, and liquid/gas [1]. Liquid-gas systems, also called absorption systems, are promising storage options because they can be pumped and used as the working heat transfer fluid. In these systems, the energy is stored by the concentration changes in a solution (strong and weak). The most promising materials studied in the literature are Calcium Chloride ($CaCl_2$), Lithium Chloride (LiCl), Lithium Bromide (LiBr), Sodium Hydroxide (NaOH), Potassium Hydroxide (KOH) and Ammonia [1]. Adsorption systems commonly involve either solid/liquid or solid/gas, storing energy by the adsorption of a sorbent (normally water) on the surface of a porous material. Zeolites, silica gel and Metal-organic frameworks (MOF's) are the most common solid adsorbents. Chemical reactions are commonly a simultaneous chemical/adsorption processes based on the reversible reaction of a solid and a gas. Normally involving a hydration/dehydration reaction (charging/discharging), which are generally assumed to be hydrated with a high number of crystal water molecules. The most promising candidates mainly include $MgSO_4 \cdot 7H_2O$, $SrBr_2 \cdot 6H_2O$, $Na_2S \cdot 9H_2O$, $MgCl_2 \cdot 6H_2O$, from which $SrBr_2 \cdot 6H_2O$ has high stability and good energy density but high-cost; the $Na_2S \cdot 9H_2O$ has the highest energy density but also highly corrosive.

PCM, in the TCM/PCM composite, could be found as well in different phase states. Solid/liquid or viscous-gel PCM's phase change undergoes an internal molecular arrangement that starts on an ordered structure (crystalline/semi-crystalline or amorphous) and ends in a more disordered structure (liquid/viscous-gel) above the phase transition. Solid/liquid PCMs commonly include paraffin (organic PCM), inorganic salts (inorganic PCM) or mixtures [2]. The main challenges when selecting a solid/liquid PCM is the need for containment or encapsulation to avoid leakage. In solid/solid PCMs, the intramolecular arrangement prevents leakage and minimizes volume change but, as a result, they exhibit relatively lower energy densities [2]. Currently, the most promising solid-solid PCMs are polyalcohols (organic), polyethylenes (polymeric) and layered perovskites (organometallics) [3]. Among polyalcohols, neopentyl glycol (NPG), pentaerythritol (PE), trihydroxy methyl-aminomethane (TAM), pentaglycerol (PG) are the prevailing subjects of investigations [4]. Polyalcohols such as PE, PG and NPG are known to have solid-solid transition enthalpies which are comparable to the fusion enthalpies of paraffin [5]. In polymeric PCMs, the phase change is structurally incorporated by different chain arrangements (side-chain grafting, bock-polymerisation, hyper-branching or crosslinking copolymerization). The transition temperature can be tailored by adjusting the chain length or the rigidity of the polymer, which could show great potential for the 3 in 1 proposed in this paper. Organometallic PCMs are another type of solid-solid PCMs, which are a group of perovskites that alternate inorganic and organic layers (sandwich crystalline structure). They absorb heat when the organic layer undergoes a phase transition while the inorganic layer remains unaltered. Even though the thermal conductivity of organometallics is higher than paraffin, the relatively high density of these materials makes them less suitable for certain weight constrained applications [2].

Figure 23. 3 in 1 system potential material's selection diagram.

The new materials can be thoroughly designed to perform in the desired working temperature range, adapting to different system configurations. The wide TCM material's combinations provides a tuneable system that can be tailored to the application's needs (input and output temperature, charging/discharging rate, system size, cost and lifetime). From the TCM technological point of view, the hybridisation with latent heat allows a more efficient low-grade heat recovery, controlled charge/discharge process and a high energy density storage media. Low percentages of PCM enables optimal TCM loadings (80-95 wt.%), which maximises the TCM content while accommodating the volume change (contraction) of the TCM when dehydrating as it can be seen in Section 9 of the thesis. This combination benefits the PCM technology prospective since it opens up a whole range of possibilities for latent heat storage materials. PCM has been always characterized to work in a narrow temperature range given its thermal heat storage characteristics. However, in this 3 in 1 system, latent heat technology is able to diversify and extend its versatility towards new sectors. The TCM active material can increase the energy density of the overall system. Besides, another

strength of the 3 in 1 system is that the TCM/PCM composite could be manufactured following conventional routes. Nowadays, the most popular method to prepare thermochemical composites is by the impregnation of an hygroscopic salt into a porous host matrix in any of its forms: direct, wet, vacuum, etc. This route has not step forward from lab scale towards large scale manufacturing. The most obvious, simple and convenient way of stabilising TCM materials is by shaping, which maximises the energy stored while shaping the pure salt in the form of granulates or pellets. The current state-of-the-art of THC does not allow the shaping route or any other simple manufacturing routes at large scale. The 3 in 1 system has the potential of marketability through tabletting (when selecting a solid-solid PCM) or extrusion (when using polymeric PCMs) that will open the manufacturing path for the TCM sector. Some of the manufacturing routes already used in PCM's could be used for this 3 in 1 system, further proving its commercial viability.

The diagram shown in Figure 24 explores how the 3 in 1 system can shape the TES system design and selection process. The decision tree, according to the authors, follows the common rationale when selecting a TES system from sensible, latent and thermochemical heat, yet we integrate the novel 3 in 1 system into the decision-making process, unlocking new potential solutions. This new concept could draw a new and revolutionary picture of TES, that includes the 3 in 1 system which in turn extends the TES application areas, previously unattainable via TCMs.
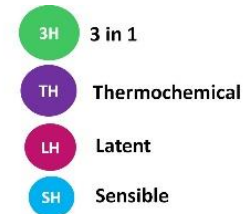
Figure 24. TES decision tree following technology selection rationale. The system (blue) and material decisions (grey) guides the storage selection.

The system selection will follow a similar rationale as the one applied for conventional TCS systems. Although in the 3 in 1, the system could be designed to meet application requirements and be tailored to the working pair selected. This will be explained later in the thesis (Chapter 11. Potential applications and prospective).

6.3 REFERENCES

[1]   Lele AF. State-of-Art of Thermochemical Heat Storage Systems. 2016. doi:10.1007/978-3-319-41228-3.

[2]   Fallahi A, Guldentops G, Tao M, Granados-Focil S, Van Dessel S. Review on solid-solid phase change materials for thermal energy storage: Molecular structure and thermal properties. Appl Therm Eng 2017;127:1427–41. doi:10.1016/j.applthermaleng.2017.08.161.

[3]   Gao W, Lin W, Liu T, Xia C. An experimental study on the heat storage performances of polyalcohols npg, tam, pe, and ampd and their mixtures as solid-solid phase-change materials for solar energy applications. Int J Green Energy 2007;4:301–11. doi:10.1080/15435070701332112.

[4]   Gao WF, Lin WX, Liu T, Li M. An experimental study on the application of polyalcohol solid-solid phase change materials in solar drying with cross-corrugated solar air collectors. IOP Conf Ser Earth Environ Sci 2017;93. doi:10.1088/1755-1315/93/1/012075.

[5]   R.W BJ. BD. W. SOLID STATE PHASE TRANSITIONS IN PENTAERYTHRITOL AND RELATED POLYHYDRIC ALCOHOLS. Sol Energy Mater 13 1986;13:133–52.

7

BENCH STUDY SPECIFICATIONS

1. Thesis timeline

2. Scientific contributions

3. Introduction

4. TCS Outlook

5. Targets and structure of the thesis

6. Hybrid TES system:

3 in 1 concept

Section 7 works as a technical specifications section including the relevant properties, the techniques/equipment used for experimentally validate the novel system proposed in the thesis and the specifications for the measurements conducted. Along the thesis this section is referenced, for concision purposes the general methodology of the thesis is summarised in this section.

7. Bench study specifications

8. Material screening and selection

9. Working pairs

10. Proof of concept and scale-up

11. Potential applications and prospective

12. Conclusions and achievements
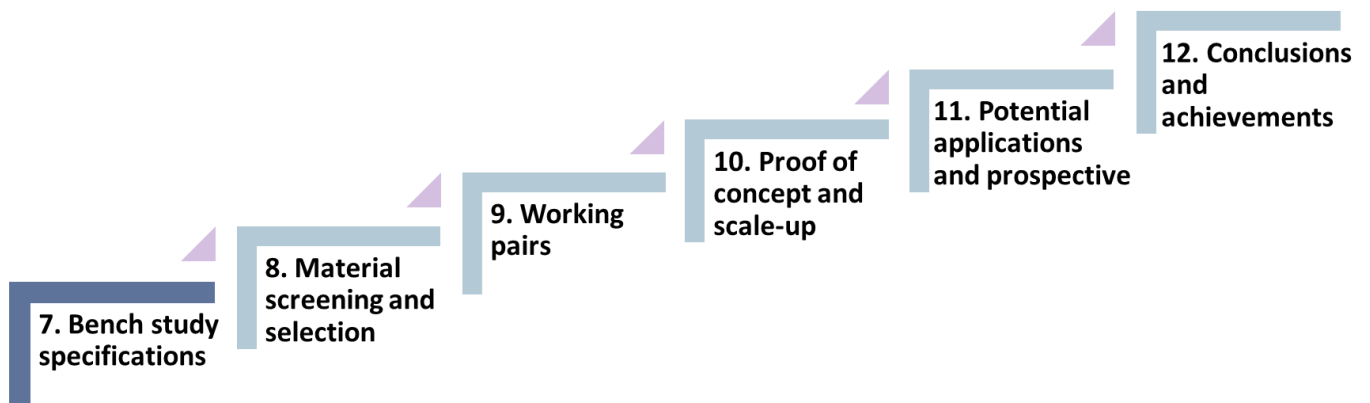
7. BENCH STUDY SPECIFICATIONS

The bench study conducted in this thesis has been mainly based on the commonly key properties measured in TES, specifically in TCS. However, some less researched properties for thermochemical materials such as specific heat and thermal conductivity have been also measured and interesting insights were raised from the study. As described in Section 5, the 3 in 1 composite component are firstly characterised separately as pure TCM and pure PCM. Then, the working pairs are investigated as TCM/PCM combinations. Different conditions are used for the pure TCMs, pure PCMs and the TCM/PCM combinations. In the base material study the specifications are the same to all TCM and PCM to ease the experimental investigation. Nevertheless, the charging/discharging conditions used for the different TCM/PCM combination were determined by the TCM working conditions and the PCM maximum temperature.

The list of properties is defined in Section 4.1 and the potential techniques used to determine them are described. The techniques used to determine the selected properties are determined by the lab facilities and equipment availability, see Section 4.2. The test conditions such as temperature range, heating rate, atmosphere, etc, are listed in Section 4.3.

7.1 PROPERTIES

In this section the relevant properties to TCS are presented and defined, considering that information already available in the thesis, here we list the relevant properties to our research (see Table 8) as well as the available methods used to measure the property and the specification for each method.

Table 8. Relevant properties to the 3 in 1 system study and potential methods/techniques used to determine them.

Property	Depends on	Influences on	Methodology	Specifications
Porosity	Material	Sorption rate Mass and heat transfer Permeability	BET	Small sample size, powder form. Preferred non-hygroscopic materials. Small pore size detection Easy and fast. Closed pores are not measured.
			Mercury porosimeter	Higher pore size detection. Small sample size. Easy and fast. Closed pores are not measured.
			Helium pycnometer	Not suitable for hygroscopic materials. Indirect measurement. Easy and fast. Closed pores are not measured.
			X-Ray Tomography	Enables tablet measurements. Open and closed porosity. Comparative between samples. Time-consuming.
Sorption rate/melting point/ Energy density/Hydration/dehydration temperature/specific heat	System and material	Input/output power	Differential Scanning Calorimetry (DSC)	Small sample size. Controlled atmosphere. Easy and simple. Difficult to control conditions (especially humidity inside the chamber)
			Simultaneous Thermal Analysis (STA)	Larger sample size than DSC. Less accurate than DSC. Controlled atmosphere. Easy and simple.
Volume change	Material	Reactor design, porosity/permeability	Dilatometry techniques	Limited sample size. Measurement during heating and cooling. Allows for tablet measurements.
Chemical and physical stability	Material and system	Input/output power Sorption rate Mass and heat transfer Permeability/porosity	X-Ray Diffraction	Crystal phases identification. Phases at different temperature steps. Dependent on grain size and crystal structure. Non-destructive technique. Difficult to measure low concentrations.
			FTIR spectroscopy	Non-destructive technique. Must be active in the IR region. Sensitive, fast and easy. Difficulty measuring low concentration components.
			Thermogravimetric analyses (TGA)	Material stability over temperature. Degradation temperature. Small sample size. Controlled atmosphere.
			Mass spectroscopy (linked to other equipment)	Volatile compounds and databased. Molecular weight obtained from a very small sample. Detection limit. Simple.
			Raman spectroscopy	Low sensitivity Difficult to measure low concentrations. Heating can lead to degradation of the sample. Simple method. Quick identification materials. Mapping of the surface.

Table 9. Continuation Table 8

Property	Depends on	Influences on	Methodology	Specifications
Cyclability	Material and system	Input/output power Sorption rate Mass and heat transfer Permeability/ porosity	DSC/TGA/STA	Small sample size Allows for in situ results and measurements. Difficult to control conditions (especially humidity inside the chamber).
			Cycling machine	Sample collection. No in-situ measurements. Larger sample size Controlled conditions.
			Humidity chamber	Sample collection. No in situ measurements. Larger sample size. Controlled conditions.
DHR	Material	Limits operational conditions and material cyclability	Dynamic Vapor Sorption (DVS) and other Water/moisture sorption analyses	Controlled conditions. Small sample size. Closed system.
			Simultenaous Thermal Analysis (STA)	Larger sample size than DVS. Controlled conditions. Open system. Difficult to control conditions (especially humidity inside the chamber).
Microstructure	Material	Input/output power Sorption rate Mass and heat transfer Permeability/ porosity	X-ray tomography (XRT)	Inner and outer microstructure. Interconnected pores. Multiple calculation tools. Complex. Time-consuming.
			Scanning electron microscopy (SEM)	Qualitative analysis. Ability to image complex shapes. Requires additional sample preparation (coating). Added value with EDS (mapping). Fast and simple.
Thermal diffusivity	Material	Heat transfer Sorption rate Input/Output power	Laser Flash analyser (LFA)	Fast and easy to handle Capable of measuring the thermal diffusivity of small samples. Wide temperature range. Complex sample preparation. Indirect calculation of thermal conductivity.
			Transient plane source)	Allows measuring of anisotropic materials. Difficult to test powders or particulate materials (planar surface required). Fast and simple. Wide temperature range
			Hot wire	Need of electrically insulating materials. Temperature range and sample thickness limitations. Fast and simple. Not recommended for anisotropic materials.

Among the properties listed in Table 8, 11 properties were targeted as relevant to the 3 in system study, and are listed in Table 10 together with the technique used to measure it.

(1)   The **volume change** is relevant to the study as we aim to control the volume change of the TCM by adding the PCM into the structure, therefore this property should be measured over the charging/discharging temperature range and through several cycles.

(2)   The **energy stored, charging/discharging temperature and kinetics of the reaction (conversion rate, time of conversion and reaction rate)** are important to understand how the addition of another heat storage material (latent heat) affects the TCM reaction, whether the reaction is favoured or non-effect is seen. Besides, the energy stored by the PCM is expected to remain stable and it should be studied to detect any subcooling or degradation over cycles.

(3)   The **melting point** of both TCM (in some cases) and PCM are key for the 3 in 1 system as the melting point of the PCM will determine the selection of the working pair (according to the three 3 in 1 system) and the melting point of the TCM has a great effect on the thermochemical reaction as explained in previous sections of this thesis. Therefore, this property must be measured for the individual components and the working pairs.

(4)   The **porosity** of the 3 in 1 system is very relevant for the mass/heat transfer and it is linked to the composite microstructure. TCM/PCM composites porosity should be studied over cycles and under the hydration/dehydration conditions.

(5)   The **chemical stability** is studied through the degradation of the material and the crystal phase stability over temperature/cycles. The study of the pure components is done to conduct the material's selection given that some materials have

not been yet studied in the literature and as a comparative control with the TCM/PCM pairs.

(6)   **Thermal diffusivity** and **specific heat capacity** are key attributes for both latent and thermochemical heat stores and have a great influence on the mass/heat transfer as well as on the energy output of the system. For that reason, these properties are measured for the pure components and the 3 in 1 working pairs. As in the previous case, pure material properties are compared to the working pairs and used for the selection process.

(7)   The **cycling stability** was studied by cycling the samples in a humidity chamber for several cycles. The non-cycled and cycled samples were then characterised through the set of techniques presented in this section. The pure samples are cycled just once to investigate the cycling stability for screening and selection purposes. The working pairs are cycled up to 15 times for the proof of concept case and up to 40 cycles for the scale-up study. The conditions for cycling are specified in the following section.

(8)   The **hydration/dehydration conditions** are studied for the pure TCM and the working pairs, they are mainly focused on the hydration equilibrium and the dehydration conditions, which were studied by STA.

(9)   The **microstructure** gives useful information about the material accommodation/distribution over cycles, especially when combining PCM and TCM. In this thesis, the microstructure has been studied at different levels through Scanning electron microscopy and X-Ray tomography.

The techniques, equipment and test conditions are detailed in the following section.

Table 10. Properties measured for the components of the 3 in 1 system and the working pairs.

Property	Pure TCM	Pure PCM	TCM/PCM combinations
Volume change	Dilatometer	Dilatometer	Dilatometer
Energy stored, charging/discharging temperature and kinetics	DSC/STA	DSC/STA	STA
Melting point	DSC/STA	DSC/STA	STA
Porosity	-	-	XRT/Calculation from helium pycnometer
Crystal phases	XRD	-	XRD
Chemical stability	Raman (just for final working pairs)	Raman (just for final working pairs)	Raman
Thermal diffusivity	LFA	LFA	-
Specific heat capacity	DSC	DSC	- (sensible heat calculated from STA data)
Cycling stability	Humidity chamber (1 cycle)	Humidity chamber (1 cycle)	Humidity chamber (up to 40 cycles)
Hydration/dehydration (DHR)	STA	-	STA
Microstructure	-	-	SEM/XRT

7.2 EQUIPMENT AND SPECIFICATIONS

(1)   Differential Scanning Calorimetry (DSC) is a thermoanalytical technique in which the difference in the amount of heat required to increase the temperature of a sample and a reference is measured as a function of temperature. This technique is used to measure enthalpy changes due to changes in the physical and chemical properties of a material as a function of the temperature or time. In this thesis, DSC (DSC2, Mettler Toledo) is used to measure the melting point, heat of reaction, latent heat and specific heat of reaction. The tests for the enthalpy of fusion and the melting

point of the pure PCM screened were performed from 25 °C to 200 °C with a heating rate of 2.5 K/min in sealed pin-holed aluminium crucibles (40 µl) under air atmosphere (100 ml/min) and a nitrogen purge gas flow of 100 ml/min. The heat of reaction tests for pure TCMs was conducted from 15 °C to 200 °C with a heating rate of 1 °C /min, 2.5 °C /min and 10 °C /min in sealed pin-holed aluminium crucibles (40 µl) under an air atmosphere and a nitrogen purge gas flow of 100 ml/min. The samples were prepared carefully making sure that the TCM was tested fully hydrated. For statistical studies, two different samples were tested for each material/composition. The specific heat capacity was obtained according to the standard (DIN51007) by the sapphire method. Different methodologies were used for calculating the specific heat of PCMs and TCMs. The PCM was measured through the areas method (high accuracy), and the TCM through two different methods, for comparison purposes; the areas and dynamic method. For statistical purposes, three different samples were tested for each material/composition. To understand the difference between both methods a brief explanation can be found in [1], the same methodology reported in that paper for both methods was followed in this study.

The specific heat of TCM was calculated at 25 °C in the hydrated form and at 25 °C and 150 °C in the dehydrated form. For the PCM, the specific heat was calculated at 25 °C and 150 °C. An example of the temperature steps followed by the dynamic and areas methods are shown in Figure 25 and Figure 26. The analysis was performed under an airflow of 100 ml/min. The amount of sample used was around 24 mg $\pm 0.1\ mg$ (similar to the sapphire sample mass used) and the sample was located into 40 µl platinum crucibles. The TCM sample weight was adjusted to calculate the specific heat in every temperature step, as the sample dehydrated through the temperature program. For that reason, the sample was carefully weighed before and after the test.

Besides, the data from the STA was used for assumptions of the number of water present in the sample through the DSC measurements.
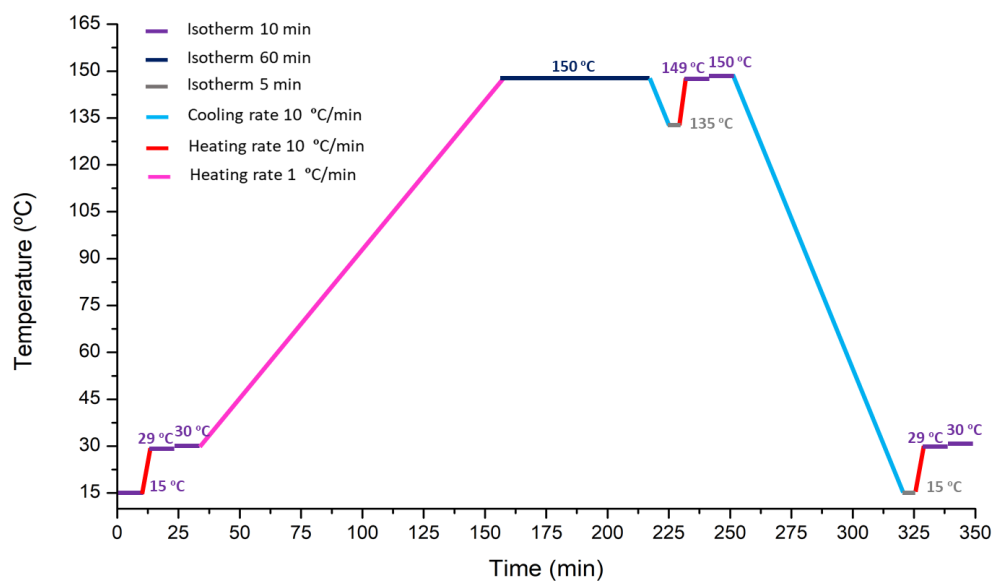
Figure 25. Methodology for specific heat capacity measurement with the areas method.
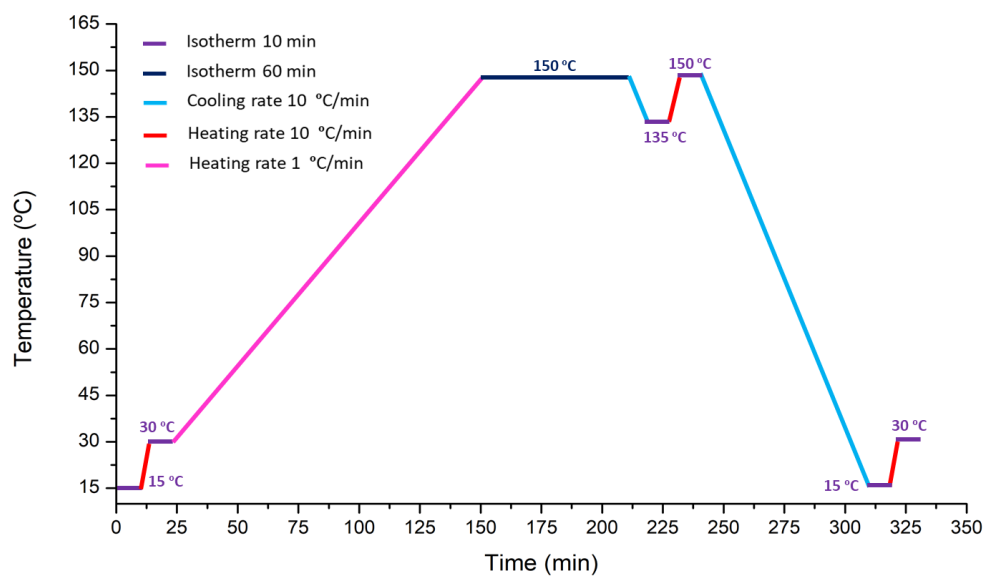
Figure 26. Methodology for specific measurement with the dynamic method.

(2)   **Simultaneous thermal analyses (STA)** Differential Scanning Calorimeter (DSC) and Thermogravimetric analysis (TG) are run in parallel, when performing the Simultaneous Thermal Analysis (STA), Netzsch STA 449 F3 Jupiter apparatus supplied by

LINSEIS company (Germany), for the thermal characterisation of the pure TCM, pure PCM and composites. The apparatus allows for controlling the relative humidity of the sample by controlling the steam flow (g/h) which was calculated from the equations stated in [2] considering the gas flow, the temperature, the pressure and the desired relative humidity. All measurements were run under air as carrier gas and nitrogen as a purge gas, in a platinum crucible with lid 50 μ L. For statistical purposes, the measurements were repeated two times.

The dehydration was performed from 30 °C to 150 °C at a heating rate of 1 °C/min with an isotherm of 1 h at 150 °C, under an air atmosphere (175 mL/min). The hydration was conducted at 30 °C with two different humidities 80% R.H. and 60% R.H. for 2.5 hours; the time used was estimated considering the hydration time needed for most of the TCM listed. For the working pairs, the proof of concept and the composite scale-up production study, specific conditions for each TCM were used (s listed in Table 11).

The energy stored by the pure TCM and PCM is calculated by integrating the heat flow curves obtained in the STA evaluation software. For each temperature program, two corrections are run to ensure accurate data and calibration for each specific test condition (heating rate, temperature range, gas flow, purge gas flow, humidity, etc) is performed. The same procedure is followed for the 3 in 1 composite (TCM/PCM), although given that two kinds of storage materials are active in the composite, the energy stored is calculated through the integration of the STA data and the calculation of the sensible heat, latent heat and thermochemical heat.

The latent heat stored (Q_{Latent}) is obtained by integrating the phase change peak in the STA software when cooling from Tmax (°C) to Tmin (°C). The water sorption N is expressed as moles of water n_{H2O} sorbed per mole of

anhydrous salt (n_x), where x is the TCM and M_x the molar mass of the anhydrous salt. When calculating the water sorption for the composites, where the content of TCM varies, the mass of the dehydrated salt is calculated from the TCM weight percentage in the host matrix. The thermochemical heat ($Q_{Thermochemical}$) is calculated by multiplying the moles of water lost (N) (following equation 4), by the energy released by the thermochemical material per mole of water. The sensible heat of the composite is then calculated by Equation 5, where Q_{Total} is the total heat stored by the composite, Q_{Latent} is the heat stored by the PCM and $Q_{Thermochemical}$ is the heat stored by thermochemical material.

$$N = \frac{n_{H_2O}}{n_x} = \frac{m_{H_2O}}{m_x} \cdot \frac{M_x}{M_{H_2O}}$$ Equation 4

$$Q_{sensible} = Q_{Total} - (Q_{latent} + Q_{Thermochemical})$$ Equation 5

The water uptake (W) and released at different temperature steps is calculated from weight loss/gain in the STA analysis described above [3] (Equation 6), where the m_{H_2O} is the mass of water lost at the reaction time t, m_x is the mass of the anhydrous, m_0 is the initial mass and the m_t is the mass at the reaction time t.

$$W \ (g/g') = \frac{m_{H_2O \ (t)}}{m_x} = \frac{m_0 - m_t}{m_x}$$ Equation 6

The total dehydration conversion ($\chi(t)$) is calculated using the following equation [4], where m_0 is the initial mass, m_t is the mass at the reaction time t, and m_a is the final mass of the anhydrous form:

$$\chi(t)(\%) = \frac{m_0 - m_t}{m_0 - m_a} \ x \ 100$$ Equation 7

The energy density is calculated by using the total energy stored and the density values from the manufacturer (HDPE 0.93 g/cm^3, erythritol 1.45 g/cm^3 and magnesium sulphate heptahydrate 2.66 g/cm^3) and calculating the density

of the composite (TCM/PCM) by the rule of mixtures. Once again, the cost/energy stored is calculated using the value provided by the manufacturer (HDPE 2.5 £/kg, erythritol 3.5 £/kg and 80 £/kg for the magnesium sulphate heptahydrate reported by [5]).

(3)   Scanning electron microscopy (SEM)

The surface morphology of the samples in this study was characterized by a scanning electronic microscope (SEM). Scanning electron microscopy (SEM) is used to obtain high-resolution images of the surface of a sample. The SEM uses the emission of secondary electrons from the surface of a specimen generated by an incident electron beam to obtain an image of the surface. The energy of the incident electrons can be as low as 100 eV or as high as 30 keV depending on the evaluation objectives. The electrons are focused into a small beam by a series of electromagnetic lenses in the SEM column. Qualitative and quantitative chemical analysis information can also be obtained using an energy dispersive x-ray spectrometer (EDS) detector coupled with the SEM.

A preliminary microstructure study and surface morphology of the proof of concept composite was carried out by Scanning Electron Microscopy (SEM) and EDS, model TM-300 (Hitachi Corp., Japan) at room temperature and 15 kV. The samples were observed in tablet form and coated with graphite to avoid the surface charge and obtain better resolution.

(4)   Dilatometer

A DIL 806 dilatometer supplied by TA instrument company (U.S.), operated by a shadowed light method, was used to characterise the dimensional change of the pellets as a function of temperature. In the screening stage, the tablets were heated from room temperature up to 150 °C at 1 °C/min under 100 mL/min airflow, the same conditions used for the thermal cycling and STA experiments. For further stages of the study, specific conditions for the different TCMs and composites are described in Table 11.

(5)   X-ray tomography uses the ability of X-ray radiation to penetrate objects. On the way through an object, part of the impinging radiation is absorbed. An X-ray detector (sensor) captures the decrease in intensity of the X-Ray radiation as a two-dimensional radiographic image [6]. X-ray microtomography analysis was performed using the Skyscan1172 (from Bruker, Germany). This technique was used to study the open and closed porosity as well as the inner microstructure over 40 cycles. Before each set of scans, the rotation stage was aligned. Samples were scanned using 90~kV and 117 mA of source voltage and current, respectively, and were exposed during 280~ms during each snap. The scans covered 360 degrees with a step of 0.2 degrees, 4 frames were averaged and the resultant projects area was recorded for each rotation step. A 0.5 mm Ti filter was required. Cross-sectional and three-dimensional images were reconstructed using NRecon software, where the ring effect and beam hardening were corrected. The misalignment was always kept between -10 and 10, as recommended for quantitative analysis.

(6)   X-ray powder diffraction (XRD) is a technique that provides information about the phase-composition of crystalline solid or powder materials. Furthermore, XRD is a non-destructive test that can distinguish between different crystallographic phases that have the same chemical formula. Typically, no more than a few hundred milligrams of the sample will be required for XRD phase analysis and a detection limit of 2 wt.%, when the samples are multicomponent ones.

A D8 Advance Plus X-ray powder diffraction (XRD) supplied by Bruker company (U.S.) equipped with an LYNXEYE detector using CuKα radiation (λ = 1.5418 Å) and θ-2θ geometry was used for the crystallinity analysis. For doing so, the pellet form of the sample was firstly ground to a powder form and then placed in the sample holder. Data collected between 10° and 50° in 2θ with a step size of 0.02° and a counting time of 8 s

per step. The X-ray diffraction patterns were recorded over-temperature stages to investigate the different crystalline phases when dehydrating the thermochemical material in pure form and the 3 in 1 composite. Two different programs were used once for chlorides thermochemical materials up to 140 °C (to avoid side reactions and any damage to the equipment) and sulphates, nitrates, carbonates materials up to 150 °C.

(7)   **Humidity chamber**: the thermal cycling was performed in a TH-ME-100 Humidity chamber from JeioTech©. The samples were cycled in tablet form (1 g and 10 g depending on the study). To avoid sample contamination from one another, the tablets were located into a muffin oven paper containers as shown in Figure 27. For the pure TCMs and PCMs cycling test, a temperature range from 30 to 150 °C was applied, a heating rate of 1 °C/min with a 1 h isothermal at 150 °C under an airflow, for dehydration; then the temperature was decreased to 30 °C with a cooling rate of 2.5 °C/min, the hydration was then performed at 30% and 80% R.H. Specific conditions for the study of each TCM were applied and are described in Table 11.

Figure 27. Making-off tablets cycling in the humidity chamber.

(8)   **Raman microscopy** is a spectroscopic technique that offers a non-destructive and non-contact method of collecting information about the chemical structure and optical images of samples. Raman experiments were performed on the surface of the tablets before and after being cycled, at room temperature using a

Renishaw confocal Raman microscope. The test was performed with a solid-state laser of 785 nm (102-3200 cm^{-1}), exposure time of 10 s and 50% of the laser power of. 3x3 image mapping was used to scan the surface of the tablets (bottom and top) and a total of 27 points were measured as shown in Figure 28.
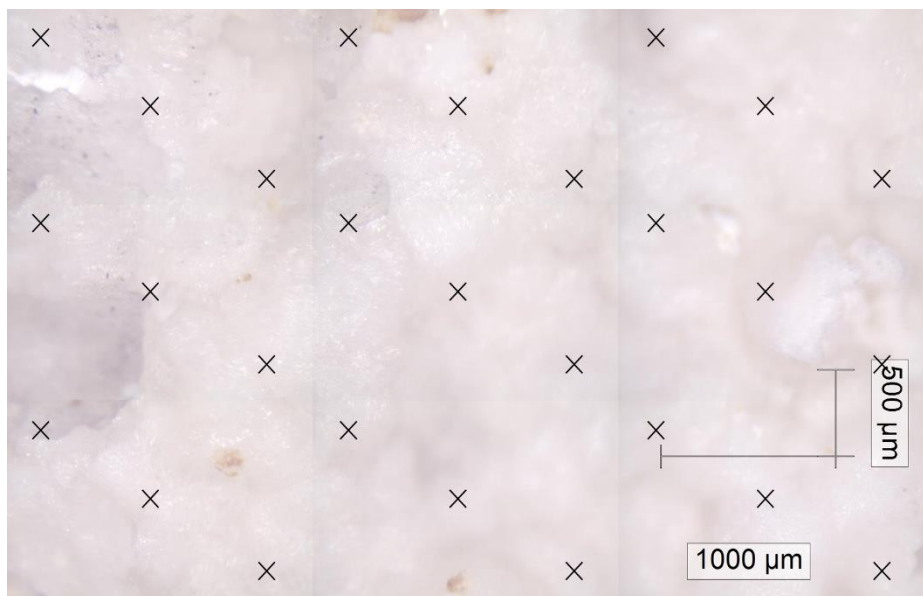
Figure 28. Example of 3x3 images mapping of Raman measurements, 27 points (9 points x 3 images).

(9) **Testing machine**. A Lloyd LS100 Plus Materials Testing Machine supplied by Lloyd Instruments company (UK) was used to compress the powders into tablets. For the working pairs study and the proof of concept, different ratios of TCM and PCM, both in powder form, were mixed and ground to a homogeneous mixture. An amount of 0.8 g ± 0.05 g was then pressed into a tablet shape with 13 mm diameter obtaining a thickness around 10 mm. The operating pressure and holding time were set to 90 MPa and 1.5 min, respectively. Same conditions were used for the pure TCMs and PCMs in the screening stage, however, an amount of 0.95 g ± 0.05 g was used to prepare the pellets in this case. For the material production scaling-up study, the amount of sample was increased to 19.5 g ± 0.05 g. Both TCM and PCM were mixed and ground to be

pressed into a tablet of 30 mm diameter and around 25 mm thickness, the pressure of 40 MPa and 1.5 holding time.

(10)   Laser Flash Analysis (LFA)

The principle of laser flash method is shown in Figure 29, where a laser pulse is applied by a laser beam on the bottom of a small sample, and an infrared detector monitors the temperature change at the opposite side of the sample. The thermal diffusivity of the specimen can be obtained by the temperature rise together with the thickness of the sample. Therefore as stated in [7], and in adiabatic conditions,

$$\alpha \; = 0.1388\,\frac{d^2}{t_{1/2}}$$

Equation 4

where α is the thermal diffusivity (cm^2/S), d is the thickness of the sample (cm), the $t_{1/2}$ is the time at 50% of the maximum temperature increase (s).

Then the thermal conductivity can be calculated with the known specific heat Cp and the density ρ of the sample following equation 5:

$$\lambda = \alpha\rho C_p$$

Equation 5

The working principle of this technique is illustrated in Figure 29 (a). Thermal diffusivity (α) measurements are performed in this thesis by using a laser flash analyser (LFA) Netzsch 427 and a sample size of 2mm thickness and 12.70 mm diameter. The tablets were prepared by pressing the samples in powder forme 0.3 g ± 0.05 g at 90 MPa for 1 min and then coating the pellet with graphite. The measurements were conducted under a nitrogen atmosphere 100 ml/min and the measurements are performed at 25°C for the hydrated and dehydrated samples. The materials are measured three times per sample and three shots per test (averaged from 3 x 3 times). The cowan plus pulse correction was used to calculate the thermal diffusivity.
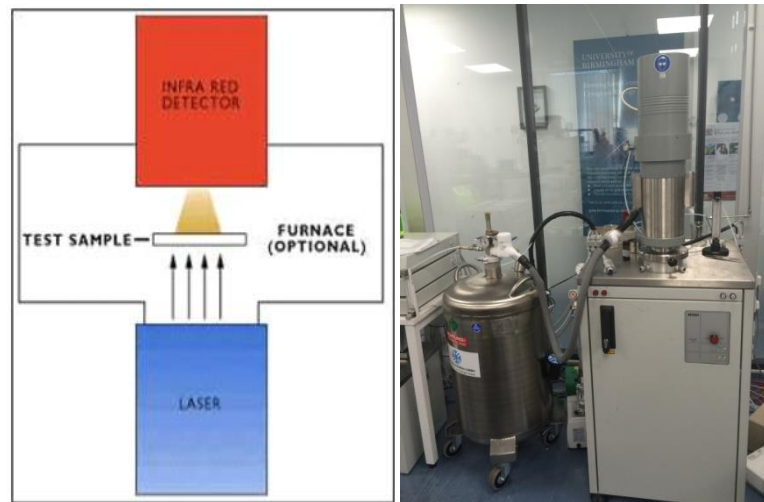
Figure 29. Laser flash analysis (LFA) （a） Basic principle（b）Equipment photo

(11)   Helium pycnometer

Helium Pycnometer is used to measure the volume of a sample by the gas displacement method, to provide high-precision volume measurements and density calculations. Helium Pycnometer allows evaluating the true density, not considering the void volume (porosity), determining the porous density and non-porous solids density. The sample is placed in a cell, which a well-known volume and the true density is calculated by dividing the sample weight by the volume measured. An AccuPyc II 1340 Pycnometer supplied by Micromeritics (U.S.) = was used to characterise the true density and, hence, calculate the open porosity of the pellets before and after the thermal cycling in the proof of concept stage. The true density of the samples was measured at room temperature. Just the open porosity is considered by using this technique. The porosity was then calculated following the Eq. 6 [8]:

Porosity (%) = $1 - \dfrac{\textbf{Bulk density}}{\textbf{True density}} \, x \, 100$ Equation 6

Table 11. Test conditions used by technique and material tested in the thesis.

Equipment	MgSO$_4$-PCM	MgCl$_2$- PCM	K$_2$CO$_3$- PCM	SrBr$_2$- PCM	Pure PCM	Pure TCM
LFA	-	-	-	-	25 °C 3 samples 3 shots per temperature step	25°C hydrated and dehydrated 3 samples 3 shots per temperature step
STA	Heating: 30-150 1 °C/min Isotherm: 1h at 150 °C Cooling: 150 °C to 30 °C 2.5 °C /min Hydrating: 30 °C 80% R.H for 2.5 h	Heating: 30-130 1 °C/min Isotherm: 1h at 130 °C Cooling: 130 °C to 30 °C 2.5 °C /min Hydrating: 30 °C 40% R.H for 2 h	Heating: 30-100 1 °C/min Isotherm: 1h at 130 °C Cooling: 100 °C to 30 °C 2.5 °C /min Hydrating: 30 °C 40% R.H for 2 h	Heating: 30-90 °C 1 °C/min Isotherm: 1h at 90 °C Cooling: 90 °C to 30 °C 2.5 °C /min Hydrating: 30 °C 50% R.H for 2 h	Heating: 30-150 1 °C/min Isotherm: 1h at 150 °C Cooling: 150 °C to 30 °C 2.5 °C /min Hydrating: 30 °C 80% R.H for 2.5 h	Heating: 30-150 1 °C/min Isotherm: 1h at 150 °C Cooling: 150 °C to 30 °C 2.5 °C /min Hydrating: 30 °C 80% R.H for 2.5 h
Humidity chamber	Heating: 30-150 1 °C/min Isotherm: 1h at 150 °C Cooling: 150 °C to 30 °C 2.5 °C /min Hydrating: 30 °C 80% R.H for 2.5 h	Heating: 30-130 1 °C/min Isotherm: 1h at 130 °C Cooling: 130 °C to 30 °C 2.5 °C /min Hydrating: 30 °C 40% R.H for 2 h	Heating: 30-100 1 °C/min Isotherm: 1h at 130 °C Cooling: 100 °C to 30 °C 2.5 °C /min Hydrating: 30 °C 40% R.H for 2 h	Heating: 30-90 °C 1 °C/min Isotherm: 1h at 90 °C Cooling: 90 °C to 30 °C 2.5 °C /min Hydrating: 30 °C 50% R.H for 2 h	Heating: 30-150 1 °C/min Isotherm: 1h at 150 °C Cooling: 150 °C to 30 °C 2.5 °C /min Hydrating: 30 °C 80% R.H for 2.5 h	Heating: 30-150 1 °C/min Isotherm: 1h at 150 °C Cooling: 150 °C to 30 °C 2.5 °C /min Hydrating: 30 °C 80% R.H for 2.5 h
DSC	-	-	-	-	Specific heat (areas) at 25 and 150 °C Latent heat: Heating: 25-200 °C 2.5 °C/min Isotherm: 10 min 200 °C Purge gas N$_2$ Carrier gas air (100 mL/min)	Specific heat (areas and dynamic) cp at 25C hydrated at 150C (dehydrated) at 25C (dehydrated) The heat of reaction: Heating: 15-200 °C 1, 2.5 and 10 °C/min Isotherm: 10 min 200 °C Purge gas N$_2$ Carrier gas air (100 mL/min)
Dilatometer	Heating: 30-150 °C at 1°C /min Cooling: 150-30 °C at 2.5 °C /min 100 mL/min air atmosphere					
XRD high temperature	Heating: 25-150 °C 1 °C/min Temperature steps: 25 °C, 30 °C, 40 °C, 70 °C, 90 °C, 120 °C, 150 °C Isotherm: 150 °C 30 min Cooling: 150-25 °C Temperature steps: 150 °C and 25 °C Air flow 100 mL/min	Heating: 25-140 °C 1 °C/min Temperature steps: 25 °C, 30 °C, 40 °C, 70 °C, 90 °C, 120 °C, 140 °C Isotherm: 140 °C 30 min Cooling: 140-25 °C Temperature steps: 140 °C and 25 °C Air flow 100 mL/min	Heating: 25-150 °C 1 °C/min Temperature steps: 25 °C, 30 °C, 40 °C, 70 °C, 90 °C, 120 °C, 150 °C Isotherm: 150 °C 30 min Cooling: 150-25 °C Temperature steps: 150 °C and 25 °C Air flow 100 mL/min	Heating: 25-150 °C 1 °C/min Temperature steps: 25 °C, 30 °C, 40 °C, 70 °C, 90 °C, 120 °C, 150 °C Isotherm: 150 °C 30 min Cooling: 150-25 °C Temperature steps: 150 °C and 25 °C Air flow 100 mL/min	-	Heating: 25-150 °C 1 °C/min Temperature steps: 25 °C, 30 °C, 40 °C, 70 °C, 90 °C, 120 °C, 150 °C Isotherm: 150 °C 30 min Cooling: 150-25 °C Temperature steps: 150 °C and 25 °C Airflow 100 mL/min
Pressing machine	Proof of concept: 0.8-0.9 g tablet 90 MPa 1.2 min Dimensions: 13 mm diameter and 10 mm thickness Scale-up: 20 g tablet 40 MPa 1.2 min Dimensions: 30 mm diameter and 25 mm thickness	Proof of concept: 0.8-0.9 g tablet 90 MPa 1.2 min Dimensions: 13 mm diameter and 10 mm thickness Scale-up: 20 g tablet 40 MPa 1.2 min Dimensions: 30 mm diameter and 25 mm thickness	Proof of concept: 0.8-0.9 g tablet 90 MPa 1.2 min Dimensions: 13 mm diameter and 10 mm thickness			

7.3 REFERENCES

[1] Ferrer G, Barreneche C, Solé A, Martorell I, Cabeza LF. New proposed methodology for specific heat capacity determination of materials for thermal energy storage (TES) by DSC. J Energy Storage 2017;11:1–6. doi:10.1016/j.est.2017.02.002.

[2] Boyle B. Humidity Generation and Humidity Measurement - The Complete Guide n.d.

[3] Korhammer K, Druske MM, Fopah-Lele A, Rammelberg HU, Wegscheider N, Opel O, et al. Sorption and thermal characterization of composite materials based on chlorides for thermal energy storage. Appl Energy 2016;162:1462–72. doi:10.1016/j.apenergy.2015.08.037.

[4] Korhammer K, Apel C, Osterland T, Ruck WKL. Reaction of Calcium Chloride and Magnesium Chloride and their Mixed Salts with Ethanol for Thermal Energy Storage. Energy Procedia 2016;91:161–71. doi:10.1016/j.egypro.2016.06.194.

[5] Jarimi H, Aydin D, Yanan Z, Ozankaya G, Chen X, Riffat S. Review on the recent progress of thermochemical materials and processes for solar thermal energy storage and industrial waste heat recovery. Int J Low-Carbon Technol 2019;14:44–69. doi:10.1093/ijlct/cty052.

[6] Kalender WA. X-ray computed tomography. Phys Med Biol 2006. doi:10.1088/0031-9155/51/13/R03.

[7] Lian T-W, Kondo A, Akoshima M, Abe H, Ohmura T, Tuan W-H, et al. Rapid thermal conductivity measurement of porous thermal insulation material by laser flash method. Adv Powder Technol 2016;27:882–5. doi:10.1016/j.apt.2016.01.008.

[8]   Yusof YA, Mohd Salleh FS, Chin NL, Talib RA. The drying and tabletting of pitaya powder. J Food Process Eng 2012;35:763–71. doi:10.1111/j.1745-4530.2010.00625.x.

8 MATERIAL SCREENING AND SELECTION

1. Thesis timeline
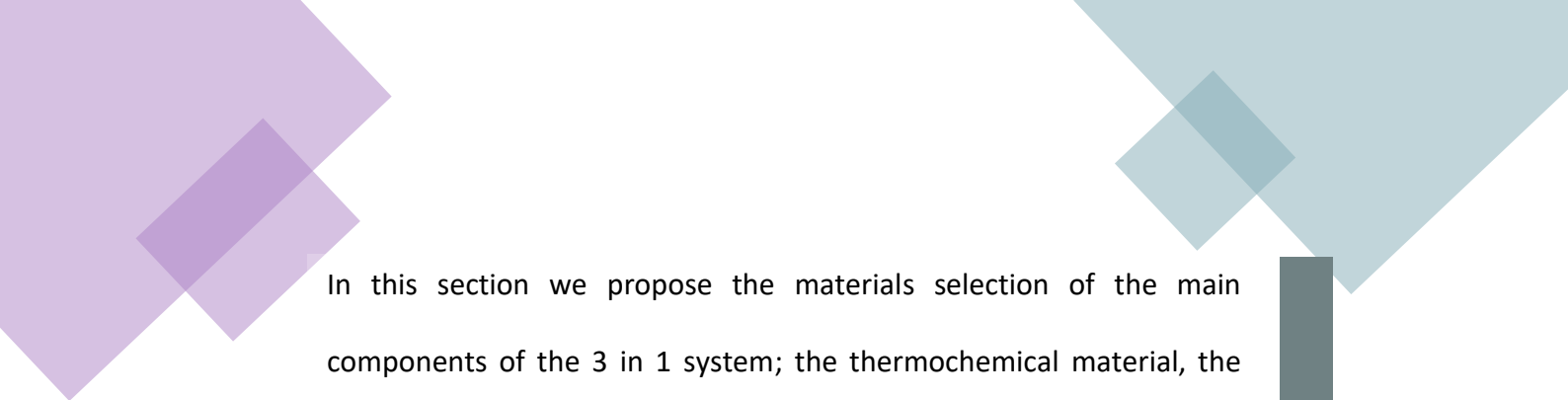
2. Scientific contributions

3. Introduction

4. TCS Outlook

5. Targets and structure of the thesis

6. Hybrid TES system:

3 in 1 concept

In this section we propose the materials selection of the main components of the 3 in 1 system; the thermochemical material, the phase change material and when necessary, the gelling agent (introduced later in the thesis). The materials are theoretically selected through a comprehensive literature review on the area. The theoretical candidates are then experimentally studied, revealing relevant properties unmeasured in the literature. The candidates are narrowed down to five TCMs, eight PCMs and two gels that will be combined to form working pairs resulting on different working temperature combinations.

7. Bench study specifications

8. Material screening and selection

9. Working pairs

10. Proof of concept and scale-up

11. Potential applications and prospective

12. Conclusions and achievements

8. MATERIAL SCREENING AND SELECTION

Material selection is defined as the act of choosing the material best suited to achieve the requirements of a given application. Many different factors go into determining the selection requirements, such as thermal properties, chemical properties, physical properties, stability, cyclability and cost. These must be weighed during the material selection process.

Material selection is used as a mathematical methodology based on the properties of the material by defining the constraints of the material based on the boundary conditions of the final system performance, the free variable, the materials' key attributes to be considered as well as the main objective this material will have in the final application. This is based on the Prof. Ashby methodology from the University of Cambridge [1], Ashby's method has been already used for TES material selection [2–5].

The first step is to identify the relevant properties so the selection process can be conducted; objectives constraints and free variables. Once the relevant properties have been identified and defined, we shall frame them to our selection methodology as described in Figure 30, where a typical selection flow chart for TES is illustrated. Following Ashby's selection methodology, we shall define the function, objective, constraints and free variables to elaborate the material index. For thermal energy storage, this should be considered for long- and short-term storage. One this has been done, the information available in the literature gains importance, as the relevant properties reported are used to screen theoretical candidates. From the set of theoretical candidates, experimental validation is performed to discard candidates that do not meet practical screening demands (filters). This is done by a set of filters that are linked to the selected variables and constraints established at the beginning of the process. The final output

is a list of candidates that fit the application requirements. A similar approach is followed in this section for the selection of the 3 in 1 component. However, given the complexity of the materials involved and that this is an early stage of development the material index is not applied in this section.
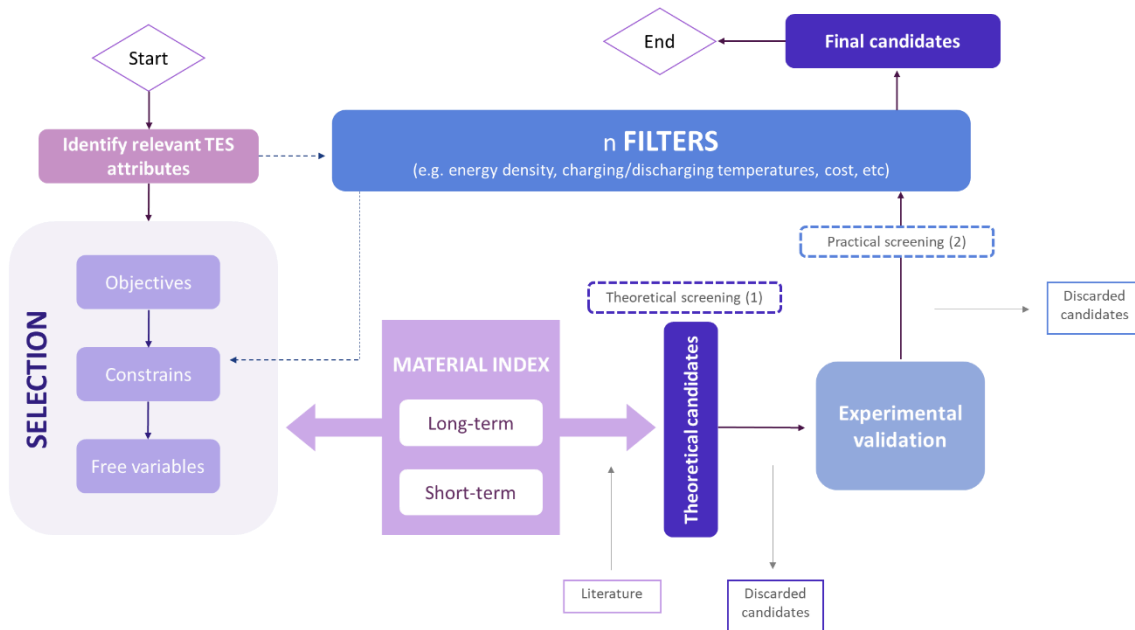
Figure 30. Material selection flow chart.

8.1 THERMOCHEMICAL MATERIAL

The thermochemical material in the 3 in 1 will work simultaneously as the primary storage media and as a co-working matrix along with the PCM material. In this section, the selection of the thermochemical material will be described and will be framed to the 3 in 1 requirement. Among all the thermochemical materials available (see Section 4), as a first approach to the 3 in feasibility, we just consider salt hydrates for low-medium temperature applications (25-150 °C). As this will ease the PCM selection, lower operational temperatures that lead to less arising problems during storage periods (such as material compatibility, chemical and physical stability). However, as stressed out in Section 6, the 3 in 1 system has a great working pair potential with a variety of material's combination.

In this section, the TCM attributes and constraints are applied for material screening and selection. Besides, experimental validation is performed, revealing interesting properties not measured before in the literature such as specific heat and thermal conductivity (in the hydrated and dehydrated state), among others. The results are discussed eventually aiming to select final TCS material candidates with different sorption behaviour and chemical nature, as well as a variety of temperatures to allow the 3 in 1 system; cascade, charging and discharging. Such final candidates will be paired to PCM's final candidates, according to the system selected to come up with a list of potential TCM/PCM working pairs (see late In Section 9).

8.1.1   TCM 3 IN 1 SYSTEM CONSTRAINS

Considering the final system where a TCM will be applied, ideally, the main objective of this material will be to store the maximum amount of energy. That means the maximum energy density possibly capable at a theoretical material level. This is also important in the 3 in 1 system as we want to provide a novel strategy for storing heat, and therefore, reach the highest possible energy density under practical conditions. However, at this stage, the main objective is to prove the feasibility of this system providing a co-working matrix between the PCM/TCM. For that reason, the energy density will be intended to be maximised but also other attributes, that are normally overlooked when selecting a TCM, will be considered (e.g. shape-ability and physical integrity). A previous knowledge acquired on the TCM thermodynamics is needed to better understand the interactions between the TCM and PCM in the 3 in 1 matrix as this will help to understand the sorption mechanism in interaction with the phase change process.

In our case of study, we have applied typical conditions for an open system, which is a suitable temperature range for space heating and domestic hot water supply [6]. The set of constraints are listed in Table 12. The hydration/dehydration temperatures were set according to the operational conditions, while the melting point is desired to be higher than the dehydration temperature as explained in Section 4. The storage media should also remain a solid/gas

sorption system (no deliquescence) at the hydration conditions, 30°C at 80% R.H. We are aware that such relative humidity might lead to a high-temperature lift in the system. However, we have set those hydration conditions as limiting conditions to ensure all conditions to work in the 3 in 1 system. The TCM should dehydrate at a temperature up to 150°C at ambient water pressure (13 mbar), which are the most common conditions of an open system. Different constraints or filters were applied in the selection process, as described below:

- The hydration/dehydration temperature defines the system input and output temperature.

- The second filter determines the energy density of the storage media, which should meet the system demands.

- The third filter makes sure the TCM can work under the operational conditions without suffering deliquescence or melting during hydration/dehydration.

- Once the material can be feasible at the service conditions the price (€/MJ) becomes a limiting factor (Filter 4), volume change (Filter 5) and chemical stability-safety (Filter 6 and 7) are applied lastly.

Table 12. Constraints for thermochemical material screening/selection.

Filters	Parameters		Importance
Filter 1	Hydration temperature	≤30°C	Must
Filter 1	Dehydration temperature	≤150°C	Must
Filter 2	Energy density	≥1.5 GJ·m^{-3}	Must
Filter 3	Deliquescence vapour pressure	Out of 30°C (80% R.H.)	Preferable
Filter 3	Melting point	> temperature dehydration	Preferable
Filter 4	Price (€/MJ)	≤ 2 €/MJ	Must
Filter 5	Volume change	≤55%	Preferable
Filter 6	Chemically stable	Stable from 30-150°C	Preferable
Filter 6	Safety	Applied in open systems	Preferable
Others		Well studied in the literature	Preferable
		Pelletizeable	Must
		Physical integrity	Preferable

8.1.2 THERMOCHEMICAL MATERIAL SCREENING

The available candidates for TCS sorption storage have been reported and researched by some authors in the last few years [6–9], the outstanding candidates are listed in Figure 31 by their deployment level. The preferred candidates by researchers and the ones that have reached higher development level are magnesium chloride [10–16], strontium bromide [17–22], magnesium sulphate [23–26], sodium sulphate [27–31] and calcium chloride [32–36]. In the last three years, potassium carbonate has appeared as a great and promising candidate for building application, although this material has not reached a deployed level yet [37–40].
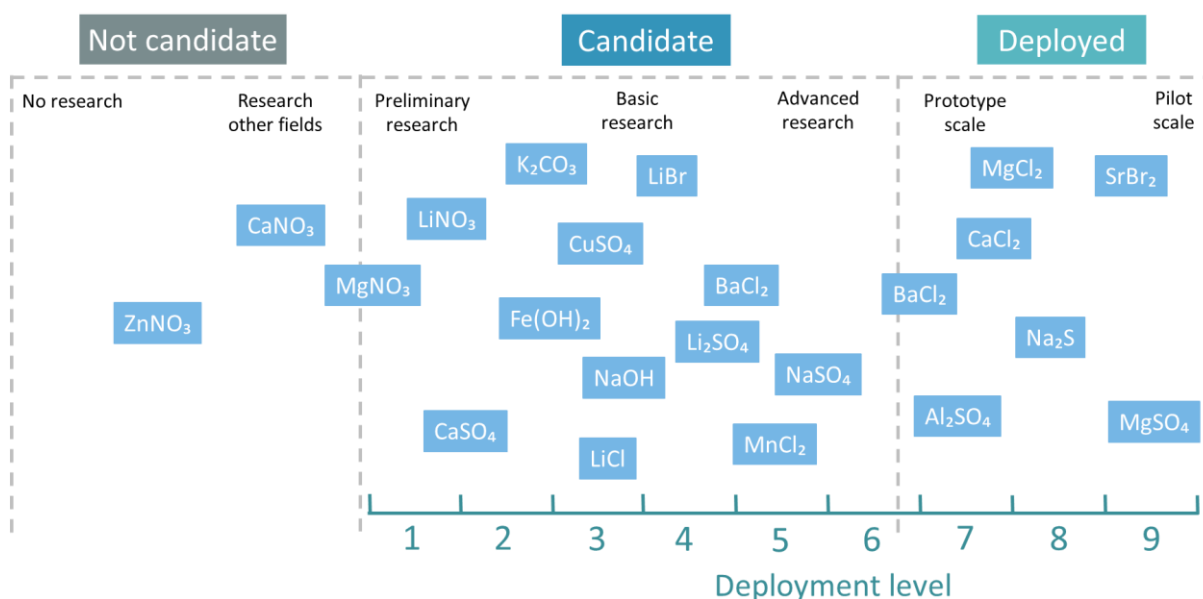
Figure 31. TCS screening candidates for building applications [6–9]. No research is defined as materials not studied in any field but that is capable of storing thermochemical heat; Research in other fields are those materials that have been studied but not in TCS; preliminary research is materials that have been briefly studied; Basic research is the stage where the materials have been studied in TCS but there is not a dep understating; Advanced research are those materials that have been deeply researched but are not yet in prototype or pilot scale; Prototype scale are those materials that have been implemented in prototype scale projects; Pilot scale are those materials that have been implemented in pilot-scale projects.

According to the selection constrains ten thermochemical materials were theoretically selected for applying the filter-screening process. This preliminary selection was done by applying the Filter 1 (hydration/dehydration temperatures), which cut off several thermochemical materials given the high energy density required and the working temperature. From those 10 materials screened by the first filter, experimental validation was conducted (see late in Section 8.1.2) to determine whether they could be used at practical conditions (hydration, dehydration temperature, volume variation and DHR). In this chapter, the ten preliminary candidates are reviewed to build up a base of knowledge for moving towards the following selection stages. The candidates are grouped by their chemical nature in the following way: sulphates (magnesium sulphate, copper sulphate and calcium sulphate), carbonates (potassium carbonate), bromides (strontium bromide), nitrates (magnesium nitrate, calcium nitrate and

zinc nitrate), chlorides (magnesium chloride and calcium chloride). For comparison purposes, values reported in the literature for dehydration steps, density, melting point, mass loss and energy stored/energy density are shown in Table 13.

Table 13. Literature review of relevant properties for the preliminary screened materials. Note that the energy density (E_d) is for an open system, specific heat (Cp) and the thermal conductivity (K) are provided for hydrated (h) and dehydrated (d) form when possible. The melting behaviour is defined as congruent (C) and incongruent (I) [21,41–45]

TCM	H_2O	Salt/water (%)	Dehydration steps	T_{dehy} (°C)	T_{Hy} (°C)	ΔH_R	T_m (°C)	Melting	ΔH_L (J/g)	Cp (J/g·K)	Density (g/cm³)	E_d (GJ·m⁻³)	K (w/m·K)	Volume change (%)	DHR (mbar at 30°C)	Others	Price
$MgSO_4$	7	49.6/50.4	7 H_2O to 6 H_2O	25 -55 [46]	30	275 (kJ/mol) [47] 2300 (kJ/kg) [11]	48.5	I	-	1.546 (h) 0.8 (d) [47]	1.680 (h) 2.660 (d) [47]	1.8-2.22	0.48 (h) [47]	-47	80% R.H (at 30C)	-	80 (€/t)
			6 H_2O to 0.1 H_2O	55-265 [46]													
			0.1 H_2O to anhydrous	276 [46]													
$SrBr_2$	6	58/42	6 H_2O to 1 H_2O	64.7-118.7 [48,49]	70-80	952.7 (kJ/mol) [49] 3192 (kJ/kg) [50]	88	I	814 kJ/kg [21]	0.457 (h) 0.986 (d) [21]	2.386 (h) [19] 1.509 (d) [21]	2.02	0.38 (h) [49]	-65	9.7-17.5 (mbar)	-	2838 (€/t)
			1 H_2O to anhydrous	158.4-212.7 [17,48,49]													

Table 14. Continuation Table 13.

TCM	H_2O	Salt/water (%)	Dehydration steps	T_{dehy} (°C)	T_{Hy} (°C)	ΔH_R	T_m (°C)	Melting	ΔH_L (J/g)	Cp (J/g·K)	Density (g/cm³)	E_d (GJ·m⁻³)	K (w/m·K)	Volume change (%)	DHR (mbar at 30°C)	Others	Price
$Mg(NO_3)_2$	6	57.84/42.16	6 H_2O to 2 H_2O	68 [6]	61	1060 (kJ/kg) [6]	89 [51] 90 [52]	C	160 [52] 167 [53]	1.81 (h) 2.480 (d) [52]	1.67 (h) 2.03 (d)[6]	1.53 [6]	0.669 (h) [52]	-41	96%	Loss of N_2	39 (€/t)
			2 H_2O to anhydrous	113 [6]													
$CaCl_2$	6	43/57	6 H_2O to 4 H_2O	29.8-63 [54–56]	32 [57]	1153 (kJ/kg) [56]	29 [58]	I	170 [52] 170190 [51] 169.98 [59] 187.49 [58]	1.42 (h) [52] 1.8 (d) [58]	1.68 (h) [52] 1.56 (d) [58]	1.84	1.088 (h) [52,58]	-35	29% (at 30C)	-	107 (€/t) 0.1-0.4 €/MJ [60]
			4 H_2O to 2 H_2O	45.3 [54,55]													
			2 H_2O to H_2O	175 [54,55] 142 [61]													
			H_2O to anhydrous	20-2600 [54–56]													

Table 15. Continuation Table 13.

TCM	H₂O	Salt/water (%)	Dehydration steps	T_{dehy} (°C)	T_{Hy} (°C)	ΔH_R	T_m (°C)	Melting	ΔH_L (J/g)	Cp (J/g·K)	Density (g/cm³)	E_d (GJ·m⁻³)	K (w/m·K)	Volume change (%)	DHR (mbar at 30°C)	Others	Price
MgCl₂	6	44/56	6 H₂O to 4 H₂O	55-69 [56,62–65]	35	1344 J/g [56] 2890 [11]	117 [52]	I	169 [52]	2.25 (h) 1.59 (d) [52]	1.560 (h) 1.450 (d) [57]	1.89-1.94 **2.3**	0.704 (h) [52]	-56	33% (at 30C)	HCl formation	154 (€/t)
			4 H₂O to 2 H₂O	75-116 [56,62–65]													
			2 H₂O to 1 H₂O	150-210 [56,64,65]													
			1 H₂O to MgOHCl + HCl	145-175 [64,65]													

Table 16. Continuation Table 13.

TCM	H_2O	Salt/water (%)	Dehydration steps	T_{dehy} (°C)	T_{Hy} (°C)	ΔH_R	T_m (°C)	Melting	ΔH_L (J/g)	Cp (J/g·K)	Density (g/cm³)	E_d (GJ·m⁻³)	K (w/m·K)	Volume change (%)	DHR (mbar at 30°C)	Others	Price
$Zn(NO_3)_2$	6	57/43	6 H_2O to 4 H_2O	39 [57]	34	-	36 [51,52,66]	C	130 [52] 146.95 [59]	1.34 (h) [51,52] 2.26 (d) [57]	2.07 (h) [52]	1.77	0.464 (h) [57]	**-57**	-	Loss of N_2	300 *(€/t)
			4 H_2O to 2 H_2O	93 [57]													
			2 H_2O to anhydrous	104 [57]													
$CaSO_4$	2	26.4/73.6	2 H_2O to 0.5 H_2O	80 [67]	25	394-500 (kJ/kg)	128	C	-	1.090 (h) [47]	1.850 (h) 2.160 (d) [47]	1.49	1.088 (d) [47]	-48	-	-	150 *(€/t)
			0.5 H_2O to 0.15 H_2O	0.5 H_2O to γ-$CaSO_4$	108 [67]												
			0.15 H_2O to anhydrous	γ-$CaSO_4$ to β-$CaSO_4$	127-227 [67]												
$Ca(NO_3)_2$	4	44/56	4 H_2O to 3 H_2O	120 [68]	43	-	42 [51]	C	140 [52] 130 [51]	1.46 (h) [52]	1.82 [52]	1.71	0.34 (d) [69]	**-45**	-	Loss of N_2	260* (€/t)
			3 H_2O to 2 H_2O	155 [68]													
			2 H_2O to 1 H_2O	160 [68]													
			1 H_2O to anhydrous	210 [68]													

Table 17. Continuation Table 13

TCM	H_2O	Salt/water (%)	Dehydration steps	T_{dehy} (°C)	T_{Hy} (°C)	ΔH_R	T_m (°C)	Melting	ΔH_L (J/g)	Cp (J/g·K)	Density (g/cm³)	E_d (GJ·m⁻³)	K (w/m·K)	Volume change (%)	DHR (mbar at 30°C)	Others	Price
$CuSO_4$	5	56.4/44.6	5 H_2O to 3 H_2O [70] 3 H_2O to H_2O [70] H_2O to anhydrous [70]	65 -102 [70–72] 90-115 [70–72] 208-250 [70–73]	35 50 [47]	78.22 [47]	110	C	-	1.050 (h) [47]	2.284 (h) 3.603 (d) [47]	1.93	0.4 (h) [47]	-59 **-60**	97% at 25 °C [70]	Toxic	134 (€/t)
K_2CO_3	1.5	19.6/80.4	1.5 H2O to anhydrous	26-57 [6,40]	65 [6]	98 kJ/mol [37]	150 [6]	-	-	-	2.33 (h) 2.18 (d) [6]	0.75 [40]	0.502 (h) [74]	-22 [6]	14 mbar (at 25 °C) [6]	-	1.67 €/MJ [6]

(1) Sulphates

(1.1)   Magnesium sulphate

Magnesium sulphate is one of the TCM that accounts higher energy density [75] and it has been widely studied for seasonal storage [46,76,77]. Even if the melting point lies in the first dehydration step this material meets other high priority requirements such as hydration/dehydration temperature, energy density, deliquescence and volume variation. Magnesium sulfate allows storing a theoretical energy up to 2.8 GJ m^{-3} [78]. However, the use of magnesium sulphate powder is difficult in a storage reactor because the particles rapidly form agglomerates during dehydration/hydration cycles, thus liming gas transfer and causing reversibility issues and low-temperature lift and resulting on poor system performance [78]. The thermochemical storage pair works following Reaction 1, the heat is released/stored by the hydration and the dehydration of magnesium sulphate. The charging/discharge processes of magnesium sulphate take place at a temperature range of 30 °C – 275 °C [46]. There are three stages of dehydration (charging) depending on the temperature [46]. The first step occurs at 30-55 °C involving a 1 molecule water loss and occurs at the same time while the melting, which reduces the bed porosity of the material, and thereby the vapour transport. The second step occurs between 65 °C – 265 °C and corresponds to a loss of approximately 5.9 water molecules. This value of energy that can be stored using this dehydration step is the largest of the three dehydration steps. In the third step, the mass loss occurs at 275 °C corresponds to 0.1 moles of water remaining. On the other hand, the hydration step (discharging) takes place at around 25-30 °C, at atmospheric pressure [46]. Since the hydration and the first dehydration step overlaps, the conversion from $MgSO_4 \cdot 7H_2O$ to $MgSO_4 \cdot 6H_2O$ gradually starts when the $MgSO_4 \cdot 7H_2O$ is stored (see phase diagram in Figure 32).

$$MgSO_4 \cdot 7H_2O \longleftrightarrow MgSO_4 + 7H_2O \tag{1}$$

The naturally occurring stable hydrated states in the $MgSO_4/H_2O$ system are epsomite ($MgSO_4 \cdot 7H_2O$), hexahydrite ($MgSO_4 \cdot 6H_2O$), amorphous monohydrate ($MgSO_4 \cdot 1H_2O$) and products of total dehydration of high hydrates ($MgSO_4$). Other metastable hydrates such as 11, 5, 4, 3, 2, 5/4 can be synthetically produced [79].

Donkers et al. [80] analysis magnesium sulphate by NRM in dynamic conditions under a dry nitrogen atmosphere. It was observed that liquid water is formed in the pore of the crystal during dehydration (at 48 °C) due to the local increase of the water vapour pressure. Such aqueous solution influences the dehydration process since it can lead to deliquescence and the crystallization of new phase can be strongly affected. Particle size, as commented previously, is also an important parameter when it comes to performing charging and discharging. Van Essen et al. [46] studied the influence of different particle size since it can also lead to the partial formation of liquid water inside the crystal especially when working with large particle size distribution 200-500 μm. Previous experimental studies performed at the Energy research Centre of the Netherlands (ECN) showed that this material presents a storage energy density of 1 $GJ \cdot m^{-3}$ when the material is used in a TC storage system with a 50% porosity packed bed reactor [63]. However, slow reaction kinetics under seasonal storage conditions [26], which might be related to the amorphization of the material [63]. This phenomenon occurs when the system works under p(H_2O) at 13 mbar (corresponding to the average value in northern Europe) [26]. Ferchaud et al. [63] studied the effect of vapour pressure in the dehydration reaction to finding the optimal conditions that should be set in a TC storage system. The dehydration was carried out between 30 °C and 150 °C with a heating rate of 1 °C/min and left for 15 minutes at 150 °C to stabilise the composition of the dehydrated material, applying six different vapour pressure ranging from 13 to 70

mbar. The two consecutive reactions taking place during the dehydration of $MgSO_4 \cdot 7H_2O$ show an increase of the reaction rate with increasing $p(H_2O)$ until 50 mbar. The reaction rate decreases again for $p(H_2O)$ above 50 mbar. This phenomenon is known as the Topley-Smith effect found in many salt hydrates [81]. This effect is often explained by assuming that the increasing water vapour pressure promotes the formation of additional structural defects (additional channels, cracks and pores), which increases the water vapour removal out of the material and thereby facilitate the formation of a new lower hydrated phase. The authors concluded that the dehydration process is directly influenced by the water vapour pressure applied in a seasonal heat storage system. The kinetics of the reaction increases when the water pressure decreases below 50 mbar and decreases when pressure is above 50 mbar. When working at lower pressures (less than 50 mbar), the water pressure seems to promote the formation of structural defects which facilitate the water removal of the material. However, above 50 mbar a saturation of the material surface in water vapour reduces the removal of the water vapour in the material.

Okhrimenko et al. [78], like other authors, stated that the full hydration/dehydration process can generate theoretical energy storage of 2.8 $GJ \cdot m^3$. However, system performance is low given the rapid particle agglomeration during the dehydration/hydration cycles, limiting gas transfer and low-temperature lift. The authors also reported the naturally occurring stable states as epsomite (7 water), hexahydrite (6 water), kieserite (1 water) and anhydrous. Other metastable phases can be produced (11, 5, 4, 3, 2, 5/4) can be produced synthetically. Under certain conditions the non-stable hydrates can also be obtained such as 4,2.4,2,1.25 and 1 using the buffering technique, to prepare magnesium sulphate monohydrate, high hydrate like $MgSO_4$ hepta- or hexahydrate was dried at 350 °C and rehydrated under saturated salt

solution. It seems that the formation of the lower crystalline hydrates of magnesium sulphate is possible in special conditions like high relative humidity. The amorphous phase obtained by rapid dehydration of the high magnesium sulphate hydrates appears like metastable phase which can retain variable water content. The authors noticed the appearance of an amorphous phase above 50 °C as reported in the literature [82]. They characterised three samples with a different specific area and sample mass in the STA (40 °C and 2 hPa water), which showed a different reaction rate (kinetics). Concluding that the final mass loss is related to temperature and water pressure and not to the specific surface. Thus, this system is bivariant and some magnesium sulphate hydrates appear as non-stoichiometric hydrates of $MgSO_4 \cdot 6H_2O$ solid phase. Posern et al. [83] explained the deliquescence phenomena that takes place above the hydration reaction or the deliquescence humidity (DRH) at a certain temperature. Scapino et al. [44] also reviewed its potential use in open systems. As demonstrated by Essen [46], the authors also experienced that magnesium sulphate is unable of taking water above 50 °C unless very high relative humidity is applied ($\sim 80\% \, R.H$). The temperature lift was increased during the first 2 hours given these two effects: continuous hydration reaction resulted on heat generation and the heated reactor was always cooled by the fed moist air. The zero-temperature lift is reached when the stored heat was completely released (absorbent hydration saturated).
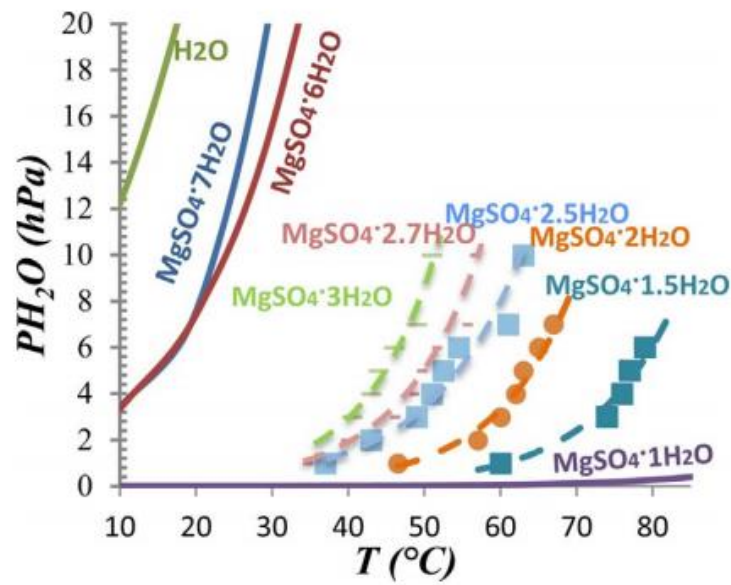
Figure 32. Magnesium sulphate phase diagram [82].

(1.1)   Calcium sulphate

Calcium sulphate is a case of less studied TCM material that presents great potential for thermal energy storage. Calcium sulphate occurs in nature in three different forms $CaSO_4 \cdot 2H_2O$ (gypsum), $CaSO_4 \cdot 1.5H_2O$ (hemihydrate) and $CaSO_4 \cdot 0.5H_2O$ (anhydrite) [84]. The hydration reaction of calcium sulphate (2 H_2O to ½ H_2O), has been studied for gas-solid chemical pumps applications [85]. However, this material is mostly used in industrial processes (limestone-gypsum flue-gas desulfurization (FGD), production of phosphoric acid or phosphate fertilizers) and has not been boarded to thermochemical storage, see phase diagram in Figure 33.

Given its application as a binder and building material, attention has been paid to the hydration-dehydration processes of calcium sulphate. Some industrial processes are accompanied by the crystallization of calcium sulphate phases such as the wet limestone-gypsum flue-gas desulfurization (FGD), the hydrometallurgical production of zinc and copper, and the recovery of natural gas and oil. Strydom et al. [86] investigated

the thermal dehydration of synthetic calcium sulphate at different heating rates. They concluded that the dehydration takes place into three steps, which are highly influenced by the number of impurities present in the salt. The first dehydration stage is ruled by the nucleation, the second and last one is diffusion-controlled.

The second dehydration (loss of 1.5 moles of water) overlaps with the first dehydration, the reaction from the dihydrate to the hemihydrate is observed to be very slow under 95 °C. While the last stage is uncertain to determine where it starts and ends, at 450 °C the authors still observe some traces of $CaSO_4 \cdot 0.15\ H_2O$ together with the anhydrous. Hudson-Lamb et al. [87] studied the dehydration of natural gypsum and pure calcium sulphate dihydrate. Although the authors stated that the dehydration takes place in two different steps; from the dihydrate to the hemihydrate, and from the hemihydrate to the anhydrous, they also found traces of $CaSO_4 \cdot 0.15 H_2O$ at 240 °C. Unlike Strydom et al. at 450 °C, only anhydrite was present in the calcium sulphate. Badens et al. [67] also studied the dehydration of gypsum powder, reporting the presence of two anhydride species γ-$CaSO_4$ and β-$CaSO_4$. The first one is called soluble anhydride because of its spontaneous hydration into hemihydrate under common atmospheric conditions, and the beta form is called as the insoluble anhydride. The transformation from alfa to beta takes place at around 127-227 °C. The thermal path highly varies on depending on the vapour pressure, the authors found that at 500 Pa or below there is only one dehydration product from gypsum to γ-$CaSO_4$. At 900 Pa the hemihydrate is an intermediate product between gypsum and γ- $CaSO_4$. Al-Abbasi et al. [47] modelled the performance of copper sulphate under open-system conditions. The authors concluded that, although it has high thermal efficiency, the reaction was really slow, and it was greatly affected by melting during dehydration over consecutive cycles. Ogura et al. [88] proposed a reversible chemical heat pump based on calcium sulphate and water

reaction. They mainly studied the reaction from the hemihydrate to the anhydrous state in open and closed systems. The main outcomes were related to the reaction rate in the open system, which was not different from the semi-open system data and quite close to that in the closed system. Considering the $CaSO_4/CaSO_4·1H_2O$ reaction the best candidate for low-temperature CHP reactant. Lee et al. [89] studied the same reaction also for a CHP system, storing heat at around 100 °C. The authors calculated the hydration and dehydration conversion after 450 cycles, they observed a reaction degradation given the irreversible transformation of III- $CaSO_4$ into II- $CaSO_4$, which are various forms of the crystal structure. From these results, they concluded that this phenomenon is dependent to proper pressure control (423 K at 30 kPa, 413 K at 151 kPa, and 403 K at 453 kPa) for ensuring the durability of the material. Richter et al. [90] in their material secreening study also included calcium sulfate, which showed appropriate temperature levels for the reversible hydration reaction and a small reaction hysteresis.
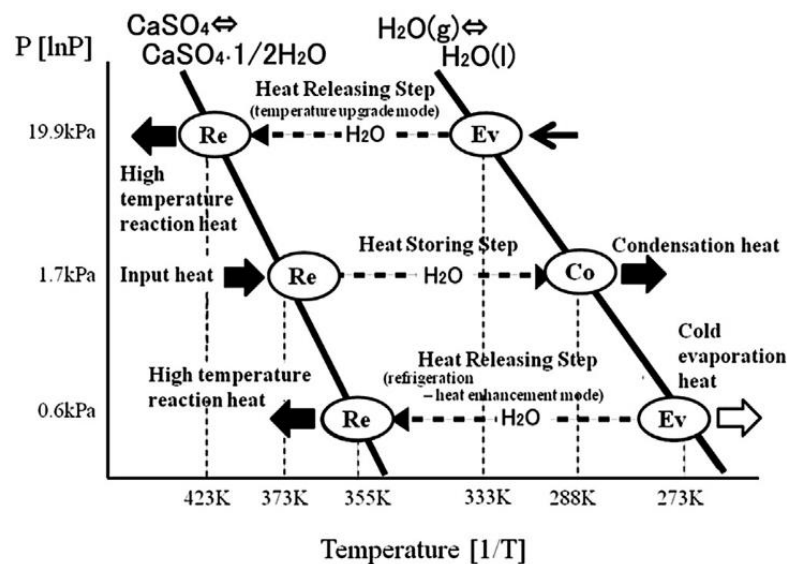

Figure 33. Phase diagram of CaSO₄ system [89].

(1.2)   Copper sulphate

Copper sulfate ($CuSO_4$) is a salt hydrate material that has the advantage of having a high DRH at ambient temperature (25 °C) and the dehydration of the first four water molecules can be driven by low-temperature heat source 60-85 °C (see phase diagram in Figure 34). Such attributes have attracted the researcher's attention as a new working pair for thermally driven adsorption desalination-cooling systems (ADCSs). Ali et al. [70] explored the use of copper sulfate in ADCS by studying the effect of changing relative pressure in the sorption reaction. The authors concluded that copper sulfate system could be driven by solar energy or other low-temperature renewable energy heat source (55-85 °C) allowing activation energy of 25.053 kJ/mol. The salt dehydration was mostly in the '60s and '80s by [71,72,91–93], and some comparative papers with other thermochemical materials have been published in the last years [7,47,94]. Wendlandt [71] studied the dehydration of copper sulfate concluding that the dehydration from the hepta- to the trihydrate happens in two steps, concluding that there was an intermediate phase $CuSO_4 \cdot$ 4 H_2O at high pressures. Borchardt and Daniels [72] studied the X-Ray diffraction as well as the dehydration stages. They found that no peaks appear between 275-725 °C, above 725 °C the two-stage decomposition from $CuSO_4$ to CuO with $CuSO_4 \cdot$ CuO as an intermediate was observed. However, they did not find any traces of the tetrahydrate, concluding that Borchardt and Daniels must have had a sample consisting of a mixture ($CuSO_4 \cdot$ 3 H_2O and adhering solution). More up to date studies have studied hybrid composites, Gordeeva et al. [94] prepared a silica gel/ copper sulfate 'salt in a porous host matrix' composite, concluding that copper sulfate allowed the lowest salt content among the salts studied (17.3 wt.% of salt content) although the ratio between the linked metal and the free metal was the highest. With increasing salt content, the free metal fraction increased as well, while the "linked" metal fraction decreased. Al-Abbasi et al. [47] overviewed the performance characteristics of copper sulphate, revealing that the salt shows a high thermal efficiency, slow reaction kinetics

and that the melting during dehydration greatly affects the lifetime over consecutive cycles. The copper sulphate can be also applied to produce hydrogen by water-splitting utilising the decomposition reaction after fully dehydration of the salt as reported by Gonzales et al. [73]. Although the dehydration reaction is considered in the cycles, this is not the driving force for the hydrogen production [95].
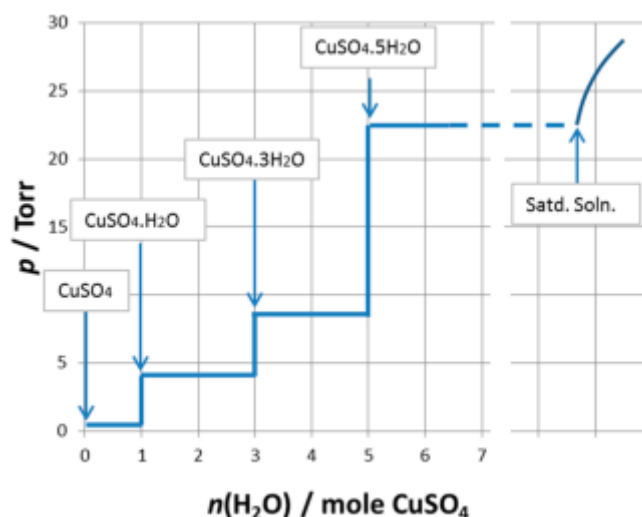

Figure 34. Vapour pressures of aqueous copper sulphate system at 25 °C [7].

(2) Carbonates

(2.1)   Potassium carbonate

Potassium carbonate was proposed by Donkers et al. [6] for an open and closed system for domestic applications, although they also stated the inconvenient of its low energy density. For this reason, we decided to include this paper in this study, aiming to provide more experimental data and evidence of the physical and chemical properties of the potassium carbonate. In Donkers's work, they apply four criteria to select a TCM according to energy density on a material level above 1.3 GJ·m^{-3}, hydration temperature above 50 °C, dehydration temperature below 120 °C and a melting point above the dehydration temperature. Among 25 candidates, the reaction of K_2CO_3 (0-1.5) was the

one that accounted for the lowest volume change while is not strongly corrosive, no higher hydrates are known, and it has no known unsafe side-reactions. The interest in potassium carbonate lies on its easy availability, reasonable capacity for water uptake and energy density at low temperature (below 100 °C), while better stability than other salts that show higher energy density attributes. After this work was published, some other authors have studied potassium carbonate for building applications. Gaeini et al. [40] studied the reaction kinetics and mechanisms of de/re-hydration of K_2CO_3. According to their outputs, the dehydration takes place on a single step from sesquihydrate to anhydrous with an enthalpy of reaction of 60.88 kJ/mol and a bulk material energy density of 0.75 GJ·m^{-3}. The performance of the material improves upon cycling since its kinetics become faster after each cycle [40]. Despite the advantages, application of K_2CO_3 is challenged by the slow hydration rate, swelling/shrinking and particle agglomeration [37]. The phase diagram of potassium carbonate sesquihydrate pressure versus temperature is shown in Figure 35.
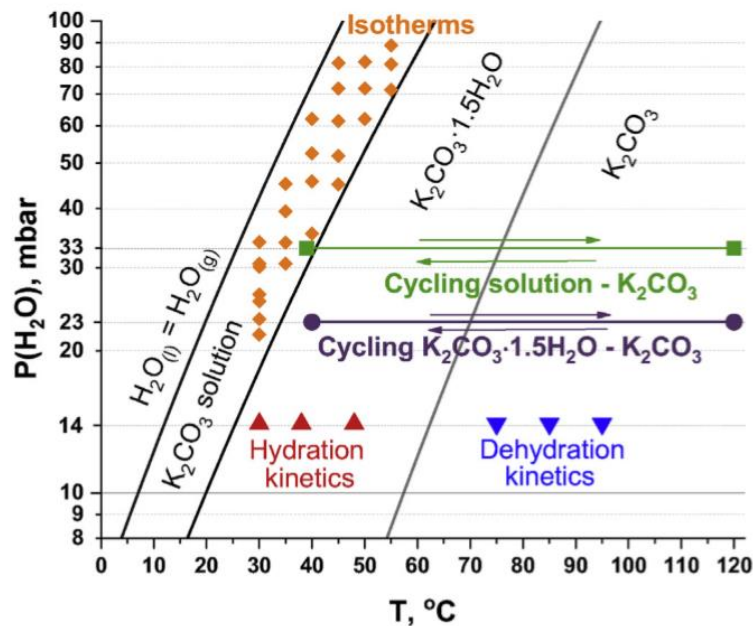

Figure 35. Diagram of K_2CO_3-H_2O system [37].

(3) Bromides

(3.1)   Strontium bromide hexahydrate

Strontium bromide has been detected as one of the most promising salts along with magnesium sulfate [96]. $SrBr_2 \cdot 6H_2O$ has been already well investigated at laboratory and prototype level for various applications either for solar cooling and heat storage in a closed process [97], or seasonal storage of solar energy in an open process [98,99]. For short storage applications, it can be considered as storage and thermal comfort material (also as phase change material). The high enthalpy (ΔH_r° = 67400 J$\cdot mol_G^{-1}$) and the density of the hexahydrated strontium bromide (2.386 g/cm^3) allow the salt to reach a high energy storage density [19]. Besides, thanks to its high melting point, which enables a charging/discharging melting-free process. Its ideal energy storage is very high with 628 kW·h·m^3, indeed it was found that the energy in an open system was 400 kW·h·m^3 [98] and 531 kW·h·m^3 [97] for a closed system. Hence, it is one of the salts that allow high-energy storage potential below 105 °C [96]. Application-wise a temperature ranging from 80-90 °C is sufficient to ensure the dehydration from the hexahydrate to the monohydrate without incongruent dissolution of water vapour in the solid phase, given the melting point [21], see phase diagram in Figure 36. The dehydration of strontium bromide has been reported to take place in two stages; from hexahydrate to monohydrate and from monohydrate to anhydrous. Richter et al. [90] studied strontium bromide in the framework of salt hydrates for a thermochemical heat transformer, concluding that $SrBr_2$ could withstand up to 10 charging/discharging, obtaining appropriate temperature levels for the reversible hydration reaction and a small reaction hysteresis. Besides, $SrBr_2$ is not toxic and forms a monohydrate with appropriate thermodynamics to thermally upgrade heat in an open process mode. Strontium bromide forms a hexahydrate that melts at 88.6 °C, for that reason for

practical use the TCM is dehydrated at a low heating rate below the melting point and stored at 110 °C. To prevent a further reaction to the hexahydrate and deliquescence, the authors suggested a minimum temperature for hydration to 150 °C, therefore, just working on the reversible reaction from monohydrate to anhydrous. Michel et al. [100] presented an approximate plot of the limit of the saturated solution of the hexahydrate, calculated by interpolation between the melting point (88.62 °C) and its eutectic (28 °C) as shown in Figure 36. $SrBr_2$ is one of the salts included in this study that has been studied up to prototype level [20,97,101–103], which denotes a higher potential for application and a deeper understanding of the salt reaction for both pure and composite formulations. According to the literature under atmospheric pressure the dehydration of the hexahydrate to the monohydrate is monotonous, desorbing 26% of the available water content (30.4%). The hydration occurs at 20 mbar and 25 °C, even though a water vapour pressure can be applied above 40 mbar at 60 °C. Above that temperature, no hydration is observed at water saturation temperature [21]. Given its latent heat, strontium bromide can also be used as a PCM. When used as a phase change material could present incongruent melting due to the insufficient release of water (uncompleted melting or charging) to dissolve the remaining salt crystals [21]. As the present salt just draws attention to heating and cooling storage application, its actual price is seen as a major inconvenient 24-17 €/kg for the hydrate and 320-210 €/kg for the anhydrous. N'Tsoukpoe et al. [96] showed that, when an external heat source is used for the evaporation and that heat is considered as free and not considered in the evaluation of either the heat storage density and the thermal efficiency, the $SrBr_2 \cdot 6H_2O$ remained the best among over 125 screened materials from a thermodynamic point of view.

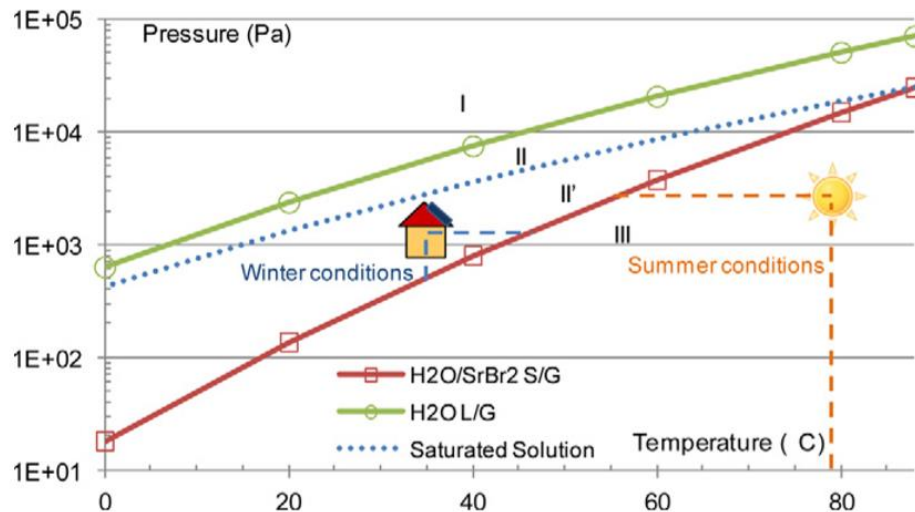Figure 36. Equilibrium lines of the solid/gas reaction and liquid vapour change of $SrBr_2$/1-6H_2O [100].

(4) Nitrates

(4.1)   Magnesium nitrate hexahydrate

Magnesium nitrate has been used as a phase change material (PCM) given its relatively high latent heat of fusion [53,104], [52]. However, it also allows storing heat in the thermochemical heat form [42]. These dual materials are called as reactive phase change materials. Although it shows a decent energy density, volume change and the melting point above hydration/dehydration process, it is usually not considered a strong candidate as it displays a tendency for significant supercooling and decomposes to magnesium oxide under strong heating conditions [52,105]. $MgNO_3$ hexahydrate turns into dehydrating if heated above 95 °C, the equilibrium diagram of magnesium nitrate and water was reported by Kenisarin et al. [52] (see Figure 37). The dehydration occurs in three steps; from the hexahydrate to the dihydrate showing that the slow dehydration is stable at lower hydrates states before decomposing at 400 °C. Two decomposition steps were observed by Paulik at al. [105] and Drake et al. [106], one from 300-400 °C with 56% mass loss of the initial hexahydrate and from 450-500 °C with a 17%. Drake et

al. [106] combined two energy storage methods aiming to harness the advantages of both (latent heat and thermochemical) by studying the eutectic composition of Magnesium nitrate and water. For that purpose, they studied the melting and dehydration of the magnesium nitrate. They found that from the dihydrate to the complete anhydride (at 270 °C) none endothermic peaks can be observed, which they attributed to an obscured of the peak due to an experiment drift. Concluding that the use of quasi-isothermal and quasi-isobaric conditions are needed for an adequate resolution. Since the study was latent heat targeted, they also studied the melting, which they found to be incongruent that is a common effect in salt-hydrate PCMs. When the magnesium nitrate melts, the water is evenly dispersed, but on freezing, the original crystalline structure may not be perfectly reformed, and these different states may have an energy disparity (supercooling) [106]. Likewise, higher dehydration temperatures are associated with increased supercooling and incongruent melting. The formation of a lower hydrate from incongruent melting is irreversible. The two stable hydrates of dehydrating are formed by incongruent melting of the hexahydrate [13].
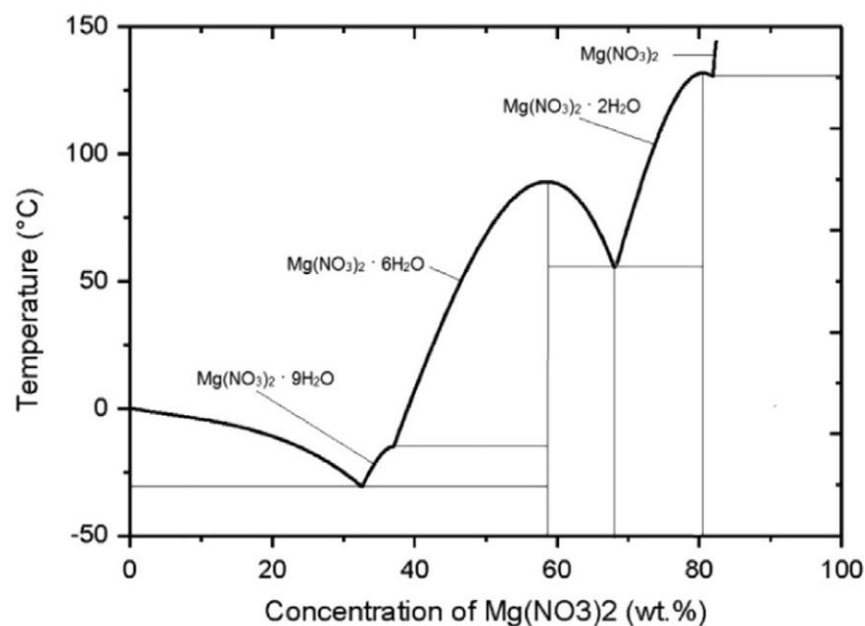

Figure 37. Phase diagram of $Mg(NO_3)_2$-$6H_2O$ system [52].

(4.2)   Zinc nitrate heptahydrate

Similarly, as for magnesium nitrate, zinc nitrate and calcium nitrate were proposed for latent heat storage [41] but have not been yet explored for thermochemical storage. The solid-liquid equilibrium was studied by [107] and they were also screened by Donkers et al. [42] for domestic applications, see phase diagram of the zinc nitrate system in Figure 38. Both have an energy density around 1.5-1.7 GJ·m^{-3} and a dehydration-hydration temperature range that meets the system requirements. The thermal decomposition of zinc nitrate has been recently studied by Malecka et al. [66], they found out that the dehydration starts at 30 °C, which is accompanied by the melting at 35 °C. According to them, the dehydration occurs in three consecutive steps that finished at 120 °C. The decomposition of nitrates groups starts at 75 °C and finalised at 265 °C forming ZnO as the final product. Literature shows that is difficult to get high purity to isolate zinc nitrate from zinc nitrate hexahydrate and compute the stoichiometric content of water [108]. Kumar et al. [108] added nucleation additives to zinc nitrate hexahydrate, to that end they also studied its thermal decomposition.
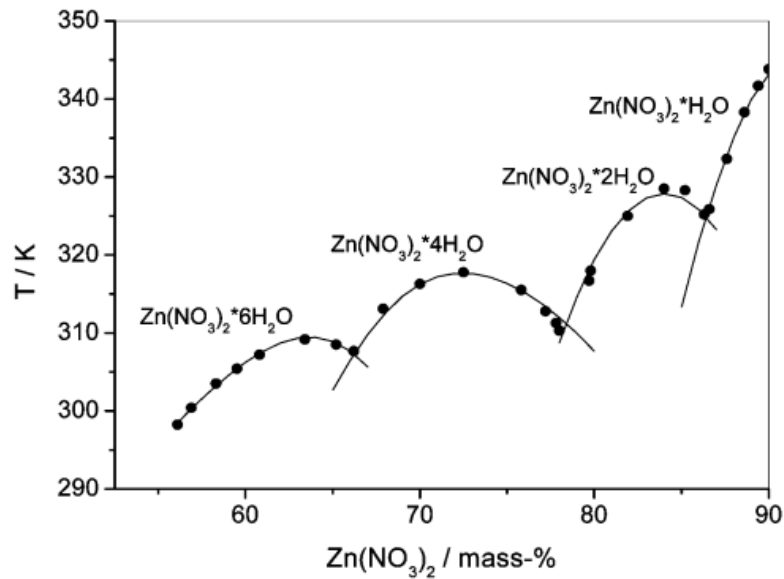
Figure 38. Phase diagram of Zn(NO₃)₂-6H₂O system [51].

(4.3)   Calcium nitrate tetrahydrate

Calcium nitrate tetrahydrate is one of the most commonly used inorganic salts given its high latent heat and low melting point [109]. However, it has not been deeply studied for thermochemical storage purposes. Liu at al. [110] added a double-layer coating technology of epoxy resin and cement to calcium nitrate tetrahydrate, which significantly enhanced the heat resistance of the crystals and reduced the deliquescence problems at room temperature. Guo et al. [111] proposed a solid-liquid calcium-based composite by adding calcium nitrate tetrahydrate to calcium nitrate hexahydrate as a modifier for latent heat applications purposes. As for magnesium nitrate, Paulik et al. [68] examined the dehydration of calcium nitrate under quasi-isothermal and quasi-isobaric conditions. They reported, as shown by other authors before, that the calcium nitrate dehydrates in four steps. The salt melts at 42.7 °C forming a saturated solution that with increasing temperature becomes unsaturated. Up to the boiling point, the salt does not lose water, above 135 °C, the solution starts losing water. Therefore, the authors concluded that the dehydration process was not based on consecutive reactions

but the course and overlapping of physical processes such as evaporation, boiling, drying and solid crust formation. The phase diagram of the calcium nitrate system is shown in Figure 39.
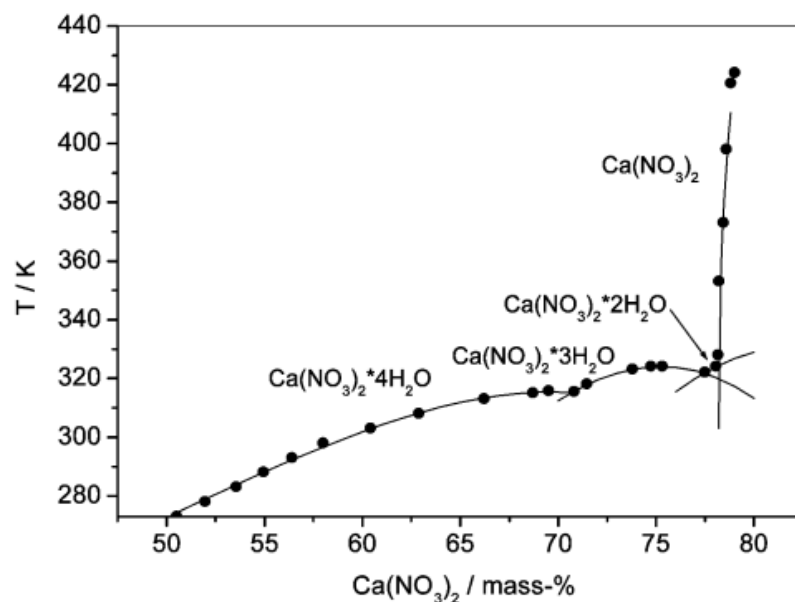

Figure 39. Phase diagram of Ca(NO$_3$)$_2$-6H$_2$O system [51].

(5) Chlorides

LiCl, MgCl$_2$ and CaCl$_2$ are of strong hygroscopicity, which could adsorb water vapour and form solution in a closed system. This phenomenon is called deliquescence (see Chapter 4), which could bring the problems: salt segregation, corrosion in sorption reactor and deterioration of heat and mass transfer of sorbents [20]. Calcium chloride and Magnesium chloride are the other two TCMs targeted with great potential for thermochemical heat storage [76]. They exhibit high energy density at the desired operational temperatures. However, magnesium chloride suffers from thermal decomposition and HCl formation as well as deliquescence below 40 °C.

(5.1) Calcium chloride

N'Tsoukpoe et al. [54] reviewed the use of calcium hydrate in applied thermal Engineering, concluding that calcium chloride is a promising material for drying and heat storage applications, which is already used for dehumidification of buildings. Calcium chloride has the potential to be used as a phase change material given its simple application around 30 °C. Its use for thermochemical storage is promising although it presents performance issues such as low melting point and a high tendency for agglomeration, see phase diagram in Figure 40. Before recording the XRD diagram, the SG62/CaCl2 composite was exposed for about 4 h to a saturated water atmosphere to prepare a composite with a high hydration rate (i.e. $CaCl_2 \cdot 4H_2O$). Between 30 °C and 50 °C, no X-ray diffraction peaks were observed showing that the $CaCl_2$ is amorphous or liquid, while crystalline $CaCl_2 \cdot 4H_2O$ was expected. This indicates the dissolution of $CaCl_2 \cdot 4H_2O$ in the composite. Between 60 °C and 80 °C, the dihydrate form of $CaCl_2$ was observed, and, for temperatures higher than 90 °C, anhydrous $CaCl_2$ was mainly observed. The monohydrate form of $CaCl_2$ was not observed regardless of the temperature applied. This explains the water vapour sorption behaviour of this composite: first, the hydration reaction of $CaCl_2$ into $CaCl_2$ dihydrate occurs followed by the hydration reaction to the $CaCl_2$ tetrahydrate, which dissolves to form a $CaCl_2$ solution. Then the absorption of water in the $CaCl_2$ solution trapped in the pores of silica gel occurs. The hysteresis observed between the sorption and desorption steps is, hence, explained by the recrystallization step. Zhao et al. [112] studied the working pair of zeolite and calcium chloride, by impregnating zeolite 13X with different aqueous solution concentration of $CaCl_2$. They found out that the samples containing 5 wt.% and 10 wt.% have much better performance than the pure zeolite, the water uptakes equilibrium of formulation with 15 wt.% and 20 wt.% were lower than the pure zeolite. Aydin et al. [113] examined the $CaCl_2$ using the incipient wetness impregnation method of different working pairs, vermiculite, silica gel, zeolite in an open-sorption pipe reactor.

Bouché et al. [114] studied the dehydration of the dehydrate to the anhydrous for industrial waste heat upgrade by using an open system in the range of 100-200°C. They perform the dehydration at 150 °C, 130 °C and 100 °C and around 40 kPa, concluding that the system enables the utilization of waste heat at 100 °C with a thermal upgrade of 65 K. P. D'Ans et al. [115] and Courbon et al. [116] proposed a working pair based on silica and calcium chloride, with a salt content of 43 wt.% and 40-43 wt.%, respectively. While [115] opted to encapsulate the salt in mesoporous silica, the authors of [116] proposed to successive impregnation of salt solution into silica gel producing high content and stability composites. Both studies lead to a cycle loading lift of 0.4 g/g. Courbon et al. [116] found out that the mechanism of water sorption goes beyond the hydration from anhydrous to 4 H_2O, the $CaCl_2 \cdot 4\ H_2O$ dissolves to form a $CaCl_2$ solution leading to water trapped in the silica gel pores. Gough et al. [117] studied the deliquescence of calcium chloride for exploring its potential in Mars. The authors used a Raman microscope to determine when occurs the deliquescence of the salt for the three phases of calcium chloride (hexahydrate, dihydrate and anhydrous). They observed that often $CaCl_2 \cdot 2\ H_2O$ deliquesced directly into liquid brine without forming $CaCl_2 \cdot 6\ H_2O$ phase, jumping the hydration step prior deliquescence. The deliquescence was observed to lower with increasing temperature for the hexahydrate, while for the dihydrate showed a weaker dependence to temperature. Gordeeva et al. [94] used the impregnation method to prepare silica gel/calcium chloride composites, concluding that the sorption equilibrium of the composites can be managed by varying conditions of the composite preparation. Jabbari-Hichri et al. [36] prepared calcium chloride composites with silica-gel, alumina and bentonite (15 wt.% of TCM), among all the matrices studied, silica gel showed the best performance given the low pore blocking and the high heat and water storage values. Jiang et al. [118] explored the development of bi and tri-salt graphite-composite sorbents by combining magnesium chloride, calcium chloride and

ammonium chloride. The multilevel sorption lead to alleviate the sorption hysteresis and a higher energy density. Karunadasa et al. [119] investigated the correlation between the stability of hydrated/anhydrous products and microstructural changes of calcium chloride, finding that there are two different phases of anhydrous calcium after dehydration (large and small unit cell). The stability of the phases is dominated by the lattice strain, larger crystallite size and small unit cell volume. Kim et al. [120] studied a composite comprising a mixture of expanded graphite, magnesium oxide and calcium chloride for a chemical heat pump application. From the study, the authors proposed a multiplied factor consisting of dehydration rate and mixing weight ratio, which suggested that 0.8 was the optimised value when the mixing molar ratio between $CaCl_2$ and $Mg(OH)_2$ was 0.10. Korhammer et al. [121] studied the reaction of the mixture between calcium chloride and magnesium chloride with alcohol, which revealed that the sorption behaviour can be controlled by the variation of ethanol pressure and, as confirmed by other authors, that the mixtures of salts from the same family lead to a superior thermal behaviour with higher heat storage capacities. Gaeni et al. [60] published a comprehensive study on the stability of calcium chloride-based materials, to that end they studied different manufacturing approaches: impregnated expanded graphite composite, impregnated vermiculite composite, encapsulated calcium chloride powder. From all the methods used, encapsulation is the one that shows the best cycling stability, although it allows for the lowest energy density than the other methods. While the impregnated samples lead to an agglomerated structure similar to the dehydrated pure salt, which reduces the conversion over cycles. Molenda et al. [55] studied the reversible reaction of calcium chloride at high H_2O partial pressures (from kPa to 96.5 kPa), which demonstrated that the reaction of calcium chloride is applicable for thermochemical energy storage up to 180 °C. They found intermediate hydration, a metastable step with 0.3 mole H_2O/mole $CaCl_2$, although they did not observe the

formation of the monohydrate as [60]. Interestingly, they noticed the dehydration of the hydrate happens in two processes depending on the pressure; at high pressures, the 0.3 H_2O intermediate step appears to be determinant, while at low pressures the monohydrate appears to be the intermediate step. This revealed a correlation between the formation temperatures the intermediate species and the partial vapour pressure. Richter et al. [114] studied the endothermic dehydration of calcium chloride dihydrate at lab scale reaction level as it exhibits complete reversibility, thermal and cycling stability and reasonable kinetics at temperatures up to 200 °C. They reported a thermal upgrade of 35 °C, discharging at 165°C and charging at 130 °C with a full conversion from the anhydrous to the dihydrate. By using the intermediate step ($CaCl_2 \cdot 0.3\ H_2O$) reported by [55], the discharging could be conducted at 180 °C, which increases the thermal upgrade to 50 °C but reduces the storage density. Therefore, to increase the thermal upgrade wither hydration needs to take place at higher temperatures or dehydration at lower ones. Two calcium chloride composites were presented by Ristic et al. [122], one disordered and the other one ordered mesoporous iron silicate matrix. Both composites showed good hydrothermal stability after 20 cycles from 150 °C to 40 °C at a water pressure of 5.6 kPa, although the authors found more suitable the disordered one for solar thermos-chemical heat storage, while the ordered one is more suitable for dehumidification applications. Skrylnyk et al. [50,123] formulate a silica gel/calcium chloride (43 wt.%) composite, the main findings were that prolonged hydration below 30 °C causes material wetting and agglomeration, although the heat upgrading performances are better. Therefore, the authors recommend a reaction advancement level between 50% and 60%. Sutton et al. [32] studied the performance of calcium chloride impregnated into porous vermiculite demonstrating that the behaviour of the storage media differ significantly between bulk material and single particle/thin layer geometries. The area of deliquescence is typically 60-100 mm into the bulk of the

material from the edge, which means that the penetration of moist air into the bulk is limited by this effect. Other authors have tried to improve the heat transfer capacity of calcium chloride by the addition of graphite based matrices, Tian et al. [124] studied the thermal conductivity, permeability and density of expanded natural graphite (ENG)/calcium chloride. They found that the permeability almost increases linearly with the mass ratio of ENG decreasing, while the thermal conductivity is proven to increase with the ENG content.
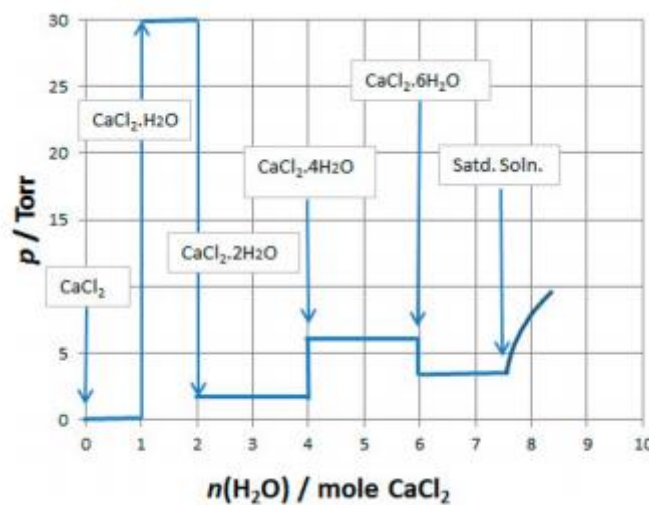
Figure 40. Vapour pressure of aqueous calcium chloride systems at 25°C [7].

(5.2)   Magnesium chloride

Several studies revealed the promising potential of magnesium chloride for seasonal heat storage in terms of energy density and temperature release. Aside from the common issues of instability and decomposition over cycles, this material is particularly disadvantaged from the fact that at ambient temperature it tends to overhydrate into a solution, which causes inhomogeneous dehydration. On top of that, above 150 °C (some authors reported even earlier decompositions), the chlorides decompose into magnesium hydroxy chloride involving a release of hydrochloric acid. Such reaction

causes obvious damages and reduces the quantity of active sorption material over time. The hydrolysis reaction occurs at the same time as the last dehydration reaction stage (from dihydrate to monohydrate) [125]. Ferchaud et al. [63] studied the XRD patterns of the hydration/dehydration intending to determine the temperature range over which magnesium chloride remains in a stable hydrated state during its dehydration/hydration reactions (13 mbar). The main outputs are that the minimum hydration temperature should be set at 40 °C to avoid the overhydration of the material; the dihydrate hydrates to the tetra- at 100 °C, and to the hexahydrate at 60 °C; the material remains in a solid-state until 30 °C; no characteristic peaks of magnesium hydroxy chloride were observed at 150 °C after 3h. Gutierrez et al. [126] recently studied the reversible reaction of a ternary equilibrium solution KCl-MgCl$_2$-H$_2$O. The authors brought more shreds of evidence of that at temperatures close to 180 °C small amount of HCL are observed from the decomposition of magnesium chloride. Also, decomposition and/ or melting was confirmed, which has a strong effect on the cycling stability of the active material. According to Zondag et al. [127], the formation of HCl was found to happen at temperatures above 150 °C, before 180 °C. They also found out that the material closer to the evaporator was overhydrated found to overhydrate, transforming to a gel-like structure, after kept long-term hydration. Mamani et al. [64] studied the viability of using bischofite (a material containing 97.4% of MgCl$_2 \cdot$ 6 H$_2$O), bringing more evidence of the hydration/dehydration behaviour of the active thermochemical material that was in accordance to the previously published work. Huang et al. [65] described the thermal decomposition of magnesium chloride in six steps (under air); from Hexa- to tetra-, from tetra- to di-, from di- to 0.3 H$_2$O/MgOHCl, from 0.3 H$_2$O/MgOHCl to MgOHCl and from MgOHCl to MgO. Rammelberg et al. [56] studied the dehydration from the hexahydrate to the dihydrate in terms of water vapour pressure and conversion independence on the heating rate. The dehydration is completed after 2 hours below 140 °C (heating rate 1

°C/min), they found that the irreversible decomposition side reaction was running side by side with the dehydration $MgCl_2 \cdot H_2O$ at lower temperatures than other authors. According to the authors, the dehydration happened in three overlapping stages, which are not highly dependent to the heating rate. Ferchaud et al. [128] studied magnesium chloride at prototype level, they concluded that the thermochemical material could be dehydrated at temperatures below 130 °C and the hydration was sufficient to provide tap water heating at 60 °C.

(1) Dehydration (<200 °C); from Hexa to tetra and from tetra to di (2) Thermal hydrolysis (>200 °C); from mono to MgOHCl and HCl (3) Dehydroxylation (>400 °C); from MgOHCl to MgO and HCl [129], see phase diagram in Figure 41.
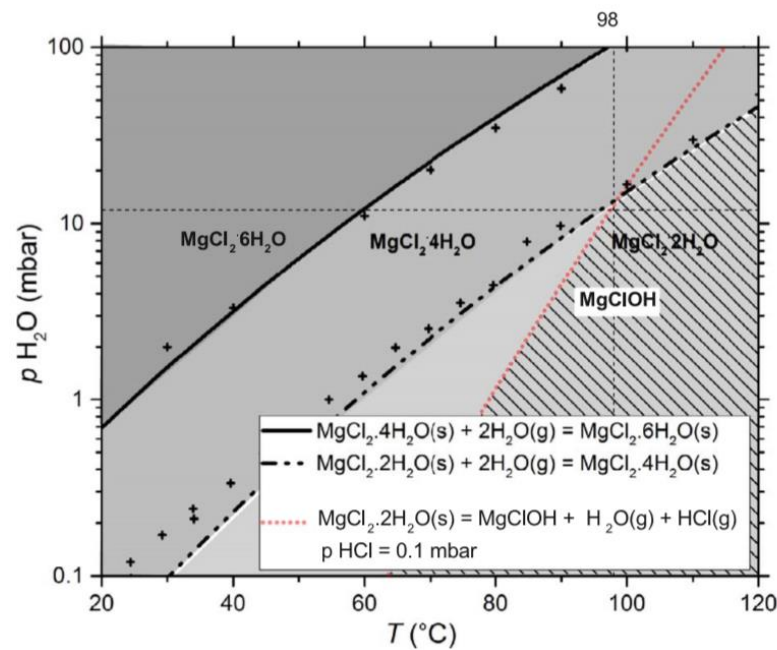
Figure 41. Phase diagram of Magnesium chloride [39].

8.1.2 TCS EXPERIMENTAL VALIDATION

(1) Materials

The magnesium sulphate, $MgSO_4$ $7H_2O$, was an analytical reagent grade (CAS: 10034-99-8, MW: 246.48) supplied by Fisher Chemical company©; the magnesium chloride, $MgCl_2$, was purchased in both anhydrous form from Acros organics (CAS: 7786-30-3, MW: 95.21, Pure) and hexahydrated form MP Biomedicals© (CAS: 7791-18-6, MW: 203.3, 98%). Potassium carbonate sesquihydrate, 98.5% purity was supplied by Acros organics™ (CAS: 6381-79-9, MW: 165.24). Strontium bromide hexahydrate, $SrBr_2$ $6H_2O$, (CAS: 7789-53-9, MW: 355.52, 99%), and Calcium chloride hexahydrate, $CaCl_2$ $6H_2O$, (CAS: 7774-34-7, MW: 219.8, 98%) both from Sigma Aldrich. Magnesium nitrate, $Mg(NO_3)_2$ $6H_2O$, 99.999% trace metals basis (CAS: 13446-18-9, MW: 256.41); Calcium nitrate hexahydrate, $Ca(NO_3)_2$ $4H_2O$, ≥99.0% (CAS: 13477-34-4, MW: 236.15); Calcium sulphate dihydrate, $CaSO_4$ $2H_2O$, ACS reagent ≥98.0% (CAS: 10101-41-4, MW: 172.17);Copper sulphate pentahydrate, $CuSO_4$ $5H_2O$, ACS reagent ≥98.0% (CAS: 7758-99-8, MW: 249.69); Zinc nitrate hexahydrate , $Zn(NO_3)_2$ $6H_2O$, reagent grade ≥98.0% (CAS: 10196-18-6, MW: 297.49), all purchased from Sigma Aldrich©.

(2) Methodology

Different techniques were used to experimentally validate the literature data and to reveal novel properties not previously studied in the literature; DSC was used to measure specific heat (dynamic and areas method hydrated and dehydrated state), the heat of reaction, reaction kinetics and melting point. The tests were repeated three times for specific heat and two times for enthalpy of reaction and melting point data. For the cycling tests and dilatometer (volume change); the samples were compressed into 1 g tablets and tested to determine their physical integrity and relative change in length up to 150 °C, respectively. The cycling test in the humidity chamber was performed under specific conditions specified

in Chapter 7. Thermal diffusivity was measured using a laser flash apparatus at room temperature for the hydrated and dehydrated TCMs. The hydration and dehydration sorption (water uptake) were studied by STA. To enable the selection of the material, the samples were characterised at the same conditions for all the TCMs (See Chapter 7). The specific methodology conditions and procedure followed are explained in Chapter 7

(3) Experimental results

The experimental data obtained from the set of characterisation techniques are presented in this section. A summary of the properties measured for each TCM is listed in Table 19, including the melting point, the enthalpy of fusion, the conversion rate/time at different hydration/dehydration conditions, the crystalline phases, the volume change and the physical integrity after cycling. The filters listed in Table 12 are applied in this section, note that filter 1 was also applied in the material screening done with the data found in the literature and presented in the previous section. For clarification, the ideal reactions that we are looking at in the working temperature range (25 to 150 °C) are shown in Table 18. The thermochemical reactions obtained in the experimental conditions are also listed in such table for both dehydration conditions and hydration at 80% R.H and 60% R.H. As Table 18 shows, the reactions observed during the experimental test can differ from those found in the literature, as in some cases the test conditions are different.

Table 18. Thermochemical reactions of the TCMs screened under operational condition and ideal (literature).

TCM	Dehydration Reaction in the literature (up to 150 °C)	Experimental dehydration (up to 150 °C)	Experimental hydration (80% R.H at 30 °C)	Experimental hydration (60% R.H at 30 °C)
$MgSO_4 \cdot 7H_2O$	7 H_2O ↔ 1 H_2O	7 H_2O → 1 H_2O	1 H_2O → 6 H_2O	1 H_2O → 3 H_2O
$SrBr_2 \cdot 6H_2O$	6 H_2O ↔ 1 H_2O	6 H_2O → 1 H_2O	1 H_2O → 6 H_2O	1 H_2O → 5 H_2O
$Mg(NO_3)_2 \cdot 6H_2O$	6 H_2O ↔ Anhydrous	6 H_2O → 2 H_2O	2 H_2O → 6 H_2O	2 H_2O → 4 H_2O
$CaCl_2 \cdot 6H_2O$	6 H_2O ↔ Anhydrous	6 H_2O → Anhydrous	Anhydrous → 6 H_2O	Anhydrous → 6 H_2O
$MgCl_2 \cdot 6H_2O$	6 H_2O ↔ 2 H_2O	6 H_2O → 2 H_2O	2 H_2O → 6 H_2O	2 H_2O → 6 H_2O
$Zn(NO_3)_2 \cdot 6H_2O$	6 H_2O ↔ Anhydrous	6 H_2O → Anhydrous	Anhydrous → 6 H_2O	Anhydrous → 5 H_2O
$CaSO_4 \cdot 2H_2O$	2 H_2O ↔ 0.15 H_2O	2 H_2O → 0.75 H_2O	0.75 H_2O → 1.55 H_2O	0.75 H_2O → 1.15 H_2O
$Ca(NO_3)_2 \cdot 4H_2O$	4 H_2O ↔ 2 H_2O	4 H_2O → 2.5 H_2O	2.5 H_2O → 4 H_2O	2.5 H_2O → 3.5 H_2O
$CuSO_4 \cdot 5H_2O$	5 H_2O ↔ 1 H_2O	5 H_2O → 1 H_2O	1 H_2O → 5 H_2O	1 H_2O → 2 H_2O
$K_2CO_3 \cdot 1/2H_2O$	1.5 H_2O ↔ Anhydrous	1.5 H_2O → Anhydrous	Anhydrous → 1.5 H_2O	Anhydrous → 1.5 H_2O

(3.1)   Filter 2 – Energy density

The energy stored was measured at three different heating rates (1 °C/min, 2.5 °C/min and 10 °C/min) up to the operational temperature selected of 150 °C, as shown in Figure 42. While some materials are strongly affected by the heating rate (e.g. magnesium chloride and calcium chloride), others do not show significant differences under different dehydration heating rates (e.g. magnesium sulphate and potassium carbonate). The materials that show higher energy density at the lowest heating rate (1 °C/min) are the ones framed in Figure 43 in the following decreasing order; magnesium chloride > calcium chloride > magnesium sulphate > strontium bromide > calcium nitrate > zinc nitrate > magnesium nitrate. Potassium carbonate, copper sulphate and calcium sulphate are the lowest one. Looking at the conversion dehydration rate (see Table 19), at 150 °C, the lowest conversion is reported for magnesium nitrate (51%), calcium nitrate (46%) and calcium sulphate (29%). Those materials cannot fully dehydrate under the test conditions as they partially dehydrate leading to intermediate hydrated species

(see Table 18). At this stage, copper sulphate and calcium sulphate are discarded since they have the lowest energy capacity among all the materials tested. Potassium carbonate is regarded as a candidate given the interesting potential of this material as it has been intensively studied these last years [6,37].
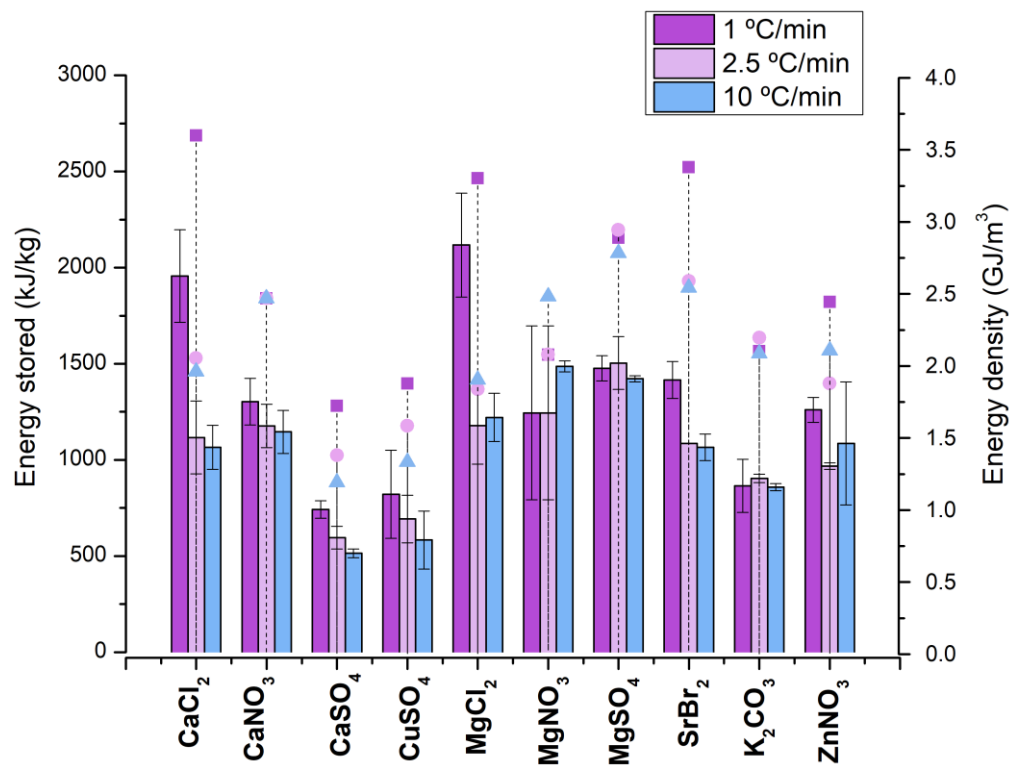

Figure 42. Energy stored and energy density of all TCMs screened under different heating rates (1 °C/min, 2.5 °C/min and 10 °C/min) from 25 °C to 150 °C in the STA.
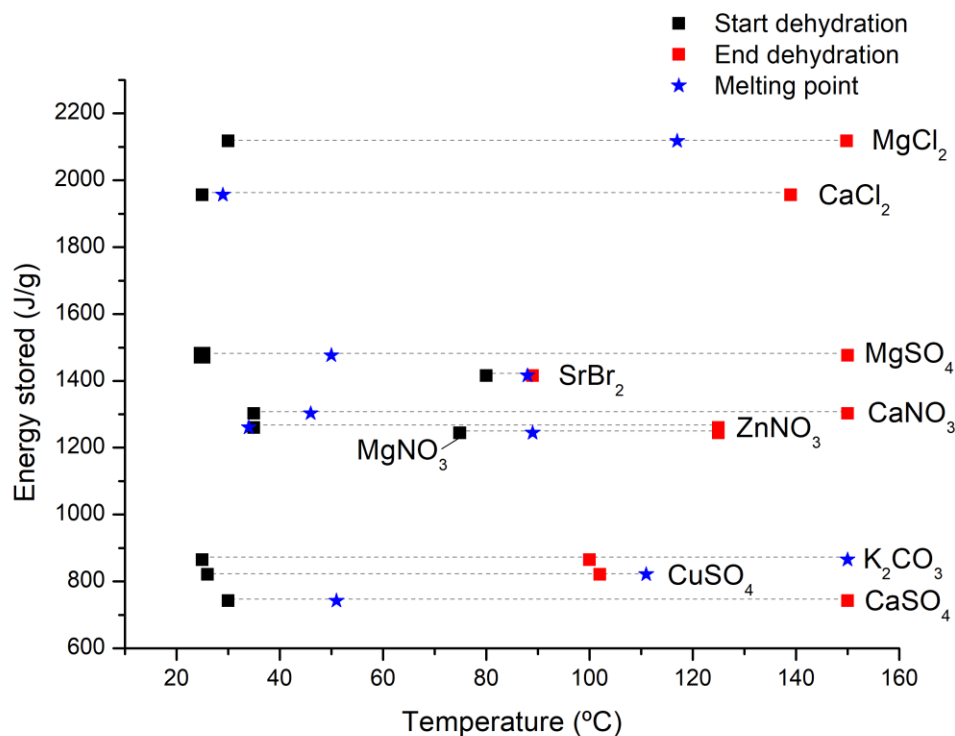
Figure 43. Energy stored, dehydration temperature range and the melting point of all the TCMs screened using the data obtained at 1 °C/min from 25 °C to 150 °C in the DSC.

(3.2)   Filter 3 – DHR and melting point

The TCM is desired to remain at solid-state, avoiding deliquescence of the salt, during the sorption/desorption process. Besides, the melting of the salt should be ideally higher than the dehydration temperature, as the melting process changes the structure of the TCM and might reduce the porosity of the system, reducing the vapour transport within the storage media. In this experimental validation, the deliquescence was studied by combining the visual inspection of the samples after hydration and the water uptake in the STA. The melting point was measured in the STA using the lowest heating rate under study (1 °C/min). Among all the TCMs studied, only potassium carbonate and copper sulphate exhibit the melting outside the hydration/dehydration region. The rest of the candidates undergo a melting transition during dehydration, as shown in Figure 43. Looking at the physical integrity after dehydration, as this is also

affected by the melting behaviour of the material, zinc nitrate and magnesium nitrate are the ones that present the worst performance as they lose the tablet shape right after dehydration. At the test conditions, Zinc nitrate decomposes, as shown in the XRD patterns Figure 50 and also observed by [66], while magnesium nitrate has a congruent melting transition to a low viscous fluid.

Regarding the deliquescence phenomenon on the salts, magnesium chloride and calcium chloride are the TCM's more sensible to high relative humidity at 30 °C, as reported in the literature and described in the previous section. They show deliquescence after 30 min of conversion at 80 % R.H., while they need more than one hour to hydrate at 60% R.H (see Figure 44). Strontium bromide, calcium nitrate and potassium carbonate also require lower conversion times to hydrate under both 80 and 60% R.H. Magnesium nitrate, copper sulphate, magnesium sulphate and calcium sulphate are more flexible regarding the hydration conditions, not showing deliquescence after reaching the total conversion to the maximum hydrated state. The lowest conversion is reported by magnesium sulphate, as it requires longer hydration times given the low kinetics reported by this TCM [77]. Further experimental validation has shown that 3 hours are enough to hydrate magnesium sulphate to the hexahydrate state at 30 °C 80% R.H., whereas 60% R.H. needs much longer times.

At this stage, zinc nitrate, calcium nitrate and magnesium nitrate are disregarded as candidates for the 3 in 1 system given their poor physical stability after one sorption/desorption cycle (see Table 22).
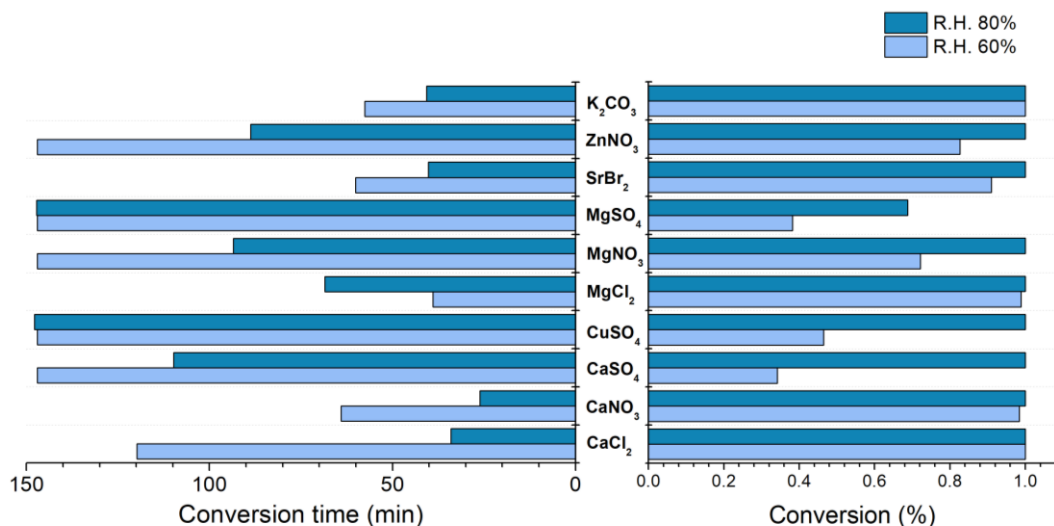
Figure 44. Hydration conversion and hydration conversion time at 30 °C and 80% R.H. and 60% R.H.

(3.4)   Filter 4 – Cost

The cost (€/MJ) listed in Table 19 has been calculated using the data collected in the literature (Table 13) and the energy stored measured in the experimental validation. As expected, given the high material cost (2800 €/t), strontium bromide has the highest storage capacity cost 2.3 €/MJ, followed by potassium carbonate 1.2 €/MJ. The other candidates range a price between 0.5 to 0.05 €/MJ, being magnesium sulphate the best candidates when it comes to energy storage versus material cost. None of the candidates is discarded in this filter as the cost is not a must for this material selection and most of the remaining materials are within the filter value.

(3.5)   Filter 5 - Volume change

The volume change of the TCMs was measured by a dilatometer, the volumetric change in percentage is used to compare the volume change among the TCMs (Table 19). The materials that do not have a value in Table 19 are the ones that became liquid during the dehydration process. Among the remaining candidates, strontium bromide is the one that presents the highest volume change (55 %), although within the filter range.

(3.6)   Filter 6 – Chemical stability and safety

From the set of TCMs characterised, as reported in the literature, nitrates present decomposition with loss of N_2 above operational temperatures [6], magnesium chloride forms HCl around 150 °C [64,65] and copper sulphate is toxic to oral exposure, therefore, should not be used in open systems. Nitrates and copper sulphate have been discarded in previous filters during the screening selection. Magnesium chloride is still a candidate for the 3 in 1 system, although the highest working temperature should not exceed 150 °C to avoid the HCl formation. The rest of the candidates are safe to be used under open-system conditions. Chemical stability has been studied through X-Ray diffraction, as chlorides should not be heated up to 150 °C, the temperature program, in this case, was set to 120 °C as the highest temperature. From the XRD patterns (Figure 48, Figure 49 and Figure 50), zinc nitrate is the only TCM that shows decomposition above to 120 °C.

(3.7)   Others

Other attributes should be considered for the 3 in 1 system; thermal diffusivity and the specific heat were also measured to provide more experimental evidence of unveiled TCM properties in the literature. Thermochemical materials specific heat has not been widely studied in the literature yet nor different methods for different TCMs compared. Folah Lele et al. [21] compared the specific heat of strontium bromide with two isothermal steps at 60 °C and 90 °C by two different methods, the displacement or the area generated during the isothermal step. Lager et al. [130] proposed a novel methodology to measure the apparent specific heat of metal hydroxides. This study has been used to optimise the methodology used in this thesis. The thermal conductivity and the specific heat of salt mixtures were measured by Carey et al. [131]. Kleiner et al. [132] also measured the thermal diffusivity of $MgSO_4$, $ZnSO_4$ and $SrCl_2$ with the light laser flash method. Folah Lele et al. [133] also measured the thermal conductivity of

calcium chloride, magnesium sulphate, strontium bromide and magnesium chloride using the DSC and the guarded hot cartridge (GHC). Since there is a lack of data in the literature for the TCMs here studied and this data can be relevant for further stages in the thesis, both thermal diffusivity and specific heat have been measured. The specific heat was determined by using the areas (Figure 45) and the dynamic method (Figure 46) for the TCM hydrated (25°C) and dehydrated (25°C and 150°C). The thermal diffusivity was measured by the laser flash method for the hydrated and dehydrated TCM form as shown in Figure 47. The main outputs from this study are that the dynamic method appears to be more accurate than the areas method as the data are in good agreement with the literature and exhibits a lower standard deviation. The thermal diffusivity values of the TCMs range from 0.3 to 0.6 mm^2/s, which are also in good agreement with the data reported [133]. As this data is added to the main database of this research, they are future filters for TCM selection and comparison in further studies.
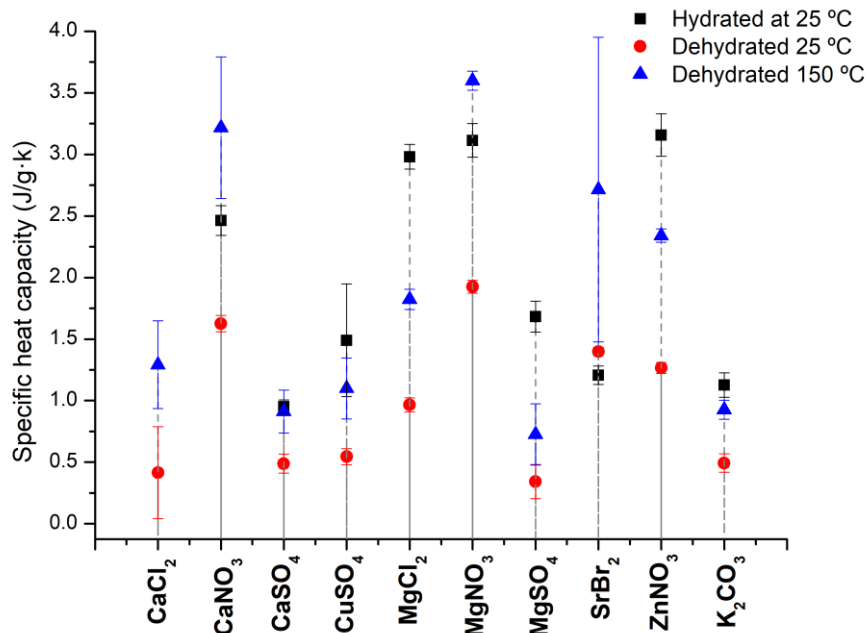
Figure 45. Specific heat capacity calculated using the areas method in the hydrated and dehydrated form at 25 °C and 150 °C.
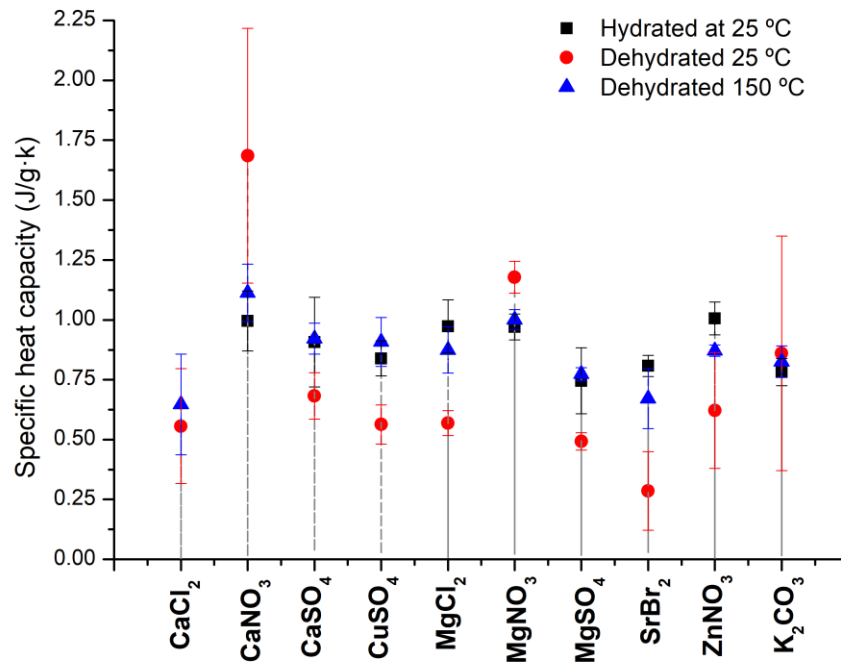
Figure 46. Specific heat capacity by using the dynamic method in the hydrated and dehydrated form at 25 °C and 150 °C.
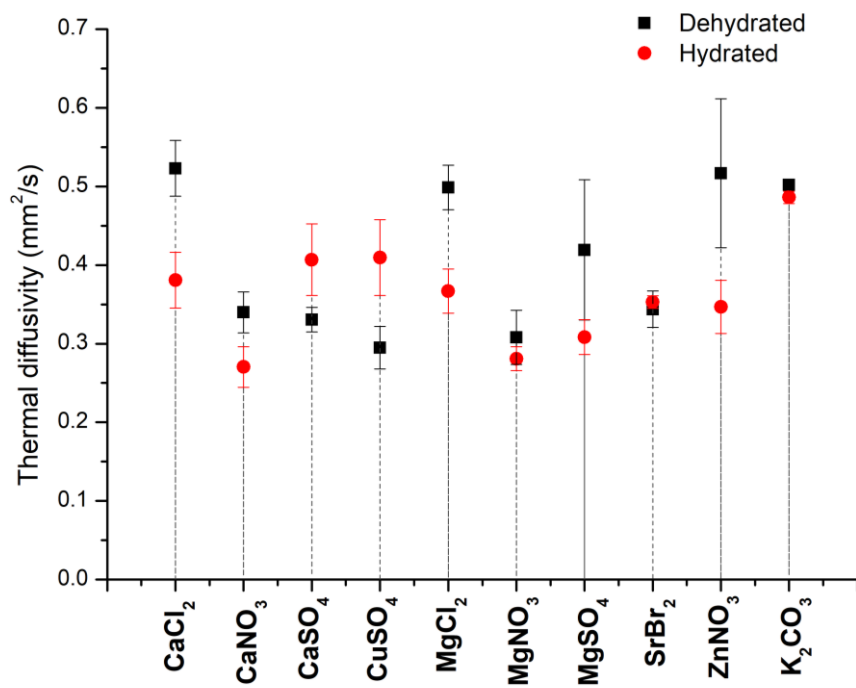
Figure 47. Thermal diffusivity in the hydrated and dehydrated form at 25 °C.
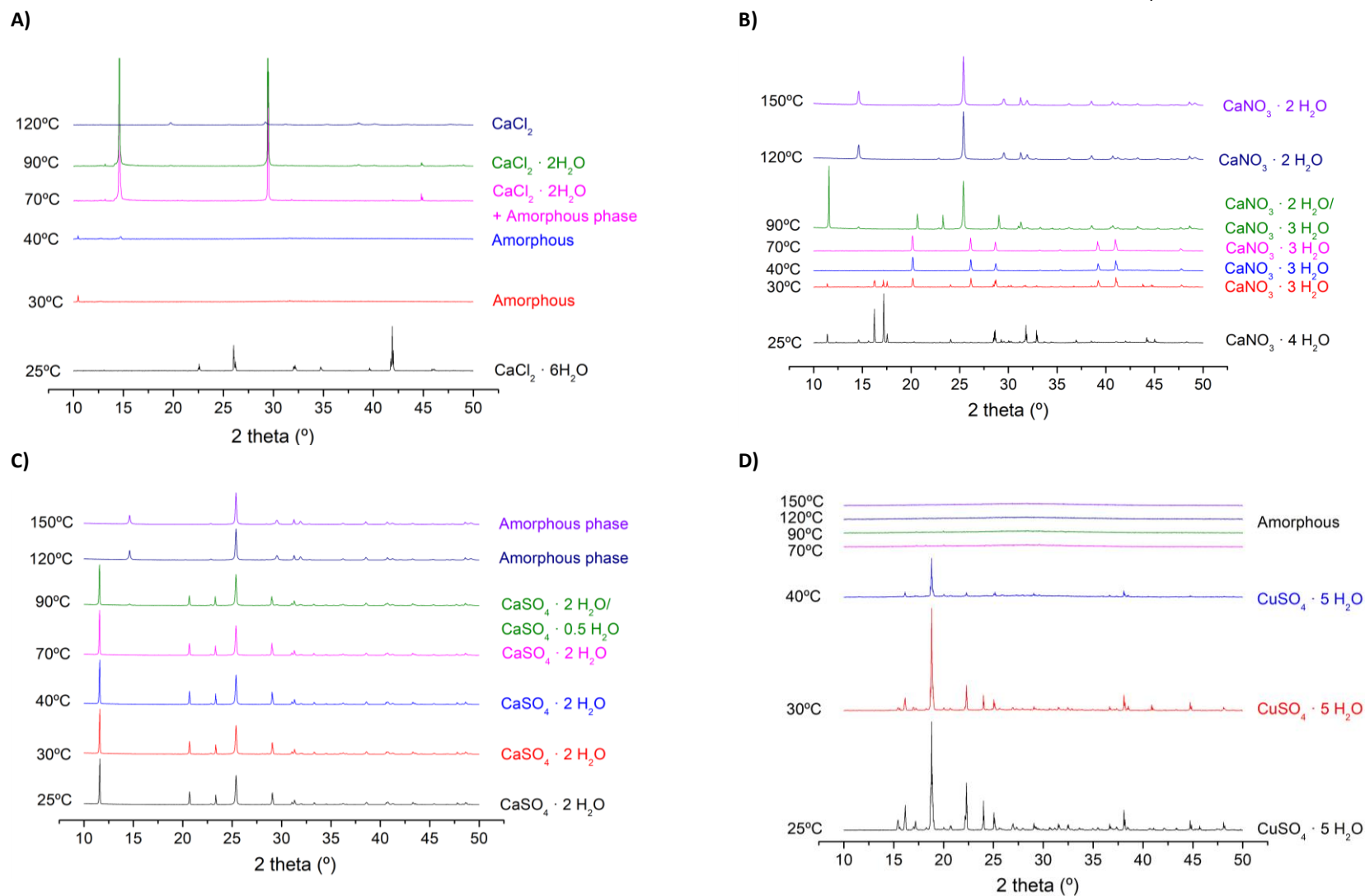
Figure 48. XRD patterns at increasing temperatures (from 25 °C to 150 °C) for (A) Calcium chloride, (B) Calcium nitrate, (C) Calcium sulphate and (D) Copper sulphate.
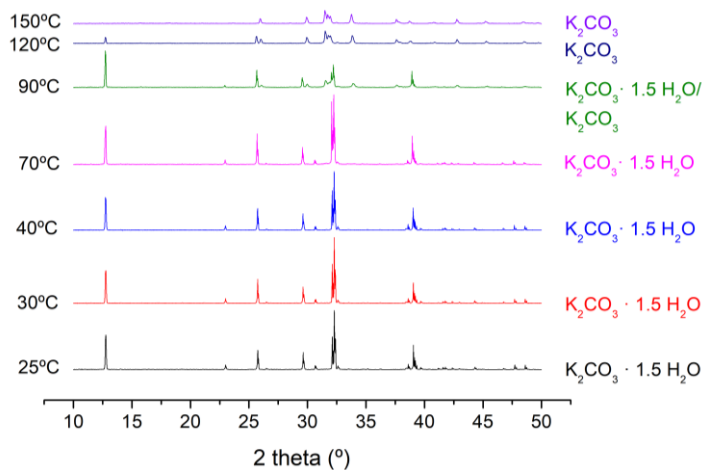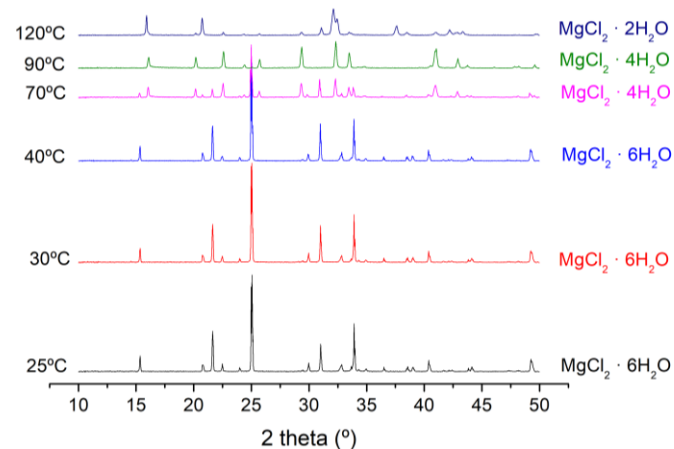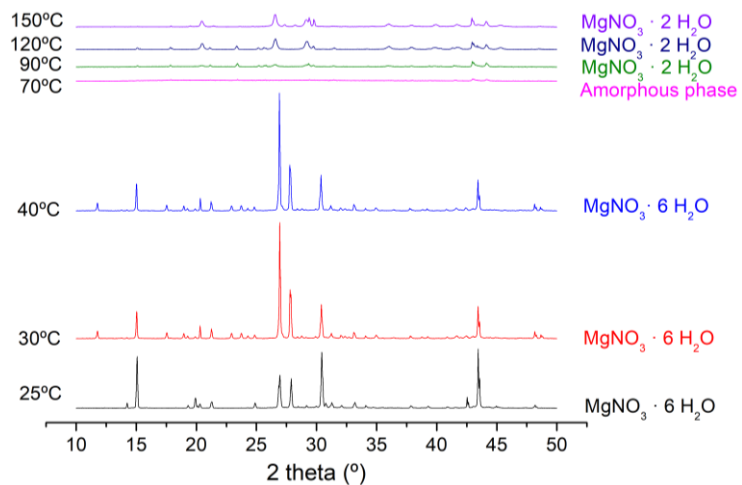
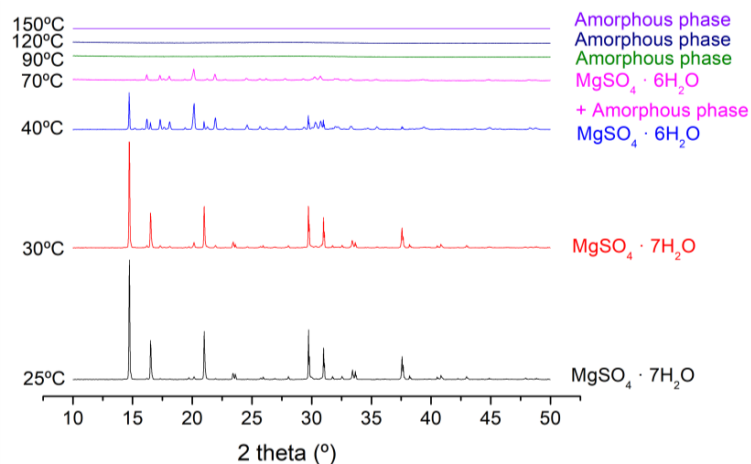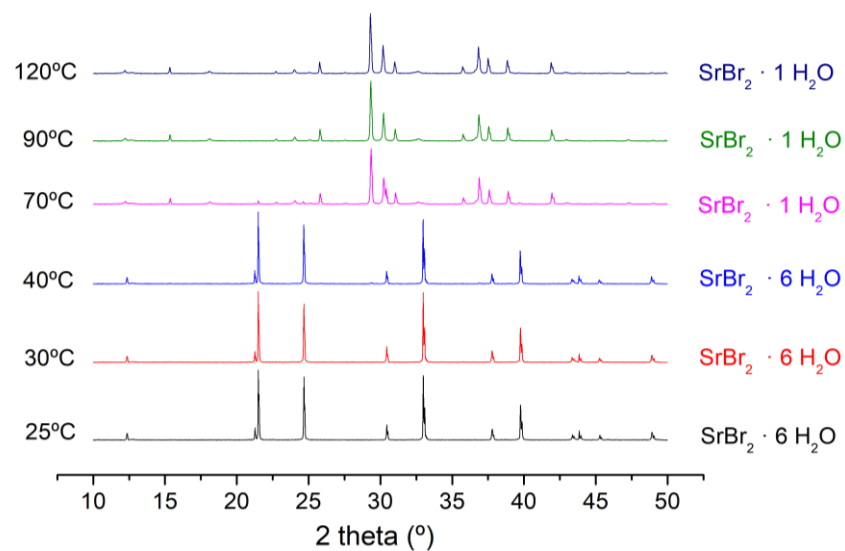Figure 49. XRD patterns at increasing temperatures (from 25 °C to 150 °C) for (A) Potassium nitrate, (B) Magnesium chloride, (C) Magnesium nitrate and (D) Magnesium sulphate.

A)

B)
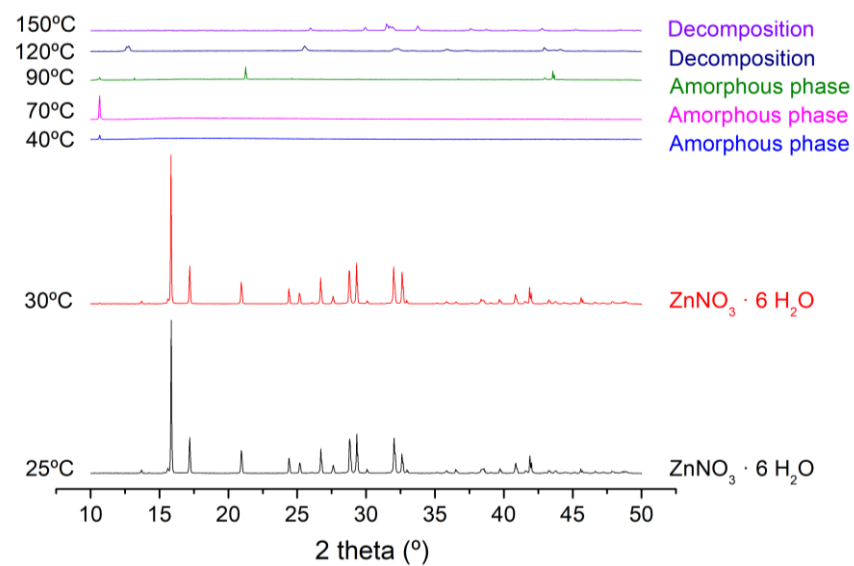
Figure 50. XRD patterns at increasing temperatures (from 25 °C to 150 °C) for (A) Strontium bromide, (B) Zinc nitrate.

Table 19. Summary of thermochemical material properties from the experimental validation for the TCMs screening. The enthalpy of reaction (ΔHr) and the energy density (E_d) has been calculated from the 1 °C/min DSC results; The χ_{dehy} is the conversion for dehydration at 1 °C/min in the STA, the conversion time and conversion for 80 and 60% R.H. is also listed $t_{60\%}$, $t_{80\%}$, $\chi_{60\%}$, $\chi_{80\%}$; the cost is calculated from the enthalpy of reaction and the cost reported in the literature. The TCM sample pictures are taken before and after one dehydration/hydration cycle in the humidity chamber.

TCM	ΔH_r (kJ/kg)	E_d (GJ·m^{-3})	T_m (°C)	χ_{dehy} (%)	$t_{60\% n}$ (min)	$\chi_{60\%}$ (%)	$t_{80\%}$ (min)	$\chi_{80\%}$ (%)	Volume change (%)	Crystalline phases	Cost (€/MJ)	Shaping	Before cycling	After cycling
MgSO$_4$·7H$_2$O		2.7	50	94	147	38	147	70	-41	Orthorombic to monoclinic to amorphous	0.05	Easy to pelletize		
SrBr$_2$·6H$_2$O	1415.9	2.6	88	90	60.08	91	40.21	100	-55	Hexagonal to orthorombic	2.3	Easy to pelletize at first but breaks after hours in the sealed plastic bag.		
Mg(NO$_3$)$_2$·6H$_2$O	1244.6	2.3	89	51	147	72	93.4	100	-	Monoclinic to monoclinic	0.03	Easy to pelletize		
CaCl$_2$·6H$_2$O	1956.6	3.6	29	100	119	100	34.1	100	-33	Hexagonal to orthorhombic	0.12	Difficult to pelletize when hydrated. Takes water from ambient.		

Continuation Table 19

TCM	ΔH_r (kJ/kg)	E_d (GJ·m^{-3})	T_m (°C)	χ_{dehy} (%)	$t_{60\% n}$ (min)	$\chi_{60\%}$ (%)	$t_{80\%}$ (min)	$\chi_{80\%}$ (%)	Volume change (%)	Crystalline phases	Cost (€/MJ)	Shaping	Before cycling	After cycling
MgCl$_2$·6H$_2$O	2117.345	3.8	117	100	38.95	98	68.5	100	-45	Monoclinic to monoclinic	0.18	Difficult to pelletize. Takes water from ambient.		
Zn(NO$_3$)$_2$·6H$_2$O	1260.2	2.3	34	98	147	82	88.8	100	-	Orthorombic to amrphous	0.24	Very difficult to pelletize. Takes water from ambient.		
CaSO$_4$·2H$_2$O	742.3	1.4	51	63	147	34	109.8	100	-35	Monoclinic to hexagonal	0.20	Easy to pelletize		
Ca(NO$_3$)$_2$·4H$_2$O	1302.8	2.4	46	76	64.1	98	26.2	100	-	Monoclinic to orthorombic	0.47	Easy to pelletize		

Continuation Table 19

TCM	ΔH_r (kJ/kg)	E_d (GJ·m⁻³)	T_m (°C)	χ_{dehy} (%)	$t_{60\% n}$ (min)	$\chi_{60\%}$ (%)	$t_{80\%}$ (min)	$\chi_{80\%}$ (%)	Volume change (%)	Crystalline phases	Cost (€/MJ)	Shaping	Before cycling	After cycling
$CuSO_4 \cdot 5H_2O$	821.5	1.5	111	98	147	46	147	100	-57	Triclinic to amorphous	0.16	Easy to pelletize, reacts easily with other components		
$K_2CO_3 \cdot 1/2H_2O$	865.2	1.6	150	100	57.8	100	40.7	100	-21	Monoclinic to monoclinic	1.16	Easy to pelletize (very low dense)		

8.1.4 THERMOCHEMICAL MATERIAL SELECTION SUMMARY
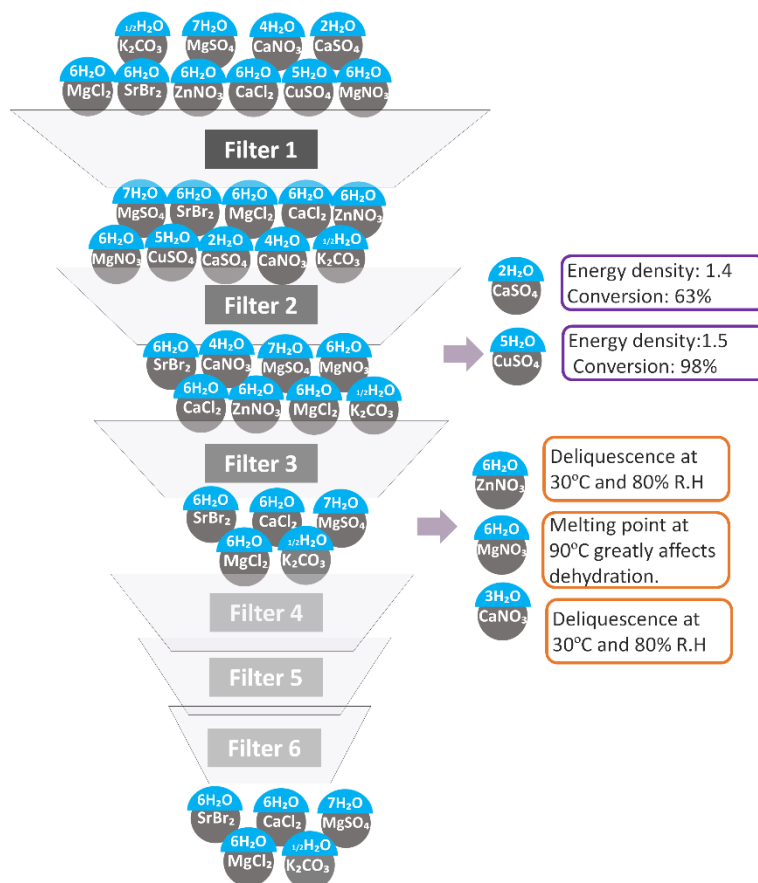
Figure 51. The screening process for the TCMs under study.

In this piece of work, a thermochemical material screening has been carried out, from the top-down approach. The authors set the operational conditions, targeting the most relevant ones and organizing them into different filters (up to 6). Ten thermochemical materials were theoretically selected according to the general thermochemical attributes reported in the literature. An experimental characterization was also conducted to ensure the TCM could perform properly under the conditions set. At the end of the screening process (Filter 6), the number of TCMs is narrowed down to magnesium sulphate, strontium bromide, calcium chloride, magnesium chloride and potassium carbonate, which exhibit high energy density while

performing properly under the practical conditions set (e.g. conversion rate, mechanical integrity, stability, etc). This selection process was possible given the experimental data that completed the set of parameters needed for the selection. Besides, the materials selected are the ones most reported in the literature, which will ease the 3 in 1 system study as there is a previous understanding of the thermochemical reaction taking place.

8.2 PHASE CHANGE MATERIAL (PCM)

The phase change material in the 3 in 1 will works simultaneously as the matrix and the secondary heat storage media. Therefore, in this section, the selection process of the latent matrix will be described and will be framed in the TCM matrix requirements. Among all the phase change materials available, we just consider solid-solid and solid-liquid (high viscous liquid) PCMs given the need for a matrix that keeps together the TCM and PCM structure. This will be discussed in this section as well as the PCM attributes and constrains applied for the material screening. An experimental validation will be also performed and discussed eventually aiming to select phase change materials with different chemical nature. Such final candidates will be paired to a TCM, according to the different systems proposed to come up with a list of potential TCM/PCM working pairs (see late in Chapter 9) Unlike the TCM selection, the PCM selection is dependent on the performance of the working pair (interaction between (TCM and PCM). Hence, the PCM selected in this chapter are just potential candidates that must be tested under the thermochemical system's operational conditions to ensure affinity with the thermochemical material paired with.

8.2.1 PCM 3 IN 1 SYSTEM CONSTRAINTS

The constrains for the phase change material screening are listed in Table 20 and classified between must and preferable, where 'must' refers to parameters that must be met for the material to be selected and 'preferable' are added values to the material that will easy

the working pair synergy. They have to be stable over the working temperature range, which will range from 25 °C to 200 °C (maximum). Another 'must' required is the latent heat higher than 150 kJ/kg, this value is considered from the hypothesis that the thermochemical heat subtracted to the TCM by the addition of PCM should be countered by the latent heat of the PCM. Besides, the PCM must be inert to water to not interfere in the sorption/desorption process and allow a porous composite structure with mass/heat channels.

The other parameters considered and labelled as 'preferable' are specific heat and thermal conductivity that should be higher than the pure TCM to enhance heat transfer. When these criteria are not achieved, additional binders could be added to the composite to optimize the performance of the composite. Likewise, easy to pelletise and high viscosity, will make the working pair to be easy to large scale manufacture and keep the mechanical integrity over cycles. If these attributes are not imperative for the selection and should be studied in detail in the following sections. Overall, PCMs are selected to have a high heat of fusion, heat capacity, and density and have a low propensity for supercooling, as some PCMs will freeze at a lower temperature than their melting point due to problems with nucleation and crystallization rate as a result of the combination of the TCM material.

Table 20. Constrains for phase change material selection

Parameters		Importance
Stability	25 – 150 °C	Must
Latent heat	>150 kJ/kg	Must
Specific heat	Higher than TCM	Preferable
Thermal conductivity	Higher than TCM	Preferable
Others	Avoid structural changes	Preferable
	Do not react with water	Must
	Easy to pelletise	Preferable
	High viscous	Preferable
	Low or none supercooling	Preferable
	Permeable to water	Preferable
Cost	Lower than TCM (or conventional matrices)	Must

8.2.2 PCM SCREENING

Potential solid-solid and solid-liquid phase change materials are reviewed in this section (see Figure 52). The candidates screened will be experimentally validated and selected as part of the working pairs. As per definition, solid-liquid phase change materials (SL-PCMs) change their internal molecular arrangement from an ordered crystalline structure to a disordered amorphous one when the temperature exceeds a critical threshold. Solid-to-liquid transitions generally involve higher energy than solid-solid transitions and avoid gas-storage problems associated with liquid–gas transitions [106]. Such phase change is accompanied by a volume change (normally increasing when the material becomes liquid). Their use present inherent drawbacks such as leakage, supercooling or higher volume change than S-S PCMs. Solid-solid transition (SS-PCMs) absorb and release heat by a reversible phase transition between a (solid) crystalline or semi-crystalline phase, and another (solid) amorphous, semi-crystalline, or

crystalline phase. Unlike solid-liquid PCMs, solid-solid retain their bulk solid properties within certain temperature ranges.
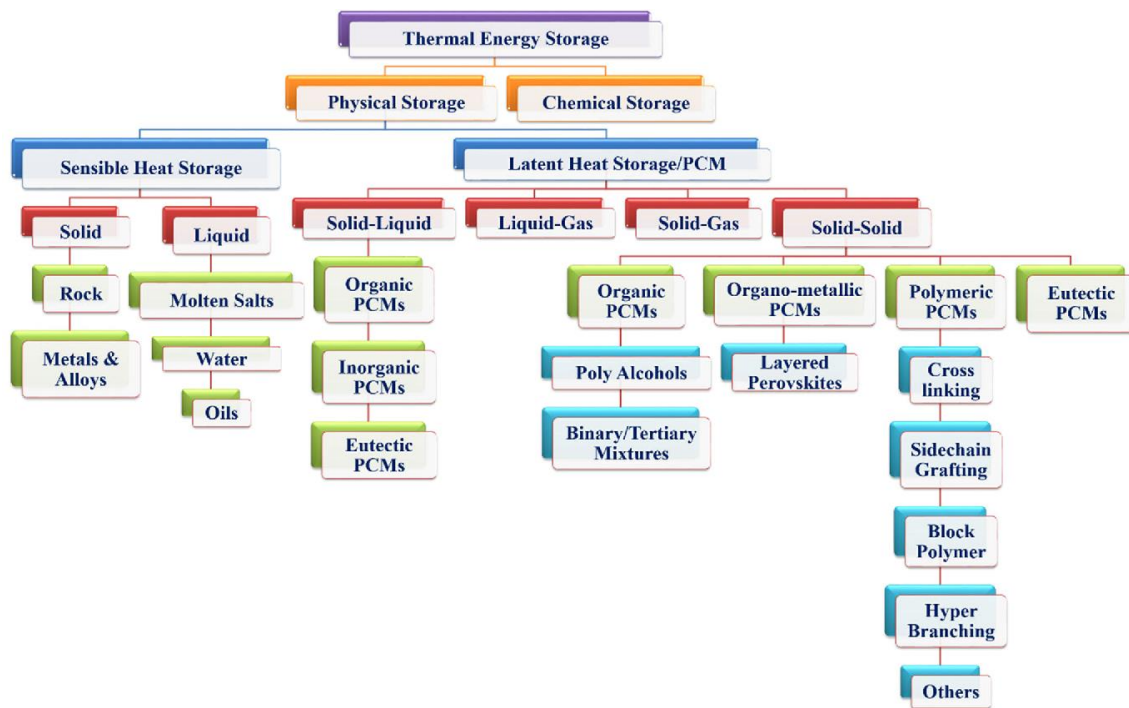
Figure 52. Overview of thermal energy storage (TES) materials, solid-solid PCM [134,135].

Another practical interest of using SS-PCMs in the 3 in 1 is that they present non-leakage, which allows them to be blended with other materials without a need for encapsulation. They also experience no phase segregation and smaller volume changes, which extends their durability by assuring performance upon cycles. [136] besides lower erosion to the device. The phase transition temperatures and enthalpies of the main types of SLPCMs and SSPCMs are shown in Figure 53. From the figure, one can see that SSPCMs generally have lower phase transition enthalpies and/or undergo phase transitions at a narrower temperature range (bottom left of the figure) when compared to SLPCMs. As stated by Falahi et al. [134] the lower enthalpy trend can be explained by the mobility restrictions imposed within SSPCMs, which hinders crystallization and therefore limits the packing efficiency. Both for solid-liquid and solid-solid PCMs are considered for the 3 in 1 system and described below.
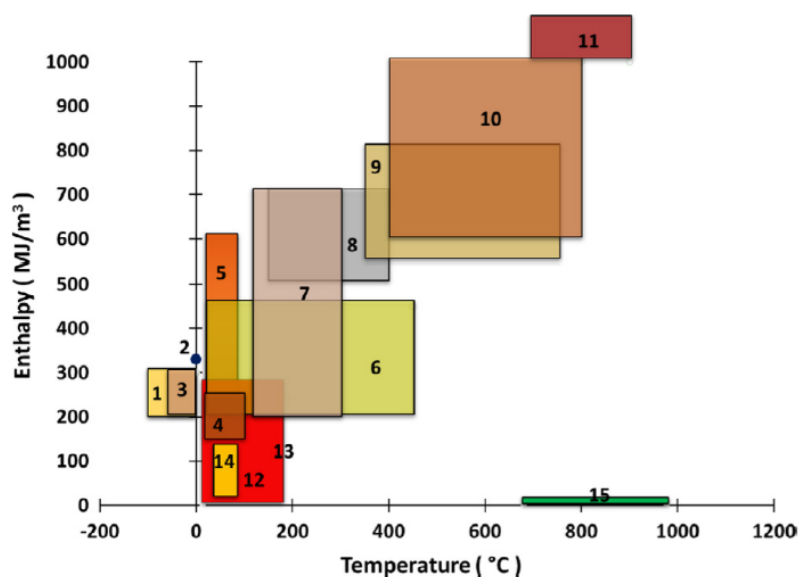
Figure 53. Enthalpy and temperature ranges for SL-PCMs and SS-PCMs; L-PCMs: (1) Water-salt solutions; (2) Water; (3) Clathrates; (4) Paraffins; (5) Salt hydrates; (6) Sugar alcohols; (7) Nitrates; (8) Hydroxides; (9) Chlorides; (10) Carbonates; (11) Fluorides; (12) Polymeric; SS-PCMS: (12) Polymeric; (13) Organics (Polyols); (14) Organometallics; (15) Inorganics (Metallics) from [134].

(1) Solid-solid PCM (SSPCM)

Solid-solid phase-change heat storage is the process in which solid materials absorb heat at a fixed temperature (charging temperature) and use it to form a lower symmetry crystal structure material; this heat can be discharged (released) in the opposite phase change direction [106].

There are currently two main approaches taken to obtain SSPCMs [106]. In the first approach, the arrangement of relatively small molecules changes from one crystalline phase to another when absorbing or releasing heat [134]. In this approach, organic PCMs and the inorganic PCM's are included. Organic PCM´s such polyalcohol's can undergo a change from layered or chain-like internal tetrahedral arrangements at low temperatures to a more disordered cubic crystalline arrangement at higher temperatures. When temperature continues to increase, these systems eventually become liquid as all their supramolecular bonds break. Regarding inorganic SS-PCM´s, they can release and absorb thermal energy due to magnetically-

induced transformations, crystalline phase transformations or order-disordered transitions (e.g phase change between ferrite and austenite). In the second approach, crystallizable moieties are incorporated through chemical bonding into a secondary structure that prevents them to flow freely when they are in their air non-crystalline state (e.g. perovskites and polymeric SSPCMs). SS-PCMs of interest for the 3 in 1 system are polyalcohol's and polymeric SSPCMs, as inorganic and organometallic do not meet the screening prerequisites and can lead to compatibility issues upfront. This selection agrees with the scientific community who stated polyalcohols, and polyethylenes as the most promising solid-solid PCMs [136]. These materials are reported below.

(1.1)   Polyalcohols:

In the '90s some authors investigated the thermophysical properties of neopentyl glycol (NPG), pentaerythritol (PE), pentaglycerol (PG), trihydroxy methyl-aminomethane (TAM), and several other polyalcohols [137–140]. It was found that these polyalcohols are heterogeneous at low temperatures, but when the temperatures rose to the solid-solid phase-change transition, their molecules became homogeneously face-centred cubic crystals with high symmetry forming hydrogen bonds as the hydrogen bonds among these square-bridge type molecules break [141]. At low temperature, polyalcohols and their amine derivatives have a body-centred tetrahedral molecular structure (a-phase). During the solid-solid phase transition, they change to homogeneous face-centred cubic crystalline structure (g-phase) accompanied by the absorption of the hydrogen bond energy. The reformation of the hydrogen bonds during cooling takes place at lower energy than the breaking of the bonds during the heating transition, which causes the subcooling in polyalcohols [142].

Some authors have reported that before reaching the solid-solid phase transition, they undergo a solid-state crystal transformation [143–145]. However, Gao et al. [136] found that polyalcohols binary mixtures have usually only one peak presented in the DSC curves either in

the charge cycle or in the discharge cycle instead of two peaks as reported by previous studies. In this section, we will focus on the primary solid-solid phase transition since it can reversibly absorb large amounts of energy. Polyalcohol PCMs have the advantages of large energy storage density, small volume, constant charging and discharging temperature, among others.

Some polyalcohols, such as PE and TAM are known to have solid-solid transition enthalpies comparable to the fusion enthalpies of many types of paraffin [143]. Among polyalcohols, NPG ($C_5H_{12}O_2$), PE ($C_5H_{12}O_4$) and TAM ($C_4H_{11}O_3N$) are the prevailing subjects of investigations [146]. AMPD is another potential candidate, although just a few studies have been published. However, Gao et al. [136] concluded that this polyalcohol is not suitable given the wide gap between the charging and discharging temperature (around 40°C). This material is also highly hygroscopic, which makes it go from powder to a waxy substance in a very short time in normal laboratory conditions. However, this material has potential application when mixed with PE (20% in weight) [136].

Lately, authors have investigated several polyalcohols mixtures, and they found out that such mixtures have the advantage of having adjusted transition temperatures which makes them attractive for low and medium-temperature utilizations [147,148]. The thermophysical properties of the mixtures of PE/ NPG and PG/NPG were explored by Font et al. [145], which reinforced the argument [143,149] about the advantage of using polyalcohols mixtures for low and medium-temperature utilizations. Qyanying et al. [150] studied four multivariate binary systems (PE-NPG, PG-NPG, TAM-NPG and AMP-NPG). They concluded that the phase change temperature and the latent heat of the four binary phase systems were lower than the single polyols phase change materials. The TAM-NPG binary system had higher phase change temperature and, PE-NPG, AMP-NPG and PG-NPG greater latent heat. Moreover, the binary mixtures with higher NPG content had greater potential for lower temperature (30-50 ℃). Conversely, higher weight ratios of TAM or PG lead to higher temperature (70-150 ℃) systems.

For the 3 in 1 system TAM, NPG and PE were selected as the screened SSPCMs polyols.

(1) TAM

TAM has been targeted as one of the most promising solid-solid PCMs, within the family of polyalcohol. It has a melting point of 172°C and an enthalpy of fusion of 270 kJ/kg, the highest among all SSPCMs polyols. TAM has a small discharge temperature ranges, which makes TAM and their binary mixtures attractive candidates [136].

(2) NPG

Neopentyl glycol (NPG) is heterogeneous at low temperature and shows a phase transition at 41.9 °C. Although it has a good latent heat value of 141.9 kJ/kg, its low decomposition temperature interval (80–150 °C) close to its melting temperature restricts considerably its usage in LHTES applications [151]. Aiming to tackle those drawbacks, Sari et al. [151] developed NPG esters as new solid-liquid PCMs through its esterification with three kinds of fatty acid chlorides. The authors concluded that the thermophysical properties of the novel NPG based PCMs make them more suitable for low-temperature applications than the pure NPG as the developed PCMs exhibit a higher decomposition temperature than the pure material, distancing it from the melting temperature.

(3) PE

Pentaerythritol is a polyalcohol with high solid-solid phase change enthalpy that makes it suited for thermal energy storage applications. At the solid-solid phase transition temperature, pentaerythritol change from body centred tetrahedral molecular structure to a face-centred cubic crystalline structure involving the creation of hydrogen bonds [152]. The phase transition occurs between 187 °C and 189 °C has a latent heat between 270 kJ/kg and 275 kJ/kg [143].

(1.2)   Polymeric

Polymeric PCMs can be implemented as solely PCMs or composite polymeric solid-solid PCMs. Regarding, composite polymeric SSPCMs, there are two kinds of polymeric compounds used in TES [153]; One kind is considered a compound material obtained by dispersing PCMs into a higher melting point polymeric materials acting as supporting materials (form stable PCMs or shape stabilized PCMs). The other kind is synthesized by chemical methods, chemical grafting or blocking copolymerization are used to make good solid-liquid PCMs as the energy storage working materials component of solid-solid phase change materials. However, this kind was reported to have some defects that limit their applications e.g. the transition temperature is too high, the transition enthalpy is low, and the thermal property is unstable. In this section, we will just consider

Many linear polymers undergo reversible liquid-solid phase transitions upon cooling from their molten amorphous state. The following groups of semi-crystalline polymers were identified as potential PCM: polyethylene (PE), polypropylene (PP), polyoxymethylene (POM), polyamides (PA) and their recycles.

Other types of linear chain SS-PCMs, are poly-(ethylene oxide) (PEO) or 4,40-diphenylmethane diisocyanate (MDI) [134]. Such polymers can serve as the "soft-segment" and are grafted onto a polymeric backbone acting as the "hard segment". In these structures when the temperature reaches the melting point, the soft segment absorbs heat through a first-order phase transition undergoing a first-order phase transition. From previous studies, the phase transition properties of crosslinking polymeric SSPCMs are influenced significantly by the movement freedom of the soft segments, and the movement freedom of the soft segments is determined to great extent by the crosslinking density of crosslinking polymeric SSPCMs [154]. Among all the polymeric SSPCMs the following were screened for the 3 in 1 selection study:

(1) MDI

MDI has a melting point of around 38 °C. It forms insoluble dimers when stored above the melting point and it tends to crystallize [155]. This material is commonly used in industry for the synthesis of polyurethane as the thermoplastic PU is synthesized by the reaction of diisocyanate and polyol [156]. Isocyanates, upon the action of water, release CO_2 that facilitates the formation of a microcellular foam [157]. MDI has been used as the hard segment in high-performance SSPCMs copolymers combined with PEG/PE [154,158,159] and PEG/polyurethane phase change materials [153]. The degradation was studied by [160], it was demonstrated to start at leading 240 °C in the air to considerable discolouration, heated in nitrogen for the same period (10 min), the samples did not show considerable discolouration until 280 °C.

(2) PEO

PEO is a nontoxic, biocompatible, and water-soluble, crystalline, thermoplastic linear polymer [161]. PEO has the same repeat structural unit —CH_2CH_2O— as polyethylene glycol (PEG). Materials with molecular weight (Mw) <100,000 are usually called PEGs, while higher molecular weight polymers are classified as PEOs. PEO has been widely used in the fields of solar energy utilization, waste heat recovery, electric energy storage, drug-controlled release, and tissue engineering. This material has the added value of allowing for chemically modified PEOs and polymer/PEO blends exhibit unique solid-solid phase transition behaviour and are efficient thermal energy storage materials [134,154,162,163]. This polymer also allows for a high degradation temperature of 360 °C [164]. The degradation mechanism of PEO proceeds via random-chain scission of C-O bonds and C-C bond cleavage, 1-3 leading to the formation of a series of molecules such as mono and diether oligomers among others.

(3) HDPE

High-density polyethylene (HDPE) has been used as a polymeric matrix for shape stabilized phase change materials [59,60]. HDPE itself can also be used as a polymeric phase change material [165–168]. It is toxicological safe, commercially available in large scale relatively cost-effective, and can be from recycled materials. These make it an interesting PCM. HDPE has a melting point (solid-viscous transition) of ~135 °C, the high specific heat of ~2 kJ/kg·K, and a decent latent heat of fusion of ~164 kJ/kg [64]. Among all the semi-crystalline polymeric materials that can be used as a PCM [169], HDPE is the one that shows the highest latent heat of fusion at temperatures lower than 150 °C. Unlike other PCMs, polymeric materials are not susceptible to phase segregation, although they are sensitive to degradation upon thermal and thermo-oxidative cycles. Associated alterations of the polymer's morphology can also affect the storage capacity [169]. HDPE can be chemically stable at temperatures up to 300 °C under air and up to 450 °C under nitrogen [170]. The thermal degradation of polyethylene (PE) in an oxidising condition takes place in two steps [171]:

1.   At a temperature below 200 °C: free-radical chain reaction and the main products are hydroperoxides and oxygenated species. At this stage, the reactions occur at a slow rate.

2.   Above 250 °C, the previous mechanism becomes irreversible and a new reaction at a high rate appears to be rate determining. Oxidised species reacts with the olefin resulting in chain scission (degradation) and release of volatiles products. At 300 °C, the PE is decomposed [170].

Weingrill et al. [165] thermally cycled HDPE under phase change conditions (oxygen atmosphere) at 160 °C and 180 °C. Their study demonstrated that a small surface area of the polymeric PCM is crucial to hold upon degradation. As the specimen dimensions determine the area of the surface through which the atmospheric oxygen can diffuse into

the polymer bulk, initiating the polymer degradation. Despite this, the storage capacity was maintained during the thermal loads applied, especially under 160 °C. Thus, HDPE can be used as a PCM under an oxidising condition as long as the upper operating temperature is kept at a temperature not far beyond the melting point and the surface exposed is minimised. Besides, HDPE has been widely used as a plastic container for packaging food and pharmaceutical products [172]. Those plastic containers are required to be permeable to moisture vapour.

(4) Cellulose

Cellulose, which is one of the most abundant, non-toxic natural resource, has recently been used as one of the matrixes (supporting) materials of PCM composites. In this case, although we know that cellulose cannot store latent heat energy, we want to explore the use of this matrix as well as the interaction with water absorption in the 3 in 1 composite. Cellulose has been studied with impregnation of PCM [173,174], as well as a polymeric blend [163,175]. Cellulose has been used as a backbone as the most common choices of polymeric matrixes, showing the best efficiencies among the options available [134]. Besides, cellulose has been studied by one author as a matrix of TCM materials [29], concluding that the cellulose fibres present may improve the mechanical stability of the salt bed during this stage and cellulose stabilized hydrate salts were observed to melt at higher temperature level than the corresponding pure salt hydrate crystals. For the reasons mentioned above, here we choose to study the compatibility of cellulose with a variety of TCM materials.

(1.2)   Solid-liquid PCM (SLPCM)

Solid-liquid PCMs commonly used for thermal energy storage include organic PCMs (paraffin and non-paraffin compounds) and inorganic (salt hydrates), or various mixtures thereof (eutectics) (see Figure 54) [134]. Organic solid-liquid PCMs are described as paraffin and nonparaffin materials (fatty acids, alcohols and glycols). Organic materials have stable

phase change temperature (without phase segregation), consequent degradation of latent heat fusion, self-nucleation (no supercooling) and usually non-corrosiveness [176]. The disadvantages of organic PCM are mainly; low thermal conductivity, low volumetric latent heat storage capacity, flammable (depending on containment). The inorganic PCM is listed as salt hydrates, inorganic compounds and metallics. The advantages of inorganic PCM are known as high volumetric latent heat storage capacity, low cost and easy availability, sharp phase change, high thermal conductivity, non-flammable. While the main disadvantages are a high volume change, supercooling and segregation issues [176]. In this section, framing the PCM selection into the 3 in 1 system requirements, we just consider organic PCM; alcohols and glycols. Figure 55 shows some examples of PCM candidates to be used at different temperature ranges. For the temperatures of interest in this thesis, the materials that show higher latent heat among all SLPCMs are sugar alcohols. Although paraffin and fatty acids show higher latent heat than polyethylene glycols, PEGs were selected given their variety of melting temperatures, non-toxicity and potential material combination. See explanation below.
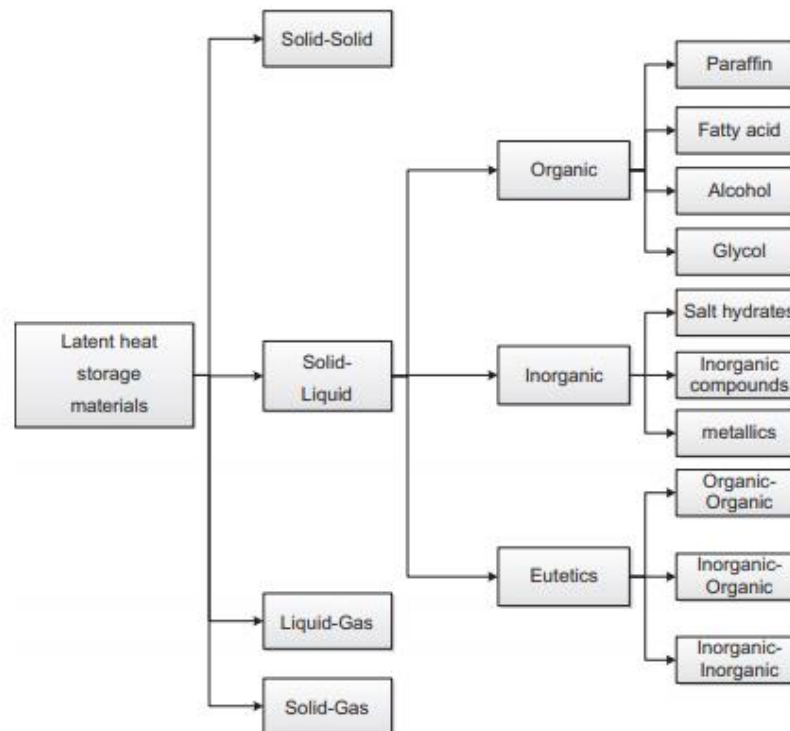
Figure 54. Classification of Solid-liquid phase change materials [177]
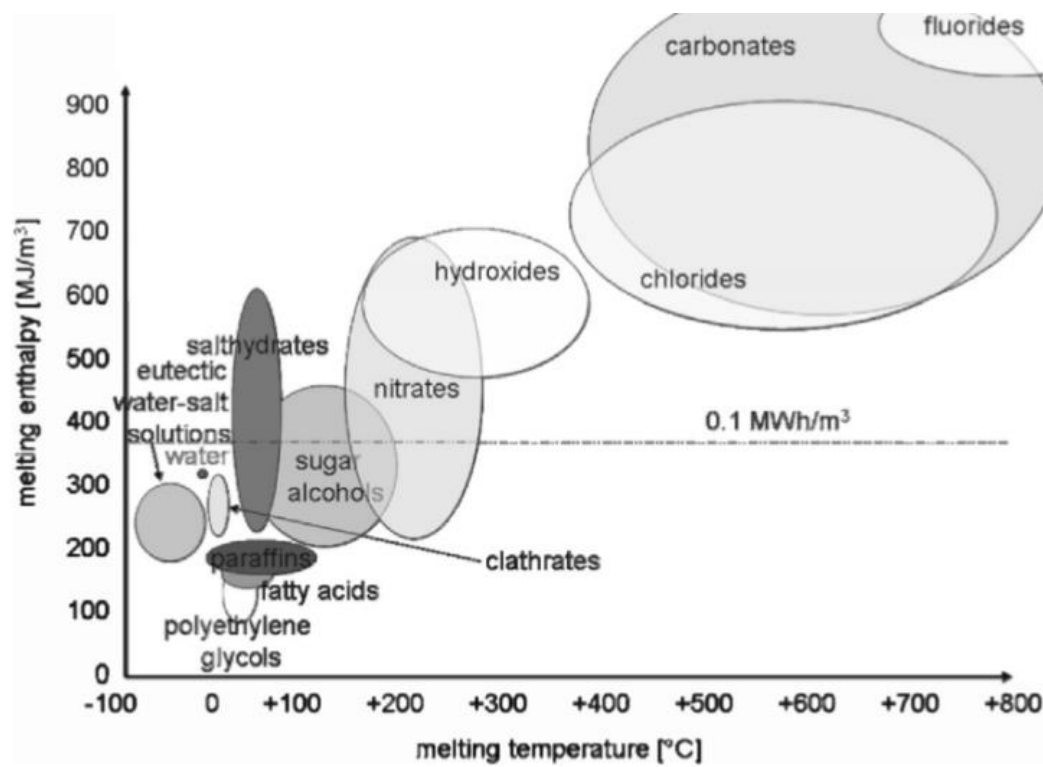
Figure 55. Classification of PCMs with their melting temperature and enthalpy [178].

(1) Sugar alcohols (SA)

Sugar alcohols (SA), also called hydrogenated carbohydrates and polyols, belong to the family of low molecular weight carbohydrates [179]. Sugar alcohols have been identified as potential phase change materials (PCMs) for a temperature range of 50–220 °C [180]. Besides, they show interesting attributes such as high phase change enthalpy values (higher than some fatty acids and paraffin), low-cost products and are non-toxic and non-corrosive. As the main disadvantages, they show supercooling, and they can exist in two or more crystalline states, called polymorphs or modifications, which can show significantly different physicochemical properties [180]. In contrast to paraffin and fatty acids, just a few studies have been published on SA, where different SA have been considered and studied for storage applications at medium temperatures (100–200 °C). Among them, erythritol has received the most attention so far and has been used in various applications (e.g. waste-heat transportation, solar cookers, etc) [179]. This SA is characterized by a melting temperature around 118 °C and relatively large latent heat of 340 J/g (see Table 21).

For applications at higher temperatures, other SA such as D-mannitol, dulcitol, myoinositol and their mixtures have also been investigated for thermal energy storage in industrial applications [179]. D-mannitol, along with erythritol are the SA that show higher latent heat, 290-316 kJ/kg. Barreneche et al. [181] concluded that D-mannitol presents suitable thermophysical properties for energy storage, but its polymorphism should be taken into account, recommending a working temperature range from 135 °C to 175 °C, where the polymorphism does not affect the thermal behaviour. Both D-mannitol and erythritol have great thermal stability showing decomposition at around 300 °C [182].

Although SA is interesting candidates given their high latent heat and proper thermal stability as well as allowing a range of melting points resulting from their mixtures, supercooling appears to be a limitation in their implementation. SA suffers from severe

supercooling and they were found to be unable to crystallize at low degrees of subcooling (~20 °C). This phenomenon must be studied in interaction with the sorption process and within the 3 in 1 matrix to understand whether this is limiting or can be overlooked when designing the hybrid composite. For the reasons stated above, D-mannitol and erythritol are the SA selected to be studied in the 3 in 1 system.

(2) Polyethylene glycols

Some authors have established polyethylene glycol (PEG) as an organic solid-liquid PCM offering a wide range of enthalpies and phase transition temperatures as a function of its molecular weight [183–185]. Other authors, Fallahi et al. [134] and Raj et al. [135] classified PEG as an organic solid-solid PCM. For concision purposes, in this thesis, PEG is classified as organic solid-liquid, although depending on the molecular weight this can be considered solid-high viscous phase change (low-melting solids). PEG is a polyalcohol, among polyalcohols, it is a linear polymeric material that is polymerized by glycol monomer with commercially available molecular weight from 300 g/mol to 100,000 g/mol. As shown in Table 21, the latent heat and melting temperature of PEG can be varied with molecular weight. While enthalpy and melting points roughly increase with increasing molecular weight, thermal conductivity does not show significant changes [186]. Besides, the density and viscosity increase with higher molecular weight but the chemical properties remain identical [187].

PEG has standing characteristics of non-toxicity, relatively high latent heat storage capacity, wide selectivity of molecular weight, low vapour pressure when melted, and good thermal and chemical stability [183]. The main disadvantages of PEG are its low commercial viability, low thermal conductivity, phase instability in the melting state and a weak interfacial combination with supporting materials [188].

Thus, and aiming to provide a solution to issues arising in the commercial development of this material, PEG and its derivatives [e.g., polyethylene glycol monomethyl ether (MPEG), carboxyl poly-Ethylene glycol (CPEG), etc.] are usually employed as the phase change functional chains (soft segments) in the molecule of polymeric SSPCMs [183]. Regarding its interaction with water, the presence of abundant oxethyl groups in the PEG molecule that are capable of forming hydrogen bonds with water makes PEG a highly water-soluble material [188]. The thermal degradation of PEG, as a pure substance, is seen at a temperature around 180 °C, depending on the molecular weight [189]. Low molecular weight esters including formic esters were produced as the main products of the thermal degradation of PEG in air. No degradation was observed for PEG aged under vacuum conditions [190]. The mechanism of thermal degradation is found to be the random chain scission of the main chain.

In the 3 in 1 system, different PEG's were screened to provide a variety of temperatures (melting point; T_m) within similar physical/chemical performance; PEG 600 (T_m: 25 °C), PEG 1,000 (T_m: 30 °C), PEG 10,000 (T_m: 50 °C), PEG 20,000 (T_m: 60 °C), and PEG 35,000 (T_m: 65 °C) have been studied. The key properties of the screened materials reviewed in this section are listed in Table 21.

Table 21. Key properties of screened SSPCMs and SLPCMs. a. Chemical database b. Manufacturer price range.

		PCM	Latent heat (J/g)	Solid-solid state transition temperature (°C)	Phase change temperature (°C)	Crystallisation temperature (°C)	Crystallisation enthalpy (J/kg)	Thermal conductivity (W m⁻¹ K⁻¹)	Specific heat capacity (J/(g·k))	Volume expansion (%)	Degradation temperature (°C)	Autoignition point (°C)	Structural changes	Price (£/kg)
Solid–Solid PCMs	Polyalcohols	TAM	270 -290 [141,143,146,150,191]	132-134 [141,143,146,150,191]	168-198 [136,141,143]	-	-	0.211 [192]	2.8 (l) [143]	-	350-400 [193]	169.7±26.5 [a]	Orthorhombic to BCC [150]	10-20 [b]
		NPG	116-139 [146] [141,143,150,191]	42-48 [146] [141,143,150,191]	124-139 [136,143]	-	-	0.12 [194]	2.8 (l) [143]	-	150 [151]	129 [a]	Monoclinic to FCC [143,150]	15-20 [b]
		PE	339.55 [141] 209.5 [191] 303 [143] 269 [143]	255-259 [136] 185.4 [141] 185.5 [191] 184-185 [143] 187 [143]	258-260 [143] 269 [143]	-	-	0.66 [195]	2.9 (l) [143]	-	-	390-490 [a]	BCT to FCC [143]	1.5-2 [b]
	Polymerics	MDI	108.7 [134]	-	38 [155] 56.7 [134] 40 [196]	70-90 [197]	-	0.126 [a]	1.067 [134]	-	240 [160]	211 [196]	-	3-5 [b]
		PEO	52.8 [134]	-	66-75 [161]	40.6-134.7 [134]	-32-(-40) [134]	0.2 [198]	40-140 [134]	-	360 [164]	370 [a]	-	5-10 [b]
		Cellulose	-	-	-	-	-	0.04 [a]	-	-	200-300 [199]	255 [a]	-	4-10 [b]
		HDPE	180-210 [200] 178.6 [201]	-	130.8 [202] 130-135 [201] 130-131 [203]	110-120 [201]	-189 [201]	0.48 [a] 0.44 0.3 [200]	1.8 [204]	-	250-300 [170]	350 [a]	-	1-5 [b]
Solid-liquid PCMs	Sugar alcohols	D-mannitol	270-316 [179,205]	-	163-169 [179,205]	-	-	1.31 (s) [179]		8.5 [179]	300 °C [182]	410 [a]	-	4-6 [b]
		Erythritol	340 [177,205]	-	116-118 [177,205]	-	-	0.326 (l) 0.733 (s)[177]	2.61 (l) 2.25 (s)[177]	4.3 [179]	300 °C [182]	-	-	1.5-2 [b]
	Glycols	PEG (Mw: 400-20,000)	148-197 [134,206]	60.4 [134]	3.1-67 [206]	-24 – 49.4 [206]	-45-(-201) [134,206]	0.19-0.29 [205,206]	139.3 [134]	-	180-200 [189]	360 [a]	-	5-10 [b]

8.2.3 PCM EXPERIMENTAL VALIDATION

To experimentally validate the results reviewed in the previous section, we have conducted a set of experiments to proceed with the selection of the PCMs for the 3 in 1 system, eventually aiming to select SSPCMs and SLPCMs candidates for the working pairs (see Chapter 9). In this section, the specifications of the materials used, the methodology followed, and the experimental results are described.

(1)   Materials

The materials used along with purity, molecular weight and supplier are listed in the following. Polyethylene glycol Bio ultra 20,000 from Sigma Aldrich (CAS: 25322-68-3, MW: 20,000). Polyethylene glycol 1,000 from Alfa Aesar (CAS: 25322-68-3, MW: 1,000). Guar gum in powder from Sigma Aldrich (CAS: 9000-30-0). Polyethylene glycol 35,000 from Sigma Aldrich (CAS: 25322-68-3, MW: 35,000). Polyethylene glycol 1,000 and polyethylene glycol 600 both from Alfa Aesar with CAS number 25322-68-3. Polyethylene oxide from Alfa Aesar (CAS: 25322-68-3, MW: >5,000,000). Methylene di-p-phenyl diisocyanate ($C_{15} H_{10} N_2 O_2$) in flakes, 98% from Acros organicsTM (CAS: 101-68-8, MW: 250.26). D-Mannitol, $C_6H_{14}O_6$, from Sigma AldrichTM (CAS: 69-65-8, MW: 128.17). Pentaerythritol, $C_5H_{12}O_4$, supplied from Alfa AesarTM (CAS: 115-77-5, MW: 136.15, <98%). Microcrystalline cellulose powder from mpBioTM (CAS: 9004-34-6, MW: N/A). Tris(hydroxymethyl)aminomethane, $(HOCH_2)_3CNH_2$, from Alfa Aesar (CAS: 77-55-1, MW: 121.14, 99%). Erythritol from Intenson (CAS: 149-32-6, MW: 122.2, 99%).

(2) Methodology

Different techniques were used to experimental validate the literature data; the DSC was used to measure the specific heat (dynamic method in liquid and solid-state), the melting temperature and latent heat; the tests were repeated three and two times,

respectively. The samples were compressed into 1g tablets and tested in the dilatometer to determine the relative change in length up to 150 °C; a laser flash was used to measure the thermal diffusivity at room temperature; the PCMs were also tested in the STA under the same conditions used for the TCMs to ensure no interaction with water and chemical stability over the working temperature range (up to 150 °C). Finally, the samples were cycled in the humidity chamber under the same conditions used for the TCMs. The specification of the methodology followed in this section are detailed in Chapter 7.

(3) Results

A summary of the properties measured for each PCM are listed in Table 22, the melting and the enthalpy of fusion are averaged from two sets of measurements The interaction with water and thermal stability refers to the results obtained by the STA while cycling is the output of the visual inspection after 1 cycle in the humidity chamber. To select the PCMs, different filters were applied in the following order of importance:

(3.1)   Filter 1 – Stability:

From the stability point of view, almost all the PCMs are stable up to 150 °C except for NPG that, as reported in the literature, decomposes with a residual mass of 30% at 150 °C. Thus, this PCM is discarded from the candidate's list.

Table 22. Summary of properties measured for the PCMs screened. The materials that have (-) in the volume change column undergo a solid-liquid transition and are in a highly viscous state after the transition. The thermal stability has been determined evaluating the STA data.

PCM	Transition	Phase change temperature (°C)	Latent heat (kJ/kg)	Volume change at 150 °C	Interaction with water	Cycling	Stability up to 150 °C
PEG 10,000	S-L	64	168	-	Absorbs small amounts of water in solid-state (5-10% water uptake))	After one cycle the material does not maintain physical integrity.	Stable
PEG 20,000		66	187				
PEG 35,000		68	188				
PEG 1,000		30	140		Liquid state		
PEG 600		25	130				
TAM	S-S	140	247	-49%	Water uptake 27%	Fairly physically stable after one cycle.	Stable
PE		255	305	-	Water uptake	After one cycle the material does not maintain physical integrity.	Stable
NPG		119	46.05	-	Decomposed at 150 °C		Residual mass 30%
D-Mannitol	S-L	167	298	-	Water uptake 20-25%		Stable
E		120	316	-			Stable
HDPE	S-S	133	170	23%	Permeable to water	Fairly physically stable after one cycle.	Stable
MDI		55	110	18%	Permeable to water		Stable
PEO		68	155	44%	Permeable to water		Stable
Cellulose		-	-	-52%	Water uptake 30%		Stable

(3.2)   Filter 2 – Melting temperature and latent heat:

Once we ensure that the PCM is stable over the working temperature range, the most important requirement is the latent heat that has been set at a minimum of 150 kJ/kg. The melting point and the latent heat are shown in Figure 56, the required values have been framed into a lilac square. Within

the framed section HDPE, PEO, Erythritol, PEG (35,000, 20,000 and 10,000), D -Mannitol and PE, they all show a latent heat higher than 150 kJ/kg and offer a variety of phase transitions points to design the 3 in 1 working pairs. PE and D-mannitol were considered for charging integrated systems, although the temperatures appear to be too high for the TCMs selected. However, lower temperature PCMs might be needed to design a kind of discharging integrated system as most of the TCMs selected are discharged at temperatures close to 25-30 °C. For that reason, PEG 600, PEG 1000 and MDI are not discarded in this filter as they can be useful for setting up discharging systems.
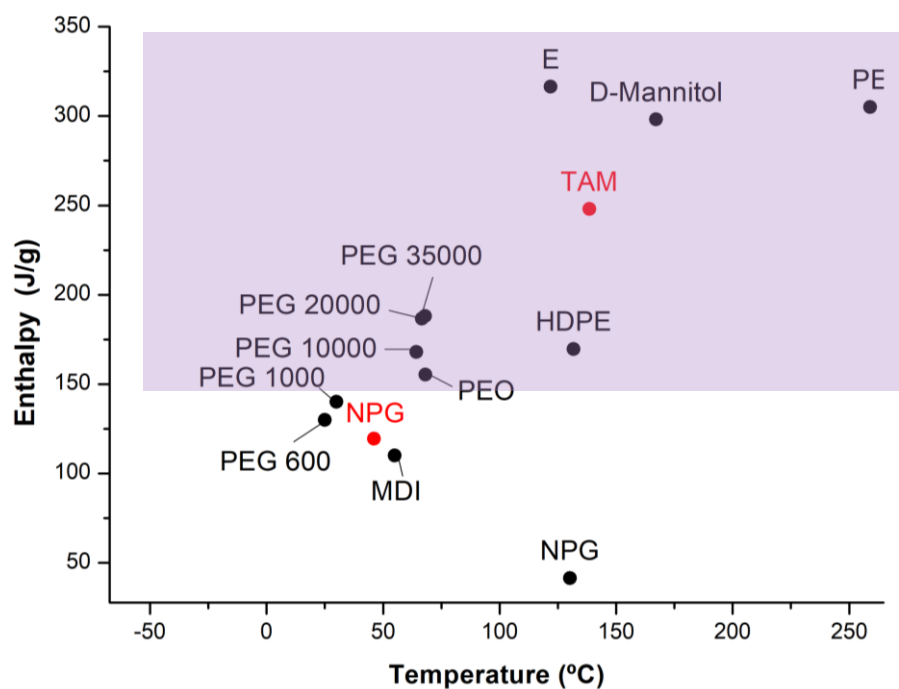
Figure 56. In black for the phase change temperature and latent heat, in red the solid-solid state transition temperature and the enthalpy of transition for NPG and TAM.

(3.3)   Filter 3 – No reaction with water and permeable:

Overall, the PCMs studied show good compatibility with water vapour although not all of them are permeable to water. Polymeric PCMs considered are all permeable to water vapour, especially HDPE have been reported to show great permeability [172], while PEG absorbs water in small amounts. Sugar alcohols and TAM have a strong tendency to absorb water under the test conditions (80% R.H. at 30 °C) with a water uptake around 20-25%.

(3.4)   Filter 4 – Specific heat and thermal conductivity not lower than the TCM:

The specific heat and the thermal conductivity are desired not to be lower than the thermochemical material, despite as being added in small amount this should not be critical to the 3 in 1 system. The average specific heat of the PCMs studied are in the range of the specific heat of the hydrated thermochemical materials with the dynamic method (Lilac line in Figure 57). Among all the PCMs, HDPE and PE are the ones that exhibit higher specific heat capacity (dynamic method in DSC test). This method was used for comparison purposes as dynamic method proved to be the most accurate for the TCMs experimental validation.

Overall, the thermal diffusivity of the PCMs is lower than the TCMs, however PE, HDPE and E show great thermal diffusivity values higher than 0.3 mm^2/s.
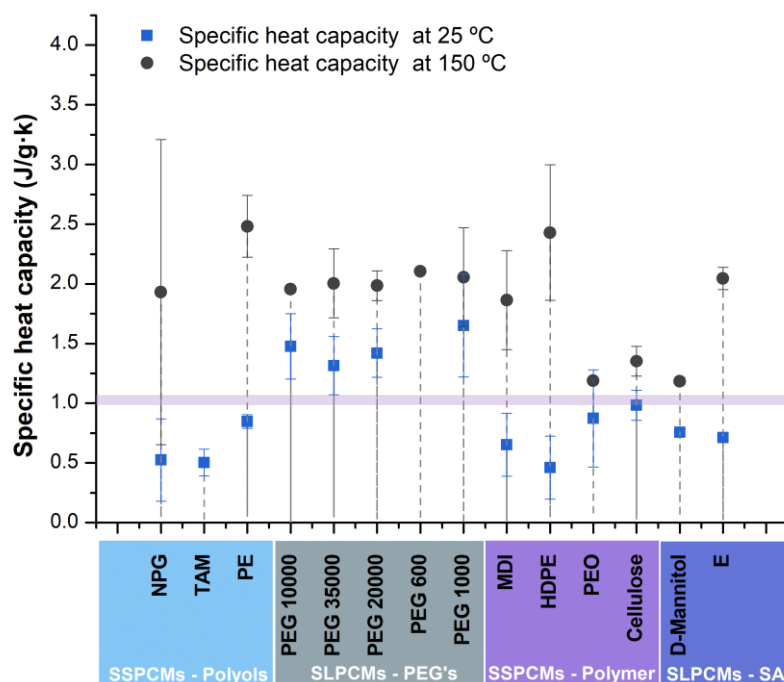
Figure 57. Averaged specific heat capacity using the dynamic method, three repetitions at 25 °C and 150 °C. Lilac line marks the average highest (hydrated) specific heat of the TCMs studied.
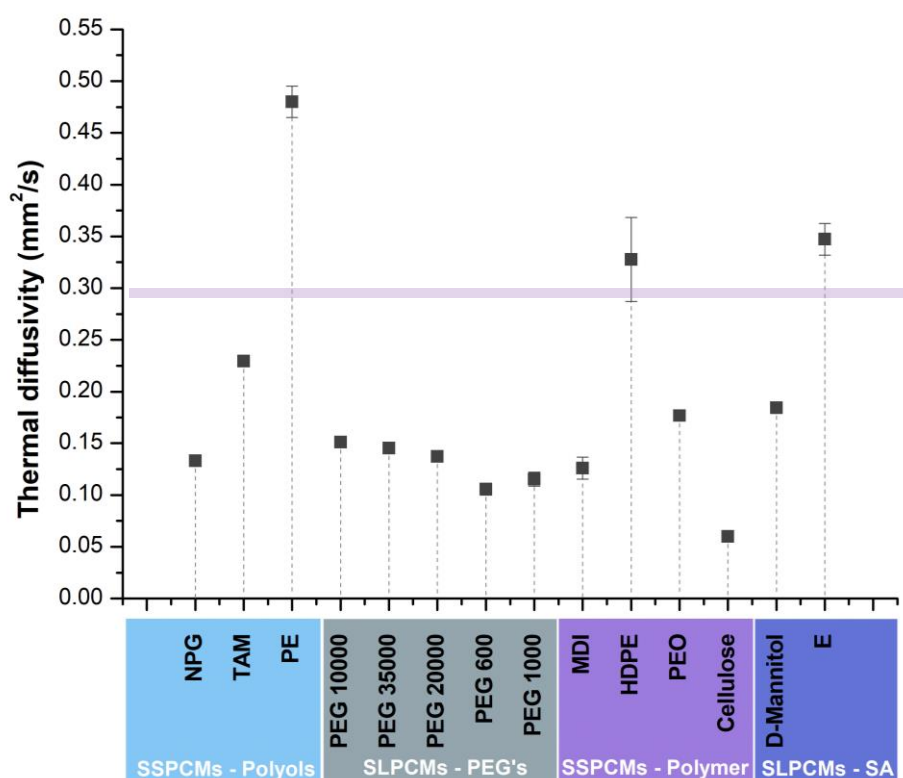
Figure 58. Averaged thermal diffusivity, three repetitions at 25 °C for the SS and SLPCM's. Lilac line marks the average specific heat of the TCMs studied.

(3.3)   Filter 5 – Cost not higher than TCM

TAM and NPG are the most expensive PCMs with a cost between 10-12 €/kg. NPG was already discarded in the filter 1, and given the high cost, TAM is also discarded at this stage. Ideally, the PCM should have a very low cost to make the 3 in 1 system cost-effective for commercialisation.

(3.4)   Filter 6 – Physical integrity and volume change

The physical integrity of the PCMs was checked by visual inspection before and after the cycling test (at the same TCMs test conditions). As expected, solid-liquid PCM showed the worst physical integrity with a volume change typical of solid-liquid transition. Hence, such materials need an additional structure to co-work in the 3 in 1 system, this will be introduced in the following section 8.3. Among them, the materials that show worse physical integrity are PE and D-mannitol, thus, these materials are discarded in this filter.

8.2.4 PCM SELECTION

A similar approach as the one followed for the TCM selection was followed for the PCM. Fourteen candidates from the literature were theoretically selected and reviewed. Experimental validation was then performed to all the candidates to ensure proper performance under operational conditions. The screening flow is illustrated in Figure 59, the theoretical candidates were narrowed down to eight, among them polymeric matrices (PEO, MDI and HDPE), polyethene glycols (PEG 1,000, PEG 600 and PEG 35,000) and one sugar alcohol (E). PEG 25,000 and 10,000 were discarded as they offer similar properties (melting point enthalpy of fusion) as PEG 35,000, but lower viscosity is given their lower molecular weight. Among the PCMs candidates as the 3 in 1 matrix, cellulose is considered as it can provide a skeleton, energy stored in sensible heat and interesting water-PCM interaction.
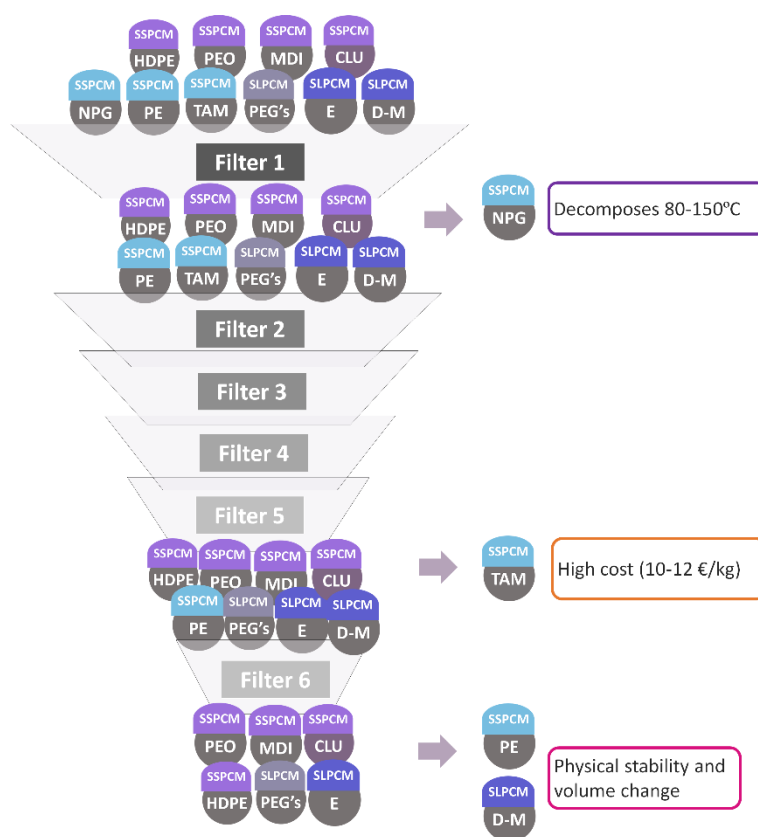
Figure 59. The screening process for the PCMs under study.

8.3 ADDITIONAL COMPONENTS: GELLING AGENTS

Given that some of the PCMs selected in the previous section are solid-liquid and might, depending on the working pair, present a structural challenge (see later Chapter 9), a potential solution to this working pair was studied upfront. A component which provides structural support to the SLPCMs/TCM working pairs, which:

- Should ensure the physical and chemical stability over cycles.

- Should not interact with latent and thermochemical processes and not react with the TCM and PCM.

- Should not increase the cost of the 3 in 1 system.

- Should be added in low percentages to strengthen the structure while not decreasing the energy density of the hybrid composite.

- Should be prepared/synthesize in a way that it does not affect the attributes of the raw materials. The resulting material should be easily shaped.

- Potential scalability of the manufacturing method.

Among the possible solutions, adding a gelling agent appear to be the most feasible as it allows low percentages (low cost) and can be prepared by dissolution in the water at room temperature or lower than 100 °C. The gel/TCM solution to prepare the 3 in 1 working pairs can be then dried and the new gel/TCM/PCM composite can be shaped, further explained in the following section. This section introduces the gelling agents as 3 in 1 material additive/component; (1) gelling agents screening (mainly hydrocolloids, as they are commercially available, cheap and soluble in water; and one hydrogel); (2) Experimental validation looking at TCMs and gelling agents compatibility (3) Selection of gelling agents for the working pairs that will be studied at the proof of concept and scale-up.

8.3.1 GELLING AGENTS SCREENING

Two types of gelling agents are screened in this section, hydrogels (polyacrylamide) and hydrocolloids (guar gum, xanthan gum, agar, carboxymethylcellulose and carrageen). Both are described in this section.

Hydrocolloids are a heterogeneous group of long-chain polymers (polysaccharides and proteins) characterised by their property of forming viscous dispersions and/or gels when dispersed in water. The functional roles of hydrocolloids are (a) thickening, which involves non-specific entanglement of conformationally disordered chains, and (b) structuring/gelling, which involve specific inter-chain association in conformationally-ordered junction zones [207]. In other words, gel formation involves the association or cross-linking of polymer chains to form a 3-D

network that traps or immobilises the water within it to form a rigid structure that is resistant to flow. Although all hydrocolloids thicken aqueous dispersions, only a comparatively few gums form gels, which according to their nature vary widely in gel character and texture.

In this section, we focused on the latter use (gelling) since they follow an associative mechanism (soluble in water), which allows the TCM (salt hydrates) to be dissolved in water along with the hydrocolloid agent to from the gel. This water thickening property is common to all hydrocolloids and varies with the type and nature of hydrocolloids, with a few giving low viscosities at a fairly high concentration but most of them giving high viscosities at low concentration, below 1% [207]. Some of them need temperatures higher than 25 °C to dissolve in water (activate the gelling agent).

In accordance to their origin and manufacturing path, hydrocolloids can be classified in four different groups (see Figure 60): 1) hydrocolloids purely isolated from plants (without chemical modification); 2) hydrocolloids obtained by fermentation; 3) plant-derived hydrocolloids chemically modified; 4) hydrocolloids from animals [208].
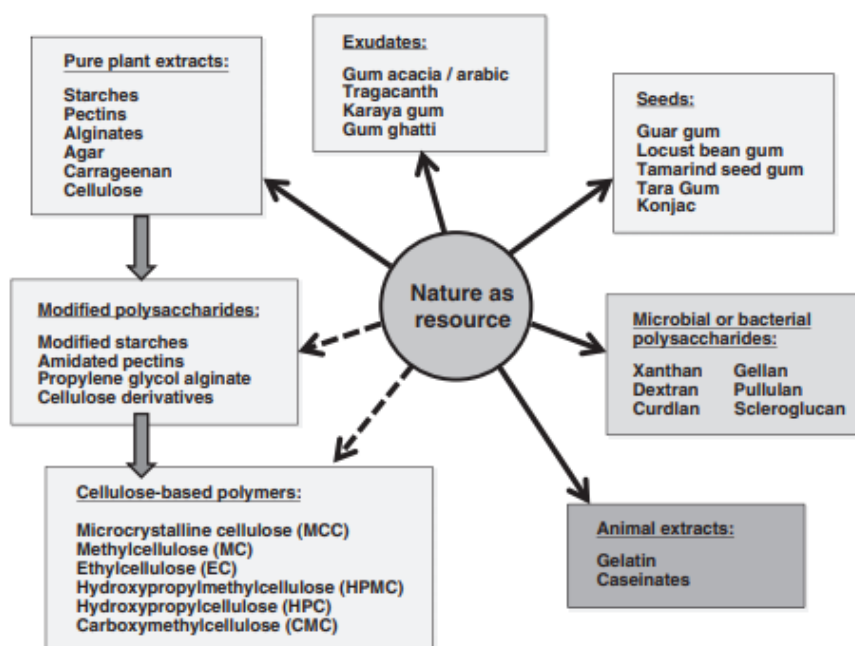
Figure 60. Overview of hydrocolloids used in industry [208].

Among all the hydrocolloids agents commercially available, in this study we have screened the most relevant ones in the literature; xanthan, carboxymethylcellulose (CMC), carrageen iota, guar gum, and agar.

(1) Xanthan Gum

Xanthan gum is a high-molecular-weight polysaccharide secreted by the microorganism Xanthomonas campestris and produced commercially in a batch fermentation process [208]. Xanthan is a long-chain polysaccharide with a high number of trisaccharide side chains [209]. Due to its soft texture, xanthan gum is widely used as a thickener or viscosifier in both food and non-food industries. It also works as a stabilizer for a wide variety of suspensions, emulsions and foams. Xanthan can be considered as a thickening and gelling agent, although most of the work has been focused on its thickening effect as it is a low strength gel. On its own does not form good gels but the gelling efficacy increases in combination with agar, locust beam guar (LGB) and some salts [210]. This is a fast-hydrating water-soluble hydrocolloid that can be dissolved at room temperature, hydration time is reduced with increased mixing speed, temperature and with higher particle sizes. With high-speed mixing, hydration takes 15 to 30 min and up to 1h with low-speed mixing [208]. It is recommended to hydrate xanthan in the water before the addition of salt. Once hydrated, xanthan has very good salt tolerance and up to 20–30% salt can be added without adversely affecting the viscosity. Xanthan has great stability over a wide pH (2.5-11) and temperature range (up to 300 °C).

(2) Guar gum

Guar gum is a polysaccharide of galactose and mannose, obtained from the endosperms of an annual leguminous plant Cyamopsis tetragonoloba [210]. Guar gum does not need to be heated for complete solubility as dissolves completely in both hot and cold water.

In gelling form, it is susceptible to decrease its viscosity by depolymerisation when applying heat (>90 °C) and pH values below 3.5 [208]. Guar gum, as a pure material, is stable over a pH range between 2 to 10 and a temperature up to 300 °C [211]. It is considered a weak gelling agent, mostly studied as a thickening, although it presents high viscosity at low concentrations and exhibits pseudo-plasticity above 0.5 wt.%. Monovalent cations do not affect, while an addition of di- or trivalent cations leads to a viscosity increase, polyols reduce it. The addition of borate ions to guar gum solutions cause a gelation rate increase. Besides, the addition of guar gum to gelling polysaccharides such as agar increases the strength and elasticity of the gels [209]

(3) CMC

Carboxymethyl cellulose (CMC) is a cellulose derivative commonly used in food applications where they are effective as viscosifiers, stabilizers and rheology modifiers. CMC, like guar gum, is soluble in either cold or hot water. The concentration, molecular weight and degree of substitution (ds) are important factors for CMC flow behaviour in aqueous dispersions. Because of the rapid hydration, particles tend to agglomerate and form lumps when the powder is added into water [208]. CMC form weak gels on heating when the temperature rises above 52 °C and under the presence of divalent and trivalent ions. Viscosity and solubility are dependent on the polymer chain length, decreasing chain length will increase solubility while it will decrease viscosity [208]. The presence of salt affects the cellulose gum solutions, depending on concentrations and type of salts. CMC should be fully hydrated before the salt is added, monovalent salts have a low impact while divalent salts may impact the solution characteristics.

(4) Carrageen iota

Carrageenans are polysaccharides (galactose) with varying degree of sulfation (between 15% and 40%) [210]. They are extracted from red seaweeds and are used as thermo-

reversible gelling agents and thickening agents. Three main commercial classes of carrageenan can be found: kappa, iota, and lambda. All are soluble in hot water, but just the lambda form is soluble in cold water although does not form a gel, and just iota/lambda are soluble in salts. κ-Carrageenan is the most used of these seaweed extracts, while λ-Carrageenan is the least utilized given its very expensive to produce [212]. Therefore, the ι-carrageenan was the one chosen for this study as the gels have a much more flexible texture and are less sensitive to shearing. The iota carrageenan network is formed by a series of double-helices and kinks that form a transparent, elastic gel [208]. This loosely-connected network can easily be destroyed by mechanical action. However, it reforms quickly once the mechanical action has stopped. Solutions of κ- and ι-types set to gels upon cooling, gels are stable at room temperature, gels melt by heating and re-set upon cooling without loss of gel strength or texture in neutral conditions [209]

(5) Agar

Agar is a seaweed hydrocolloid, or phycocolloid, with a long use history as a food additive for gelling, thickening and stabilising [208]. It has also been widely used as a solid culture media in microbiology. This material can work both as gelling and thickening agent and it is a family of linear galactan polysaccharides obtained from the cellular walls of red seaweeds. Agar can form reversible gels by simply cooling hot water since it is insoluble in cold water, but hydrates to form random coils in boiling water (melting point 80-90 °C). The agar gelation process is completely reversible; the gel melts on heating and resets on cooling. This cycle can be repeated many times without any significant change in the mechanical properties of the gel, provided the agar is not used in very low pH conditions (below 4) or used with oxidising agents. Agar forms gels at very low concentrations, with a concentration threshold for gelation around 0.2%. Gel

strength is strongly influenced by concentration, pH and sugar content. Higher sugar contents (>60 vol.%) have shown to exhibit enhanced gel strength [208].

Hydrogels are water-based hydrophilic crosslinked polymers, such as poly-N, N-dimethyl acrylamide (PDMAA), 2-hydroxy-ethyl methacrylate (HEMA), and vinyl pyrrolidone (VP)—that is capable of swelling to absorb and hold vast amounts of water (10 − 1,000 times its weight) within their three-dimensional network [213]. Hydrogels possess high biocompatibility and high permeability. Unlike hydrocolloids, hydrogels are not reversible (no hysteresis temperature. Hydrogen gels form the gel structure through a radical polymerisation reaction while hydrocolloids are held together in a gel-like structure by a non-covalent interaction like hydrogen bonds and electrostatic interactions.

(1) Polyacrylamide

Polyacrylamide gels are three-dimensional networks of acrylamide reacted with the bifunctional reagent N, N'-methylene-bis-acrylamide (abbreviated as Bis) via a free-radical initiated vinyl polymerization mechanism [214]. The pore size of the gel is very reproducible and is directly related to the ratio of acrylamide to Bis. It is highly water-absorbent, forming a soft gel when hydrated. In the straight-chain form, it is also used as a thickener and suspending agent. The viscosity of the polyacrylamide solution has a linear correlation with its molecular weight; besides, the higher the temperature, the lower the viscosity. Polyacrylamide can easily be dissolved in water an activated at temperatures close to 90 °C, when polymerisation takes place.

Table 23. Key properties of the screened gelling agents for the 3 in 1 system. [208–210] Note: melting temperature refers to the temperature when stops being a firm gel. Hysteresis is the temperature when it solidifies again. Gelling temperature is the temperature to be soluble in water.

Gelling agents	T. Gelling (°C)	T. Melting (°C)	T. Hysteresis (°C)	T. Decomposition (°C)	Concentration on the gel (vol.%)	Comments	Cost (U$/kg)
Agar	30-40	80-90	45-50	250 [215]	0.5-8	Gel strength dependent on Concentration, time, pH (4.5-9.0) and sugar content. High gel strength (highly heat stable). Clarity gel.	1-3
Xanthan	Room temperature	270	100	290 [211]	0.1-5	High strength gels in combination with LBG (50:50 or 60:40) Otherwise, weak-gel. pH (2.5-11), wide temperature range and under salts and acids concentration.	3-6
CMC	52	274	100	260 [216]	0.7-4	Soluble at cold water. Stable over a pH from 3-10 Gel formation with the number of ions ($^+2,^+3$). Not in pure water. Strong bonds. Opaque gels.	3-6
Carrageenan iota	75-80	50-80	40-50	220 [217]	4	Strongest gels with Ca^+. Gels break by shear but recover and re-gel after shear stress are removed. Clear gel.	10-12
Polyacrylamide	50-65	210	-	250 [218]	4	Chemically inert. Control of different pore sizes. pH neutral or basic (3-9).	1-3
Guar gum	Room temperature	220	<90	310 [216]	0.2-5	Degradable at low pH (2-12) poor clarity gel due to the presence of impurities. Low strength gels, strong gelation with borate ions.	1-3

8.3.2 GELLING AGENTS EXPERIMENTAL VALIDATION

The compatibility between the gelling agents listed in the previous section and the thermochemical materials selected was experimentally studied. Currently, there are not many studies looking at the compatibility of hydrated salts and the gelling agents selected. To that end, preliminary tests were conducted to find whether the gelling agents can work with the TCMs and, when compatible, which is the highest TCM loading admitted by the gelling solution. Since all the gelling agents can be dissolved in water (warm or cold), the same procedure was normalised for all the TCM/gelling agents working pairs for comparison purposes, as described below.

(1) Materials

The gel used, manufacturer and CAS number of the TCM-gel study are described in the following. The polyacrylamide (C3H5NO)n was supplied by Sigma Aldrich (CAS: 9003-05-8), guar gum powder ($C_{10}H_{14}N_5Na_2O_{12}P_3$) from Sigma Aldrich (CAS: 9000-30-0), Xanthan gum ($C_{35}H_{49}O_{29}$) from Xanthomonas campestris supplied by Sigma Aldrich (CAS: 11138-66-2), ι-Carrageenan commercial-grade Type II ($C_{24}H_{36}O_{25}S_2^{-2}$) also from Sigma Aldrich (CAS: 9062-07-1), agar-agar for microbiology ($C_{12}H_{18}O_9$)n from Sigma Aldrich (CAS: 9002-18-0) and carboxymethylcellulose $C_8H_{16}O_8$ (CAS: 9004-32-4) from Sigma Aldrich.

(2) Methodology

As explained in the previous section, the gel could be formed through dissolution into cold or hot water. Therefore, in this section two different methodologies are reported, for hot and cold water, depending on the gel used, this will be explained later.

In the hot water- TCM/gel synthesis was conducted in six steps (see Figure 61); (1) The gelling agent was added into 10 mL of water at room temperature followed by stirring at a constant rate of 250-300 rpm. (2) The gel solution was heated up to 90 °C in the hot plate while stirring at the same rpm to allow the gel to dissolve. (3) Once the gel has been activated (viscosity of the solutions is visibly increased), the salt was added in percentages between 80-100 wt./vol.% in volume into the gel solution. The percentages are intended to maximise the TCM percentage while allowing the salt homogeneously to disperse into the gel structure. Hence, 100 wt./vol.% of TCM would be ideal for the composite, though this might saturate and collapse the gel structure (see later). When the salt was completely dispersed in the gel structure, the temperature was reduced to room temperature, stirring at a constant rate was maintain during the whole preparation process. (4) The stirring magnet was removed from the gel/TCM solution and poured into a silicone mould (2 cm x 4 cm), to allow the gel stabilisation the gel/TCM was left to settle for 2 hours in the silicon moulds at ambient conditions. This step was skipped when working with highly hygroscopic (e.g. $CaCl_2$ and $MgCl_2$) materials as they needed to be dried right after the synthesis to avoid any extra saltwater absorption. (5) The silicon trays were located into a humidity chamber under vacuum conditions (10^{-3} bar) and heated up to 60 °C with the slowest heating rate allowed by the chamber (1 °C/min). Followed by an isotherm at 60 °C for 1.2 hours. Note that in Chapter 9 this temperature is studied and readjusted for the TCM/PCM (6) Once the TCM/gel is completely dry, it was easily unmoulded from the silicon tray and kept in a sealed bag.

The cold water- TCM/gel synthesis was conducted in six steps (see Figure 62); similar to the hot water procedure but without heat during the addition of the gel and the TCM into the water solution.
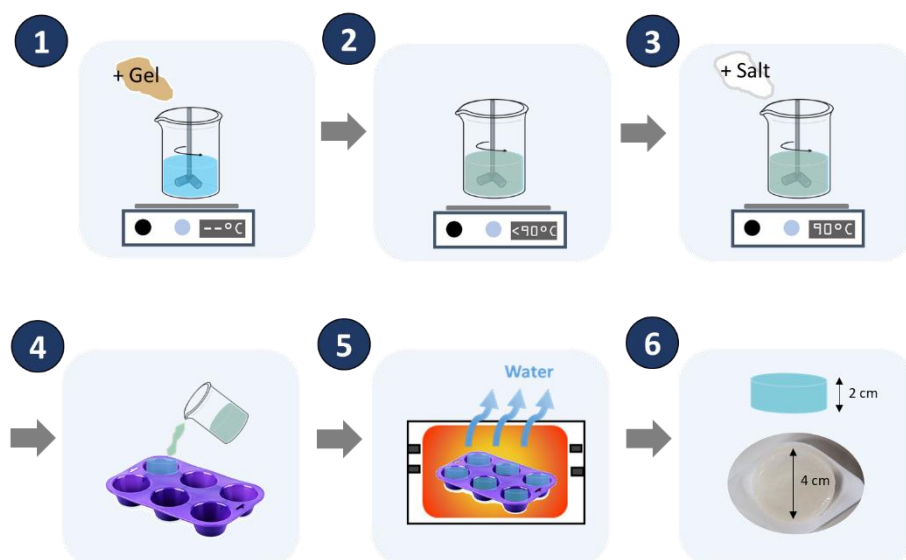
Figure 61. Hot gel/TCM synthesis procedure, gel content ranging from 2-4 wt./vol.%. and TCM from 80-100wt./ vol.%. Note that a temperature of 90°C is applied during the mixing process.
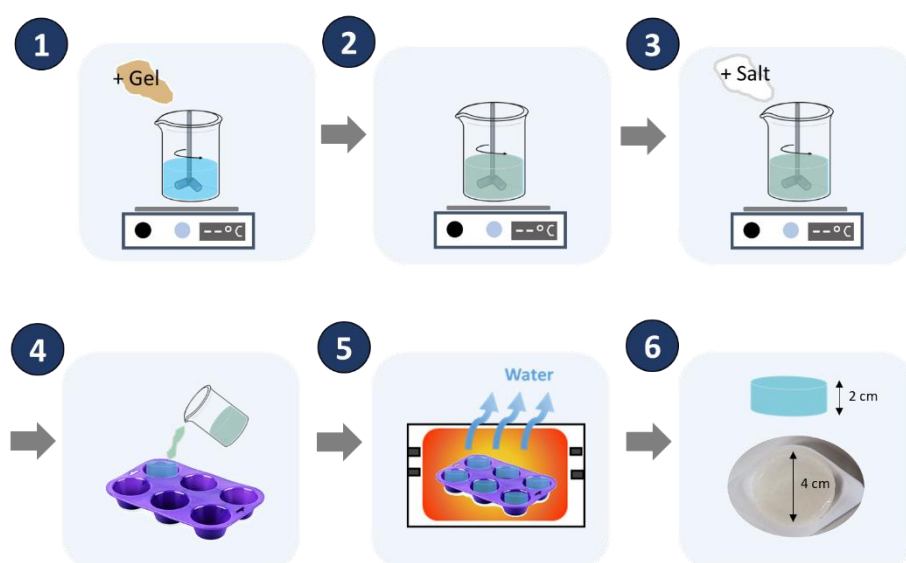
Figure 62. Cold gel/TCM synthesis procedure, gel content ranging from 2-4 wt./vol.% and TCM from 80-100 wt./vol.%. Note that the mixing process is conducted at room temperature.

(3) Compatibility

To study the compatibility between the TCMs and the gelling agents selected, the first approach is oriented to find the minimum gel load that achieves a gel structure with the

minimum TCM load of the study (80 wt./vol.%). When that is accomplished, the TCM loading is increased if possible to 100 wt./vol.%).

Therefore, a first preliminary study was performed, which consisted on the addition of different percentages of gel, from 2 to 6% in volume (preliminary test showed that 1% vol. was not enough to allow jellification of 80% vol. TCM). It is worth mentioning that the order of addition must be first the gel, and then the TCM, as the contrary does not lead to satisfactory results; as shown in Figure 63. The gelling agent must be fully dissolved to form the structure and well hydrated before adding the salt (as also reported in the literature), otherwise, the gel is not formed, and the mixture is formed with lumps of gel and TCM solution.

Figure 63. Left; Mixture of Gel and TCM with an order of addition 1st TCM and 2nd gel following the procedure described in the methodology section. Right; Mixture of Gel and TCM with an order of addition 1st gel and 2nd TCM following the procedure described in the methodology section.

Figure 64. Left; Mixture of Guar gum and TCM (Magnesium sulphate as an example) prepared through the cold method. Right; Mixture of polyacrylamide and TCM (Magnesium sulphate as an example) prepared though hot preparation method.

From this first experiment, we can conclude that, overall, the minimum amount of gel required to form a gel is 4 wt./vol.% (see Table 24). Some of the TCMs such as strontium bromide and calcium chloride allow for a lower amount of gel given that the salt does not interact strongly with the gelling agent. However, this preliminary study aimed to find a minimum percentage common for all TCMs so next experiments could be performed under the same conditions to determine the TCM load in the gel solution. Regarding the preparation method, all gels needed heat to activate and form the gel (Figure 61) except Guar gum, that it can be dissolved at a cold temperature and form the gel afterwards (Figure 62 and Figure 64). Among all the gels, it is worth noticing that carrageen iota needed longer times and higher shear rates to dissolve, while guar gum was the easiest and simplest to prepare. Xanthan, agar and CMC were the less compatible with TCMs, whereas guar gum, carrageen iota and polyacrylamide showed fairly good compatibility (except for potassium carbonate that just shows synergies with guar gum). Polyacrylamide showed good interaction with all the TCMs tested and a wide range of gel concentrations (2-8 wt./vol.%) (see Figure 64). As expected, the gel strength was increased with the gel concentration till reaching a point were gel formed a heavy paste and no more gelling agent could be dissolved as the water may already be trapped into the formed gel structure. The main outcomes of these experiments are reviewed below for each of the TCMs;

- **Potassium carbonate** reacts with all the gels given the high basic pH of the solution, which was measured to be 12; it forms a yellowish solution when dissolving in the gel solution. That results in lumps of gel and solution (see Figure 65). This TCM just forms weak gels with guar gum (GG), that is less sensitive to basic pH, and do not require heat to dilute.
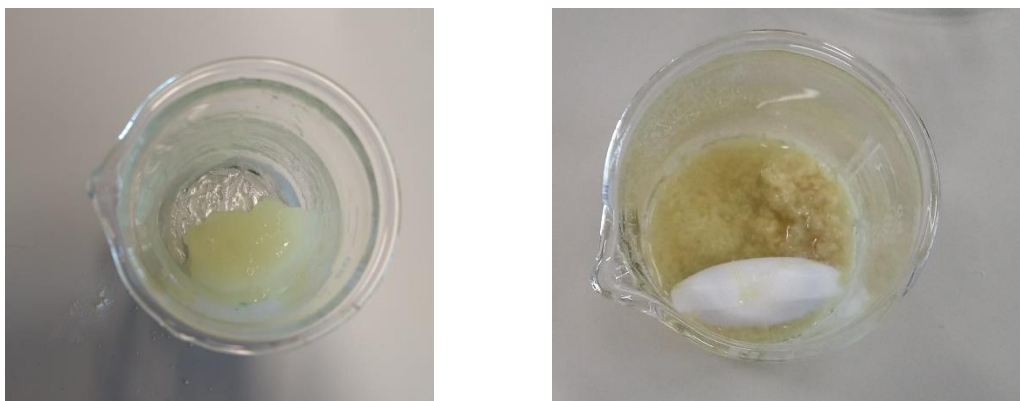
Figure 65. The yellowish solution resulted from potassium carbonate reaction with gels, guar gum in the left-hand side and xanthan in the right.

-   **Magnesium sulfate** does not work with agar given the presence of Mg^{2+} ion, resulting on the formation of a solution similar to the one shown in Figure 63, with percentages of TCM ranging from 70-100 wt./vol.% and 4 wt./vol.% of agar. The first approach to solve this was to check the solution pH (6.15-6.8). Along with this, as reported in the literature, agar is stable over pH from 4.5, as reported in the screening section, so this theory was discarded. From visual inspection, when adding the magnesium sulphate into the agar solution, phase separation can be seen, magnesium sulphate attracts the water into its solvation structure breaks the hydrogen bonds in the gels. Thus, it appears to be a matter of electric charges or water affinity for the different particles dissolved in the water solution as magnesium ions have shown to be a problem in the gelation of some hydrocolloids [219]. Although, this was not confirmed in this study as-is out of the scope of the thesis and should be further studied to validate this hypothesis. This phenomenon was not observed with the rest of the gels. Carboxymethylcellulose, guar gum and polyacrylamide are the ones that allow higher loads and stronger/stable gels. In the case of guar gum, the gel was strengthened by the addition of magnesium sulphate.

For xanthan, the gels are very weak and not fully homogeneous, although do not behave as agar gels.

- **Magnesium Chloride** shows a similar behaviour as magnesium sulphate given the Mg^{2+} ion. Although it appears to be very difficult to dry the gels given the low deliquescence of the salt.

- **Calcium chloride** works very well with gum-based gels, especially agar. Very difficult to dry the gels given the low deliquescence of the salt. It is also suitable with carrageen iota given the presence of Ca^{2+}.

- **Strontium bromide** works well with all gels except for xanthan that does not even form a gel. This effect was attributed to similar behaviour as the one reported with Mg^{2+} ions and agar gel. In this case, the strongest gels formed are with agar and CMC.

Table 24. Minimum and maximum (min-max) loading of the gelling agent into an 80 wt./vol.% solution of TCM.

TCM	Guar gum	Polyacrylamide	CMC	Xanthan	Agar	i-Carrageen
Potassium carbonate	4-6 wt./vol.%	-	-	-	-	-
Magnesium sulphate	4-8 wt./vol.%	2-8 wt./vol.%	4-8 wt./vol.%	4-6 wt./vol.%	-	2-4 wt./vol.%
Strontium bromide	4-8 wt./vol.%	2-8 wt./vol.%	4-8 wt./vol.%	-	2-8 wt./vol.%	2-4 wt./vol.%
Calcium chloride	4-8 wt./vol.%	2-8 wt./vol.%	-	-	2-8 wt./vol.%	2-8 wt./vol.%
Magnesium chloride	4-8 wt./vol.%	2-8 wt./vol.%	4-8 wt./vol.%	4-6 wt./vol.%	-	2-4 wt./vol.%

Hence, from the explained above, the optimum minimum percentage for all the gels studied was set to 4 wt./vol.%. The next step was focused on determining the TCM load range for the TCM/gel working pair. To that end, loadings of TCM ranging from 80-100 wt./vol.% were dissolved into 4 wt./vol.% gelling agent solutions, see Table 25. The solubility of the salt plays

a key role in this experiment, although most of the salts here considered are highly soluble in water. Since the aim here was to ensure the gel formation while maximising the loading of TCM, some of the salt was assumed to be partially dissolved. This was considered not a limiting issue as the important feature is that gel can contain the TCM and homogeneously disperse it within its structure. The gel will be dried and just the salt will remain, therefore the salt does not must to be fully dissolved as it is just accommodated in the 3D gel structure, which could cause non-homogeneities. Besides, some gels are formed when cooling down (e.g. agar) and others are already formed when adding the salt (e.g. guar gum). In further steps, when working pairs have been selected and thermal properties need to be studied, this will be considered more in detail.

Table 25. Maximum TCM load in 4 wt./vol.% in volume gelling agent solution.

TCM	Guar gum	Polyacrylamide	CMC	Xanthan	Agar	i-Carrageen
Potassium carbonate	80 wt./vol.%	-	-	-	-	-
Magnesium sulphate	80 wt./vol.%	80 wt./vol.%	80 wt./vol.%	80 wt./vol.%	-	-
Strontium bromide	90 wt./vol.%	90 wt./vol.%	90 wt./vol.%	-	90 wt./vol.%	-
Calcium chloride	90 wt./vol.%	80 wt./vol.%	-	-	100 wt./vol.%	90 wt./vol.%
Magnesium chloride	90 wt./vol.%	90 wt./vol.%	90 wt./vol.%	80 wt./vol.%	-	-

From this second experiment, the main outcomes are that, in general, the maximum loads vary from 80 to 90 wt./vol.%, 100 wt./vol.% appear to be too high for most of the gels, except for agar/calcium chloride. In the other cases, when adding a higher percentage two phenomena are observed: (1) There is phase segregation where there is a solution underneath the gel (see Figure 66), this happened for polyacrylamide, guar gum CMC and xanthan; and (2) The lumps gel are heterogeneously dispersed into a TCM solution as shown in Figure 66. This was observed for agar and i-carrageena.

Figure 66. Right: phase segregation; Left: lumps heterogeneously distributed.

8.3.3 GELLING AGENTS SELECTION

From the experiments described above, it was concluded that guar gum and polyacrylamide were selected as the gelling agents to be studied in the working pair's stage. A 4 wt./vol.% in vol. of the gelling agent was set as the optimum to synthesize the gel, while a maximum loading of TCM was set to 80-90 wt./vol.% (depending on the TCM/gel working pair) was determined. Polyacrylamide and guar gum are both compatible with all TCMs understudy, but they are cost extensive (1-3 $/kg). Besides, they offer two different gelling nature as one is a hydrogel (polyacrylamide) and the other one a hydrocolloid gel (guar gum). This allows us to compare two different gelling mechanisms and preparation methods (hot and cold).

8.4 CONCLUDING REMARKS

In this section, a comprehensive screening and selection study of TCMs available for building applications, following a top-down approach was presented. The main outcomes of this research concern the thermochemical material screening process flow and the importance of considering a set of theoretical candidates when selecting a TCM for a specific application. Besides, other relevant properties such as thermal diffusivity and specific heat capacity not often characterized

in the TCM research studies found in the literature have been measured, providing more experimental evidence for comparison between studies. The outputs from the overall selection process are a list of candidates narrowed down to 9 thermochemical materials; $MgSO_4 \cdot 7H_2O$, $MgCl_2 \cdot 6 H_2O$, $CaCl_2 \cdot 6H_2O$, $SrBr_2 \cdot 6 H_2O$ and $K_2CO_3 \cdot 1.5 H_2O$, eight-phase change materials; High density polyethylene (HDPE), 4,40-diphenylmethane diisocyanate (MDI), polyethylene oxide (PEO), polyethylene glycols (PEG) (1,000 MW, 600 MW and 35,000 MW), erythritol (E), plus one matrix cellulose (CLU) and two gels (polyacrylamide (PA) and guar gum (GG)) that will be combined to working pairs according to the working temperature combinations.

The compatibility study of TCM/gel working pair has proved that gelling agents have a great potential in TCS technology, not just for the 3 in 1 system but for pure TCMs, as they provide a skeleton structure. This opens a new way to TCM manufacturing and fabrication, the research here presented can be used as a guide for future studies as a layout of gel/TCM compatibility is provided.

8.4 REFERENCES

[1]   Ashby MF. Materials Selection in Mechanical Design. Second Edi. Oxford: Butterworth-Heinemann; 1999.

[2]   Fernandez AI, Martnez M, Segarra M, Martorell I, Cabeza LF. Selection of materials with potential in sensible thermal energy storage. Sol Energy Mater Sol Cells 2010. doi:10.1016/j.solmat.2010.05.035.

[3]   Khare S, Dell'Amico M, Knight C, McGarry S. Selection of materials for high temperature sensible energy storage. Sol Energy Mater Sol Cells 2013;115:114–22. doi:10.1016/j.solmat.2013.03.009.

[4]   Liu M, Fernández AI, Segarra M. Materials for Phase Change Material at High

Temperature. Elsevier Ltd; 2018. doi:10.1016/B978-0-12-805323-2.00008-4.

[5]   Ruiz-Cabañas FJ, Prieto C, Madina V, Fernández AI, Cabeza LF. Materials selection for thermal energy storage systems in parabolic trough collector solar facilities using high chloride content nitrate salts. Sol Energy Mater Sol Cells 2017;163:134–47. doi:10.1016/j.solmat.2017.01.028.

[6]   Donkers PAJ, Sögütoglu LC, Huinink HP, Fischer HR, Adan OCG. A review of salt hydrates for seasonal heat storage in domestic applications. Appl Energy 2017. doi:10.1016/j.apenergy.2017.04.080.

[7]   Glasser L. Thermodynamics of inorganic hydration and of humidity control, with an extensive database of salt hydrate pairs. J Chem Eng Data 2014;59:526–30. doi:10.1021/je401077x.

[8]   Clark RJ, Mehrabadi A, Farid M. State of the art on salt hydrate thermochemical energy storage systems for use in building applications. J Energy Storage 2020. doi:10.1016/j.est.2019.101145.

[9]   Hawwash AA, Hassan H, Ahmed M, Ookawara S, Feky K El. Long-term Thermal Energy Storage Using Thermochemical Materials. Energy Procedia 2017;141:310–4. doi:10.1016/j.egypro.2017.11.111.

[10]   Sutton R, Jewell E, Searle J, Elvins J. Discharge performance of blended salt in matrix materials for low enthalpy thermochemical storage. Appl Therm Eng 2018;145:483–93. doi:10.1016/j.applthermaleng.2018.09.052.

[11]   Whiting GT, Grondin D, Stosic D, Bennici S, Auroux A. Zeolite-MgCl2 composites as potential long-term heat storage materials: Influence of zeolite properties on heats of water sorption. Sol Energy Mater Sol Cells 2014;128:289–95. doi:10.1016/j.solmat.2014.05.016.

[12]   Posern K, Osburg A. Determination of the heat storage performance of thermochemical heat storage materials based on SrCl2 and MgSO4. J Therm Anal Calorim 2017;131:2769–73. doi:10.1007/s10973-017-6861-8.

[13]   Soda M, Beyene A. Multiphase ultra-low grade thermal energy storage for organic Rankine cycle. Int J Energy Res 2016;40:51–60. doi:10.1002/er.3300.

[14]   Kim ST, Zamengo M, Ryu J, Kato Y. Kinetic Characterization of Expanded Graphite, Calcium Chloride, and Magnesium Hydroxide Composite for the Chemical Heat Pump. Heat Transf Res 2014;46:91–107. doi:10.1615/heattransres.2014006874.

[15]   Pathak AD, Nedea S, Zondag H, Rindt C, Smeulders D. Diffusive transport of water in magnesium chloride dihydrate under various external conditions for long term heat storage: A ReaxFF-MD study. Eur J Mech B/Fluids 2017;64:93–101. doi:10.1016/j.euromechflu.2016.12.011.

[16]   Nedea S, Zondag H, Rindt C, Pathak AD, Smeulders D, van Duin ACT. Reactive force field development for magnesium chloride hydrates and its application for seasonal heat storage. Phys Chem Chem Phys 2016;18:15838–47. doi:10.1039/c6cp02762h.

[17]   Zhang YN, Wang RZ, Zhao YJ, Li TX, Riffat SB, Wajid NM. Development and thermochemical characterizations of vermiculite/SrBr2 composite sorbents for low-temperature heat storage. Energy 2016;115:120–8. doi:10.1016/j.energy.2016.08.108.

[18]   Fopah-lele A, Gaston J. Solar Energy Materials & Solar Cells A review on the use of SrBr 2 · 6H 2 O as a potential material for low temperature energy storage systems and building applications. Sol Energy Mater Sol Cells 2017;164:175–87. doi:10.1016/j.solmat.2017.02.018.

[19]   Courbon E, D'Ans P, Permyakova A, Skrylnyk O, Steunou N, Degrez M, et al. A new composite sorbent based on SrBr2and silica gel for solar energy storage application with

high energy storage density and stability. Appl Energy 2017;190:1184–94. doi:10.1016/j.apenergy.2017.01.041.

[20]   Zhao YJ, Wang RZ, Zhang YN, Yu N. Development of SrBr2composite sorbents for a sorption thermal energy storage system to store low-temperature heat. Energy 2016;115:129–39. doi:10.1016/j.energy.2016.09.013.

[21]   Fopah-Lele A, Tamba JG. A review on the use of SrBr2·6H2O as a potential material for low temperature energy storage systems and building applications. Sol Energy Mater Sol Cells 2017;164:175–87. doi:10.1016/j.solmat.2017.02.018.

[22]   Gilles D, Segato T, Courbon E, Degrez M, D'Ans P. Affordable Process for the Production of Strontium Bromide Used in Low Grade Heat Recovery Applications. Procedia CIRP 2018;69:383–8. doi:10.1016/j.procir.2017.11.056.

[23]   Posern K, Kaps C. Humidity controlled calorimetric investigation of the hydration of MgSO4 hydrates. J Therm Anal Calorim 2008;92:905–9. doi:10.1007/s10973-007-8640-4.

[24]   Whiting G, Grondin D, Bennici S, Auroux A. Heats of water sorption studies on zeolite-MgSO 4 composites as potential thermochemical heat storage materials. Sol Energy Mater Sol Cells 2013;112:112–9. doi:10.1016/j.solmat.2013.01.020.

[25]   Calabrese L, Brancato V, Palomba V, Frazzica A, Cabeza LF. Assessment of the hydration/dehydration behaviour of MgSO4·7H2O filled cellular foams for sorption storage applications through morphological and thermo-gravimetric analyses. Sustain Mater Technol 2018;17:e00073. doi:10.1016/j.susmat.2018.e00073.

[26]   Ferchaud CJ, Scherpenborg RAA, Zondag HA, De Boer R. Thermochemical seasonal solar heat storage in salt hydrates for residential applications - Influence of the water vapor pressure on the desorption kinetics of MgSO4·7H2O. Energy Procedia 2014;57:2436–40.

doi:10.1016/j.egypro.2014.10.252.

[27] Sharma SK, Jotshi CK, Kumar S. Thermal stability of sodium salt hydrates for solar energy storage applications. Sol Energy 1990;45:177–81. doi:10.1016/0038-092X(90)90051-D.

[28] De Jong AJ, Trausel F, Finck C, Van Vliet L, Cuypers R. Thermochemical heat storage - System design issues. Energy Procedia 2014;48:309–19. doi:10.1016/j.egypro.2014.02.036.

[29] Roelands M, Cuypers R, Kruit KD, Oversloot H, De Jong AJ, Duvalois W, et al. Preparation & Characterization of Sodium Sulfide Hydrates for Application in Thermochemical Storage Systems. Energy Procedia 2015;70:257–66. doi:10.1016/j.egypro.2015.02.122.

[30] Scapino L, Zondag HA, Van Bael J, Diriken J, Rindt CCM. Energy density and storage capacity cost comparison of conceptual solid and liquid sorption seasonal heat storage systems for low-temperature space heating. Renew Sustain Energy Rev 2017;76:1314–31. doi:10.1016/j.rser.2017.03.101.

[31] Solé A, Barreneche C, Martorell I, Cabeza LF. Corrosion evaluation and prevention of reactor materials to contain thermochemical material for thermal energy storage. Appl Therm Eng 2016;94:355–63. doi:10.1016/j.applthermaleng.2015.10.156.

[32] Sutton RJ, Jewell E, Elvins J, Searle JR, Jones P. Characterising the discharge cycle of CaCl2and LiNO3hydrated salts within a vermiculite composite scaffold for thermochemical storage. Energy Build 2018;162:109–20. doi:10.1016/j.enbuild.2017.11.068.

[33] Bouché M, Richter M, Linder M. Heat transformation based on CaCl2/H2O - Part B: Open operation principle. Appl Therm Eng 2016;102:641–7. doi:10.1016/j.applthermaleng.2016.03.102.

[34] Molenda M, Bouché M, Linder M, Blug M, Busse J, Wörner A. Thermochemical Energy

Storage for Low Temperature Applications : Materials and First Studies in a Gas-Solid Reactor 2012;2:1–10.

[35]   van der Pal M, Critoph RE. Performance of CaCl2-reactor for application in ammonia-salt based thermal transformers. Appl Therm Eng 2017;126:518–24. doi:10.1016/j.applthermaleng.2017.07.086.

[36]   Jabbari-Hichri A, Bennici S, Auroux A. CaCl2-containing composites as thermochemical heat storage materials. Sol Energy Mater Sol Cells 2017;172:177–85. doi:10.1016/j.solmat.2017.07.037.

[37]   Shkatulov AI, Houben J, Fischer H, Huinink HP. Stabilization of K2CO3 in vermiculite for thermochemical energy storage. Renew Energy 2020. doi:10.1016/j.renene.2019.11.119.

[38]   Linnow K, Niermann M, Bonatz D, Posern K, Steiger M. Experimental studies of the mechanism and kinetics of hydration reactions. Energy Procedia 2014;48:394–404. doi:10.1016/j.egypro.2014.02.046.

[39]   Sögütoglu LC, Donkers PAJ, Fischer HR, Huinink HP, Adan OCG. In-depth investigation of thermochemical performance in a heat battery: Cyclic analysis of K2CO3, MgCl2 and Na2S. Appl Energy 2018;215:159–73. doi:10.1016/j.apenergy.2018.01.083.

[40]   Gaeini M, Shaik SA, Rindt CCM. Characterization of potassium carbonate salt hydrate for thermochemical energy storage in buildings. Energy Build 2019. doi:10.1016/j.enbuild.2019.05.029.

[41]   Xie N, Huang Z, Luo Z, Gao X, Fang Y, Zhang Z. Inorganic Salt Hydrate for Thermal Energy Storage 2017:1–17. doi:10.3390/app7121317.

[42]   Donkers PAJ, Sögütoglu LC, Huinink HP, Fischer HR, Adan OCG. A review of salt hydrates for seasonal heat storage in domestic applications. Appl Energy 2017;199:45–68.

doi:10.1016/j.apenergy.2017.04.080.

[43]   Riffat S, Ozankaya G, Yanan Z, Jarimi H, Aydin D, Chen X. Review on the recent progress of thermochemical materials and processes for solar thermal energy storage and industrial waste heat recovery. Int J Low-Carbon Technol 2018:44–69. doi:10.1093/ijlct/cty052.

[44]   Scapino L, Zondag HA, Van Bael J, Diriken J, Rindt CCM. Sorption heat storage for long-term low-temperature applications: A review on the advancements at material and prototype scale. Appl Energy 2017;190:920–48. doi:10.1016/j.apenergy.2016.12.148.

[45]   Donkers PAJ, Pel L, Adan OCG. Experimental studies for the cyclability of salt hydrates for thermochemical heat storage. J Energy Storage 2016;5:25–32. doi:10.1016/j.est.2015.11.005.

[46]   van Essen VM, Zondag H a., Gores JC, Bleijendaal LPJ, Bakker M, Schuitema R, et al. Characterization of MgSO4 Hydrate for Thermochemical Seasonal Heat Storage. J Sol Energy Eng 2009;131:041014. doi:10.1115/1.4000275.

[47]   Al-Abbasi O, Abdelkefi A, Ghommem M. Modeling and assessment of a thermochemical energy storage using salt hydrates. Int J Energy Res 2017;41:2149–61. doi:10.1002/er.3776.

[48]   Michel B, Mazet N, Neveu P. Experimental investigation of an open thermochemical process operating with a hydrate salt for thermal storage of solar energy: Local reactive bed evolution. Appl Energy 2016;180:234–44. doi:10.1016/j.apenergy.2016.07.108.

[49]   Cammarata A, Verda V, Sciacovelli A, Ding Y. Hybrid strontium bromide-natural graphite composites for low to medium temperature thermochemical energy storage: Formulation, fabrication and performance investigation. Energy Convers Manag 2018;166:233–40. doi:10.1016/j.enconman.2018.04.031.

[50] Descy G, Frère M, Bougard J, Heymans N, Skrylnyk O, Courbon E. Performance characterization of salt-in-silica composite materials for seasonal energy storage design. J Energy Storage 2018;19:320–36. doi:10.1016/j.est.2018.08.015.

[51] Voigt W, Zeng D. Solid–liquid equilibria in mixtures of molten salt hydrates for the design of heat storage materials. Pure Appl Chem 2007;74:1909–20. doi:10.1351/pac200274101909.

[52] Kenisarin M, Mahkamov K. Salt hydrates as latent heat storage materials:Thermophysical properties and costs. Sol Energy Mater Sol Cells 2016;145:255–86. doi:10.1016/j.solmat.2015.10.029.

[53] Wang Z, Jing Y, Jia Y, Zhang Y, Ma G, Xie S, et al. Hydrophilic expanded graphite-magnesium nitrate hexahydrate composite phase change materials: Understanding the effect of hydrophilic modification on thermophysical properties. Int J Energy Res 2019;43:1121–32. doi:10.1002/er.4336.

[54] Korhammer K, Rammelberg HU, Ruck WKL, N'Tsoukpoe KE, Lele AF, Watts BA, et al. A review on the use of calcium chloride in applied thermal engineering. Appl Therm Eng 2014;75:513–31. doi:10.1016/j.applthermaleng.2014.09.047.

[55] Molenda M, Stengler J, Linder M, Wörner A. Reversible hydration behavior of CaCl2 at high H2O partial pressures for thermochemical energy storage. Thermochim Acta 2013;560:76–81. doi:10.1016/j.tca.2013.03.020.

[56] Urs Rammelberg H, Schmidt T, Ruck W. Hydration and dehydration of salt hydrates and hydroxides for thermal energy storage - kinetics and energy release. Energy Procedia 2012;30:362–9. doi:10.1016/j.egypro.2012.11.043.

[57] Chacartegui R, Valverde JM, Barrios-Padura A, Lizana J, Ortiz C. Identification of best available thermal energy storage compounds for low-to-moderate temperature storage

applications in buildings. vol. 68. 2018. doi:10.3989/mc.2018.10517.

[58]   Berroug F, Lakhal EK, El Omari M, Faraji M, El Qarnia H. Thermal performance of a greenhouse with a phase change material north wall. Energy Build 2011;43:3027–35. doi:10.1016/j.enbuild.2011.07.020.

[59]   Canbazoğlu S, Şahinaslan A, Ekmekyapar A, Aksoy YG, Akarsu F. Enhancement of solar thermal energy storage performance using sodium thiosulfate pentahydrate of a conventional solar water-heating system. Energy Build 2005;37:235–42. doi:10.1016/j.enbuild.2004.06.016.

[60]   Gaeini M, Rouws AL, Salari JWO, Zondag HA, Rindt CCM. Characterization of microencapsulated and impregnated porous host materials based on calcium chloride for thermochemical energy storage. Appl Energy 2018;212:1165–77. doi:10.1016/j.apenergy.2017.12.131.

[61]   Rammelberg HU, Schmidt T, Ruck W. Hydration and dehydration of salt hydrates and hydroxides for thermal energy storage - Kinetics and energy release. Energy Procedia 2012;30:362–9. doi:10.1016/j.egypro.2012.11.043.

[62]   Chen J, Ma P, Chen G, Chen F. The measurement of hydration heats for magnesium chloride with low water by means of DSC. J Therm Anal Calorim 2001;65:777–86. doi:10.1023/A:1011963712794.

[63]   Ferchaud CJ, Zondag HA, Veldhuis JBJ, De Boer R. Study of the reversible water vapour sorption process of MgSO4.7H2O and MgCl2.6H2O under the conditions of seasonal solar heat storage. J Phys Conf Ser 2012;395. doi:10.1088/1742-6596/395/1/012069.

[64]   Mamani V, Gutiérrez A, Ushak S. Development of low-cost inorganic salt hydrate as a thermochemical energy storage material. Sol Energy Mater Sol Cells 2018;176:346–56. doi:10.1016/j.solmat.2017.10.021.

[65]   Huang QZ, Lu GM, Wang J, Yu JG. Mechanism and kinetics of thermal decomposition of MgCl 2 × 6H 2O. Metall Mater Trans B Process Metall Mater Process Sci 2010;41:1059– 66. doi:10.1007/s11663-010-9390-4.

[66]   Małecka B, Łącz A, Drozdz E, Małecki A. Thermal decomposition of d-metal nitrates supported on alumina. J Therm Anal Calorim 2015;119:1053–61. doi:10.1007/s10973-014-4262-9.

[67]   Badens E, Llewellyn P, Fulconis JM, Jourdan C, Veesler S, Boistelle R, et al. Study of Gypsum Dehydration by Controlled Transformation Rate Thermal Analysis (CRTA). J Solid State Chem 1998;139:37–44. doi:10.1006/jssc.1998.7797.

[68]   Paulik J, Paulik F, Arnold M. Thermogravimetric examination of the dehydration of calcium nitrate tetrahydrate under quasiisothermal and quasi-isobaric conditions. J Therm Anal 1983;27:409–18. doi:10.1007/BF01914678.

[69]   Zhao CY, Ji Y, Xu Z. Investigation of the Ca(NO3)2–NaNO3 mixture for latent heat storage. Sol Energy Mater Sol Cells 2015. doi:10.1016/j.solmat.2015.04.005.

[70]   Ali ES, Askalany AA, Harby K, Diab MR, Alsaman AS. Adsorption desalination-cooling system employing copper sulfate driven by low grade heat sources. Appl Therm Eng 2018;136:169–76. doi:10.1016/j.applthermaleng.2018.03.014.

[71]   W. Wendlandt W. A new apparatus for simultaneous differential thermal analysis and gas evolution analysis. Anal Chim Acta 1962;27:309–14. doi:10.1016/s0003-2670(00)88506-2.

[72]   Borchardt HJ, Daniels F. Differential thermal analysis of inorganic hydrates. J Phys Chem 1957;61:917–21. doi:10.1021/j150553a016.

[73]   Gonzales RB, Law VJ, Prindle JC. Analysis of the hybrid copper oxide-copper sulfate cycle for the thermochemical splitting of water for hydrogen production. Int J Hydrogen Energy

2009;34:4179–88. doi:10.1016/j.ijhydene.2008.12.026.

[74]   Noorsyakirah A, Mazlan M, Afian OM, Aswad MA, Jabir SM, Nurazilah MZ, et al. Application of Potassium Carbonate as Space Holder for Metal Injection Molding Process of Open Pore Copper Foam. Procedia Chem 2016. doi:10.1016/j.proche.2016.03.052.

[75]   Abedin A, Rosen M, Choi JC, Kim SD, Eindhoven TU, Habashy GM, et al. A Critical Review of Thermochemical Energy Storage Systems. Open Renew Energy J 2011;4:42–6. doi:10.2174/1876387101004010042.

[76]   van Essen VM, Cot Gores J, Bleijendaal LPJ, Zondag H a., Schuitema R, Bakker M, et al. Characterization of Salt Hydrates for Compact Seasonal Thermochemical Storage. ASME 2009 3rd Int Conf Energy Sustain Vol 2 2009;2:825–30. doi:10.1115/ES2009-90289.

[77]   Hongois S, Kuznik F, Stevens P, Roux JJ. Development and characterisation of a new MgSO4-zeolite composite for long-term thermal energy storage. Sol Energy Mater Sol Cells 2011;95:1831–7. doi:10.1016/j.solmat.2011.01.050.

[78]   Okhrimenko L, Favergeon L, Johannes K, Kuznik F, Pijolat M. Thermodynamic study of MgSO4– H2O system dehydration at low pressure in view of heat storage. Thermochim Acta 2017;656:135–43. doi:10.1016/j.tca.2017.08.015.

[79]   Grevel KD, Majzlan J, Benisek A, Dachs E, Steiger M, Fortes AD, et al. Experimentally Determined Standard Thermodynamic Properties of Synthetic MgSO4 center dot 4H(2)O (Starkeyite) and MgSO4 center dot 3H(2)O: A Revised Internally Consistent Thermodynamic Data Set for Magnesium Sulfate Hydrates. Astrobiology 2012;12:1042–54. doi:DOI 10.1089/ast.2012.0823.

[80]   Donkers PAJ, Beckert S, Pel L, Stallmach F, Steiger M, Adan OCG. Water Transport in MgSO4·7H2O during Dehydration in View of Thermal Storage. J Phys Chem C 2015;119:28711–20. doi:10.1021/acs.jpcc.5b08730.

[81]   L'vov B V. Thermal Decomposition of Solids and Melts 2007;7. doi:10.1007/978-1-4020-5672-7.

[82]   Zondag H, Essen M Van, He Z, Schuitema R, Helden W Van. CHARACTERISATION OF MgSO 4 FOR THERMOCHEMICAL STORAGE 2007.

[83]   Posern K, Linnow K, Niermann M, Kaps C, Steiger M. Thermochemical investigation of the water uptake behavior of MgSO4 hydrates in host materials with different pore size. Thermochim Acta 2015;611:1–9. doi:10.1016/j.tca.2015.04.031.

[84]   Freyer D, Voigt W. Crystallization and Phase Stability of CaSO4 and CaSO 4 - Based Salts. Monatshefte Fur Chemie 2003;134:693–719. doi:10.1007/s00706-003-0590-3.

[85]   Xu C, Yu Z, Xie Y, Ren Y, Ye F, Ju X. Study of the hydration behavior of zeolite-MgSO4 composites for long-term heat storage. Appl Therm Eng 2017;129:250–9. doi:10.1016/j.applthermaleng.2017.10.031.

[86]   Strydom CA, Hudson-Lamb DL, Potgieter JH, Dagg E. The thermal dehydration of synthetic gypsum. Thermochim Acta 1995;269–270:631–8. doi:10.1016/0040-6031(95)02521-9.

[87]   Hudson-Lamb DL, Strydom CA, Potgieter JH. The thermal dehydration of natural gypsum and pure calcium sulphate dihydrate (gypsum). Thermochim Acta 1996;282–283:483–92. doi:10.1016/0040-6031(95)02819-6.

[88]   Ogura H, Haguro M, Shibata Y, Otsubo Y. Reaction characteristics of CaSO4/CaSO4·1/2H2O reversible reaction for chemical heat pump. J Chem Eng Japan 2007;40:1252–6. doi:10.1252/jcej.07WE223.

[89]   Lee JH, Ogura H, Sato S. Reaction control of CaSO4 during hydration/dehydration repetition for chemical heat pump system. Appl Therm Eng 2014;63:192–9. doi:10.1016/j.applthermaleng.2013.10.043.

[90]   Richter M, Habermann EM, Siebecke E, Linder M. A systematic screening of salt hydrates as materials for a thermochemical heat transformer. Thermochim Acta 2018;659:136–50. doi:10.1016/j.tca.2017.06.011.

[91]   Sørensen OT. Quasi-isothermal methods in thermal analysis. Thermochim Acta 1981;50:163–75. doi:10.1016/0040-6031(81)85052-6.

[92]   Reisman A, Karlak J. Observations on the Differential Thermal Analysis of Copper Sulfate Pentahydrate. J Am Chem Soc 1958;80:6500–3. doi:10.1021/ja01557a009.

[93]   Mu J, Perlmutter DD. Thermal Decomposition of Inorganic Sulfates and Their Hydrates. Ind Eng Chem Process Des Dev 1981;20:640–6. doi:10.1021/i200015a010.

[94]   Savchenko E V., Gordeeva LG, Glaznev IS, Aristov YI, Malakhov V V. Impact of phase composition on water adsorption on inorganic hybrids "salt/silica." J Colloid Interface Sci 2006;301:685–91. doi:10.1016/j.jcis.2006.05.009.

[95]   Bhosale R, Dardor D, Kumar A, Al Momani F, Ghosh U. Thermochemical copper Oxide - Copper sulfate water splitting cycle for solar hydrogen production. Adv Mater - TechConnect Briefs 2016 2016;2:2–6.

[96]   N'Tsoukpoe KE, Schmidt T, Rammelberg HU, Watts BA, Ruck WKL. A systematic multi-step screening of numerous salt hydrates for low temperature thermochemical energy storage. Appl Energy 2014;124:1–16. doi:10.1016/j.apenergy.2014.02.053.

[97]   Lahmidi H, Mauran S, Goetz V. Definition, test and simulation of a thermochemical storage process adapted to solar thermal systems. Sol Energy 2006;80:883–93. doi:10.1016/j.solener.2005.01.014.

[98]   Michel B, Mazet N, Neveu P. Experimental investigation of an innovative thermochemical process operating with a hydrate salt and moist air for thermal storage of solar energy: Global performance. Appl Energy 2014. doi:10.1016/j.apenergy.2014.04.073.

[99]   Marias F, Neveu P, Tanguy G, Papillon P. Thermodynamic analysis and experimental study of solid/gas reactor operating in open mode. Energy 2014. doi:10.1016/j.energy.2014.01.101.

[100]   Michel B, Mazet N, Mauran S, Stitou D, Xu J. Thermochemical process for seasonal storage of solar energy: Characterization and modeling of a high density reactive bed. Energy 2012;47:553–63. doi:10.1016/j.energy.2012.09.029.

[101]   Guillaume R. Modélisation de transfert de vapeur d'eau à faible pression à travers un milieu poreux réactif 2007:4–10.

[102]   Mauran S, Lahmidi H, Goetz V. Solar heating and cooling by a thermochemical process. First experiments of a prototype storing 60 kW h by a solid/gas reaction. Sol Energy 2008;82:623–36. doi:10.1016/J.SOLENER.2008.01.002.

[103]   Fopah Lele A, Kuznik F, Opel O, Ruck WKL. Performance analysis of a thermochemical based heat storage as an addition to cogeneration systems 2015. doi:10.1016/j.enconman.2015.10.068.

[104]   Ding Q, Luo X, Lin X, Zhang H. Study of magnesium nitrate hexahydrate and magnesium chloride hexahydrate mixture as phase change material. Asia-Pacific Power Energy Eng Conf APPEEC 2012:2–5. doi:10.1109/APPEEC.2012.6306921.

[105]   Paulik F, Paulik J, Arnold M, Naumann R. Investigation on the thermal behaviour of $Mg(NO_3)_2 \cdot 6H_2O$ I. The decomposition behaviour. J Therm Anal 1988;34:627–35. doi:10.1007/BF02331764.

[106]   Drake G, Freiberg L, AuYeung N. Reactive Phase-Change Materials for Enhanced Thermal Energy Storage. Energy Technol 2018;6:351–6. doi:10.1002/ente.201700495.

[107]   Voigt W, Zeng D. Solid–liquid equilibria in mixtures of molten salt hydrates for the design of heat storage materials. Pure Appl Chem 2002;74:1909–20.

doi:10.1351/pac200274101909.

[108]   Kumar N, Banerjee D, Chavez R. Exploring additives for improving the reliability of zinc nitrate hexahydrate as a phase change material (PCM). J Energy Storage 2018;20:153–62. doi:10.1016/j.est.2018.09.005.

[109]   Vranes M, Gadzuric S, Dozic S, Zsigrai I. Stability and thermodynamics of thermochromic cobalt(II) chloride complexes in low-melting phase change materials. J Chem Eng Data 2010;55:2000–3. doi:10.1021/je9009267.

[110]   Liu D, Zhu J. Investigation of Anti-Deliquesce Properties of Ca(NO3)24H2O Crystal Particles in Double-Layer |Coated Materials with Epoxy Resins and Portland Cement. Asian J Chem 2015;27:3097–100. doi:10.3153/jfscom.2010021.

[111]   Guo L, Yu X, Gao D, Guo Y, Ma C, Deng T. Synthesis and thermal energy storage properties of a calcium-based room temperature phase change material for energy storage. J Therm Anal Calorim 2019;135:3215–21. doi:10.1007/s10973-018-7610-3.

[112]   Tang X, Jia S, Zhao H, Zhang M, Cheng J, Yan H, et al. Experimental Investigations of Composite Adsorbent 13X/CaCl2 on an Adsorption Cooling System. Appl Sci 2017;7:620. doi:10.3390/app7060620.

[113]   Aydin D, Casey SP, Chen X, Riffat S. Novel "open-sorption pipe" reactor for solar thermal energy storage. Energy Convers Manag 2016;121:321–34. doi:10.1016/j.enconman.2016.05.045.

[114]   Richter M, Bouché M, Linder M. Heat transformation based on CaCl2/H2O - Part A: Closed operation principle. Appl Therm Eng 2016;102:615–21. doi:10.1016/j.applthermaleng.2016.03.076.

[115]   D'Ans P, Skrylnyk O, Hohenauer W, Courbon E, Malet L, Degrez M, et al. Humidity dependence of transport properties of composite materials used for thermochemical

heat storage and thermal transformer appliances. J Energy Storage 2018;18:160–70. doi:10.1016/j.est.2018.04.027.

[116]   Courbon E, D'Ans P, Permyakova A, Skrylnyk O, Steunou N, Degrez M, et al. Further improvement of the synthesis of silica gel and CaCl2 composites: Enhancement of energy storage density and stability over cycles for solar heat storage coupled with space heating applications. Sol Energy 2017;157:532–41. doi:10.1016/j.solener.2017.08.034.

[117]   Gough R V., Chevrier VF, Tolbert MA. Formation of liquid water at low temperatures via the deliquescence of calcium chloride: Implications for Antarctica and Mars. Planet Space Sci 2016;131:79–87. doi:10.1016/j.pss.2016.07.006.

[118]   Jiang L, Gao J, Wang L, Wang R, Lu Y, Roskilly AP. Investigation on performance of multi-salt composite sorbents for multilevel sorption thermal energy storage. Appl Energy 2017;190:1029–38. doi:10.1016/j.apenergy.2017.01.019.

[119]   Karunadasa KSP, Manoratne CH, Pitawala HMTGA, Rajapakse RMG. Relative stability of hydrated/anhydrous products of calcium chloride during complete dehydration as examined by high-temperature X-ray powder diffraction. J Phys Chem Solids 2018;120:167–72. doi:10.1016/j.jpcs.2018.04.034.

[120]   Kim ST, Ryu J, Kato Y. Optimization of magnesium hydroxide composite material mixed with expanded graphite and calcium chloride for chemical heat pumps. Appl Therm Eng 2013;50:485–90. doi:10.1016/j.applthermaleng.2012.07.005.

[121]   Korhammer K, Apel C, Osterland T, Ruck WKL. Reaction of Calcium Chloride and Magnesium Chloride and their Mixed Salts with Ethanol for Thermal Energy Storage. Energy Procedia 2016;91:161–71. doi:10.1016/j.egypro.2016.06.194.

[122]   Yu N, Wang RZ, Wang LW. Sorption thermal storage for solar energy. Prog Energy Combust Sci 2013;39:489–514. doi:10.1016/j.pecs.2013.05.004.

[123]   Skrylnyk O, Courbon E, Heymans N, Frère M, Bougard J, Descy G. Energy Performances of Open Sorption Reactor with Ultra-Low Grade Heat Upgrading for Thermochemical Energy Storage Applications. Energy Procedia, vol. 135, 2017, p. 304–16. doi:10.1016/j.egypro.2017.09.522.

[124]   Tian B, Jin ZQ, Wang LW, Wang RZ. Permeability and thermal conductivity of compact chemical and physical adsorbents with expanded natural graphite as host matrix. Int J Heat Mass Transf 2012;55:4453–9. doi:10.1016/j.ijheatmasstransfer.2012.04.016.

[125]   Kirsh Y, Yariv S, Shoval S. Kinetic analysis of thermal dehydration and hydrolysis of $MgCl_2\cdot6H_2O$ by DTA and TG. J Therm Anal 1987;32:393–408. doi:10.1007/BF01912692.

[126]   Gutierrez A, Ushak S, Linder M. High Carnallite-Bearing Material for Thermochemical Energy Storage: Thermophysical Characterization. ACS Sustain Chem Eng 2018;6:6135–45. doi:10.1021/acssuschemeng.7b04803.

[127]   Zondag H a, van Essen VM, Bleijendaal LPJ, Kikkert BWJ, Bakker M. Application of $MgCl_2\cdot6H_2O$ for thermochemical seasonal solar heat storage. 5th IRES Conf 2011:22–4.

[128]   Ferchaud CJ, Zondag HA, Rubino A, de Boer R. Seasonal sorption heat storage – Research on thermochemical materials and storage performance. Proc Heat Power Cycle 2012 2012:1–7.

[129]   Mohan G, Venkataraman M, Gomez-Vidal J, Coventry J. Assessment of a novel ternary eutectic chloride salt for next generation high-temperature sensible heat storage. Energy Convers Manag 2018;167:156–64. doi:10.1016/j.enconman.2018.04.100.

[130]   Lager D, Hohenauer W, Knoll C, Weinberger P, Werner A. Methodology to determine the apparent specific heat capacity of metal hydroxides for thermochemical energy storage. J Therm Anal Calorim 2018. doi:10.1007/s10973-017-6883-2.

[131]   Carey EM, Vu T, Choukroun M, Zhong F, Cohen B, Barmatz M, et al. Thermal Conductivity

and Specific Heat Measurements of Hydrated Salt Mixtures with Implications for Icy Satellites. 49th Lunar Planet Sci Conf 2018 2018;49:6–7.

[132] Kleiner F, Posern K, Osburg A. Thermal conductivity of selected salt hydrates for thermochemical solar heat storage applications measured by the light flash method. Appl Therm Eng 2017;113:1189–93. doi:10.1016/j.applthermaleng.2016.11.125.

[133] Fopah Lele A, Edem N 'tsoukpoe K, Osterland T, Ed Eric Kuznik F, Ruck WKLL, N'Tsoukpoe KE, et al. Thermal conductivity measurement of thermochemical storage materials. Appl Therm Eng 2015;89:916–26. doi:10.1016/j.applthermaleng.2015.06.077.

[134] Fallahi A, Guldentops G, Tao M, Granados-Focil S, Van Dessel S. Review on solid-solid phase change materials for thermal energy storage: Molecular structure and thermal properties. Appl Therm Eng 2017;127:1427–41. doi:10.1016/j.applthermaleng.2017.08.161.

[135] Raj CR, Suresh S, Bhavsar RR, Singh VK. Recent developments in thermo-physical property enhancement and applications of solid solid phase change materials: A review. J Therm Anal Calorim 2020. doi:10.1007/s10973-019-08703-w.

[136] Gao W, Lin W, Liu T, Xia C. An experimental study on the heat storage performances of polyalcohols npg, tam, pe, and ampd and their mixtures as solid-solid phase-change materials for solar energy applications. Int J Green Energy 2007;4:301–11. doi:10.1080/15435070701332112.

[137] Ruan D, Zhang T, Liang S, Hu Q. DSC investigation of phase change materials. Acta Energiae Solaris Sin 1994;15:19–24.

[138] Xiang D, Chi G, Ruan D, Huo L, Li D, Zhang T, et al. Solid state phase transition in binary systems of polyhydric alcohols. Acta Energiae Solaris Sin 1995;16:131–7.

[139] Zhang ZY, Yang ML. Heat-capacity and phase-transitions of 2-amino2-methyl1,3-

propanediol from 280K to the melting point. Thermochim Acta 1990;169:263–9.

[140] Zhang ZY, Yang ML, Li HP. Heat-capacity and phase-transitions of mixtures of neopentylglycol and pentaerythritol from 270K to their melting point. Thermochim Acta 1992;202:105–12.

[141] Wang X, Lu E, Lin W, Wang C. Micromechanism of heat storage in a binary system of two kinds of polyalcohols as a solid-solid phase change material. Energy Convers Manag 2000;41:135–44. doi:10.1016/S0196-8904(99)00096-5.

[142] Barrio M, Font J, Muntasell J, Navarro J, Tamarit JL. Applicability for heat storage of binary systems of neopentylglycol, pentaglycerine and pentaerythritol: A comparative analysis. Sol Energy Mater 1988. doi:10.1016/0165-1633(88)90051-2.

[143] R.W BJ. BD. W. SOLID STATE PHASE TRANSITIONS IN PENTAERYTHRITOL AND RELATED POLYHYDRIC ALCOHOLS. Sol Energy Mater 13 1986;13:133–52.

[144] Son C., Morehouse J. An Experimental Investigation of Solid-State Phase-Change Materials for Solar Thermal Storage. J Mech Des 1991;113:244–9. doi:10.1115/1.2898876.

[145] Font J, Muntasell J, Navarro J, Tamarit JL, Lloveras J. Calorimetric study of the mixtures PE/NPG and PG/NPG. Sol Emergy Mater 1987;15:199–310.

[146] Gao WF, Lin WX, Liu T, Li M. An experimental study on the application of polyalcohol solid-solid phase change materials in solar drying with cross-corrugated solar air collectors. IOP Conf Ser Earth Environ Sci 2017;93. doi:10.1088/1755-1315/93/1/012075.

[147] Wang X, Lu E, Lin W, Liu T, Shi Z, Tang R, et al. Heat storage performance of the binary systems neopentyl glycol/pentaerythritol and neopentyl glycol/trihydroxy methyl-aminomethane as solid-solid phase change materials. Energy Convers Manag 2000;41:129–34. doi:10.1016/S0196-8904(99)00097-7.

[148] Son C., Morehouse J. An Experimental Investigation of Solid-State Phase-Change Materials for Solar Thermal Storage. J Mech Des 1991;113:244–9. doi:10.1115/1.2898876.

[149] Benson DK, Chandra D. Solid-state phase change materials for thermal energy storage. US DOE Contract No DE'AC02'-83CH10093 1985.

[150] Jianjun ZJLXWKZ, Shumei. H. Phase diagram of Binary NPG-TAM n.d.:1–6.

[151] Sar A, Alkan C, Bicer A. Development , Characterization , and Latent Heat Thermal Energy Storage Properties of Neopentyl Glycol-Fatty Acid Esters as New Solid – Liquid PCMs 2013. doi:10.1021/ie403039n.

[152] K P V, Suresh S, Praveen B, Venugopal A, C Nair S. Pentaerythritol with alumina nano additives for thermal energy storage applications. J Energy Storage 2017;13:359–77. doi:10.1016/j.est.2017.08.002.

[153] Su JC, Liu PS. A novel solid-solid phase change heat storage material with polyurethane block copolymer structure. Energy Convers Manag 2006;47:3185–91. doi:10.1016/j.enconman.2006.02.022.

[154] Peng K, Chen C, Pan W, Liu W, Wang Z, Zhu L. Preparation and properties of β-cyclodextrin/4,4'-diphenylmethane diisocyanate/polyethylene glycol (β-CD/MDI/PEG) crosslinking copolymers as polymeric solid-solid phase change materials. Sol Energy Mater Sol Cells 2016;145:238–47. doi:10.1016/j.solmat.2015.10.031.

[155] Fink JK. Reactive Polymers Fundamentals and Applications: A Concise Guide to Industrial Polymers: Second Edition. 2013. doi:10.1016/C2012-0-02516-1.

[156] Dutta AS. Polyurethane Foam Chemistry. Recycl. Polyurethane Foam., 2018. doi:10.1016/b978-0-323-51133-9.00002-4.

[157] Chevali V, Kandare E. Rigid biofoam composites as eco-efficient construction materials. Biopolym. Biotech Admixtures Eco-Efficient Constr. Mater., 2016. doi:10.1016/B978-0-08-100214-8.00013-0.

[158] Li WD, Ding EY. Preparation and characterization of cross-linking PEG/MDI/PE copolymer as solid-solid phase change heat storage material. Sol Energy Mater Sol Cells 2007;91:764–8. doi:10.1016/j.solmat.2007.01.011.

[159] Liu Z, Fu X, Jiang L, Wu B, Wang J, Lei J. Solvent-free synthesis and properties of novel solid-solid phase change materials with biodegradable castor oil for thermal energy storage. Sol Energy Mater Sol Cells 2016;147:177–84. doi:10.1016/j.solmat.2015.12.009.

[160] Shieh YT, Chen HT, Liu KH, Twu YK. Thermal degradation of MDI-based segmented polyurethanes. J Polym Sci Part A Polym Chem 1999. doi:10.1002/(SICI)1099-0518(19991115)37:22<4126::AID-POLA11>3.0.CO;2-A.

[161] Shi Z, Xu H, Yang Q, Xiong C, Zhao M, Kobayashi K, et al. Carboxylated nanocellulose/poly(ethylene oxide) composite films as solid–solid phase-change materials for thermal energy storage. Carbohydr Polym 2019;225:115215. doi:10.1016/j.carbpol.2019.115215.

[162] Chen C, Liu W, Wang Z, Peng K, Pan W, Xie Q. Novel form stable phase change materials based on the composites of polyethylene glycol/polymeric solid-solid phase change material. Sol Energy Mater Sol Cells 2015;134:80–8. doi:10.1016/j.solmat.2014.11.039.

[163] Li Y, Wu M, Liu R, Huang Y. Cellulose-based solid-solid phase change materials synthesized in ionic liquid. Sol Energy Mater Sol Cells 2009;93:1321–8. doi:10.1016/j.solmat.2009.02.005.

[164] Barroso-Bujans F, Fernandez-Alonso F, Cerveny S, Parker SF, Alegría A, Colmenero J. Polymers under extreme two-dimensional confinement: Poly(ethylene oxide) in graphite

oxide. Soft Matter 2011;7:7173–6. doi:10.1039/c1sm05661a.

[165]   Weingrill HM, Resch-Fauster K, Lucyshyn T, Zauner C. High-density polyethylene as phase-change material: Long-term stability and aging. Polym Test 2019;76:433–42. doi:10.1016/j.polymertesting.2019.04.009.

[166]   Zauner C, Hengstberger F, Etzel M, Lager D, Hofmann R, Walter H. Durability of a fin-Tube latent heat storage using high density polyethylene as PCM. IOP Conf. Ser. Mater. Sci. Eng., 2017. doi:10.1088/1757-899X/251/1/012123.

[167]   Salyer IO, Davison JE. Thermal-energy storage in crosslinked pellets of high-density polythylene for home heating and cooling via off-peak electric power utilization. J Appl Polym Sci 1983. doi:10.1002/app.1983.070280919.

[168]   Yang C, Navarro ME, Zhao B, Leng G, Xu G, Wang L, et al. Thermal conductivity enhancement of recycled high density polyethylene as a storage media for latent heat thermal energy storage. Sol Energy Mater Sol Cells 2016. doi:10.1016/j.solmat.2016.02.022.

[169]   Weingrill HM, Resch-Fauster K, Zauner C. Applicability of Polymeric Materials as Phase Change Materials. Macromol Mater Eng 2018;303:1–17. doi:10.1002/mame.201800355.

[170]   Zhao L, Guo Z, Cao Z, Zhang T, Fang Z, Peng M. Thermal and thermo-oxidative degradation of high density polyethylene/fullerene composites. Polym Degrad Stab 2013;98:1953–62. doi:10.1016/j.polymdegradstab.2013.07.020.

[171]   Zanetti M, Bracco P, Costa L. Thermal degradation behaviour of PE/clay nanocomposites. Polym Degrad Stab 2004;85:657–65. doi:10.1016/j.polymdegradstab.2004.03.005.

[172]   Chen Y, Li Y. Determination of water vapor transmission rate (WVTR) of HDPE bottles for pharmaceutical products. Int J Pharm 2008. doi:10.1016/j.ijpharm.2008.02.031.

[173]   KONUKLU Y, ERZİN F, AKAR HB, TURAN AM. Cellulose-based myristic acid composites for thermal energy storage applications. Sol Energy Mater Sol Cells 2019;193:85–91. doi:10.1016/j.solmat.2019.01.006.

[174]   Feczkó T, Kardos AF, Trif L, Gyenis J. Thermal energy storage by microcomposite of a phase change material and ethyl cellulose. WIT Trans Built Environ 2014;142:279–90. doi:10.2495/ARC140251.

[175]   Asghar A, Abdul Y, Hashaikeh R. Cellulose/PEO Blends with Enhanced Water Absorption and Retention Functionality. J Appl Polym Sci 2012;125:2121–7. doi:10.1002/app.

[176]   Kuznik F, David D, Johannes K, Roux JJ. A review on phase change materials integrated in building walls. Renew Sustain Energy Rev 2011;15:379–91. doi:10.1016/j.rser.2010.08.019.

[177]   Su W, Darkwa J, Kokogiannakis G. Review of solid-liquid phase change materials and their encapsulation technologies. Renew Sustain Energy Rev 2015;48:373–91. doi:10.1016/j.rser.2015.04.044.

[178]   Mehling H, Cabeza LF. Heat and cold storage with PCM. 2008. doi:10.1007/978-3-540-68557-9.

[179]   del Barrio EP, Godin A, Duquesne M, Daranlot J, Jolly J, Alshaer W, et al. Characterization of different sugar alcohols as phase change materials for thermal energy storage applications. Sol Energy Mater Sol Cells 2017;159:560–9. doi:10.1016/j.solmat.2016.10.009.

[180]   Solé A, Neumann H, Niedermaier S, Martorell I, Schossig P, Cabeza LF. Stability of sugar alcohols as PCM for thermal energy storage. Sol Energy Mater Sol Cells 2014;126:125–34. doi:10.1016/j.solmat.2014.03.020.

[181]   Barreneche C, Gil A, Sheth F, Inés Fernández A, Cabeza LF. Effect of d-mannitol

polymorphism in its thermal energy storage capacity when it is used as PCM. Sol Energy 2013;94:344–51. doi:10.1016/j.solener.2013.05.023.

[182] Kumaresan G, Velraj R, Iniyan S. Thermal analysis of D-mannitol for use as phase change material for latent heat storage. J Appl Sci 2011. doi:10.3923/jas.2011.3044.3048.

[183] Prajapati DG, Kandasubramanian B. A review on Polymeric-Based Phase Change Material for Thermo-Regulating Fabric Application. Polym Rev 2019;0:1–31. doi:10.1080/15583724.2019.1677709.

[184] Yang Y, Pang Y, Liu Y, Guo H. Preparation and thermal properties of polyethylene glycol/expanded graphite as novel form-stable phase change material for indoor energy saving. Mater Lett 2018;216:220–3. doi:10.1016/j.matlet.2018.01.025.

[185] Sarı A. Thermal energy storage characteristics of bentonite-based composite PCMs with enhanced thermal conductivity as novel thermal storage building materials 2016. doi:10.1016/j.enconman.2016.02.078.

[186] Wojda M, Wójcik TM. Novel solid - Solid phase change material based on polyethylene glycol and cellulose used for temperature stabilisation. MATEC Web Conf 2014;18:0–3. doi:10.1051/matecconf/20141803009.

[187] Joshi R, Kandpal ND. Viscometric properties of aqueous solutions of Poly (ethylene) glycols at 15°C. Der Pharm Lett 2015;7:126–33.

[188] Zhao H, Xiong S, Li M, Zhang Q, Liu G. Comparison of gelation time and polyalcohol effect on hydrogels from domestic and wild silk fibroins. Adv Mater Sci Eng 2012. doi:10.1155/2012/819464.

[189] Royer A, Barriere T, Gelin JC. The degradation of poly(ethylene glycol) in an Inconel 718 feedstock in the metal injection moulding process. Powder Technol 2015. doi:10.1016/j.powtec.2015.07.032.

[190] Han S, Kim C, Kwon D. Thermal/oxidative degradation and stabilization of polyethylene glycol. Polymer (Guildf) 1997;38:317–23. doi:10.1016/S0032-3861(97)88175-X.

[191] Quanying Y, Lili J. Research on the Thermal Storage Performance of Solid-Solid Phase-Change Material Used in the Wall 2012;07:2801–4. doi:10.4028/www.scientific.net/AMR.347-353.2801.

[192] Wu CB, Wu G, Yang X, Liu YJ, Liang T, Fu WF, et al. Preparation of microencapsulated medium temperature phase change material of Tris(hydroxymethyl)methyl aminomethane@SiO2with excellent cycling performance. Appl Energy 2015;154:361–8. doi:10.1016/j.apenergy.2015.05.029.

[193] Wu R, Yao Y. Tris(hydroxymethyl)aminomethane, a pure organic thermal stabilizer for poly(vinyl chloride). ICMREE 2013 - Proc. 2013 Int. Conf. Mater. Renew. Energy Environ., 2013. doi:10.1109/ICMREE.2013.6893748.

[194] Praveen B, Suresh S. Experimental study on heat transfer performance of neopentyl glycol/CuO composite solid-solid PCM in TES based heat sink. Eng Sci Technol an Int J 2018;21:1086–94. doi:10.1016/j.jestch.2018.07.010.

[195] Praveen B, Suresh S. Engineering Science and Technology , an International Journal Experimental study on heat transfer performance of neopentyl glycol / CuO composite solid-solid PCM in TES based heat sink. Eng Sci Technol an Int J 2018;21:1086–94. doi:10.1016/j.jestch.2018.07.010.

[196] Center for the Polyurethanes Industry. Working with MDI and Polymeric MDI 2012.

[197] Li X, Lu Y, Wang H, Pöselt E, Eling B, Men Y. Crystallization of hard segments in MDI/BD-based polyurethanes deformed at elevated temperature and their dependence on the MDI/BD content. Eur Polym J 2017. doi:10.1016/j.eurpolymj.2017.10.014.

[198] Lu C, Chiang SW, Du H, Li J, Gan L, Zhang X, et al. Thermal conductivity of electrospinning

chain-aligned polyethylene oxide (PEO). Polymer (Guildf) 2017. doi:10.1016/j.polymer.2017.02.024.

[199] Shen D, Xiao R, Gu S, Zhang H. The Overview of Thermal Decomposition of Cellulose in Lignocellulosic Biomass. Cellul - Biomass Convers 2013. doi:10.5772/51883.

[200] Yang C, Navarro ME, Zhao B, Leng G, Xu G, Wang L, et al. Thermal conductivity enhancement of recycled high density polyethylene as a storage media for latent heat thermal energy storage 2016;152:103–10. doi:10.1016/j.solmat.2016.02.022.

[201] Sewda K, Malti SN. Crystallization and Melting Behavior of HDPE in HDPE/Teak Wood Flour Composites and Their Correlation with Mechanical Properties. J Appl Polym Sci 2010;116:2658–67. doi:10.1002/app.

[202] . KAT. EXPERIMENTAL INVESTIGATION OF POSSIBLE USE OF HDPE AS THERMAL STORAGE MATERIAL IN THERMAL STORAGE TYPE SOLAR COOKERS. Int J Res Eng Technol 2015. doi:10.15623/ijret.2015.0412019.

[203] Gu J, Xu H, Wu C. Thermal and crystallization properties of HDPE and HDPE/PP blends modified with DCP. Adv Polym Technol 2014;33:1–5. doi:10.1002/adv.21384.

[204] Tavman I, Aydogdu Y, Kök M, Turgut A, Ezan A. Measurement of heat capacity and thermal conductivity of HDPE/expanded graphite nanocomposites by differential scanning calorimetry. Arch Mater Sci Eng 2011;50:56–60.

[205] Gunasekara SN, Pan R, Chiu JN, Martin V. Polyols as phase change materials for surplus thermal energy storage. Appl Energy 2016;162:1439–52. doi:10.1016/j.apenergy.2015.03.064.

[206] Sundararajan S, Samui AB, Kulkarni PS. Versatility of polyethylene glycol (PEG) in designing solid-solid phase change materials (PCMs) for thermal management and their application to innovative technologies. J Mater Chem A 2017;5:18379–96.

doi:10.1039/c7ta04968d.

[207] Saha D, Bhattacharya S. Hydrocolloids as thickening and gelling agents in food: A critical review. J Food Sci Technol 2010;47:587–97. doi:10.1007/s13197-010-0162-6.

[208] Imeson A. Food Stabilisers, Thickeners and Gelling Agents. 2009. doi:10.1002/9781444314724.

[209] Wüstenberg T. General Overview of Food Hydrocolloids. Cellul. Cellul. Deriv. Food Ind., 2014, p. 1–68. doi:10.1002/9783527682935.ch01.

[210] Das N, Triparthi N, Basu S, Bose C, Maitra S, Khurana S. Progress in the development of gelling agents for improved culturability of microorganisms. Front Microbiol 2015. doi:10.3389/fmicb.2015.00698.

[211] Srivastava A, Mishra V, Singh P, Srivastava A, Kumar R. Comparative study of thermal degradation behavior of graft copolymers of polysaccharides and vinyl monomers. J Therm Anal Calorim 2012;107:211–23. doi:10.1007/s10973-011-1921-y.

[212] Kulkarni VS, Shaw C. Use of Polymers and Thickeners in Semisolid and Liquid Formulations. Essent. Chem. Formul. Semisolid Liq. Dosages, 2016. doi:10.1016/b978-0-12-801024-2.00005-4.

[213] Omidian H, Park K. Hydrogels. Fundam. Appl. Control. Release Drug Deliv., 2012. doi:10.1007/978-1-4614-0881-9_4.

[214] Otter D. PROTEIN | Determination and Characterization. Encycl. Food Sci. Nutr., 2003. doi:10.1016/b0-12-227055-x/00980-9.

[215] Basumatary K, Daimary P, Das SK, Thapa M, Singh M, Mukherjee A, et al. Lagerstroemia speciosa fruit-mediated synthesis of silver nanoparticles and its application as filler in agar based nanocomposite films for antimicrobial food packaging. Food Packag Shelf Life 2018;17:99–106. doi:10.1016/j.fpsl.2018.06.003.

[216] Linea IEN. PREPARACIÓN Y CARACTERIZACION DE MEMBRANAS DE CELULOSA Desarrollo y aplicación de nuevos materiales-DANUM . Universidad Pedagogica y Tecnologica de Colombia-UPTC , leidyypaola@hotmail.com Instituto de Investigacion en Materiales-IIM . Universidad Nacional 2015;2015.

[217] Elnashar MMM, Hassan ME. Novel epoxy activated hydrogels for solving lactose intolerance. Biomed Res Int 2014. doi:10.1155/2014/817985.

[218] Yang MH. Two-stages thermal degradation of polyacrylamide. Polym Test 1998. doi:10.1016/S0142-9418(97)00036-6.

[219] Topuz F, Henke A, Richtering W, Groll J. Magnesium ions and alginate do form hydrogels: A rheological study. Soft Matter 2012. doi:10.1039/c2sm07465f.

9

WORKING PAIRS

1. Thesis
timeline

2. Scientific
contributions

3. Introduction

4. TCS Outlook

5. Targets
and structure
of the thesis

6. Hybrid TES
system:

3 in 1 concept

The 3 in 1 working pairs selected in the previous section are experimentally validated in this section. The working pairs are studied in two main blocks; SSPCM and SLPCM-gel. The energy stored and the chemical stability of SSPCMs are studied, while the compatibility/synergies between TCM/PCM-gel working pairs (SLPCMs) are investigated. The use of gels proofs to have potential for thermochemical synthesis as it reduces the leakage and enhances the cycling stability even of pure TCMs. The final working pairs for proof of concept and scale-up validation are selected as the main outputs of this chapter; $MgSO_4$/E/PA and $MgSO_4$/HDPE for charging integrated system, $MgSO_4$/MDI, $MgSO_4$/CLU, $MgCl_2$/PEO and $MgCl_2$/MDI for cascade system and $MgCl_2$/HDPE for charging integrated.

7. Bench study specifications

8. Material screening and selection

9. Working pairs

10. Proof of concept and scale-up

11. Potential applications and prospective

12. Conclusions and achievements

9. WORKING PAIRS

In the previous section we narrowed down the 3 in 1 system candidates to five TCMs (magnesium sulphate, potassium carbonate, magnesium chloride, calcium chloride and strontium bromide); four SSPCMs (MDI, PEO and HDPE); four SLPCMs (PEG 600, PEG 1,000, PEG 35,000 and Erythritol); one matrix (CLU); and two gels (Guar gum and Polyacrylamide), as shown in Figure 67.
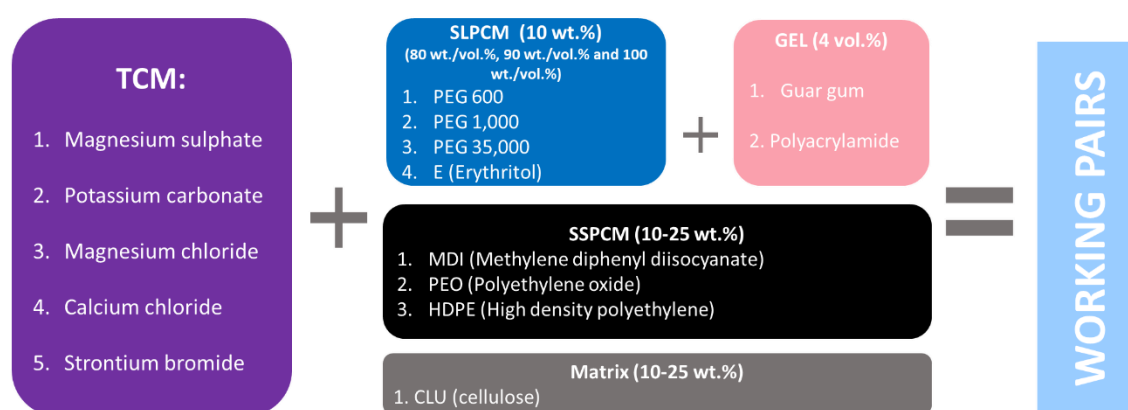
Figure 67. Selected materials, percentages and combinations for the 3 in 1 working pairs

The working pair validation process was conducted in sequential steps (1) Theoretical combinations, (2) Potential SSPCM working pairs, (3) Potential SLPCM working pairs and as described below and seen in Figure 69. The eventual aim is to provide suitable working pair(s) to further study scale-up manufacturing (20 g) through hydration/dehydration cycles (step (4) Proof of concept/Scale-up study):

(1)   Theoretical combinations: The selected TCMs and PCMs were paired accordingly to come up with a set of working pairs for each 3 in 1 system presented in this thesis (cascade, charging integrated and discharging integrated). Note that SLPCM requires the gel addition for better stability as established in the previous chapter of the thesis, see Figure 68. The criteria for the working pairs formulation was to combine a TCM with three SSPCMs (MDI, HDPE, PEO),

cellulose as a matrix that is included in the SSPCM study and two SLPCM to come up with at least one working pair for each system if possible two. The outcome will be limited by the possible temperature-wise combination. The compatibility study was then divided into SSPCM step (2) and SLPCM step (3) as explained in the following points.
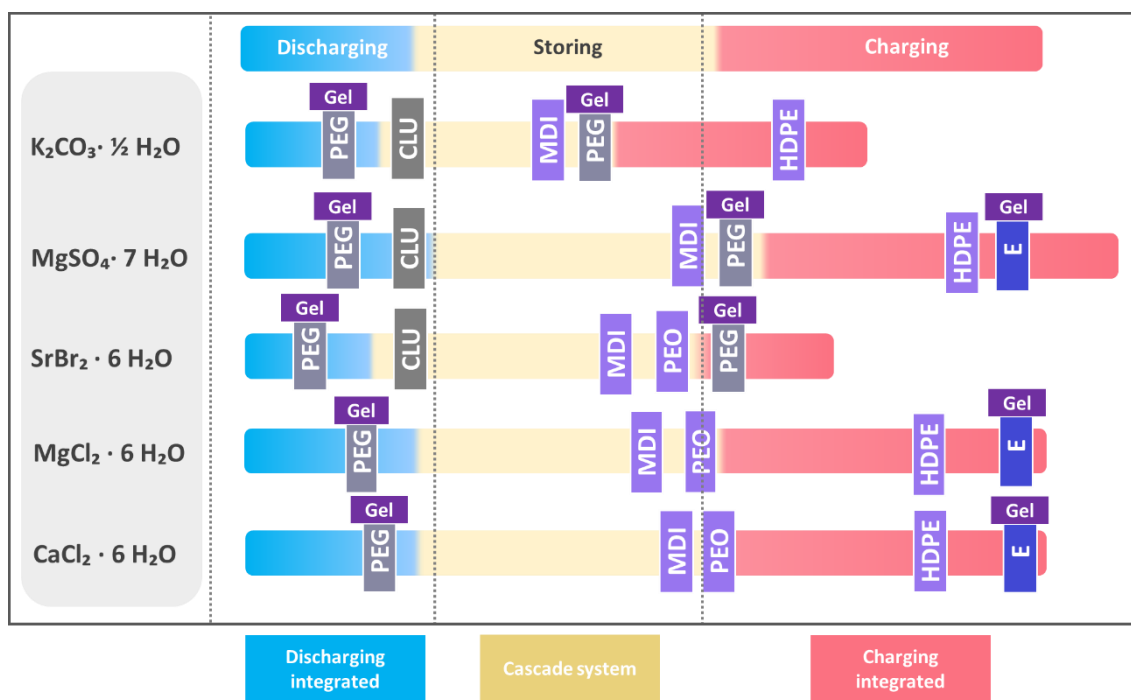
Figure 68. Potential working pairs combining TCMs with SSPCMs and gel-SLPCMs classified into the three 3 in 1 system.

(2) Potential SSPCM working pairs: The lowest amount of SSPCM in the co-working matrix was tested for each of the proposed working pairs (90 wt.% TCM/10 wt.% PCM). This is to assess the working pair composition limitations and that they have a good PCM/TCM synergy (avoid side reactions, degradation, etc). Thus, tablets of 1 g were prepared to contain 90 wt.% TCM and 10 wt.% PCM and tested in a humidity chamber over 5 cycles. Most of the working pairs failed at this stage as they presented chemical incompatibilities and/or structural problems, further explained in this section The working pairs that did not show chemical incompatibilities, were reformulated with higher PCM content to investigate

whether they could withstand the structure over a larger number of thermal cycles in the proof of concept/scale-up level.

(3) Potential SLPCM working pairs: Similarly, as for SSPCMs, SLPCM validation was first conducted through a compatibility study between PCM and TCM. Once the compatibility between the TCM and the SLPCM has been proved, the best performing working pair(s), regarding physical integrity (cyclability) criteria, is studied by adding the gel parameter interaction to the SLPCM/TCM working pair. Given the gel synthesis process, 1 g tablet is not enough to produce a representative tablet for the gel-TCM/PCM interaction study. Therefore, 10 g tablets are fabricated and cycled (5 cycles) to reveal the most promising gel-SLPCM/TCM candidates.

(4) Proof of concept/Scale-up study: At the end of the process, a set of SSPCM/TCM and SLPCM/TCM/gel are proposed as potential candidates. (4.1) One working pair is selected for a full feasibility study (up to 15 cycles) at lab-scale (1 g tablet) and as a proof of concept of the 3 in 1 system. (4.2) A comprehensive study at scale-up level (20 g tablets) is then presented for all the potential candidates.

For clarification, the overall working pairs identification flow chart is shown in Figure 69. The characterisation techniques used in each of the stages are also presented, the eventual goal is to narrow down the possible working pairs and identify the best candidates to prove the feasibility of the 3 in 1 system. Note that stage 4 will be shown in Chapter 10 of this thesis.
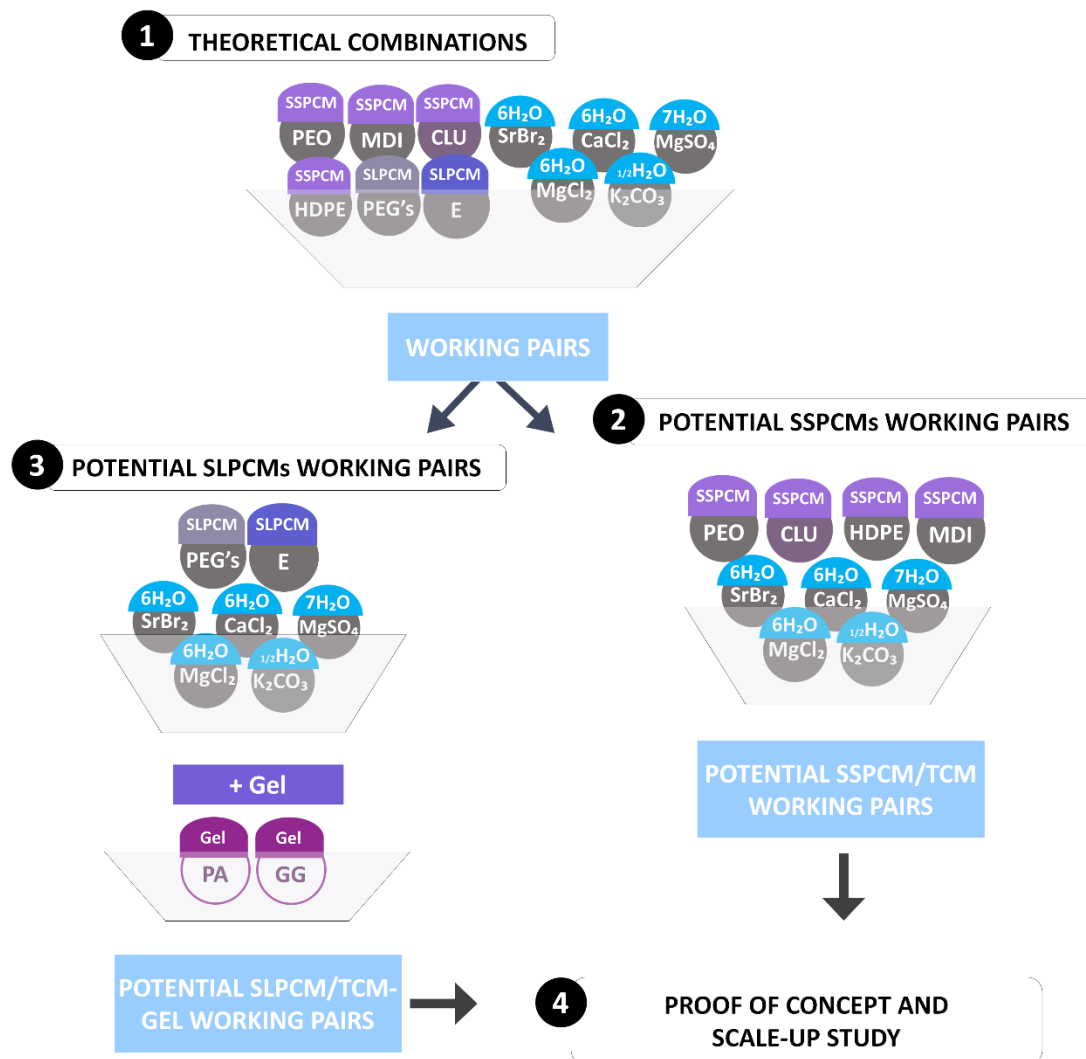
Figure 69. Working pair identification flow chart.

9.1 POTENTIAL SSPCMS WORKING PAIRS

(1) Methodology

Different ratios of TCM and PCM, both in powder form, were mixed and ground to a homogeneous mixture. An amount of 1 g ± 0.05 g was then pressed into a tablet shape with 13 mm diameter obtaining a thickness around 10 mm using a Lloyd LS100 Plus Materials Testing Machine supplied by Lloyd Instruments company (UK). The operating pressure and

holding time for the machine was set to 90 MPa and 1.5 min, respectively. Note that since magnesium chloride and calcium chloride hydrated salts easily take water from the ambient, to ease the manufacturing process, this material was prepared from the anhydrous form in combination with the PCM. The tablet was then fully hydrated below deliquescence conditions, and the hydrated tablet was then cycled as for the rest of TCM working pairs. The rest of the materials were prepared from the hydrated forms (magnesium sulphate hexahydrate, strontium bromide hexahydrate and potassium carbonate sesquihydrate).

Preliminary work conducted varying the TCM content from 60 wt. % to 95 wt. % and subjected to several charging/discharging cycles, obtained suitable working pairs with TCM loadings varying from 80 wt.% to 90 wt.%, which maximised the TCM content while maintained the composite shape. Hence, the first attempt was to prepare 90/10 tablets (90 wt.% TCM/ 10 wt.% PCM). For the samples that did not withstand one cycle with 90/10 ratio, the PCM loading was lowered down to find the maximum TCM content possible (ratios from 90/10 to 85/25... 80/20). In extreme cases, where the composite exhibited leakage or breakage (e.g Magnesium chloride) the ratio was even extended to 75/25, which was eventually set as the maximum TCM load. For clarification, breakage is considered when the tablet collapses showing cracks in the structure, while leakage is considered when there is a visible component leaking from the composite structure

The tablets were then cycled, for 5 times, in the humidity chamber following the specific conditions required for each TCM, as described in Chapter 7. The samples that withstand 5 cycles were characterised in the STA, to measure the energy stored by the composite, and in the X-Ray diffraction to ensure chemical stability (TCM crystalline phases are the same as for the pure TCM and no new species are formed), see conditions Chapter 7. Samples with minor leakage issues were considered for further study as this could be

potentially solved reformulating the composite. On the contrary, samples presenting major leakage issues and breakage were discarded for the experimental validation.

As verified in the material screening section, the following reactions for each of the TCM's are studied, (note that magnesium sulphate reaction cannot hydrate to heptahydrate after the first dehydration as explained in the screening section):

$MgCl_2 \cdot 6H_2O \leftrightarrow MgCl_2 \cdot 2H_2O + 4\ H_2O$ T; ~40 °C-140 °C   Reaction 1

$SrBr_2 \cdot 6H_2O \leftrightarrow SrBr_2 \cdot 1H_2O + 5\ H_2O$ T; ~60 °C- 90 °C   Reaction 2

$MgSO_4 \cdot 6H_2O \leftrightarrow MgSO_4 \cdot 1H_2O + 5\ H_2O$ T; ~55 °C-150 °C   Reaction 3
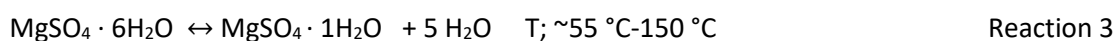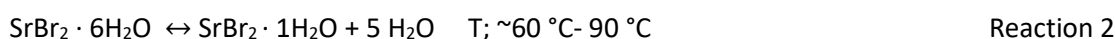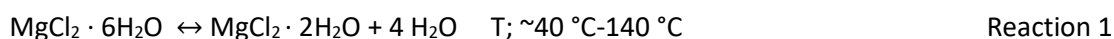
(2) Experimental validation

Among the SSPCM's, 90/10 formulation succeed for strontium bromide and magnesium sulphate working pairs. They showed minor leakage (or none) and do not visibly break during cycling. MDI/$MgSO_4$ shows some leakage that can be reduced by increasing the amount of PCM in the composite. This strategy is also applied in other working pairs, which present similar problems (this will be studied Chapter 10). Potassium carbonate reacts with all PCM and shows major chemical incompatibilities as seen in Table 27. When it comes to calcium chloride and magnesium chloride, they both require higher content of SSPCMs, given that 90-10 does not withstand even one cycle and they break and leak dramatically whereas 80/20 samples show decent results after 5 cycles, as shown in Table 27. Besides, given that $MgCl_2$ and $CaCl_2$ show very similar behaviour, in terms of potential working pairs (see Table 26), and similar thermochemical energy storage attributes, just $MgCl_2$ is studied in the experimental validation (XRD and STA).
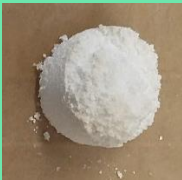
Interestingly, cellulose failed when combined with highly hygroscopic TCMs (tendency to undergo deliquescence) such as magnesium chloride and calcium chloride. For that reason, these working pair were not even considered. The reason for that is the intrinsic water

absorption capacity of cellulose that affects the sorption rate of the TCM driving the system to deliquescence conditions. For strontium bromide and magnesium sulphate, cellulose can act as a matrix without interfering the sorption processes; while this matrix does not provide additional energy storage capacity, it does allow stable, cost-extensive and easily to pelletize composites using it in 10% in weight in percentages.

Table 26. Outputs from the 5-cycle test of SSPCM and SLPCM/TCM working pairs. The red squares show the failure of the test (major structural problems), while the ones in green showed decent physical integrity (minor or no changes).

	Solid-Solid PCM			
TCM	PEO	HDPE	MDI	Cellulose
Potassium carbonate	75/25	75/25	75/25	75/25
Magnesium sulphate	-	90/10	90/10	90/10
Strontium bromide	90/10	-	90/10	90/10
Calcium chloride	80/20	80/20	80/20	-
Magnesium chloride	80/20	80/20	80/20	-

Table 27. Pictures after cycling the SSPCM working pairs. The squares in red failed during cycling (major structural problems), while the ones in green showed decent physical integrity (minor or no changes).

	Solid-Solid PCM			
TCM	**PEO**	**HDPE**	**MDI**	**Cellulose**
Potassium carbonate				
Magnesium sulphate	-			
Strontium bromide		-		
Calcium chloride				-
Magnesium chloride				-

For the working pairs that withstand 90/10 formulation, they are further studied in the following percentages; 90/10 and 80/20. However, the working pairs that can just work at 80/20 percentage, they are formulated as follows; 80/20 and 75/25. Thus, the experimental validation will be conducted on the following working pairs; $MgCl_2$/MDI- $MgCl_2$/PEO- $MgCl_2$/HDPE ranging from 80/20 to 75/25, $SrBr_2$/MDI- $SrBr_2$/MDI- $SrBr_2$/PEO- $SrBr_2$/CLU and $MgSO_4$/HDPE- $MgSO_4$/MDI- $MgSO_4$/CLU both TCM working pairs ranging from 90/10 to 80/20. The study is described in the following section divided into; (2.1) Sorption process/energy stored (STA) and (2.2) Chemical stability (XRD).

(2.1)   Sorption process/ energy stored (STA)

To study the sorption process of the different working pairs after the 5-cycles test, hydration conversion time, hydration conversion, energy stored, and dehydration conversion were calculated from the STA data (procedure described in equations shown in Chapter 7). This data will draw some conclusions on how the working pairs work in terms of sorption/desorption reaction.

As expected, the highest enthalpies of reaction are reported by the ones that have the highest PCM content. Conversion rates range from 70% to 90% in most of the cases, but they do not always concur the highest conversion with highest TCM percentage. Although the data shown is an average of two measurements, the accuracy of results is affected by the measurement error itself as well as the heterogeneity of the samples. Thus, in some cases, energy density differences, which are less than 10% between the same working pairs/different formulation percentages, could be not significantly different. Energy stored vs hydration conversion is shown in Figure 70, while hydration conversion time and hydration conversion is shown in Figure 71. Looking at the results for each TCM;

(1) Magnesium sulphate: the highest energy stored is reported by MDI 90/10 and HDPE 90/10, while conversions achieved by HDPE 80/20 and CLU 80/20 are close to the pure TCM. The hydration step (discharging) takes place at around 25–30 °C at a relative humidity from 60% to 80%, depending on pressure [1,2]. Since the hydration (~25–30 °C) and the first dehydration stage (starting at ~25 °C) overlap, the conversion from $MgSO_4 \cdot 7H_2O$ to $MgSO_4 \cdot 6H_2O$ occurs gradually when $MgSO_4 \cdot 7H_2O$ is formed. All working pairs show full hydration to the hexahydrate state, the experimental hydrated state achieved by magnesium sulphate after rehydration. While cellulose and MDI require 2.5 hours to fully hydrate, HDPE composites need almost 3 hours to complete hydration ~96% (similar as for the

pure TCM). Higher content of PCM shows to facilitate the hydration as higher conversion rates are achieved at lower times.

(2) Strontium bromide: among the working pairs, cellulose 80/20 and 90/10 are the ones that store the highest energy. PEO 80/20 is the PCM pair that leads to lower energy, while 90/10 appears to be an optimal formulation with a similar conversion rate as pure TCM. Strontium bromide working pairs show the shortest hydration times given the high reaction rate of strontium bromide [3]. Under the same conditions, pure strontium bromide hydrate in 80 min while 90/10 MDI, PEO and CLU hydrate faster (~ 60 min) (see Figure 44). Therefore, it is proved that the PCM matrix can help the sorption process allowing faster reaction times.

(3) Magnesium chloride: this TCM has an intrinsic high energy capacity, although this is reduced by the addition of PCM, some working pairs still present large energy density compared to the rest of working pairs studied, such as MDI 80/20 and PEO 80/20. As for the other TCMs, the higher the content of TCM the higher the energy stored by the $MgCl_2$ 3 in 1 composite. From the SSPCMs, PEO based are the ones that show higher conversion while MDI the lowest ones. In general, higher amounts of PCM lead to higher conversion rates, thus, better desorption values, although lower energy is stored given the higher amount of PCM in the composite. Regarding the hydration, 80/20 show lower hydration times than the pure TCM for MDI and HDPE. All the working pairs are hydrated after 2.5 h, being 80/20 HDPE the fastest (88 min), whereas pure magnesium chloride hydrates in 124 min.
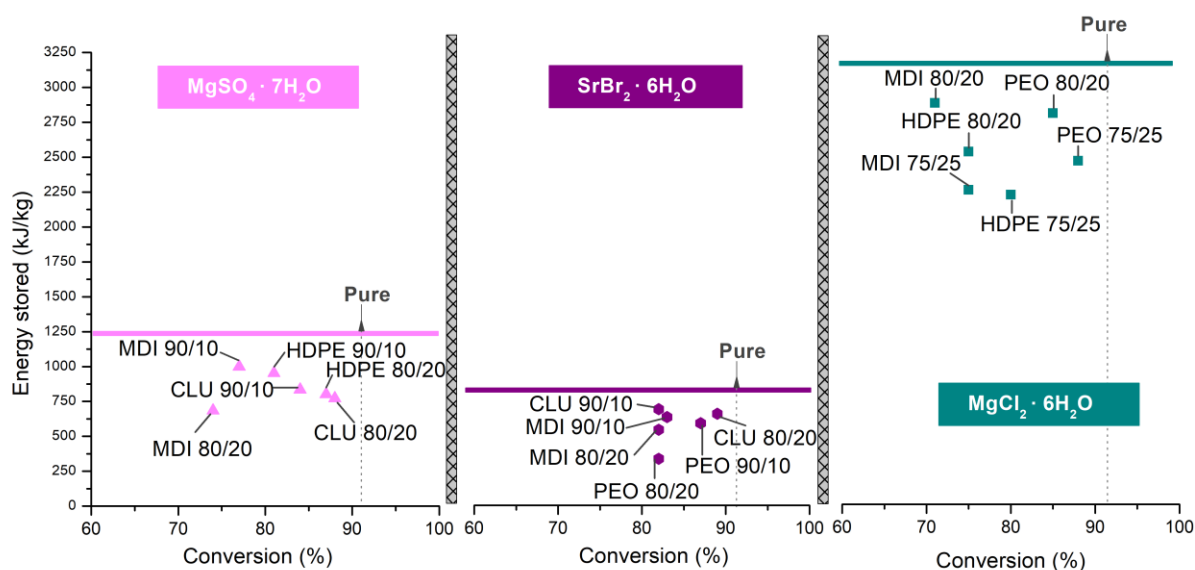
Figure 70. Dehydration conversion and enthalpy of fusion for the formulation containing 80 wt.%. TCM/20 wt.% PCM (80/20), 90 wt.% TCM/ 10 wt.% PCM (90/10) and 75 wt.% TCM/25 wt.% PCM (75/25) at the different test conditions; for magnesium sulphate 25-150 °C at 1 °C /min-60 min hold, for strontium bromide 25-90 °C at 1 °C /min-60 min hold.; and for magnesium chloride 25-140 °C at 1 °C /min-60 min hold in the STA. Pure PCM data is illustrated with a flat line for the energy stored and dotted line for the conversion.
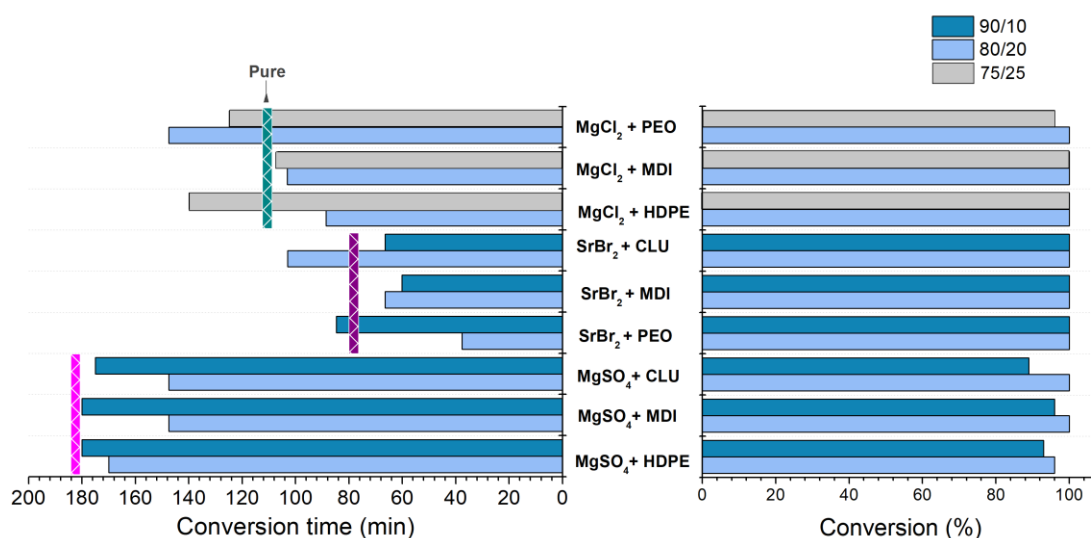
Figure 71. Hydration conversion and hydration conversion time for the formulation containing 80 wt.% TCM/ 20 wt.% PCM (80/20), 90 wt.% TCM/10 wt.%. PCM (90/10) and 75 wt.% TCM/25 wt.% PCM (75/25) at the different conditions; for magnesium sulphate 3h at 30 °C-80 % R.H, for strontium bromide 2.5h at 30 °C-50 % R.H.; and for magnesium chloride 2.5h at 40 °C-30 % R.H. Note that the initial magnesium chloride sample was anhydrous, thus these values are for the second hydration of the composite. Pure TCM conversion time is illustrated with a vertical line; green for magnesium chloride, purple for strontium bromide and pink for magnesium sulphate.

(2.2)   Chemical stability (XRD)

The chemical stability was studied using a high-temperature X-Ray diffraction apparatus, each TCM working pair was subjected to a different temperature program according to their nature. The hydration/dehydration conditions from 25 °C to 120 °C in case of strontium bromide, magnesium chloride from 25 °C to 140 °C to avoid secondary reactions; and magnesium sulphate from 25 °C to 150 °C. The XRD patterns, at the highest test temperature, were recorded after a 30 min isotherm to ensure the stabilisation of the crystalline phase. The patterns of the pure TCM sample are also shown for comparison purposes (Figure 72 to Figure 74). This technique is used to check that no other crystalline phases are present in the composite after dehydration and that the species obtained from the hydrated to dehydrated form are the same as the pure material ones. For that reason, just the working pairs containing the highest PCM (80/20 for $MgSO_4$/$SrBr_2$ and 75/25 for $MgCl_2$) percentages are characterised. The results obtained are discussed for each TCM;

(4) Magnesium sulphate: pure magnesium sulphate dehydrates in three different steps, from hepta- to hexa- in the range from 25 °C to 40 °C; the hexahydrate form is stable up to 70 °C when the transition from hexa- to an amorphous monohydrate form takes place up to a temperature range of 150 °C as also reported by Ferchaud et al. [4]. HDPE and Cellulose working pairs show similar behaviour as the pure TCM, the amorphous phase appears at 70 °C. From 70 °C to 120 °C just two visible crystal diffraction peaks from HDPE can be seen around $2\theta = 21.6°$ and 23.8° [5]. Above 120 °C HDPE is melted and just a "flat" amorphous signal is reported. The MDI working pair shows interesting results as the amorphous phase is in this case delayed to appear at higher temperatures, while a new hydrated form can be seen in the XRD patterns $MgSO_4 \cdot 4\,H_2O$. At the light of the results, this was repeated to proof the validity of this data, which was

confirmed by a second test. This form has not been reported in the literature as a natural form of magnesium sulphate but it is just achieved by synthetic processes [6]. The tetrahydrate is formed at 90 °C, where normally the amorphous phase would be formed. At 120 °C, the amorphous phase appears to coexist with the tetrahydrate as the intensity of the peaks lower. The amorphous phase is then seen at 150 °C when the TCM has completely dehydrated. This evidences that PCM matrices can affect and change the dehydration steps followed by the TCM and might stabilise forms that are not naturally stable within the PCM structure. Another hypothesis is that given the melting point of the PCM (MDI), around 50 °C- 60 °C, this process interacts with the desorption reaction through the heat involved in the phase change as the dehydration from Hexa- to mono starts (55- 60 °C), which may affect the reaction rate/ kinetics of the TCM.

(5) **Strontium bromide:** the pure TCM dehydrates in two steps, firstly from 25 °C to 40 °C to the hexahydrate form, then at approximately 60 °C a transition from Hexa- to mono starts and the form is stable up to 120 °C (see Figure 73), which is in good agreement with the literature [7]. Unlike magnesium sulphate, strontium bromide TCM/PCM working pair show similar XRD patterns as the pure TCM. Therefore, the interaction between TCM and PCM is a factor that determines the effect seen for magnesium sulphate and MDI. The difference in intensities strength can be attributed to a modification of the grain size in the powder sample as reported for other TCMs [4].

(6) **Magnesium chloride:** the dehydration reaction of $MgCl_2.6H_2O$ until 150 °C performed at 1 °C/min was reported to present two dehydration steps with the formation of the crystalline phases $MgCl_2.4H_2O$ in the temperature range of 80-110 °C and $MgCl_2.2H_2O$ in the temperature range of 120-140 °C, as described by Ferchaud et al. [4]. The XRD patterns obtained in this study, show a slightly earlier

transition from $MgCl_2.4H_2O$ to $MgCl_2.2H_2O$ phase, given that the tetrahydrate phase is detected already at 70 °C, as shown in Figure 72. Same heating rate and XRD program conditions have been used, thus this might be attributed to the atmosphere as we operate under open air and the authors worked under controlled partial vapour pressure of 13 mPa atmosphere. Besides, no XRD peaks characteristic of the crystalline phase of magnesium hydroxy chloride MgClOH has been observed on the spectra at 140 °C after 30 min, therefore no side reaction or decomposition is seen. TCM/PCM formulations crystalline peaks sequence is modified for the MDI and PEO composites. In both cases, the $MgCl_2.6H_2O$ phase is formed up to 70 °C, and the crystalline phase of $MgCl_2.4H_2O$ is formed at 80 °C as reported by Ferchaud et al. [4]. In both cases, the intensity of the peaks is very low, and the intensity of the peaks dramatically change before the dehydration from Hexa- to tetra. This was also reported by Ferchaud et al. [4], they attributed this to a preferential orientation change of the material during the measurement. The same explanation for the phenomena observed in the magnesium sulphates pairs can be applied in this case, regarding the tetrahydrate formation temperature shifts. The two plausible hypotheses are that (1) the latent heat reaction can affect the sorption reaction by shifting the crystalline phase formation or (2) the polymeric structure can affect the crystalline phase transformation driving a shift in the transition from one crystalline phase to the other one.

A)

B)

C)

D)
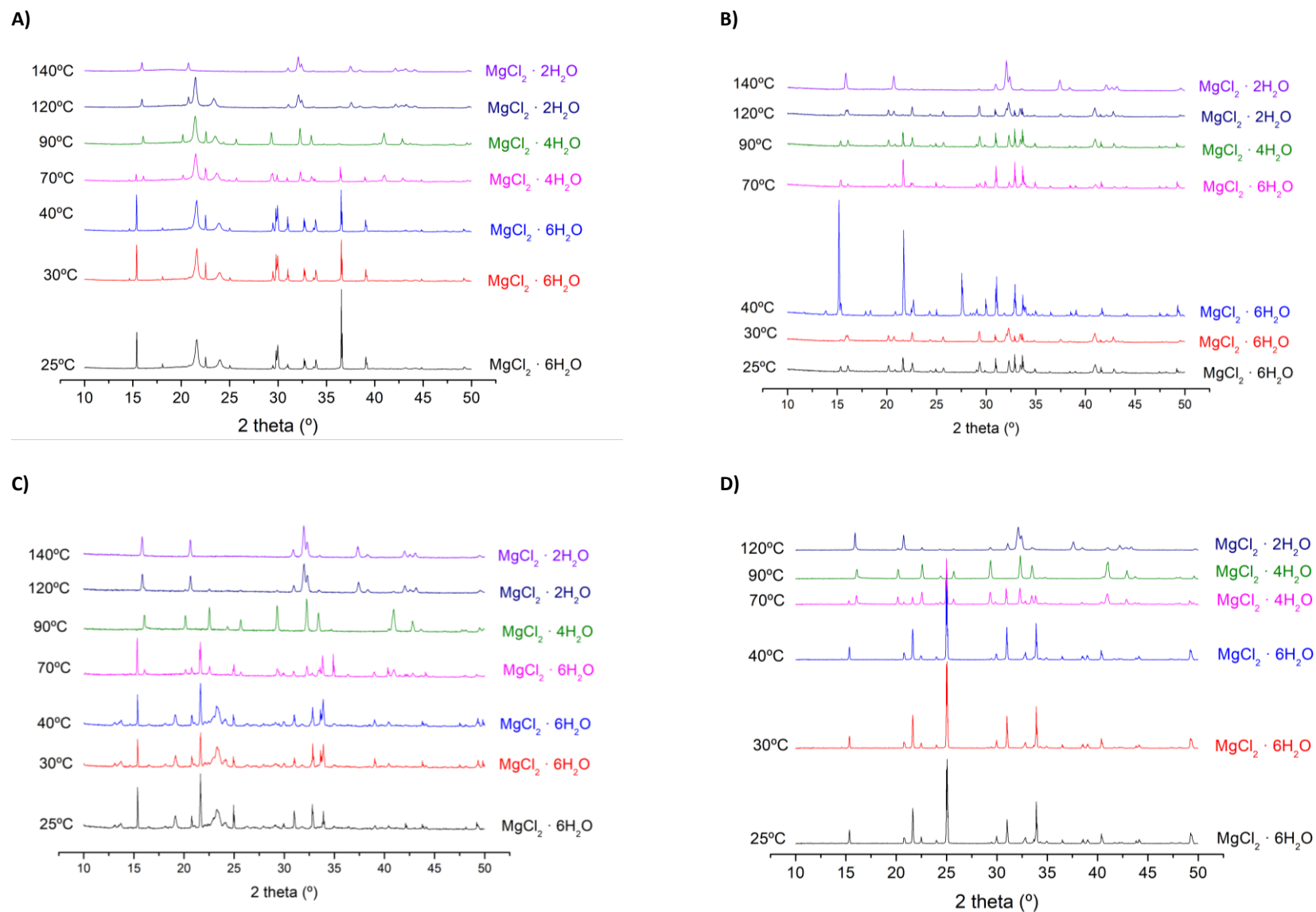
Figure 72. XRD patterns at increasing temperatures (from 25 °C to 140 °C 1 °C/min-hold 30 min) for (A) 75 wt.% $MgCl_2$/25 wt.% HDPE, (B) 75 wt.% $MgCl_2$/25 wt.% MDI (C) 75 wt.% $MgCl_2$/25 wt.% PEO and (D) Pure $MgCl_2$.

A)
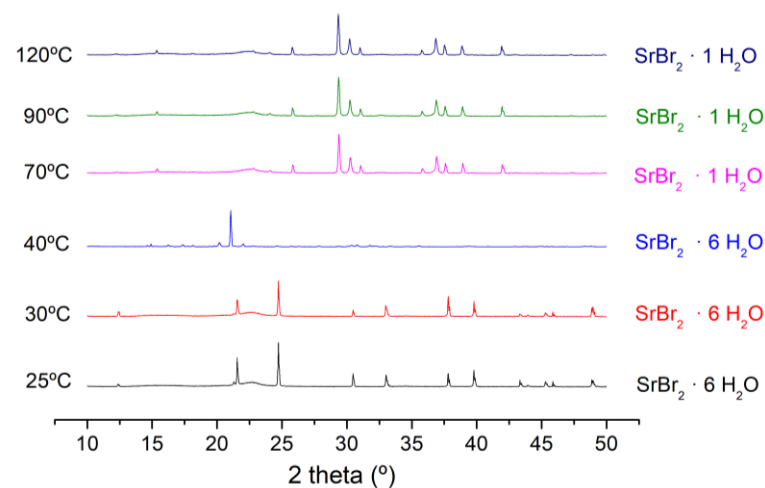
B)
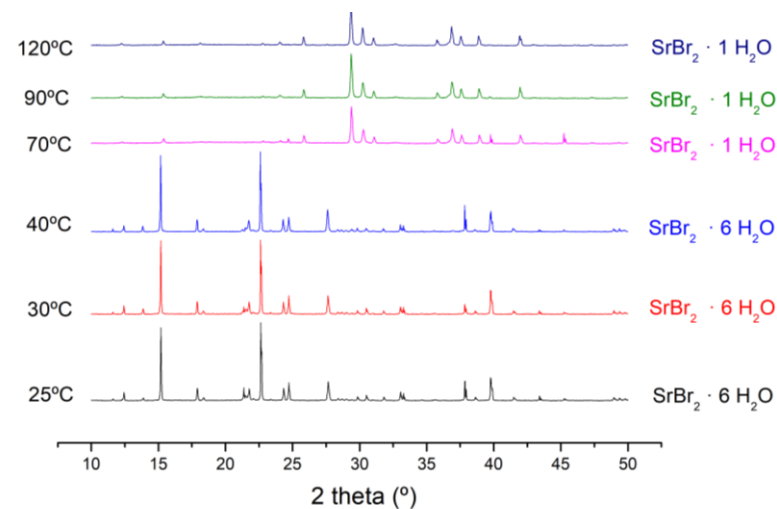
C)
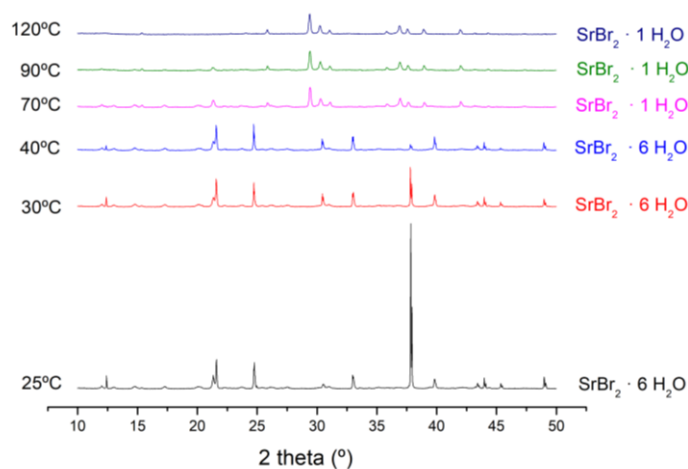
D)
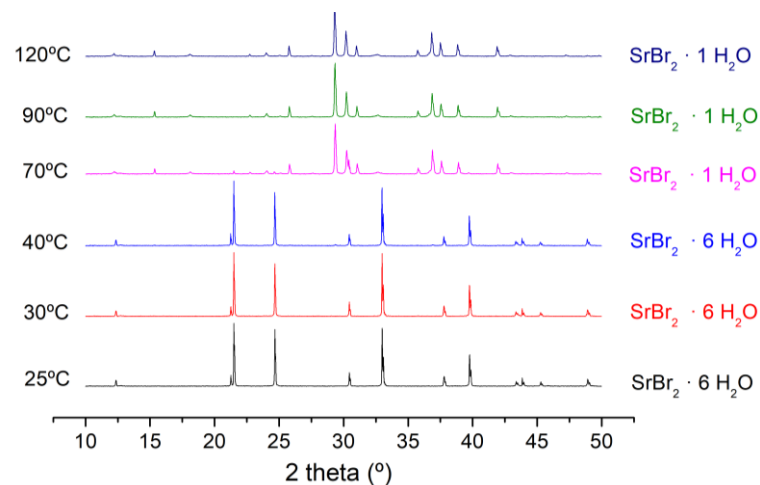
Figure 73. XRD patterns at increasing temperatures (from 25 °C to 120 °C at 1 °C/min-hold 30 min) for (A) 80 wt.% $SrBr_2$/20 wt.% CLU, (B) 80 wt.% $SrBr_2$/20 wt.% MDI (C) 80 wt.% $SrBr_2$/20 wt.% PEO and (D) Pure $SrBr_2$.
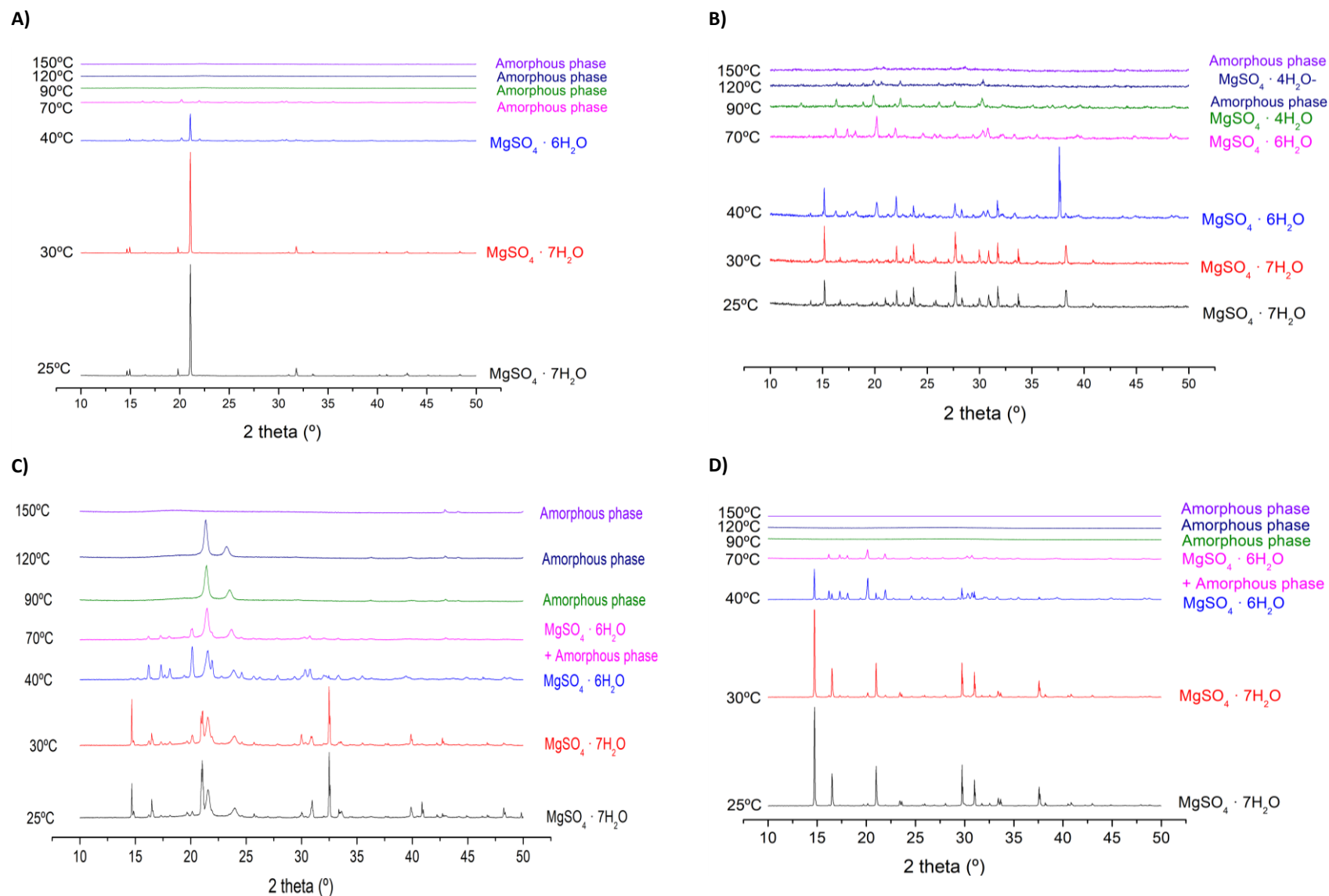
Figure 74. XRD patterns at increasing temperatures (from 25 °C to 150 °C at 1 °C/min-hold 30 min) for (A) 80 wt.%.MgSO₄/ 20 wt.% CLU, (B)80 wt.% MgSO₄/ 20 wt.% MDI (C) 80 wt.% MgSO₄/ 20 wt.% HDPE and (D) Pure MgSO₄.

(1) Outputs

This section discusses the experimental results of the SSPCM/TCM working pair selected. Interesting and ground-breaking results have been obtained as such combinations have not been yet studied elsewhere. Thus, the full understanding of the characterisation performed is a challenge at this stage as there not enough shreds of evidence in the literature to compare and further experimental investigation should be performed. For that reason, the behaviour of the 3 in 1 working pairs have been mainly compared to the pure TCM, and the following outputs were drawn from that process.

The 3 in 1 system is feasible with the use of SSPCM while SLPCM has proved to need an additional component (gel), as they exhibit leakage and breakage after cycling. PCM can affect reaction times, can work as a matrix and can change the dehydrated species of the TCM stabilising or changing the dehydration steps reported in the literature. The working pairs containing higher PCM content show higher conversion rates overall, but lower energy stored given there is a lower TCM content in the composite. Calcium chloride was not experimentally validated as showed very similar behaviour to magnesium chloride. Potassium carbonate was discarded for material incompatibility with all the PCM tested. A maximum 80/20 TCM/PCM ratio is obtained for magnesium chloride while a 90/10 ratio works for magnesium sulphate and strontium bromide. Among all the working pairs experimentally validated magnesium chloride is the one that shows higher energy density while magnesium sulphate composites suppose a compromise between energy stored and structural stability. Strontium bromide performs very well under cycling conditions, although shows the lowest energy stored. Hence, the final candidates for the proof of concept selected are $MgSO_4$/MDI/HDPE/CLU ranging from 90-80 wt.% of TCM and $MgCl_2$/MDI/PEO/HDPE ranging from 80-75 wt.% of TCM.

9.2 POTENTIAL SLPCMs WORKING PAIRS

Previous experimental validation (chapter 8) proved that SLPCMs should be added maximum in 10 wt.% percentages for two main reasons; (1) lower PCM percentages (5 wt.%) tested proved not to be enough to sustain the TCM/PCM structure even though using gelling agents; and (2) the addition of the assisted matrix (gel) allows maximising the TCM content in the 3 in 1 composite. As investigated in the previous section, 4 wt./vol.% of gel into the structure ensures the gel formation while allowing a stable structure. Thus, the highest percentage of TCM loading was set to 80-90 wt./vol.% in this case the loading will be TCM/PCM. The PCM range was extended to 10-25 wt.%. when working with SSPCM as they require large amounts of PCM to sustain the structure given the absence of gel or any other additive into the structure. In this section, we add up another parameter as the SLPCM is added into the synthesis process.

(1) Methodology

Firstly, as done for SSPCMs, the compatibility between PCM and TCM is studied following the same procedure shown previously. Then, a compatibility study between the SLPCMs candidates/TCM/gel is conducted. The eventual goal is to find out the potential SLPCM/TCM/gel working pairs, for that reason, in this section, the experimental validation is targeted to study the synergies between the gel and the TCM/PCM working pair. Given that most of the candidate combinations are expected to fail either for gel formation issues (incompatibilities with PCM/TCM) or cycling issues (leakage, breakage, agglomeration) the energy stored and chemical stability will be studied in further steps (Chapter 10), just for the potential candidates found in this study.

Ideally, the TCM selected in this process should match the ones selected for SSPCM so a comparison between both storage strategies can be provided. Hence, magnesium sulphate and magnesium chloride will be prioritized over the other candidates, although

potential working pairs for the five selected TCM will be proposed as this might be of help for future researchers' guidelines.

The schematic flow chart for the compatibility study is shown in Figure 75. To maximise the TCM content in the composite and take full advantage of the gel component in the mixture, just one formulation will be studied, 90 wt.% of TCM/ 10 wt.% of PCM. The TCM/PCM content is then added in the solution in 80 wt./vol.%. The samples were cycled 5 times under the specific conditions for each TCM (as described in Chapter 7). The combination that could withstand the cycling was then studied in the proof of concept/scale-up stage.
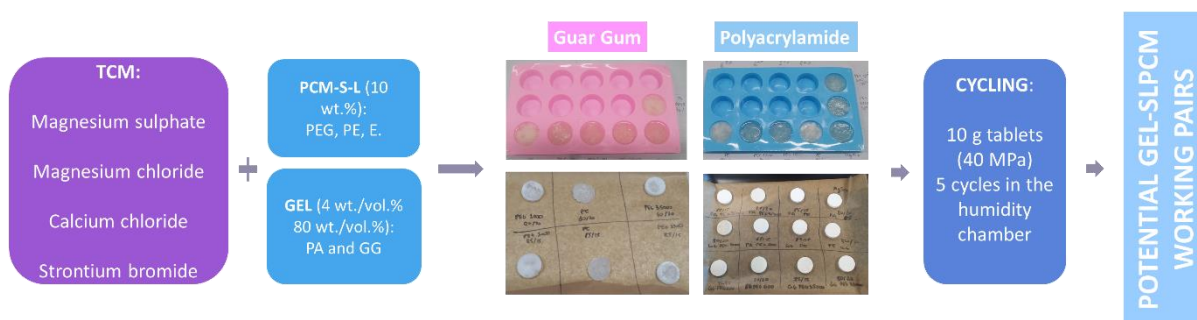
Figure 75. Flow chart for the TCM/PCM-gel compatibility study.

Regarding the preparation methodology, guar gum and polyacrylamide follow two different synthesis method, hot and cold process for GG and PA respectively. For comparison purposes, 10 g of TCM/PCM-gel tablets were prepared for the cycling study. In the hot water synthesis (Chapter 8), the PCM was added along with the TCM (90/10) as seen in Figure 61; (1) A 4 wt./vol.% the gelling agent was added into water at room temperature followed by stirring at a constant rate of 250-300 rpm. (2) The gel solution was heated up to 90 °C while stirring at constant rpm to allow the gel to dissolve. (3) Once the gel has been activated (viscosity of the solutions is visibly increased), TCM/PCM was added in 80 wt./vol.%. The percentages are intended to maximise the TCM percentage while allowing the salt to

homogeneously dispersed into the gel structure. At that point, when the TCM/PCM mixture was completely dispersed in the gel structure, the temperature was reduced to room temperature, stirring at a constant rate was maintain during the whole preparation process. (4) The stirring magnet was removed from the TCM/PCM-gel solution and poured into a silicone mould (2 cm x 4 cm), to allow the gel stabilisation and it was left to settle for 2h in the silicon mould at ambient conditions. This step was skipped when working with highly hygroscopic (e.g. $CaCl_2$ and $MgCl_2$) materials as they needed to be dried right after the synthesis to avoid any extra water absorb into the structure. (5) The silicon trays were located into a humidity chamber under vacuum conditions (10^{-3} bar) at 90 °C with the slowest heating rate allowed by the chamber (1 °C/min). The TCMs were then partially dehydrated in this process, however, this was required since lower temperatures did not lead to completely dry TCM/gel composites.

Different gel drying conditions were studied; 60 °C, 70 °C, 80 °C and 90 °C, the higher the temperature the better the results found as the bottom part of the composites was completely dry. For lower temperatures, the samples were not to completely dry in the lower part of the tablet, as shown in Figure 78 and a water solution was formed for magnesium chloride and calcium chloride. 90 °C, as the drying temperature, was found to be a good compromise for all the TCMs to compare different TCM synthesis under the same conditions and reduce the number of parameters affecting the outputs. During the drying process, some TCMs were partially or completely dehydrated. For that reason, the first cycling step was used to completely dehydrate the composite to ensure that the starting point of the cycling tests was the dehydrated TCM form. Right before the cycling study, the samples were pressed into tablets (40 mPa holding for 1 min) to ensure equal geometry/shape (3 cm x 2.5 $\pm 0.3\ cm$). (8) The tablets were labelled and located into an oven tray with oven paper to avoid them to stick together. The tablets were cycled for 5

dehydration/hydration cycles under the conditions specified for each of the TCMs (see Chapter 7).

The cold water- TCM/gel synthesis was conducted in eight steps as well (see Figure 62); similar to the hot water procedure but without applying heat during the process.
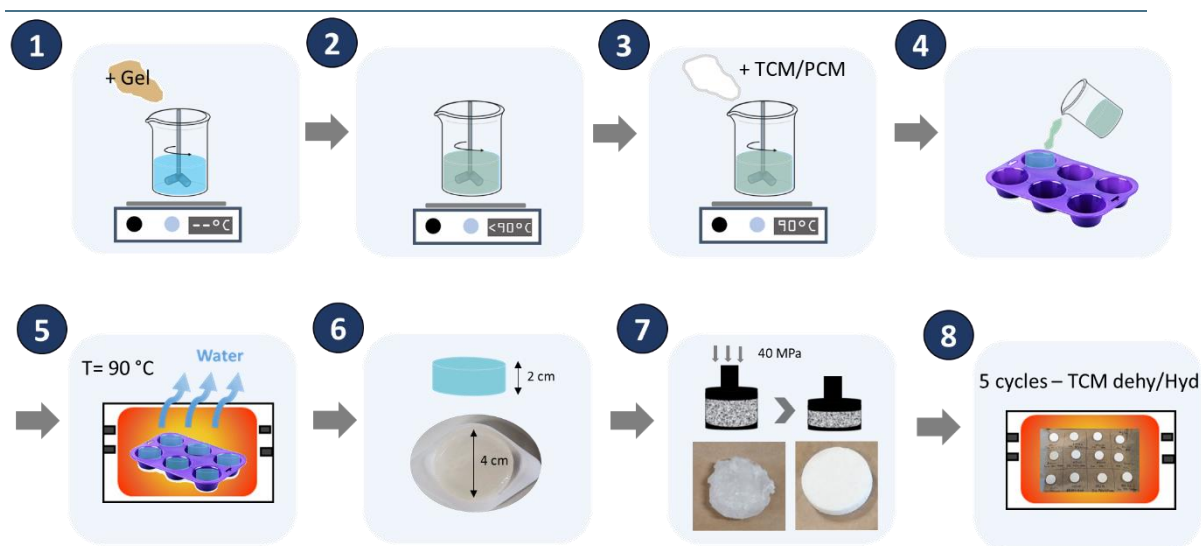
Figure 76. Hot TCM/PCM-gel synthesis procedure, gel content 4 wt./vol.% and TCM/PCM content of 80 wt./vol.% (polyacrylamide). Note that a temperature of 90°C is applied during the mixing process."
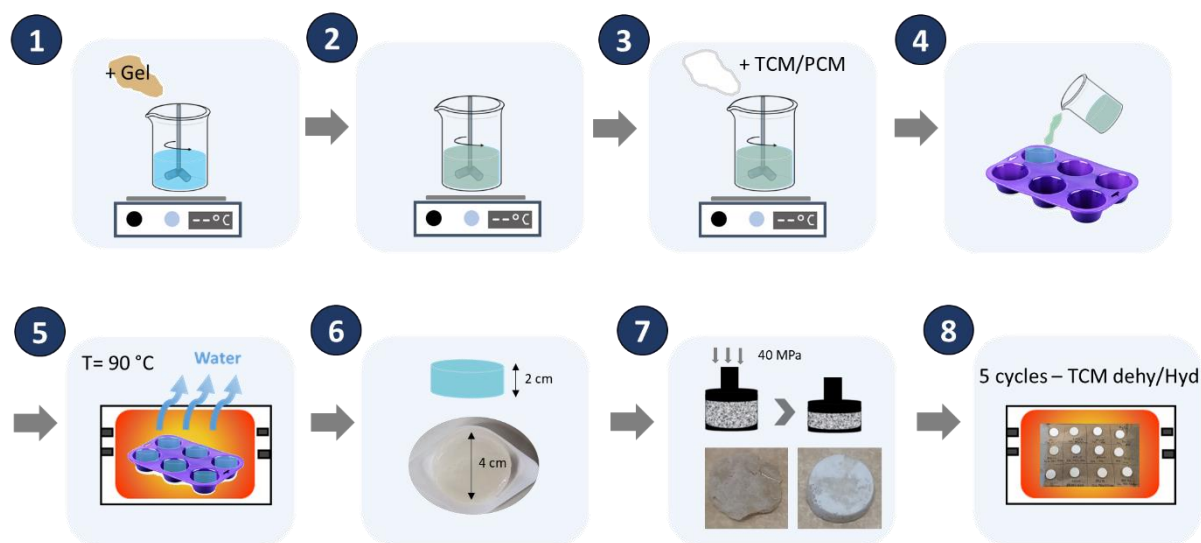
Figure 77. Cold TCM/PCM-gel synthesis procedure, gel content 4 wt./vol.% and TCM/PCM content of 80 wt./vol.% (guar gum). Note that the mixing process is conducted at room temperature.
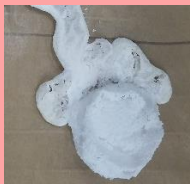
Figure 78. TCM/PCM-gel preparation after drying in the humidity chamber at 70 °C

(2) Experimental validation

From the cycling study, as expected, the SLPCM/TCM pairs failed as they presented major leakage issues (see Table 28). Only the working pair SrBr$_2$/PEG's (35,000 and 1,000) show fairly good structural integrity, proving that when finding optimal compatibility conditions SLPCM/TCM has the potential to offer a consistent alternative to SSPCMs. At this stage, the need for the gel in the SLPCM appears to be crucial given that most of the SLPCM/TCM working pair fail after one cycle. Regarding the compatibility study, just potassium carbonate exhibit chemical incompatibilities with the different PCMs studied.

Table 28. Pictures after cycling the SLPCM/TCM working pairs. The squares in red failed during cycling (major structural problems), while the ones in green showed decent physical integrity (minor or no changes). Note that as PEG 600 and PEG 1,000 have similar attributes just one of them was studied in each case depending on the desired temperature to match hydration conditions (discharging integrated system).

TCM	PEG's		E	
Potassium carbonate	90/10	-	90/10	-
Magnesium sulphate	90/10		90/10	
Strontium bromide	90/10		-	-
Calcium chloride	90/10		90/10	
Magnesium chloride	90/10		90/10	

For comparison purposes, the pure TCMs were also synthesised with the gels (80 wt./vol.% of TCM and 4 wt./vol.% gel). The results for pure TCM-gel and TCM/PCM-gel tablets after cycling are also shown in Table 29. As foresaw, most of the working pairs failed after 5 cycles given the high difficulty of finding compatible TCM/PCM-gel working pair. However, the pure TCM samples show great prospective as they can maintain the structural integrity over cycles in all the cases. When adding the PCM parameter into the equation, the scenario is not as optimistic, only $MgSO_4$ and $SrBr_2$ allowed potential candidates. In general, the addition of PEG and erythritol into the mixtures appears to strengthen the gelling effect given that higher gel strength in

comparison to the TCM/gel combinations can be visibly seen. Thus, the failure is related to incompatibilities and side degradation reactions during hydration/dehydration and melting/solidification. Among the magnesium sulphate working pairs, MgSO$_4$/E/PA is the only one that can withstand 5 cycles, while the other composites show breakage (none suffers leakage), which was the main issue of the SLPCM/TCM composites. The samples containing PEG show clear degradation, which is mainly attributed to the PCM/TCM incompatibility, as the TCM/gel was proved to be stable over the temperature range (no degradation is observed). Similarly, to SSPCMs, magnesium chloride and calcium chloride show very similar behaviour as they both show extreme degradation when combined with GG and leakage when added to PA/PCM. While GG shows clear decomposition, which might be attributed to the acidic conditions during hydration/dehydration that leads to side decomposition reactions. The best performance is shown by strontium bromide working pairs, they all show no leakage either breakage over cycles. Both guar gum and polyacrylamide are compatible with this TCM. Besides, strontium bromide dehydrates at 90 °C, which means that the working pair is not subjected to high temperatures (at least not as high as magnesium sulphate and magnesium chloride). This might have played an important role in the incompatibility shown on the other composites.
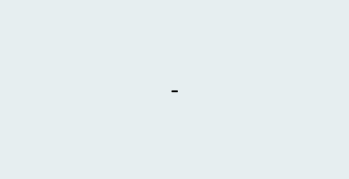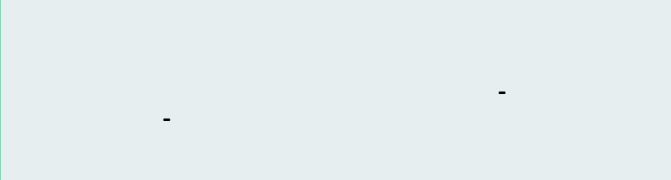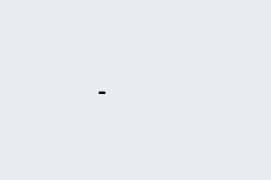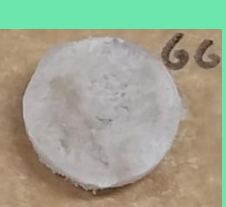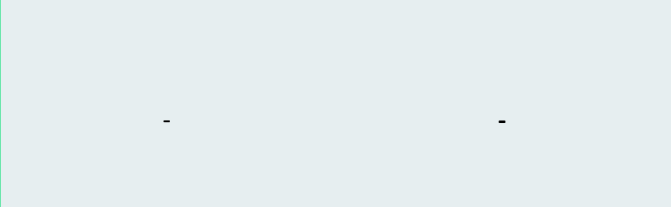
(3) Outputs

Overall, the main issues exhibited by the gel formulations are related to material compatibility besides leakage. Thus, the gel can work as a complementary component to hold the phase change and allow the sorption reaction. Although this section has proven that the technology is effective and can pave the future TCM manufacturing, a complete material selection is needed to find potential TCM/gel candidates. Besides, the same methodology has been used for all the TCM/PCM-gel working pairs to reduce

the number of parameters affecting the composites comparison. However, further study is required to understand the effect of such parameters in the performance of the composite (drying temperature, compressing pressure, shape, particle size, agitation speed, etc).

Looking at the three 3 in 1 system proposed; discharging integrated has shown to be the most complex as it is challenging to find a solid-liquid PCM that can hold the composite together through hydration/dehydration. In this case, TCM integrity is crucial for successful working pairs, e.g. strontium bromide is the only TCM that works with PEG 600/PEG 1,000. In this respect, further combinations should be studied and other low temperatures (25-30 °C) phase change materials explored ensuring stability at temperatures around 120 °C. Charging integrated system can be achieved by combining magnesium sulphate and erythritol, which has shown very good stability while providing high temperature stored given that sugar alcohols possess a high latent heat (see later). Cascade system could have been designed by the combination of PEG 35,000 with either magnesium sulphate or magnesium chloride. Although the leakage problem shown in the previous section has been solved, the addition of gel does not yet lead to a stable working pair over cycles, as degradation appears after 5 cycles.

Table 29. Pictures after cycling of SLPCM/TCM-gel working pairs after 5 cycles. The squares in red failed during cycling (major leakage), while the ones in green showed decent physical integrity (minor leaking).

TCM	Gel	Pure TCM	PEG 35,000	PEG 1,000	PEG 600	E
Magnesium sulphate	GG			-		
	PA			-		
Strontium bromide	GG				-	-
	PA				-	-

Continuation Table 4.

TCM	Gel	Pure TCM	PEG 35,000	PEG 1,000	PEG 600	E
Calcium chloride / Magnesium chloride	GG				-	
	PA				-	

9.3. FINAL WORKING PAIRS FOR PROOF OF CONCEPT AND SCALE-UP STUDY

A summary of the selected working pairs for an in-depth material behaviour study and the scale-up process is shown in Figure 79. Magnesium sulphate has proven to be the best candidate as it offers working pairs that allow SSPCM with relatively high energy density and physical integrity, plus a feasible option to study the gel interaction with PCM/TCM working pairs. Besides, such combinations can be proposed for the three different systems configurations; $MgSO_4$/E/PA and $MgSO_4$/HDPE for charging integrated, $MgSO_4$/MDI for cascade system and $MgSO_4$/CLU for discharging integrated. Thus, for the proof of concept study, which involves a full set of characterisation techniques of 1 g tablets and a 15- cycles test, magnesium sulphate working pair was selected; $MgSO_4$/HDPE.

Once the system was shown to be feasible, the study was upgraded to the next level that involved bigger tablets (20 g) and a larger number of cycles (40 cycles) as the scale-up validation. For such study two thermochemical materials were selected; magnesium sulphate (for the reasons stated above), and magnesium chloride given that was the working paired that showed the highest energy stored. Since magnesium chloride did not show excellent cycling stability, the PCM ratio in their working pairs was raised to 25 wt.% aiming to improve the physical integrity of $MgCl_2$ working pairs. Due to $MgCl_2$ incompatibilities with the gels, just SSPCM are considered for the $MgCl_2$-working pair: $MgCl_2$/PEO and $MgCl_2$/MDI for cascade system and $MgCl_2$/HDPE for charging integrated. This will be presented in the following sections of the thesis.

(4.1) PROOF OF CONCEPT (1 g)

TCM:

MgSO₄

PCM-S-S (80-95 wt.%):
HDPE

CYCLING:
1 g tablets
(90 MPa)

15 cycles in
the humidity
chamber (1,
5, 10 and 15)

XRD   DSC

STA

Porosity

BET

SEM   Dilatometer

(4.2) SCALE-UP (20 g)

TCM:

MgSO₄

MgCl₂

PCM-S-S (75-90 wt.%):
PEO, HDPE, MDI, CLU

PCM-S-L (90 wt.%):
Erythritol

GEL (4% gel, 80 % and 90% in vol.):
PA

CYCLING:

20 g tablets
(40 MPa)

40 cycles in
the humidity
chamber (1,
5, 15, 25, 40)

XRD   DSC

STA   RAMAN

FT-IR

XRT
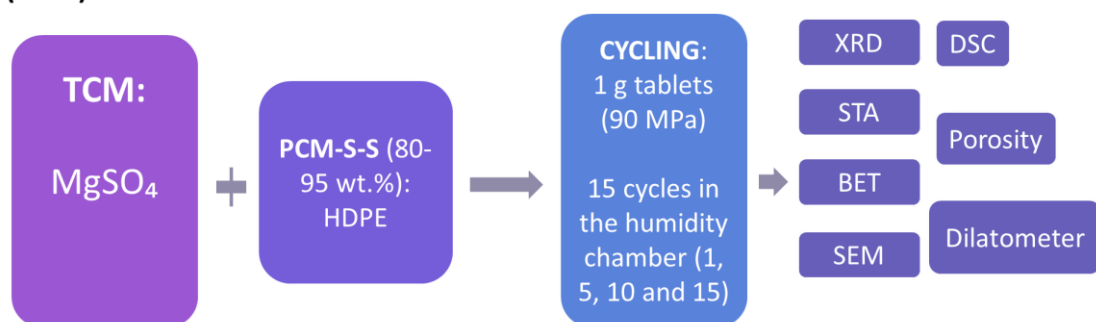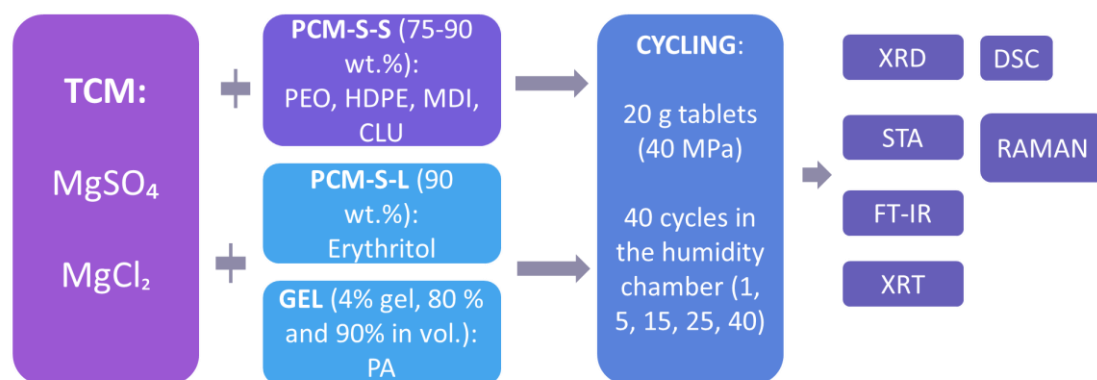
Figure 79. Flow chart for proof of concept section (4.1) and scale-up (4.2) validation of the 3 in 1 system.

9.4 REFERENCES

[1]   Donkers PAJ, Beckert S, Pel L, Stallmach F, Steiger M, Adan OCG. Water Transport in MgSO4·7H2O during Dehydration in View of Thermal Storage. J Phys Chem C 2015;119:28711–20. doi:10.1021/acs.jpcc.5b08730.

[2]   Okhrimenko L, Favergeon L, Johannes K, Kuznik F, Pijolat M. Thermodynamic study of MgSO4– H2O system dehydration at low pressure in view of heat storage. Thermochim Acta 2017;656:135–43. doi:10.1016/j.tca.2017.08.015.

[3]   Fopah-Lele A, Tamba JG. A review on the use of SrBr2·6H2O as a potential material for low temperature energy storage systems and building applications. Sol Energy Mater Sol Cells 2017;164:175–87. doi:10.1016/j.solmat.2017.02.018.

[4]   Ferchaud CJ, Zondag HA, Veldhuis JBJ, De Boer R. Study of the reversible water vapour sorption process of MgSO4.7H2O and MgCl2.6H2O under the conditions of seasonal solar heat storage. J Phys Conf Ser 2012;395. doi:10.1088/1742-6596/395/1/012069.

[5]   Gu J, Xu H, Wu C. Thermal and crystallization properties of HDPE and HDPE/PP blends modified with DCP. Adv Polym Technol 2014;33:1–5. doi:10.1002/adv.21384.

[6]   Grevel KD, Majzlan J, Benisek A, Dachs E, Steiger M, Fortes AD, et al. Experimentally Determined Standard Thermodynamic Properties of Synthetic MgSO4 center dot 4H(2)O (Starkeyite) and MgSO4 center dot 3H(2)O: A Revised Internally Consistent Thermodynamic Data Set for Magnesium Sulfate Hydrates. Astrobiology 2012;12:1042–54. doi:DOI 10.1089/ast.2012.0823.

[7]   Morris MC, McMurdie HF, Evans EH, Paretzkin B, Parker HS, Pyrros NP, et al. STANDARD

X-RAY DIFFRACTION POWDER PATTERNS. NBS Monogr (United States) 1982.

X-RAY DIFFRACTION POWDER PATTERNS. NBS Monogr (United States) 1982.

Anabel Palacios Trujillo   HYBRID 3 IN 1 SYSTEM

10 PROOF OF CONCEPT AND SCALE-UP

1. Thesis timeline

2. Scientific contributions

3. Introduction

4. TCS Outlook

5. Targets and structure of the thesis

6. Hybrid TES system:

3 in 1 concept

The 3 in 1 system is brought to the ultimate level in the thesis, with the proof of concept and the scale-up study. In the proof of concept, the $MgSO_4$/HDPE working pairs (charging integrated system) is studied in a temperature range between 30 °C and 150 °C. Regarding the scale-up study, the final working pairs candidates from Chapter 9 are experimentally validated through a complete set of characterisation techniques.

7. Bench study specifications

8. Material screening and selection

9. Working pairs

10. Proof of concept and scale-up

11. Potential applications and prospective

12. Conclusions and achievements

10. PROOF OF CONCEPT AND SCALE-UP

10.1 PROOF OF CONCEPT

To prove the feasibility of the 3 in 1 technology proposed in this thesis, we have pictured a $MgSO_4$-HDPE system for the in-principle demonstration of the concept. We established a charging integrated system for such a purpose and studied it in a temperature range between 30 °C and 150 °C, which working conditions are suitable for space heating and domestic hot water supply [51]. This section presents the details.

(1) Materials

The TCM selected for the proof of concept was magnesium sulphate heptahydrate ($MgSO_4 \cdot 7H_2O$). It was an analytical reagent grade (CAS: 10034-99-8, MW: 246.48) supplied by Fisher ScientificTM. The high-density polyethylene (HDPE; CAS: 9002-88-4, MFI: 3.2) was used as the PCM and supplied by Matrix company©.

(2) Methodology

Different ratios of magnesium sulphate heptahydrate and HDPE from 80–95 wt.%, both in powder form, were mixed and ground to a homogeneous mixture. An amount of 0.8 g ± 0.05 g was then pressed into a tablet shape with 13 mm diameter and ~10 mm height using a Lloyd LS100 Plus Materials Testing Machine supplied by Lloyd Instruments company (UK). The operating pressure and holding time was set to 90 MPa and 1.2 min, respectively. Three pellets for each of the formulations and cycling testing were prepared. The compacted composites were tested to determine the cycling stability after 1, 5, 10 and 15 charging/discharging cycles. The energy stored (STA), chemical stability (XRD), volume change (Dilatometer), porosity (helium pycnometer) and microstructure (SEM) of the 3 in 1 composite

before and after cycling were studied following the specifications described in Chapter 7. The experimental data were averaged from the three pellets prepared.

(3)   **Experimental validation**

The working pairs that withstand the highest number of cycles were the 80/20 and 85/15 (see Figure 80). The criteria to select the best working pairs was to consider just the ones that did not show any cracks or major structural problems such as leakage or breakage. In the first selection stage, the structural integrity was prioritised over other attributes, and only the pellets that maintain their structural integrity up to 15 cycles were fully characterised. Although the cycling was stopped at 15 cycles, these formulations showed the potential to withstand a higher number of cycles (see Section 10.2).
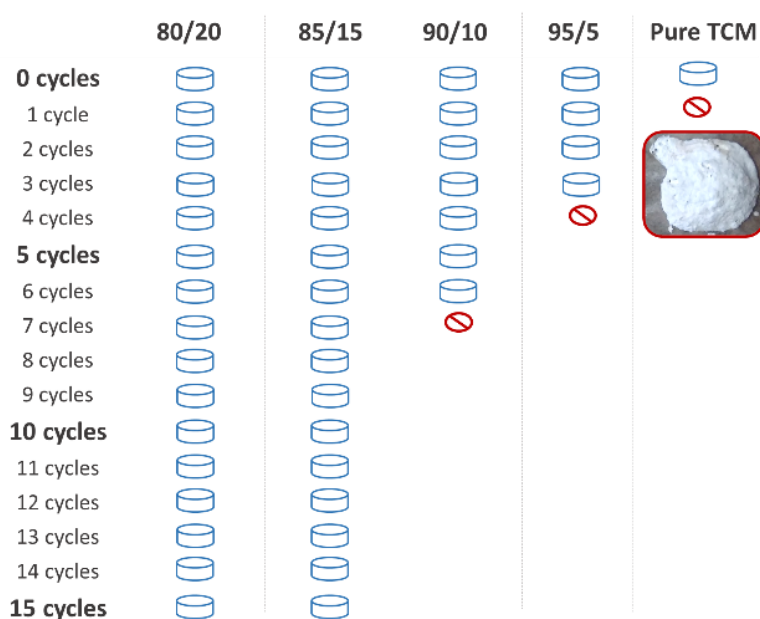
Figure 80. Tablets prepared cycled from 0 to 15 cycles and mechanical integrity obtained and pictures from the 80 wt.% TCM/20 wt.% PCM tablets after cycling.

As stated in previous sections, magnesium sulphate suffers from cracking and eventual breakage during sorption/desorption cycles [1]. This is mainly triggered by three interrelated phenomena: (1) volume change between hepta- to mono form of the TCM; (2) reduction of the composite porosity; and (3) change between crystal to amorphous phases. The addition of the HDPE into the TCM skeleton can give flexibility to the structure due to the viscous fluid state of the PCM upon melting, besides thermal energy storage capacity. Donkers et al. [2], observed cracks of the TCM because of the volume change when heptahydrate magnesium sulphate transforms into hexahydrate. In the 3 in 1, the TCM volume change during the desorption of water molecules is counterbalanced by the volume change of the PCM; see Figure 81 for an illustration of the mechanism. Although the thermochemical material has been reported to experience a theoretical volume change of ~69% between a state with 7 water molecules and an anhydrous state (Figure 82) [3], this study only found a volume change around 20%. The two formulations prepared (80/20 and 85/15), show that the PCM in the composite structure helps to accommodate the TCM volume change after 15 cycles (Figure 82).
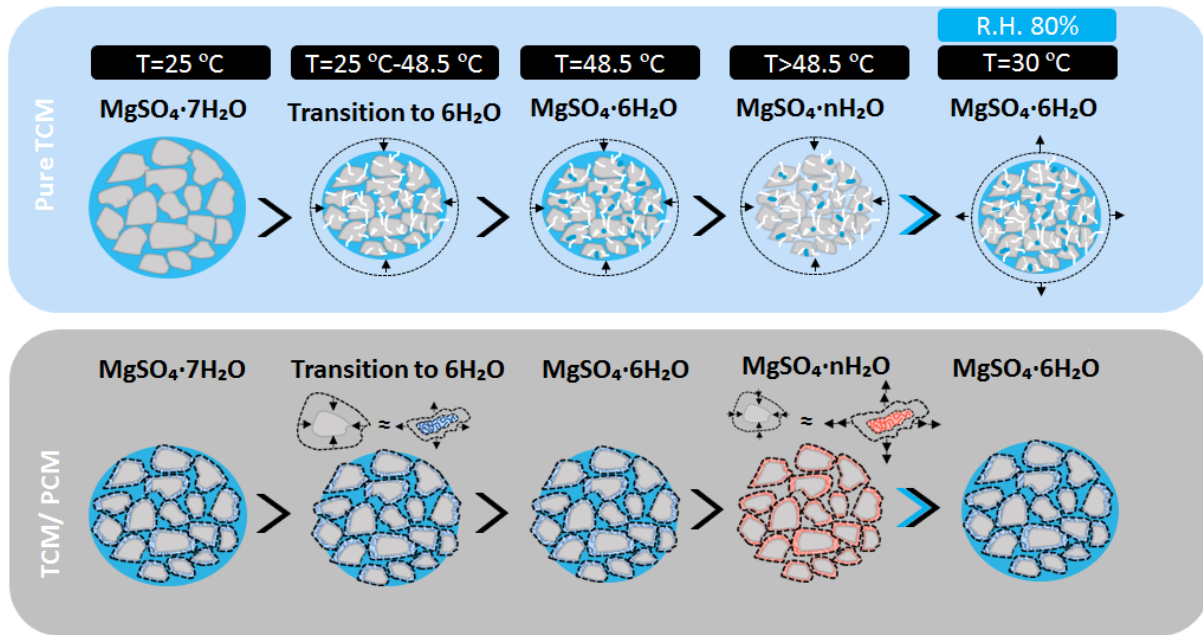
Figure 81. Pure TCM and TCM/PCM microstructure during dehydration and hydration.
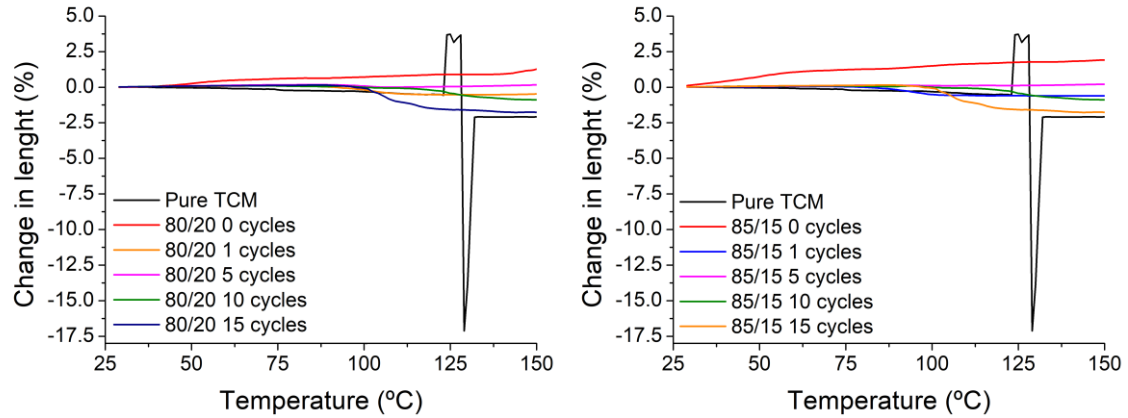
Figure 82. Change in length of 85 wt.% TCM/15 wt.% PCM (right) and 80 wt.% TCM/20 wt.% PCM (left).

Associated with the volume change during the TCM thermal cycles is the decrease of porosity over cycles [1]. Such a decrease in the porosity hinders the water vapour transport and significantly reduces the reaction rate. The 3 in 1 system alleviates this through reducing and accommodating the volume change and thus enabling water transport to the TCM (due to the hydrophobic and permeable character of the polymer-based PCM). The two effects co-work synergistically to keep the structure together avoiding structural degradation and mechanical breakage. Figure 83 shows the microstructural changes of the composite after 15 cycles when a stable porosity of ~55% is reached (hydrated). The 85/15 TCM/PCM composite had a slightly higher porosity than the 80/20 one which might be due to the lower loading of PCM, as seen in the SEM images, a less compacted composite. As reported by Ferchaud et al.[4], two main structural changes of the material can be observed in the XRD patterns (see Figure 85); the change from heptahydrate to hexahydrate crystalline phases (between 30 °C and 40 °C), and from hexahydrate to amorphous phase (between 60 °C and 80 °C). The formation of the amorphous phase has been related to a slow reaction rate at pressures <13 mbar, which is related to an inhomogeneous and slow reorganization of the crystal structure forming a disordered arrangement. Likewise, this phenomenon is observed in the PCM/TCM composites, the amorphous phase appears at 70 °C. From 70 °C to 120 °C just two visible crystal diffraction peaks from HDPE can be seen around $2\theta = 21.6°$ and $23.8°$ [5] (see Figure 85).
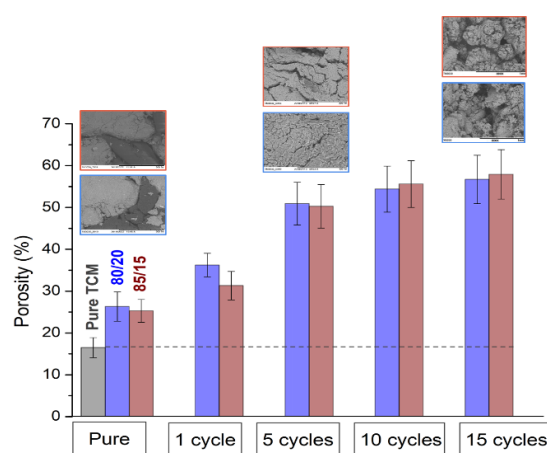
Figure 83. Porosity over cycles for the pure TCM, 80 wt.% TCM/20 wt.% PCM and 85 wt.% TCM/ 15 wt.% PCM formulations.
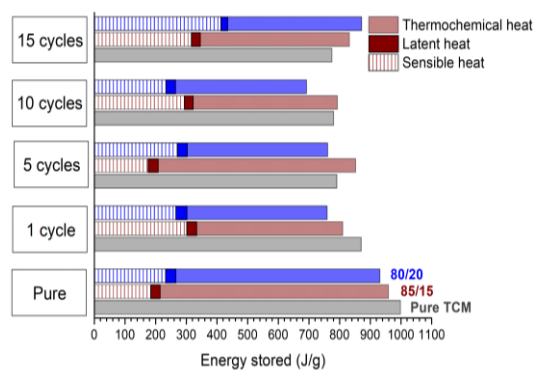
Figure 84. Energy stored by form (sensible, thermochemical and latent) for the pure TCM, 80 wt.% TCM/20 wt.% PCM and 85 wt.% TCM/ 15 wt.% PCM
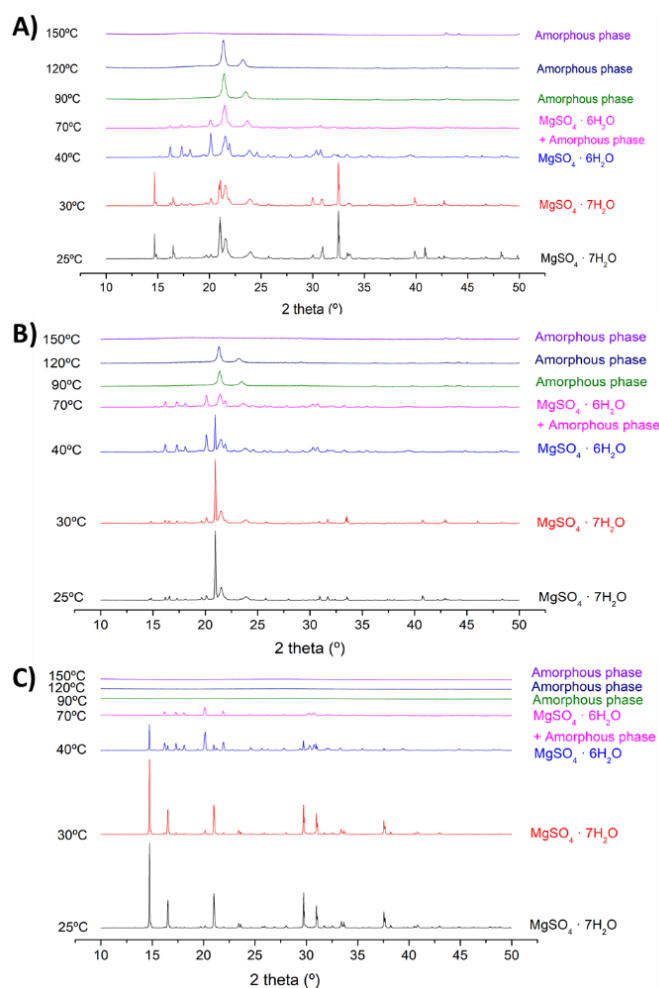
Figure 85. In-situ XRD patterns of the dehydration reaction of 80 wt.% TCM/20 wt.% PCM (A), 85 wt.% TCM/ 15 wt.% PCM (B) and pure TCM (C), in powder form.

After validating the 3 in 1 system's structural and physical integrity, both the stored energy and water uptake behaviour of the composites were studied. Although the pure TCM breaks after one cycle, the energy stored for 1, 5, 10 and 15 cycles were also included for comparison purposes. The energy stored by the pure composite (tested in powder form) after the first dehydration cycle is 18% higher than the composites (cycled in tablet form in the humidity chamber) (see Figure 84). However, looking at the hydration curves (see Figure 86), it can be seen that the hydration process of the composites, both 80/20 and 85/15, is faster than the pure TCM, with conversion rates of 90% for the hydration reaction in less than two hours. Comparing the cycled composites in the tablet form to the initial powders (0 cycles), the powders take longer to reach χ_{90} (90% conversion). This might be because, as for the pure TCM, the powders rapidly agglomerate when dehydrating, hindering the water mass transfer and hence reducing the conversion rate. Thus, the structure created by the polymer and the thermochemical material is key to allow higher and more stable conversion rates over cycles.
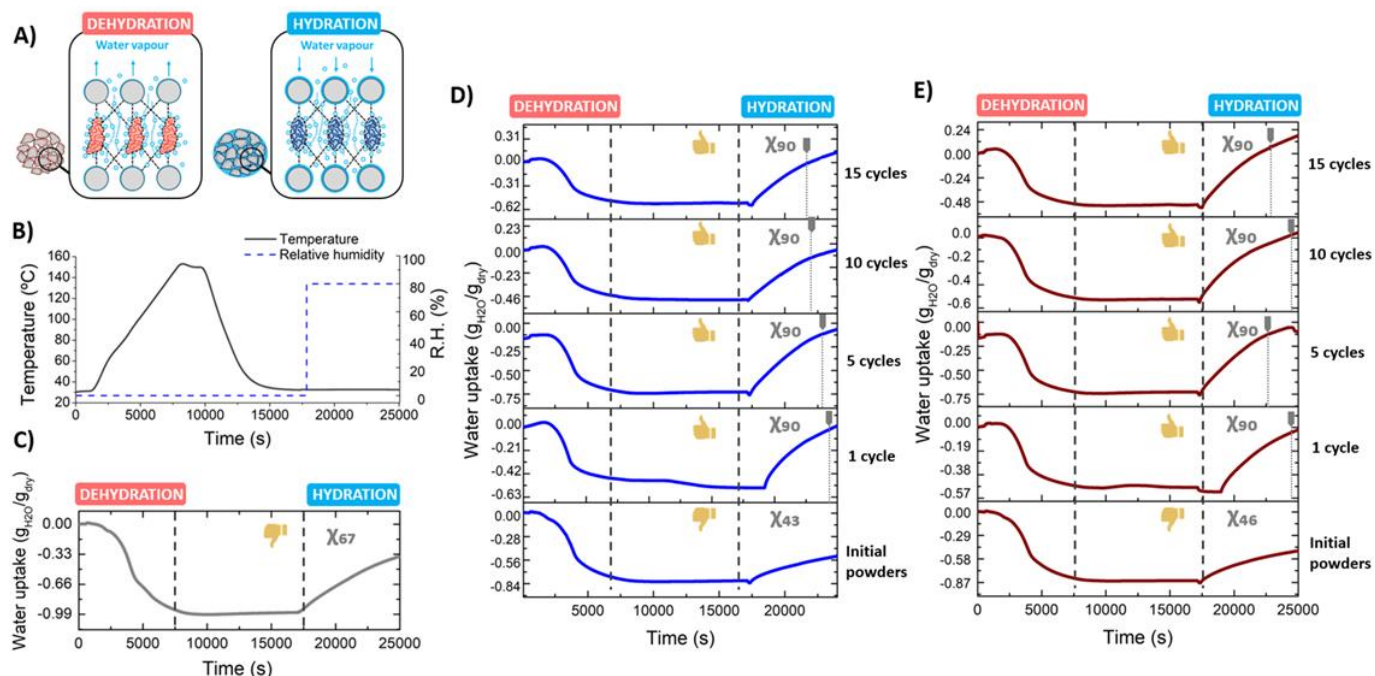
Figure 86. A) Dehydration (left) and hydration (right) mechanism of the PCM/TCM composites; B) Temperature and relative humidity program set for the measurements shown in the figure; C) Water uptake of the pure raw magnesium sulphate heptahydrate (dehydration/hydration); D) Water uptake of the 80 wt.% $MgSO_4 \cdot 7H_2O$ and 20 wt.% HDPE (hydration/dehydration); E) Water uptake of the 85 wt.% $MgSO_4 \cdot 7H_2O$ and 15 wt.% HDPE (hydration/dehydration).

Besides the fact that the polymer keeps the structure together given the adhesion forces and does not experience any leakage given the polymer's high viscosity, the 3 in 1 structure also enables the water vapour transport due to the hydrophobic nature of the polymer (Figure 86 (A)).

Under the investigated conditions, the 3 in 1 system can store ~2 GJ·m^{-3}, after 15 charging/discharging cycles (see Figure 87). Although no significant differences can be observed between the hydration/dehydration behaviour of 80/20 and 85/15, the polymer-based PCM loading might affect the distribution of the components in the structure. The quantity of polymer determines the contact area between the thermochemical material and the polymeric PCM. A higher percentage of PCM gives a higher contact area but at the same time makes the structure more compact, and hence hindering the water vapour transport (due to low porosity). While a lower percentage of the polymeric PCM may not be enough to provide enough contact area and allow the structural stability, leading to the agglomeration of the TCM particles (structural degradation) and hindering mass transfer. To finish off this section, the energy stored cost (€/kJ) of the material has been also calculated (Figure 87). The pure thermochemical material is already cost-intensive in the first dehydration-hydration cycle; by increasing the number of cycles, the energy density gradually decreases resulting in an even higher cost per unit of energy stored. Whereas the 3 in 1 system, despite suffering a slight cost increment over cycles, the low cost of the HDPE and the structural stability of the composite gives an offset, leading to a lower cost per unit energy stored than that of the pure TCM.
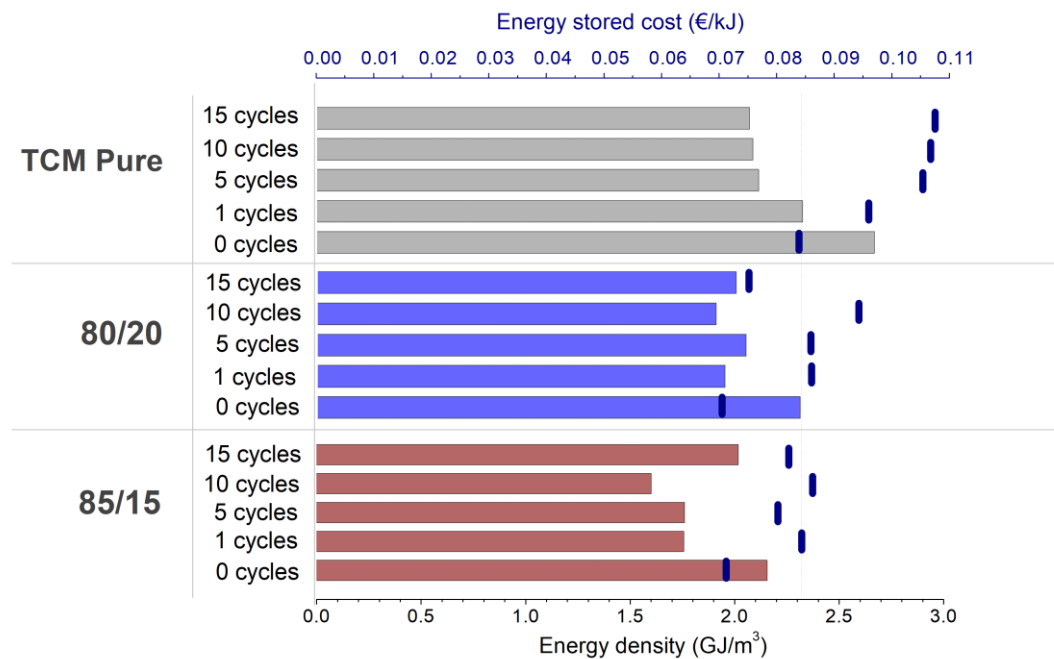
Figure 87. The energy density (GJ·m^{-3}) and energy stored cost (€/kJ) of pure TCM, 80 wt.% TCM/20 wt.% PCM and 85 wt.% TCM/ 15 wt.% PCM formulations.

(4)   Outputs

The configuration here presented, serves as a proof of concept of the 3 in 1 system. It showed great potential storing heat in a large temperature range, from 30 °C to temperatures closer to 150 °C. Where the composite compiles the strengths of all three TES systems (sensible, latent and thermochemical) by using its components as a synergic matrix that allows structural integrity along with the different storage processes. PCMs, help to maintain the physical integrity of the composite by accommodating the volume change and holding the structure together during cycles. The unique combination of a polymer and a thermochemical material allows for a cost-effective storage media that can store up to 2 GJ·m^{-3}. As we have discussed in the material selection section, there are numerous working pairs combinations for the 3 in 1 system that can adapt to the requirements of various applications. The studied

combination in this section provides evidence of the synergistic entanglement of the three forms of energy storage.

10.2 SCALE-UP STUDY

In the previous section, the 3 in 1 system was proven to be feasible up to 15 thermal cycles. Aiming to transit to the next manufacturing level, the set of working pairs obtained in Chapter 9 (including the one tested in the proof of concept) are validated at a scale-up level in this section. The tablets are scaled up from 1 g to 20 g of sample mass, following the same manufacturing process (tabletting) used throughout the thesis. Besides, cycling stability at a larger number of cycles is tested, from 15 to 40 cycles. This section presents the details.

(1)   Materials

The TCMs selected for the scale-up study were magnesium sulphate heptahydrate ($MgSO_4 \cdot 7H_2O$) and magnesium chloride ($MgCl_2 \cdot 6H_2O$). The first one was an analytical reagent grade (CAS: 10034-99-8, MW: 246.48) supplied by Fisher Scientific[TM] and the second one was purchased in anhydrous form from Acros Organics[TM] (CAS: 7786-30-3, MW: 95.21, Pure). The high-density polyethylene (HDPE; CAS: 9002-88-4, MFI: 3.2) was used as the PCM and supplied by Matrix company©. The other polymeric PCMs used were the 4,40-diphenylmethane diisocyanate (MDI) supplied by Acros Organics[TM] ($C_{15}H_{10}N_2O_2$) in flakes, 98% (CAS: 101-68-8, MW: 250.26), polyethylene oxide, ($-CH_2CH_2O-$)n, from Alfa Aesar[TM] (CAS: 25322-68-3, MW: >5,000,000) and erythritol, SLPCM, $C_4H_{10}O_4$, Intenson (CAS: 149-32-6, MW: 122.2, 99%). The gel used for the SLPCM working pairs was polyacrylamide, supplied by Sigma Aldrich (CAS: 9003-05-8). The cellulose matrix was the Microcrystalline cellulose powder from MPBioTM (CAS: 9004-34-6, MW: N/A).

(2)   Methodology

Different ratios of TCM and PCM, both in powder form, were mixed and ground to a homogeneous mixture. An amount of 19.5 g ± 0.05 g was then pressed into a tablet shape with 30 mm diameter and ~25 mm thickness using a Lloyd LS100 Plus Materials Testing Machine supplied by Lloyd Instruments company (UK). The operating pressure and holding time for the machine was set to 40 MPa and 1.5 min, respectively. Two pellets for each of the formulations and cycling test were prepared. $MgSO_4$/SSPCM (HDPE, MDI and CLU) were mixed in PCM ratios of 10 wt.%, 15 wt.%, 20 wt.% and 25 wt.% Given the promising results shown in the proof of concept section, the PCM content was extended from 80/20 to 75/25 to study the effect of PCM into the $MgSO_4$ working pairs. $MgSO_4$/SLPCM-gel (E/PA) composites were prepared by firstly mixing 10 wt.% PCM and 90 wt.% TCM and then adding the mixture in a ratio of 80 wt./vol.%, 90 wt./vol.% and 100 wt./vol.% on a 4 wt./vol.% the water solution of the gelling agent (PA). $MgCl_2$/SSPCM (HDPE, MDI and PEO) were mixed in PCM ratios of 15 wt.%, 20 wt.% and 25 wt.%. None SLPCM/$MgCl_2$ formulations were tested in this section as they all failed the TCM/PCM-gel compatibility test (see Chapter 9). Note that $MgSO_4$ was formulated from hydrated form (7 H_2O), while $MgCl_2$ composites were prepared from the anhydrous form as explained in the previous section. The compacted composites were tested to determine the cycling stability after 1, 5, 15, 25 and 40 charging/discharging cycles. The energy stored (STA), chemical stability (XRD and Raman), porosity (XRT) and microstructure (XRT) of the 3 in 1 composite before and after cycling were studied following the specifications described in Chapter 7. The experimental data were averaged from the two pellets prepared.

Given the large number of samples studied in this section, a nomenclature is assigned to each of them as shown in Table 21 to Table 34. The sample is assigned a letter e.g. 90 wt.% $MgSO_4$/ 10 wt.% HDPE is the letter A, whereas the cycling stage is identified by a number e.g. 1 cycle is number 1. (see Table 21 to Table 34). Therefore, sample A cycled once would be A1, like this consecutively for the rest of the samples.

(3)   Experimental validation

(3.1) Cycling stability

Magnesium sulphate working pairs stand up as the most promising candidates for the 3 in 1 composite as they can withstand up to 40 cycles without showing major leakage, breakage or chemical degradation (see Table 21 to Table 34). Among the SSPCM working pairs, MgSO4/HDPE shows the best compatibility as well as physical integrity over cycles for either 80 wt.%, 85 wt.% or 75 wt.% formulations (see Table 21). These results are in good agreement with the proof of concept section and proves that using a larger tablet size does not affect, cycling stability-wise neither the synergy between magnesium sulphate and high-density polyethylene. With a visual inspection, one can conclude that the sample M (75/25) does contract throughout the thermal cycles while B and C tablets size remains the same. The working pair containing MDI shows leakage after 1 cycle and major breakage after 5 cycles, concluding that MDI polymer, unlike HDPE, does not work as a supporting matrix for the 3 in 1 system. This might be due to the MDI acting as a hard segment (using as an analogy a polymer blend) not allowing mobility and restructuring of the TCM in the composite after one cycle not providing a contained-flexible structure, which leads to leakage of the PCM; and after 5 cycles resulting on the collusion of the structure (breakage). In this case, a polymer-based blend (e.g. PEG-MDI) could be an alternative to improve this behaviour [6,7]. Cellulose exhibits promising behaviour under 5 thermal cycles, especially for 90/10, however above 5 cycles all the samples break following a similar behaviour as the one shown by the pure TCM, 1) collapsing – 2) cracking- 3) breakage.

The SLPCM-gel magnesium sulphate samples (G, H and I), show fairly good physical integrity over cycles with no visible breakage or leakage. However, they seem to expand, especially after 1 cycle, creating noticeable hollow channels in the tablet. This phenomenon is aggravated by the higher content of PCM/TCM in gel solution, for instance, 100 wt./vol.% in

the gel, the solution appears to have a higher tendency to form macro channels as it can be seen in the 40 cycles's pictures (Table 32).

Regarding magnesium chloride working pairs, all the formulation studied were not able to withstand more than 5 thermal cycles, some of them broke just after 1 cycle, like the ones containing PEO and MDI. Increasing the size of the tablet in this case, leads to major leakage issues, the magnesium chloride leaks from the bottom part of the tablet, as seen in the images from Table 34. A noticeable difference between magnesium sulphate and magnesium chloride working pairs lies in intrinsic lower viscosity of magnesium chloride when melting, which makes more challenging to find a suitable PCM that can synergistically work as a co-matrix and keep the TCM in the structure. Thus, given the poor physical integrity over cycles, magnesium chloride candidates are discarded for further experimental validation.

The working pairs B, C, M, containing HDPE and G, H, I, with Erythritol and PA are the ones that will be a further study in this section.

Table 30. Cycling outputs of the MgSO₄/HDPE working pairs studied in the scale-up section for 1, 5,15, 25 and 40 cycles. Note that samples in green are considered suitable in the validation study, while samples in red are discarded.

Working pair (TCM/PCM)	Cycles	A-90 wt.%/10 wt.%	B-85 wt.%/15 wt.%	C-80 wt.%/20 wt.%	M-75 wt.%/25 wt.%
MgSO₄/HDPE	1 cycle				
	5 cycles				
	15 cycles				
	25 cycles				
	40 cycles				

Table 31. Cycling outputs of the MgSO4/MDI and MgSO4/CLU working pairs studied in the scale-up section for 1, 5 and 15 cycles. Note that samples in green are considered suitable in the validation study, while samples in red are discarded.

Working pair (TCM/PCM)	Cycles	J-85 wt.%/15 wt.%	K-80 wt.%/20 wt.%	L-75 wt.%/25 wt.%
MgSO₄/MDI	1 cycle	-		
	5 cycles	-		

	Cycles	D-90 wt.%/10 wt.%	E-85 wt.%/15 wt.%	F-80 wt.%/20 wt.%	
MgSO₄/CLU	1 cycle				-
	5 cycles				-
	15 cycles				-

Table 32. Cycling outputs of the MgSO$_4$/E/PA working pairs studied in the scale-up section for 1, 5,15, 25 and 40 cycles. Note that samples in green are considered suitable in the validation study, while samples in red are discarded.
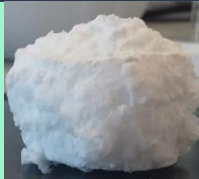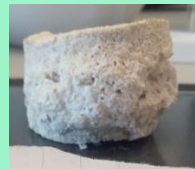
Working pair (TCM/PCM)	Cycles	G- 80 wt./vol.%	H-90 wt./vol.%	I-100 wt./vol.%
MgSO$_4$/E/PA	1 cycle			
	5 cycles			
	15 cycles			
	25 cycles			
	40 cycles			

Table 33. Cycling outputs of the MgCl$_2$/HDPE working pairs studied in the scale-up section for 1, 5 and 15 cycles. Note that samples in green are considered suitable in the validation study, while samples in red are discarded.

Working pair (TCM/PCM)	Cycles	N-85 wt.% /15 wt.%	O-80 wt.% /20 wt.%	P-75 wt.% /25 wt.%
MgCl$_2$/HDPE	1 cycle			
	5 cycles			
	10 cycles		-	-

Table 34. Cycling outputs of the $MgCl_2$/MDI and $MgCl_2$/PEO working pairs studied in the scale-up section for 1 and 5 cycles. Note that samples in green are considered suitable in the validation study, while samples in red are discarded.

Working pair (TCM/PCM)	Cycles		Q-85 wt.% /15 wt.%	R-80 wt.% /20 wt.%	S-75 wt.% /25 wt.%
$MgCl_2$/MDI	1 cycle	-			
	5 cycles	-			
	Cycles		T-85 wt.% /15 wt.%	U-80 wt.% /20 wt.%	V-75 wt./% 25 wt.%
$MgCl_2$/PEO	1 cycle	-			
	5 cycles	-			

(3.2) Sorption process/Energy stored (STA)

The dehydration conversion of 1 cycle and 40 cycles samples are compared in Figure 88, the reaction rate at the highest conversion rate is also shown in the graph. The conversion rate appears to be slightly higher at larger cycling stages, as demonstrated in the proof of concept section. The 3 in 1 composite reaches a stable structure over cycles that enables the hydration/dehydration processes in the TCM/PCM structure. The dehydration process consists of one stage, which involves the loss of 5 mols of water from hexahydrate to monohydrate from 25 °C to 150 °C (see Figure 102). As stated, the dehydration step of epsomite (from Hexa to hepta) is complex and can be described as a deceleration reaction controlled by interface advancement [8].

Conversions rates range around 80-97% for the HDPE working pairs and 70-90% for the PA/Erythritol working pairs. Note that a small amount of sample is tested (20-30 mg), which might increase the error of the test due to heterogeneities in the actual sample composition. Calculations are made assuming that the ratio of TCM/PCM is constant and homogeneous throughout the composite. Hence, this data is compared within samples, but larger mass should be tested to ensure accurate results. Generally, reaction rates are slightly lower than pure magnesium sulphate (0.066 min^{-1} at hydration/dehydration cycle), especially for M, that is the one with the highest content of HDPE 25 wt.% Thus, lower percentages of HDPE seem to favour the TCM reaction while 25 wt.% leads to a third of the reaction rate of the pure TCM. Besides, the reaction rate value is consistent after 40 cycles. The formulation I (100 wt./vol.% of 90/10 MgSO$_4$/E in the gel solution) exhibits the highest reaction rate, whereas no significant differences can be seen between MgSO$_4$/HDPE and MgSO$_4$/E/PA samples, dehydration-wise. Ruiz-Agudo et al. [8] observed during the latest stages of the reaction a reduction in the reaction rate when adding additives into pure Epsomite, among them polyacrylamide acid, which was associated with the obstruction of the diffusional

removal of the gaseous product by the surface product layer and the stronger bonding of H_2O molecules in lower hydrates.
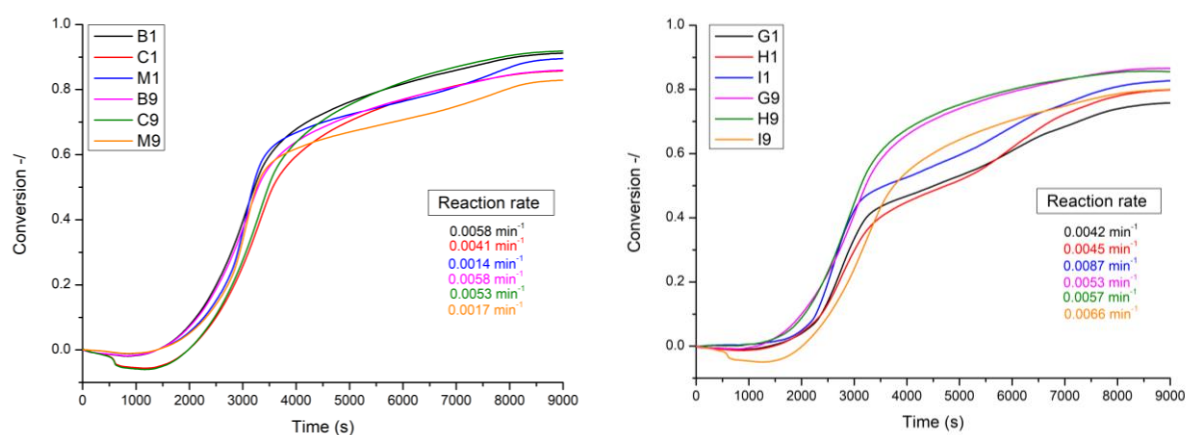
Figure 88. Dehydration conversion vs time of the samples containing erythritol and gel (G, H, I) for one cycle (1) and 40 cycles (9) in the left figure and the formulations with HDPE (B, C, M) for one cycle (1) and 40 cycles (9) in the right figure. Note that the data is averaged from two sets of measurements. STA program from 25 °C to 150 °C at 1 °C/min-hold 60 min.

The hydration also takes place in one step, enabling the full hydration of the TCM up to 5 mols of water. Comparing the hydration curves of the 1 g tablets with the scaled-up (20 g) ones, similar behaviour can be seen as the hydration process of the composites is faster than the pure TCM, with conversions of 90% for the hydration reaction in less than two hours and a half (pure TCM needs 3h to fully hydrate). However, the 20 g tablets show larger hydration times (114-180 min) than the 1 g tablets (70-150 min). Comparing the 40-cycled composites in the tablet form to the 1-cycled samples, the 40 cycled one takes longer to reach χ90 (90% conversion). This might be because, as stated in the proof of concept, the structure created by the polymer and the thermochemical material takes some cycles to stabilize and it is key to allow for a higher and a more steady conversion rate.
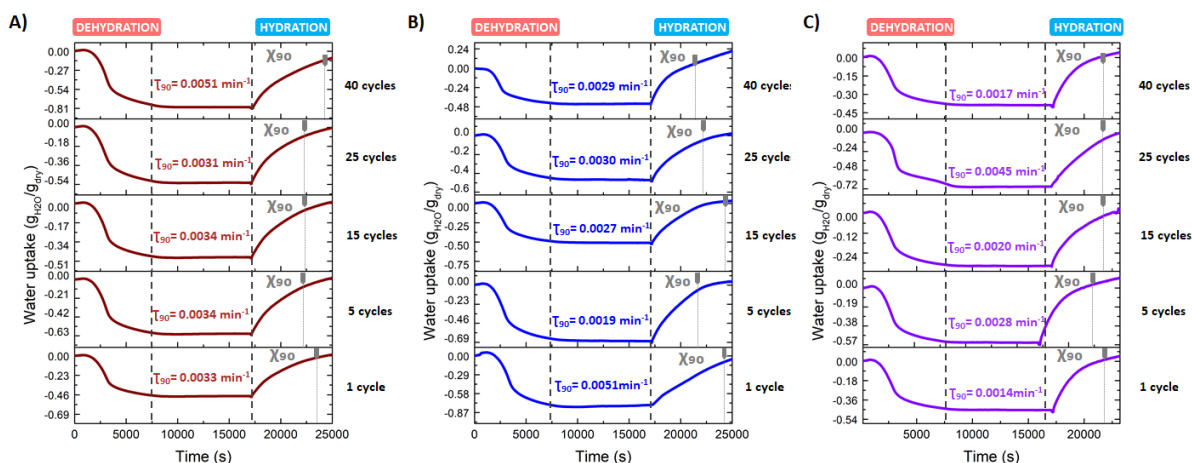
Figure 89. A) Water uptake of the 85 wt.% $MgSO_4 \cdot 7H_2O$ and 15 wt.% HDPE (hydration/dehydration); B) Water uptake of the 80 wt.% $MgSO_4 \cdot 7H_2O$ and 20 wt.% HDPE (hydration/dehydration) and C) Water uptake of the 75 wt.% $MgSO_4 \cdot 7H_2O$ and 25 wt.% HDPE (hydration/dehydration). Note that the data is averaged from two sets of measurements. STA program from 25 °C to 150 °C at 1 °C/min-hold 60 min; hydration at 30 °C 80% R.H. for 2.5 h.
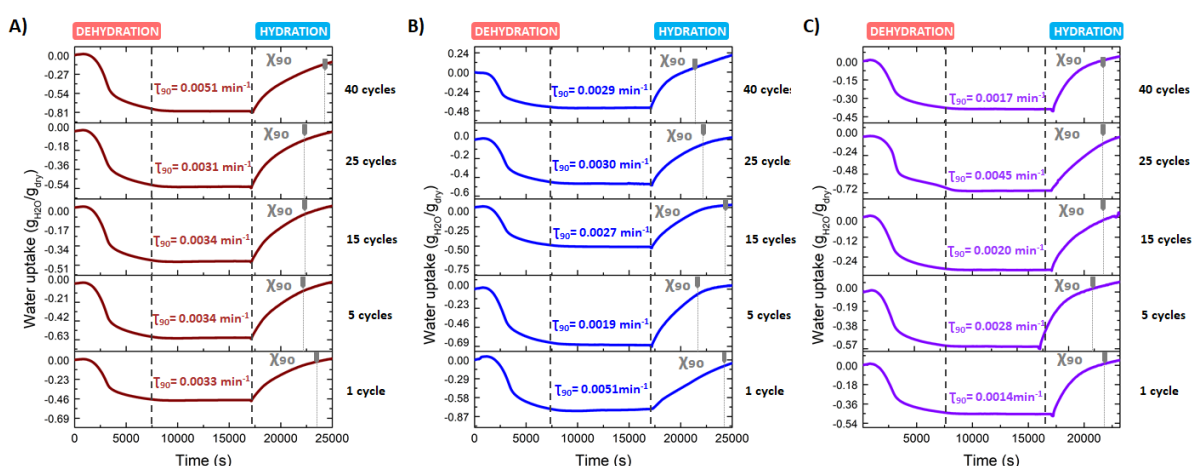
Figure 90. A) Water uptake of $MgSO_4 \cdot 7H_2O$/E 80 wt./vol.% of gel solution (hydration/dehydration) B) Water uptake of $MgSO_4 \cdot 7H_2O$/E 90 wt./vol.% of gel solution (hydration/dehydration) and C) Water uptake of $MgSO_4 \cdot 7H_2O$/E 100 wt./vol.% of gel solution (hydration/dehydration). Note that the data is averaged from two sets of measurements. STA program from 25 °C to 150 °C at 1 °C/min-hold 60 min; hydration at 30 °C 80% R.H. for 2.5 h.

The energy stored by the working pairs is illustrated in Figure 91 (B and D), overall, the samples containing erythritol exhibit significantly higher energy storage values as the SLPCM has a higher specific heat capacity and larger latent heat capacity than the SSPCM, HDPE (see Chapter 8). The sample B10 and G10 (40 cycles) are the ones that show higher energy storage, 1040 kJ/kg for G10 and 1120 kJ/kg for B10, both higher than pure TCM. The 20 g MgSO4/HDPE working pairs are also compared to the 80/20- 1 g tested in the proof of concept, concluding that the energy stored by the 20 g tablets is higher after 15 thermal cycles. The energy density (see Figure 91 (A) and (C)) reach values up to 2.4 GJ·m^{-3} for the MgSO$_4$/E/PA working pair and 2.1 GJ·m^{-3} for the MgSO$_4$/HDPE working pairs. The cost of the material per energy stored is in the range shown for the proof of concept, just slightly higher for B-15 cycles and G-25 cycles.
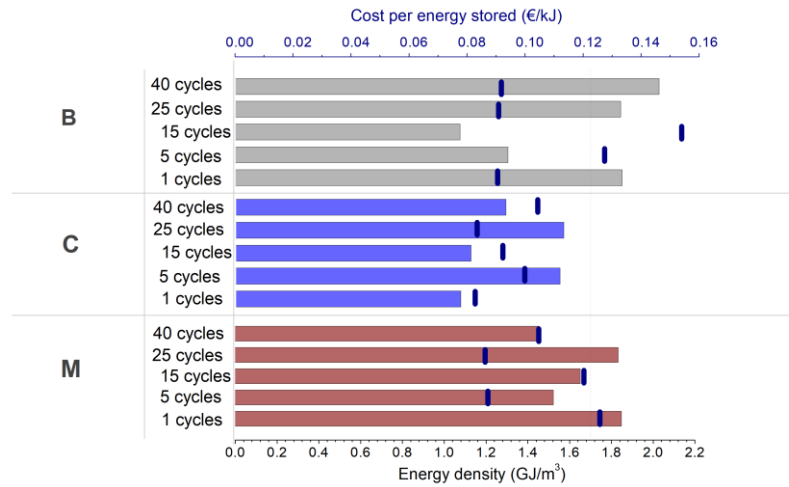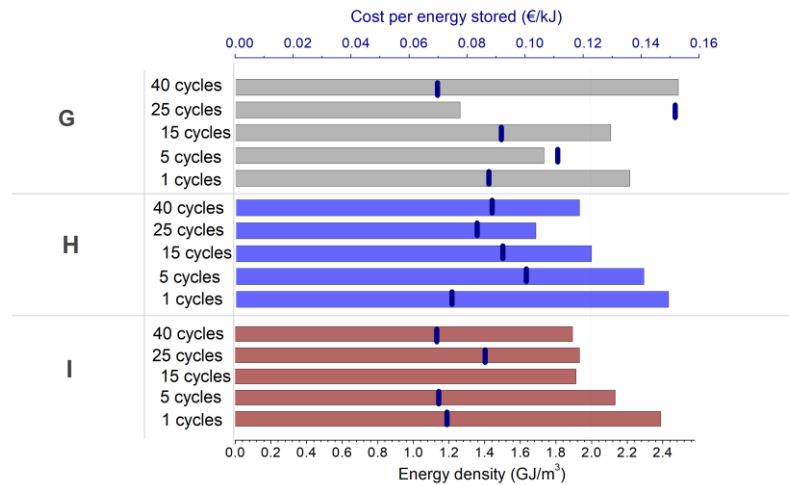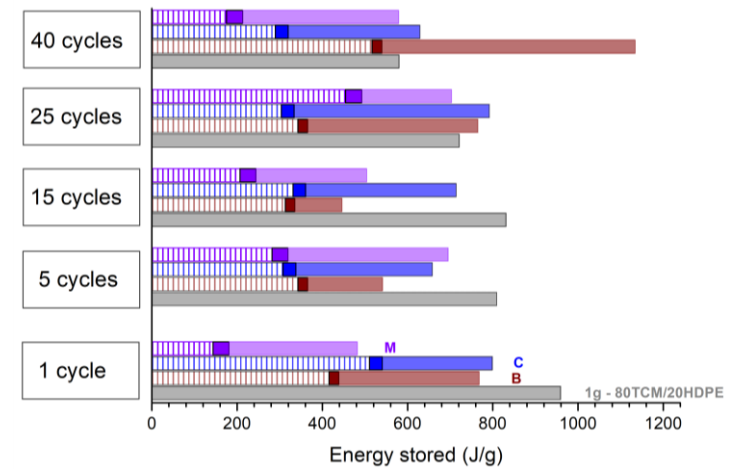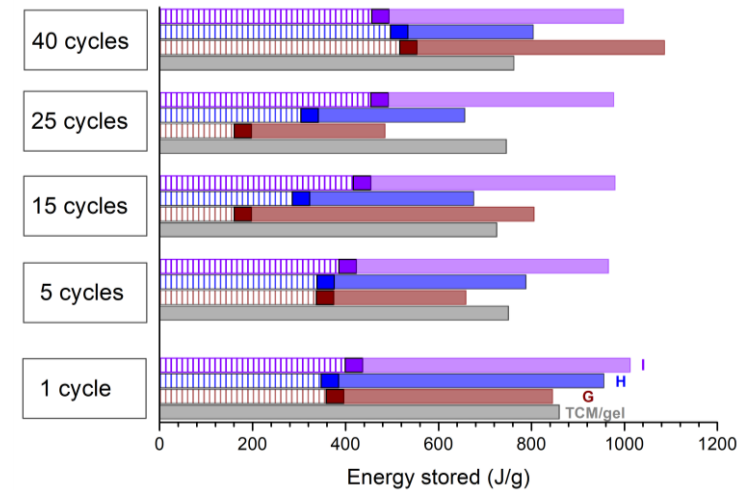
Figure 91. (A) The energy density (GJ·m⁻³) and material cost (€/kJ) of B, C and M formulations. (C) The energy density (GJ·m⁻³) and material cost (€/kJ) of G, I and H formulations. (B) Energy density stored by component (sensible, thermochemical and latent) for the 1g- 80 wt. % TCM/20 wt.% PCM, B, C and M. (D) Energy density stored by component (sensible (vertical lines) , thermochemical (deep colour) and latent (light colour)) for the TCM/gel, G, H and I.

(3.3) Chemical stability (XRD and Raman)

The $MgSO_4$/HDPE from 25 °C to 150 °C XRD patterns are very similar to the ones reported by pure magnesium sulfate after the first dehydration/hydration cycle, as well as the absence of low hydrated magnesium sulfate phases (e.g. less than 6 mol H_2O per mol $MgSO_4$) [9]. Interestingly, the XRD patterns of the samples after cycling (1, 15 and 40 cycles) reveal that a portion of the TCM material converts into kieserite, the crystalline structure of $MgSO_4·1$ H_2O [9,10] above 70 °C, instead of fully converting into the monohydrate amorphous structure as reported in the literature [4], and like the powder samples characterised in the proof of concept section. Such structure has been reported to be synthetically formed at specific and controlled pressure and temperature conditions [11]. Kieserite is a monoclinic structure, while HDPE, which has a crystallinity of up to 80%, can be found in orthogonal and monoclinic cells [12]. Tetragonal, orthorhombic and monoclinic phases are only slight distortions of the cubic structure [13]. Besides, the selection of nucleating agents mainly follows the rules proposed by Telkers that nucleating agents must have less than 15% variation in the unit cell from the existing structure [14]. Thus, given their crystal structure similarities, they could act as nucleation agents when present in small percentages in the main crystalline structure (monoclinic or orthorhombic in this case) and favour the partial formation of the crystalline monohydrate phase. Even though, the amorphous phase is still present as confirmed by the XRD patterns (note that $MgSO_4· 1$ H_2O* refers to patterns with a noticeable content of amorphous phase). Therefore, a percentage of the TCM might follow the route (1) from hexahydrate to monohydrate monoclinic and another portion route (2), from hexahydrate to monohydrate amorphous. The intensity of kieserite varies within the XRD patterns, which denotes that the ratio amorphous/crystalline phase is heterogeneous throughout the tablet TCM/PCM content. Besides, a tendency to an increasing crystallinity content over cycles is observed in the XRD patterns from 1 to 40 cycles as the intensity of the peaks is higher and

broad X-ray scattering profiles from the amorphous phase can be seen. Given the heterogeneity of the samples and the small amount tested, it is difficult to draw any conclusions related to the percentage of crystalline monohydrate formed.

While in the literature the formation of the amorphous phase has been related to slow reaction rates at pressures <13 mbar, in the 3 in 1 system this seems to be partially tackled by the addition of HDPE, which favours the reorganization of the crystal structure forming an ordered arrangement (monoclinic). Along with this, HDPE appears to recrystallize into the initial structure not increasing the amorphous content within the polymer structure as seen in the X-Ray diffraction patterns (see Figure 72 to Figure 94). The crystal diffraction peaks from HDPE can be seen around $2\theta = 21.6°$ and $23.8°$ [75] up to 120 °C, they disappear at 150 °C due to the melting of the polymer and reappear given the recrystallisation at 25 °C after cooling down. This is also seen in the DSC curves as proven in the latent heat study in the following Section 3.4.

The MgSO$_4$-E-PA working pairs X-Ray diffractograms are similar to the ones of MgSO$_4$-HDPE in terms of the dehydration behaviour of magnesium sulphate (see Figure 95 to Figure 97). The crystalline monohydrate phase Kieresite is also present in this case, sharper peaks with lower amorphous content than in the HDPE samples, which is also attributed to the amorphous content of the polymer in the MgSO$_4$-HDPE samples. Following the same rationale; erythritol is a symmetrical molecule and therefore it exists in only one form, the mesoform [15], meso erythritol forms a tetragonal structure in which the molecules are centrosymmetric [16]. Hence, the formation of kieserite in the gel/E dopped samples could be attributed as well to the tetragonal structure, which acts as nucleating agent that along with the reaction rate reduction favour the formation of the crystalline MgSO$_4$·1H$_2$O. The crystal diffraction peaks from erythritol are identified at around $2\theta = 15°$ and $21°$-$20°$ [17,18] as observed in Figure 98 (B and C), where the pure erythritol and erythritol prepared in gel solution (4 wt./vol.% PA and

100 wt./vol.% E) are measured for reference purposes. Looking at the diffractograms of the MgSO$_4$-E-PA (see Figure 95 to Figure 97), it can be seen that given the lower and heterogeneous concentration of the sugar in the composite, the peaks are low-intensity and cannot be easily identified in all the samples. For instance, G5, H1, H5, H9 and I5 diffractograms are a good example to identify the erythritol peaks, visible up to 90 °C as the melting takes place at around 120 °C. Recrystallisation peaks cannot be identified in the MgSO$_4$-E-PA, although a semicrystalline/amorphous phase is identified in pure Erythritol and PA-Erythritol samples after cooling down at 2.5 °C/min, as reported by Nakano et al. [17]. Such cooling rate has been reported to be slow enough to allow the recrystallisation of the sugar at 25 °C [17,18]. Also, the presence of magnesium sulphate affects the recrystallisation process of erythritol when cooling down as the initial crystalline peaks (2θ = 15° and 21°-20°) can be identified from 1 to 40 cycles. It has been reported that, in the bulk state, a solid/solid transformation, from a crystalline phase immediately after cold-crystallization to another crystalline phase similar to the single crystal of erythritol, occurred after leaving the solid at 293 K for several hours or during the heating process [18]. Such a process was also reported not to involve heat, with no appreciable peak in the DSC as it is driven as a diffusional process. Nakano et al. [17] studied the effect of confining erythritol into different mesoporous structures. They observed an interesting effect in one their formulations suggesting a similar solid/solid transformation occurred involving heat when erythritol became semi-amorphous in the heating process, whereas such a solid/solid transformation did not occur when erythritol crystallized (at around room temperature) in the cooling process. This is what appears to happen in the MgSO$_4$-E-PA composites, as confirmed by the DSC peaks, where no-peaks can be seen for Erythritol while the pure erythritol crystallises under the same conditions (see Figure 103).

Once the monohydrate crystalline phase has been identified in the XRD patterns, the conversion rates for hydration and dehydration as the rehydration from kieserite is studied and compared with the values from the amorphous phase. However as reported by Steiger et al. [9] the complete conversion to hexahydrite was rapidly achieved at 65%, 70%, 75%, and 80% RH, which are within the hydration conditions of this study. Besides, the hydration of MgSO4 · 1 H$_2$O (kieserite) and the formation of MgSO$_4$ · 6H$_2$O (hexahydrite) was defined as kinetically hindered. The authors found out that above the deliquescence humidity of kieserite, the reaction proceeds via a two-stage reaction pathway involving the dissolution of kieserite and the subsequent crystallization of hexahydrite from a highly supersaturated solution [9]. Therefore, the initial hexahydrite state can be reached for both amorphous and crystalline monohydrate.

Raman spectroscopy was used as a complementary technique to X-Ray diffraction. A mapping of the bottom (part in contact with the tray) and top (part contact with the environment) surfaces of the tablets was conducted to 1-cycle and 40-cycles samples. Kieresite, hexahydrite, erythritol and HDPE peaks were identified (see Figure 99 (D) and Figure 100 (D)) as reported in the literature; Wang et al. [19] for magnesium sulphate species, Mignani et al. [20] for erythritol peaks and Ibrahim et al. [21] for HDPE. The hydrated magnesium sulphates could just be identified in the spectral region of SO$_4$ fundamental vibrational modes, given that the Mg-sulfates peaks are in the spectral region of water OH stretching vibrational modes and could not be identified in these measurements.

A coloured mapping of the surface is provided for MgSO$_4$-HDPE working pairs in Figure 99 A, B and C. From the 27 points measured in different locations of the tablet surface, one can conclude that HDPE has a higher concentration at the bottom of the tablet, an effect that is aggravated over cycles. This might be given to the higher viscosity of HDPE in comparison to magnesium sulphate. While magnesium sulphate remains "static" in the structure, HDPE has

mobility and flows when melting, which leads to an apparent higher content of polymer in the bottom of the tablet. However, this cannot be quantified by the Raman technique. Besides, amorphous content can be observed as the patterns present a tendency to the Boson peak [22,23], which is characteristic of non-crystalline or semicrystalline structures (amorphous HDPE content). Again, the monohydrate crystalline phase has also been identified in the hydrated tablet, which confirms that part of the hexahydrite is converting into kieserite. This data indicates that a percentage of kieserite might not be transforming to hexahydrate and remain in the lattice structure of the magnesium sulfate hexahydrate as the crystalline monohydrate, which would lower the reaction rate and conversion. However, there are just a few points identified in this test and other techniques should be used to confirm this phenomenon, among them high-temperature Raman, calorimetry measurement at a very slow heating rate, etc.

The $MgSO_4$PA-gel working pairs could just be characterised at 1 cycle, due to the high scattering of the 40 cycle measurements that severely reduce Raman signal-to-noise ratios (backscattering mode), no peaks were recorded in those measurements, this might be related to the particle size as reported by Gómez et al. [24]. The 1 cycle samples showed a homogeneous distribution of magnesium sulphate hexahydrate and erythritol at the bottom and top of the tablet, unlike $MgSO_4$-HDPE working pairs, that showed a heterogeneous distribution of PCM and TCM in the composite. This is provided by the 3D gel structure that allows proper distribution of the components. In this case, it was difficult to identify magnesium sulphate monohydrate as the main peak overlaps with the main erythritol peak 1046.1 cm^{-1} and 1046 cm^{-1}, respectively. However, some spectrums, as the one shown in Figure 100 (D), enable the identification of 6 points containing hexahydrite, kieserite and erythritol.
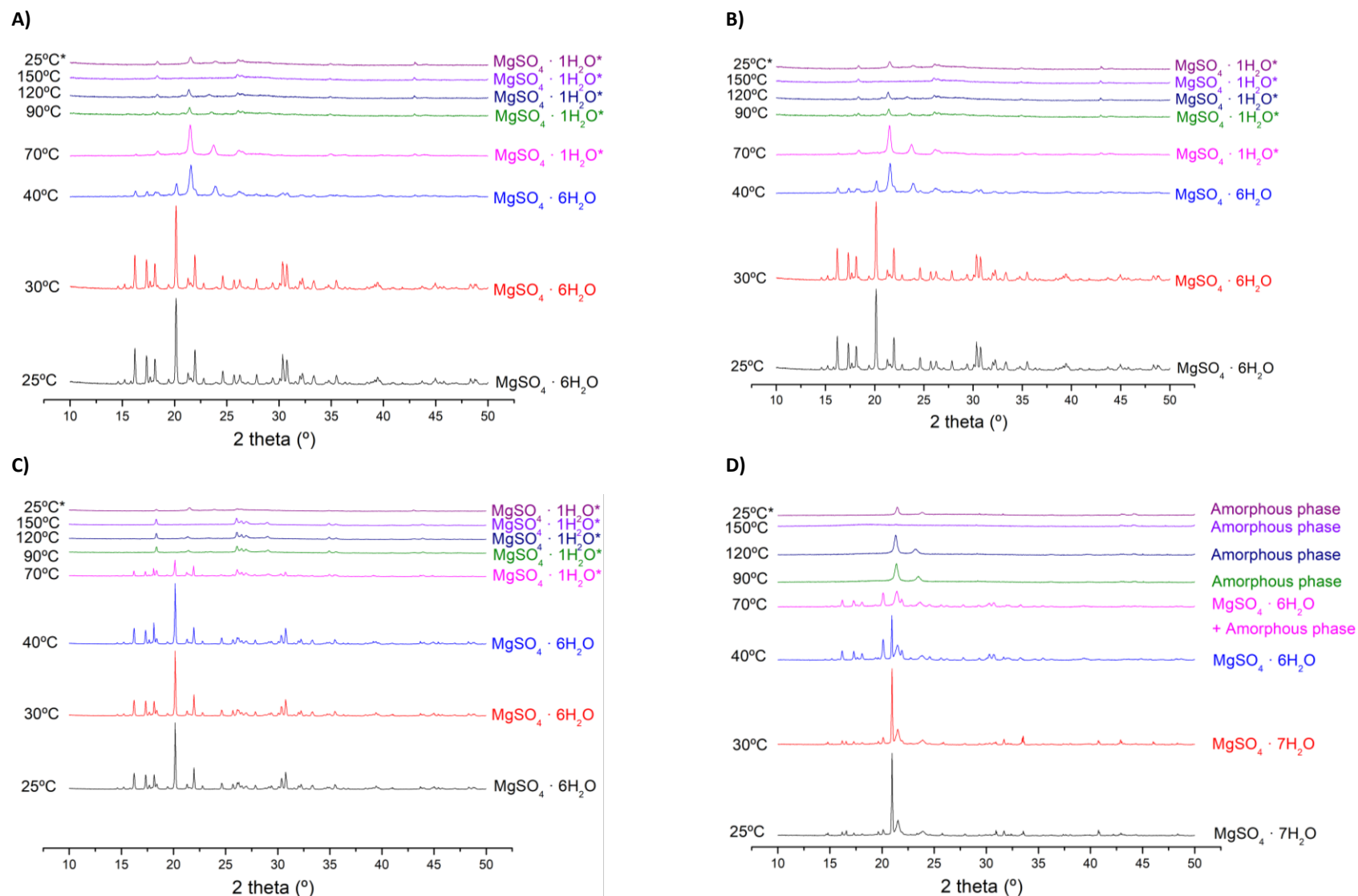
Figure 92. XRD patterns at increasing temperatures (from 25 °C to 150 °C at 1 °C/min-hold 30 min and cooling from 150 °C to 25°C at 2.5 °C /min) for (A) M1 (1 cycle), (B) M5 (15 cycles), (C) M9 (40 cycles) and (D) 75% $MgSO_4$/25% HDPE. Note that $MgSO_4 \cdot 1H_2O$ * identify patterns with a high content of the amorphous phase and 25 °C* are the diffraction patterns for the cooling process.
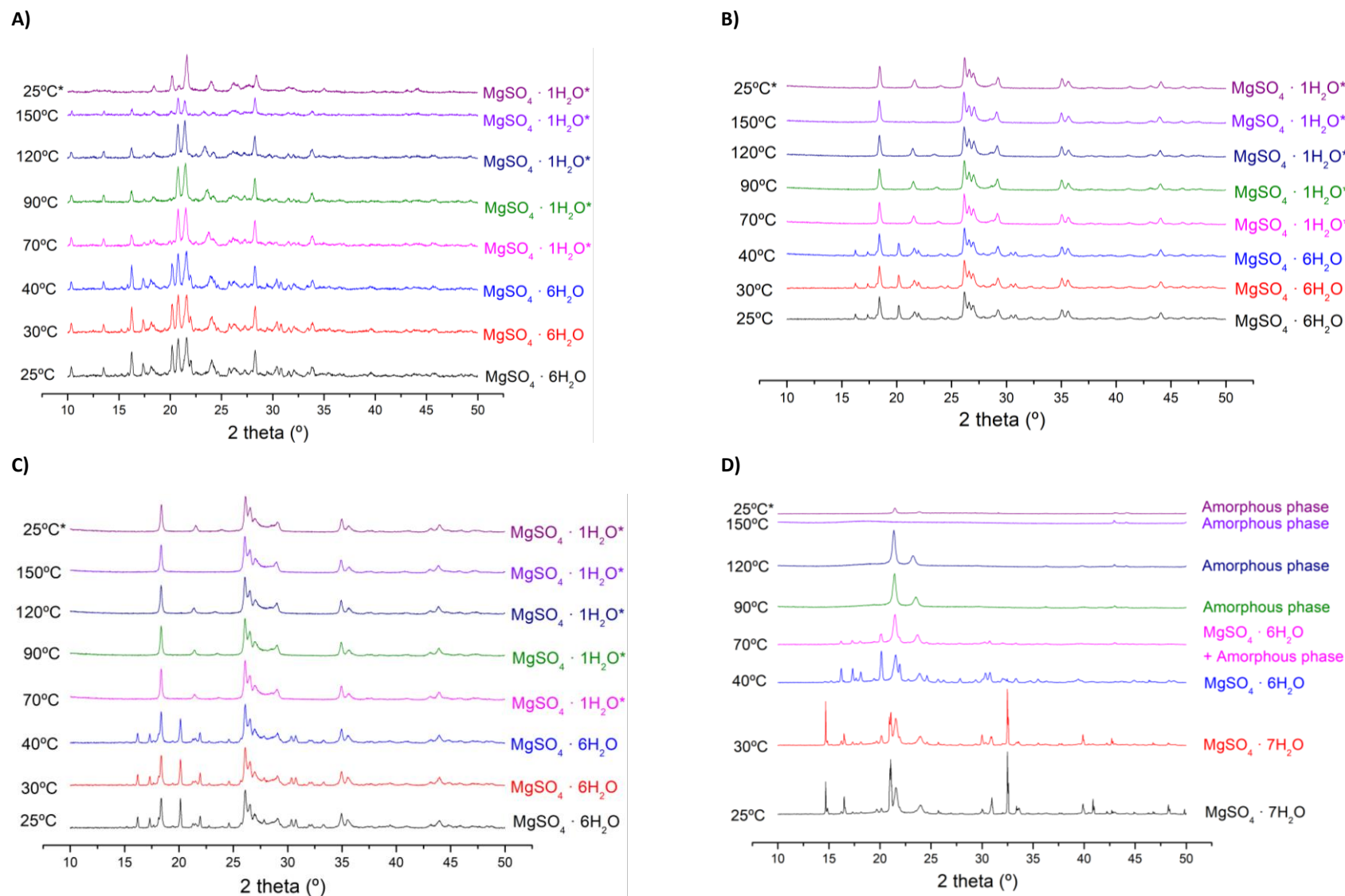
Figure 93. XRD patterns at increasing temperatures (from 25 °C to 150 °C at 1 °C/min-hold 30 min and cooling from 150 °C to 25°C at 2.5 °C /min) for (A) C1 (1 cycle), (B) C5 (15 cycles), (C) C9 (40 cycles) and (D) 80 wt.% MgSO$_4$/20 wt.% HDPE. Note that MgSO$_4$·1H$_2$O * identify patterns with a high content of the amorphous phase and 25 °C* are the diffraction patterns for the cooling process.
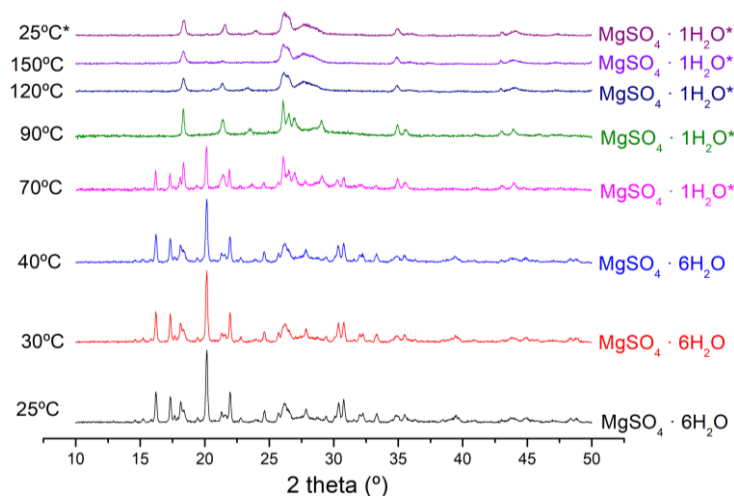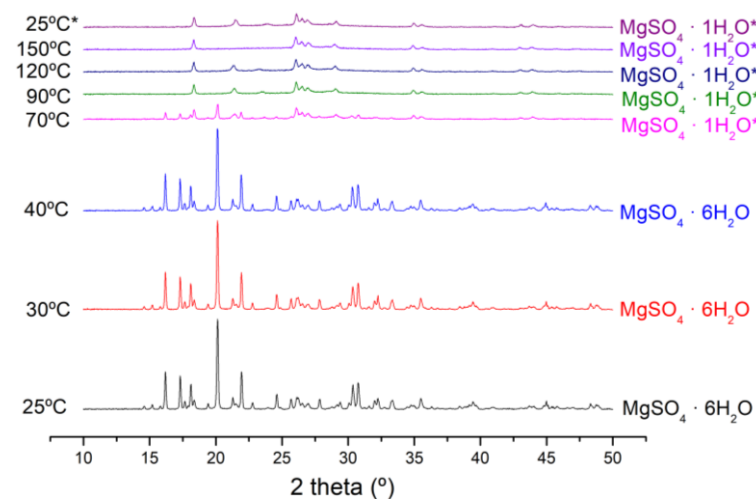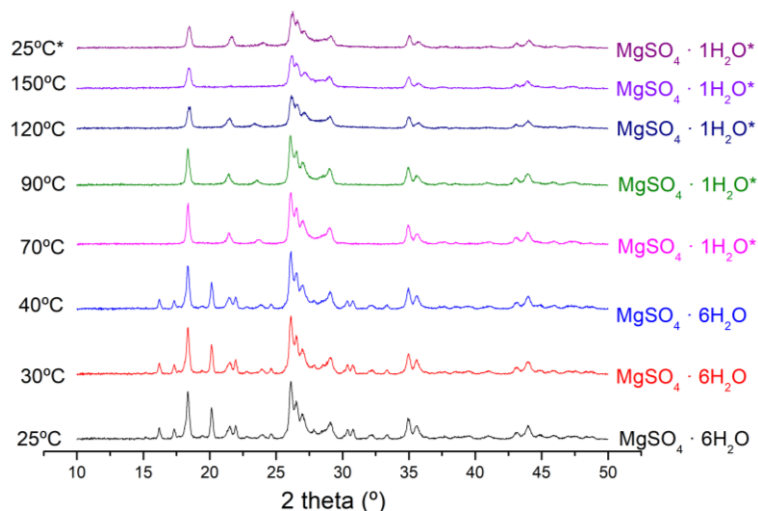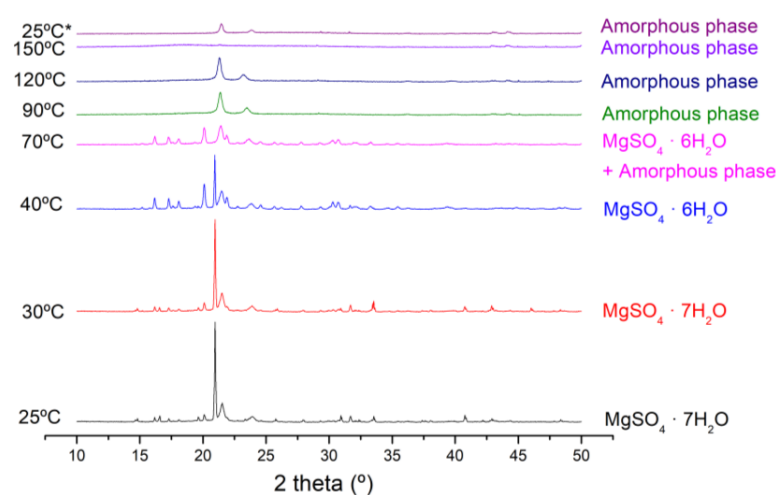
Figure 94. XRD patterns at increasing temperatures (from 25 °C to 150 °C at 1 °C/min-hold 30 min and cooling from 150 °C to 25°C at 2.5 °C /min) for (A) B1 (1 cycle), (B) B5 (15 cycles), (C) B9 (40 cycles) and (D) 85 wt.% $MgSO_4$/15 wt.% HDPE. Note that $MgSO_4$ $1H_2O$ * identify patterns with a high content of the amorphous phase and 25 °C* are the diffraction patterns for the cooling process.
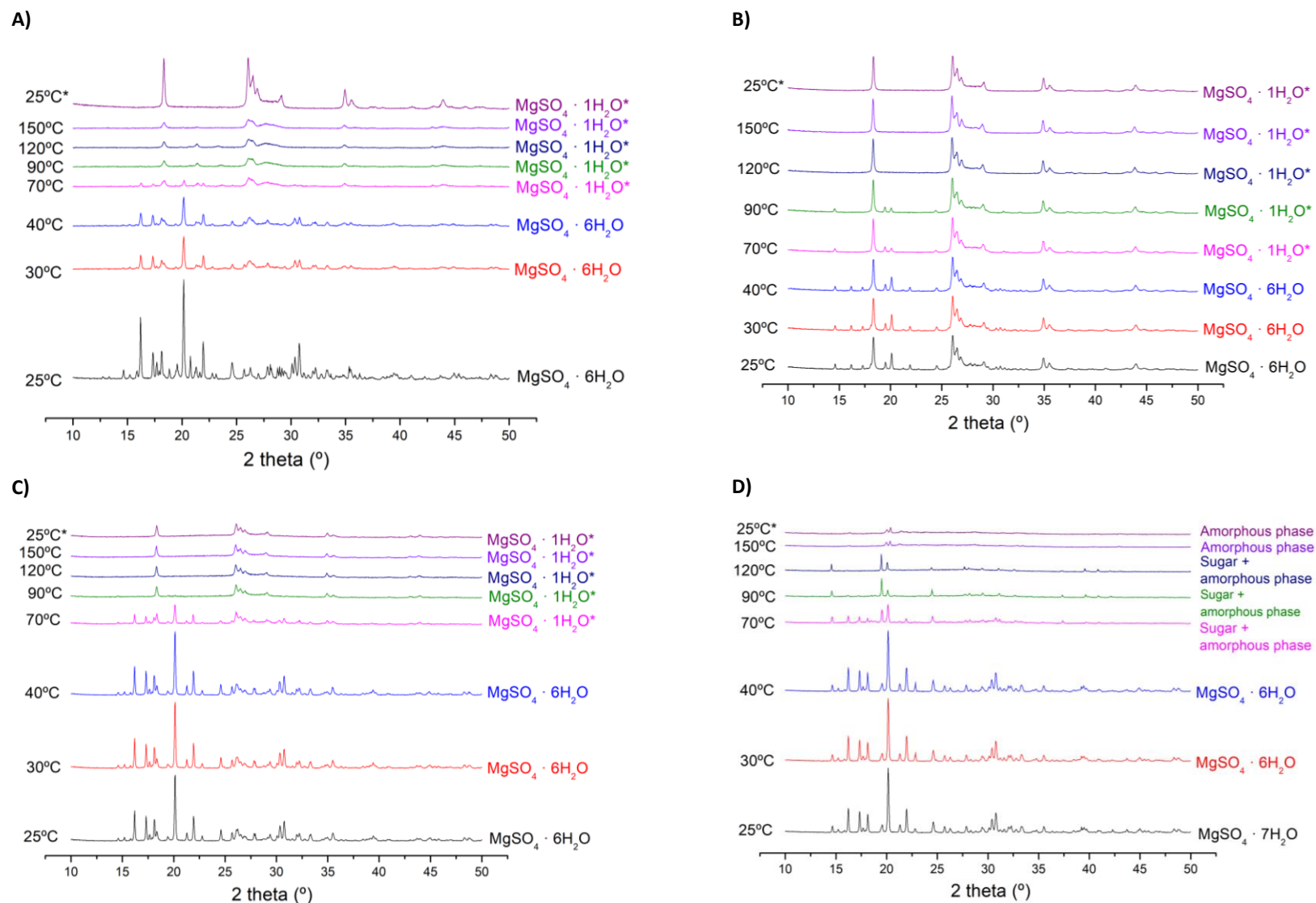
Figure 95. XRD patterns at increasing temperatures (from 25 °C to 150 °C at 1 °C/min-hold 30 min and cooling from 150 °C to 25°C at 2.5 °C /min) for (A) G1 (1 cycle), (B) G5 (15 cycles), (C) G9 (40 cycles) and (D) 80 wt./vol. of $MgSO_4$/E/PA. Note that $MgSO_4 \cdot 1H_2O$ * identify patterns with a high content of the amorphous phase and 25 °C* are the diffraction patterns for the cooling process.

A)

B)

C)

D)
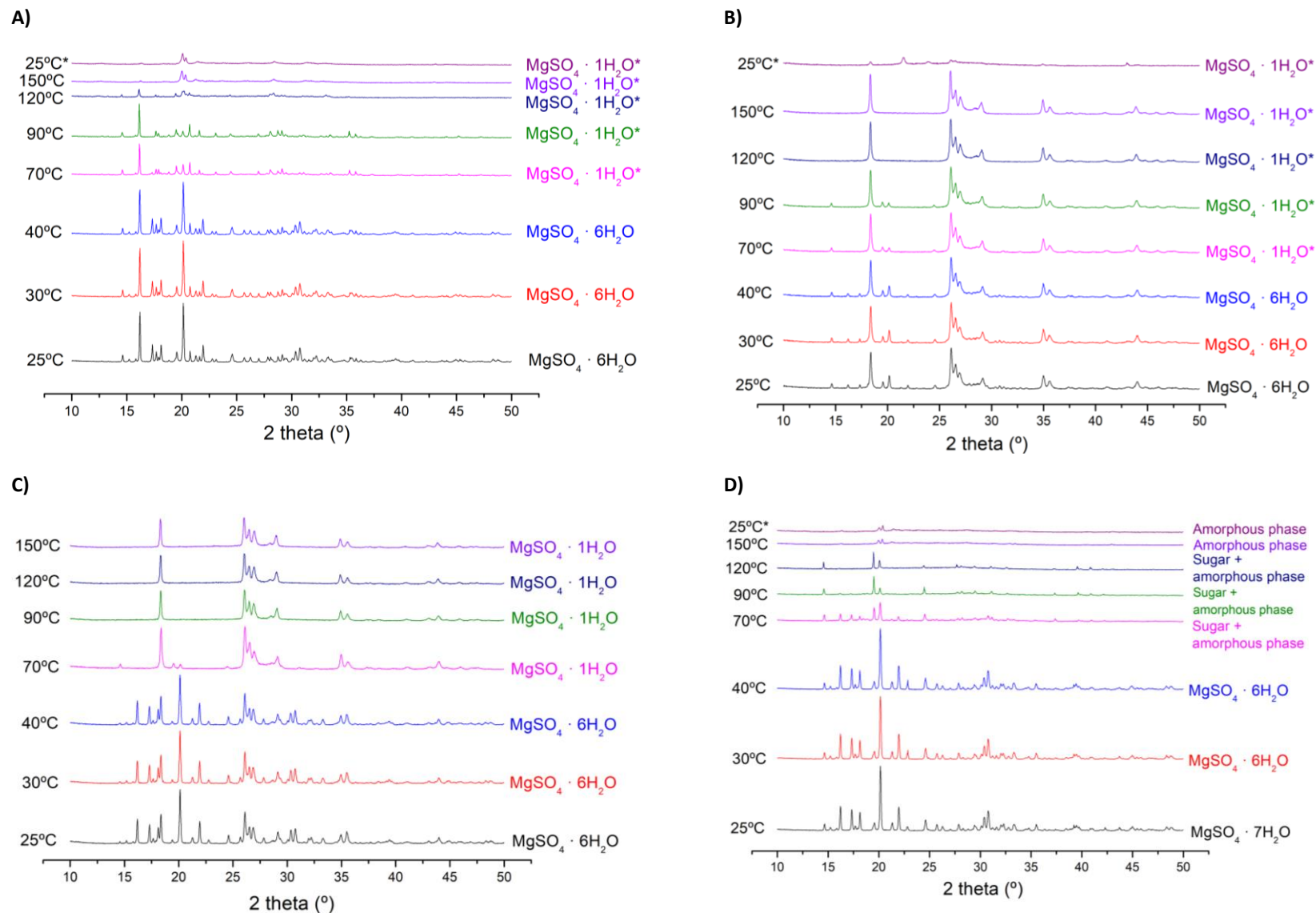
Figure 96. XRD patterns at increasing temperatures (from 25 °C to 150 °C at 1 °C/min-hold 30 min and cooling from 150 °C to 25°C at 2.5 °C /min) for (A) H1 (1 cycle), (B) H5 (15 cycles), (C) H9 (40 cycles) and (D) 90 wt./vol. of MgSO$_4$/E/PA. Note that MgSO$_4$·1H$_2$O * identify patterns with a high content of the amorphous phase and 25 °C* are the diffraction patterns for the cooling process.
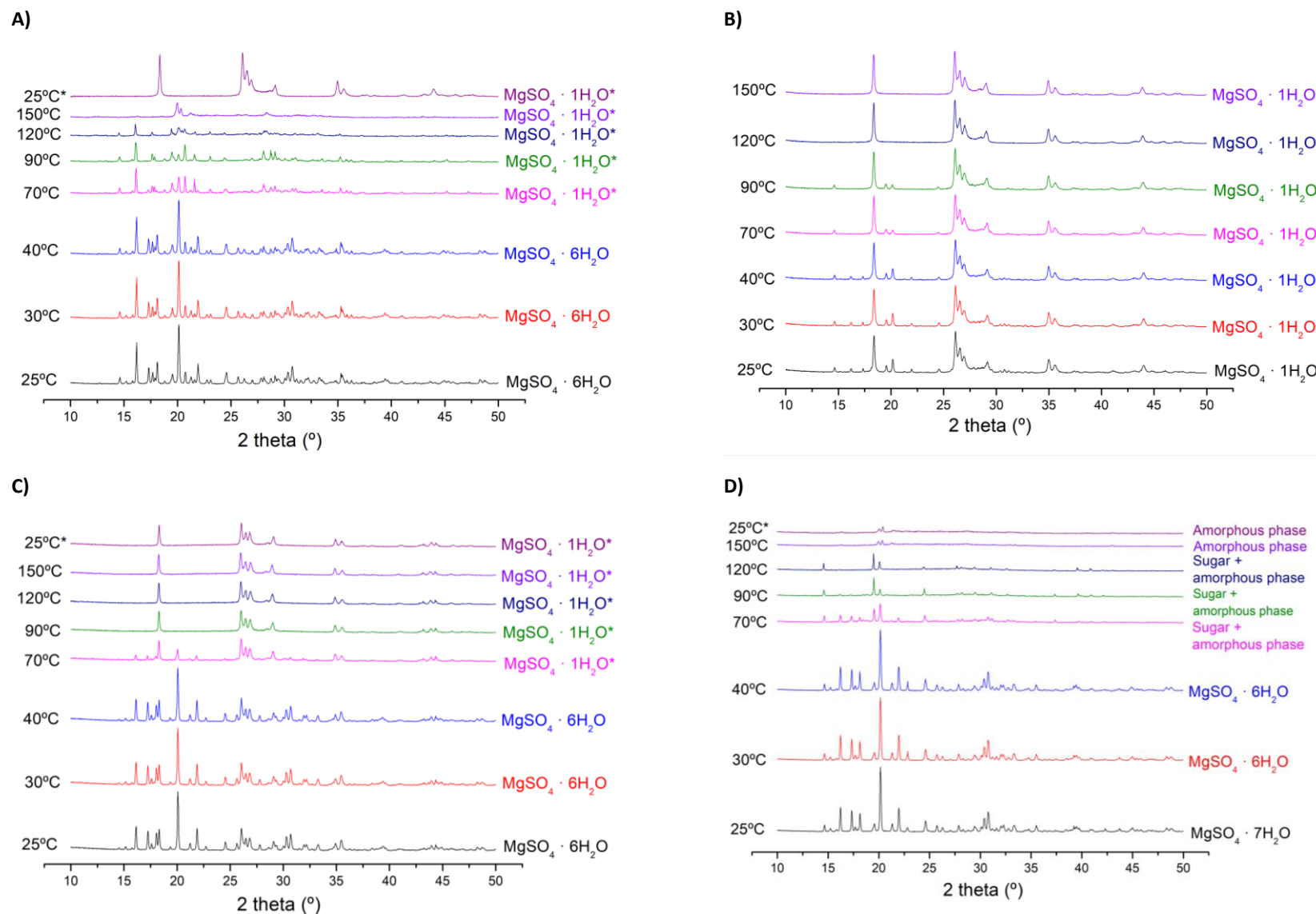
Figure 97. XRD patterns at increasing temperatures (from 25 °C to 150 °C at 1 °C/min-hold 30 min and cooling from 150 °C to 25°C at 2.5 °C /min) for (A) I1 (1 cycle), (B) I5 (15 cycles) (C), I9 (40 cycles) and (D) 100 wt./vol. of MgSO$_4$/E/PA. Note that MgSO$_4$·1H$_2$O * identify patterns with a high content of the amorphous phase and 25 °C* are the diffraction patterns for the cooling process.
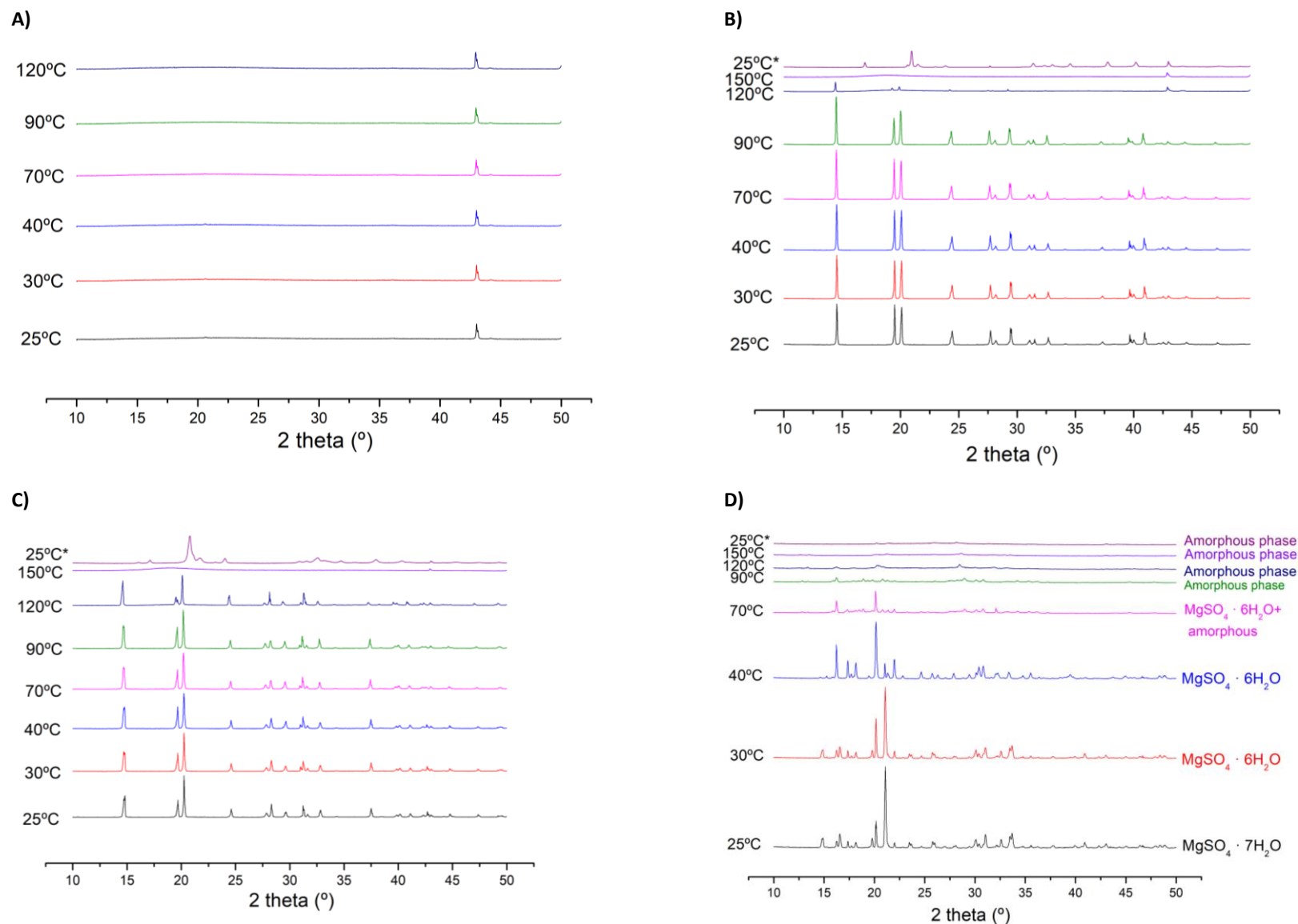
Figure 98. XRD patterns at increasing temperatures (from 25 °C to 150 °C at 1 °C/min-hold 30 min and cooling from 150 °C to 25°C at 2.5 °C /min) for (A) PA, (B) Erythritol (C), Erythritol/PA and (D) MgSO$_4$/PA. Note that 25 °C* is the diffraction patterns for the cooling process.
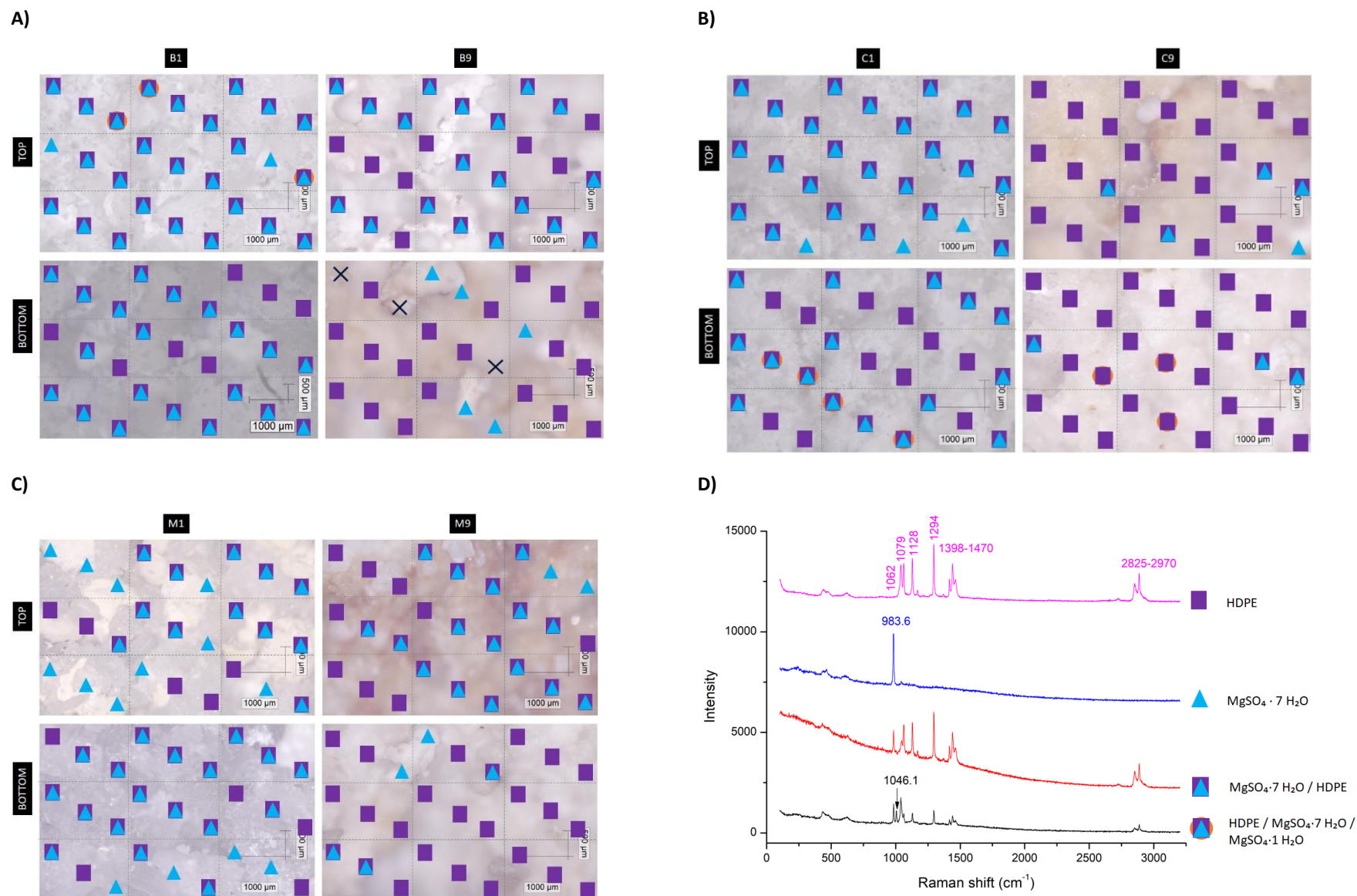
Figure 99. Raman 3x3 mapping images (bottom and top) with scanned points identified, following legend on the graph (D); (A) B1 and B9 samples, (B) C1 and C9 samples, (C) M1 and M9 samples.
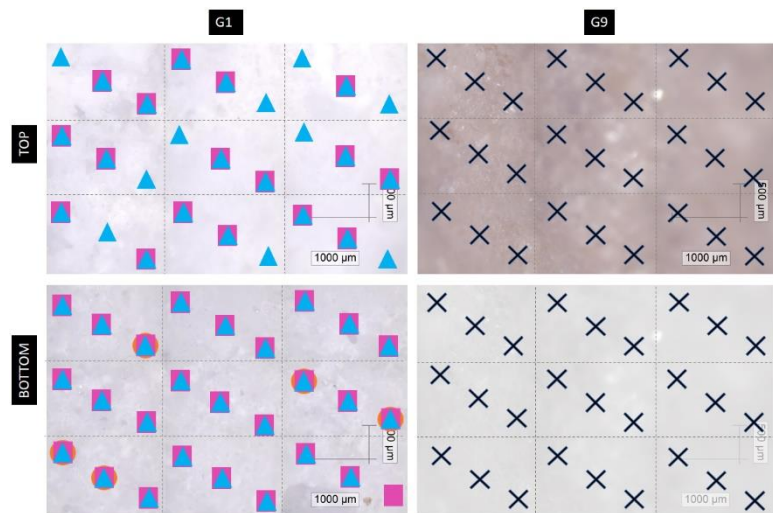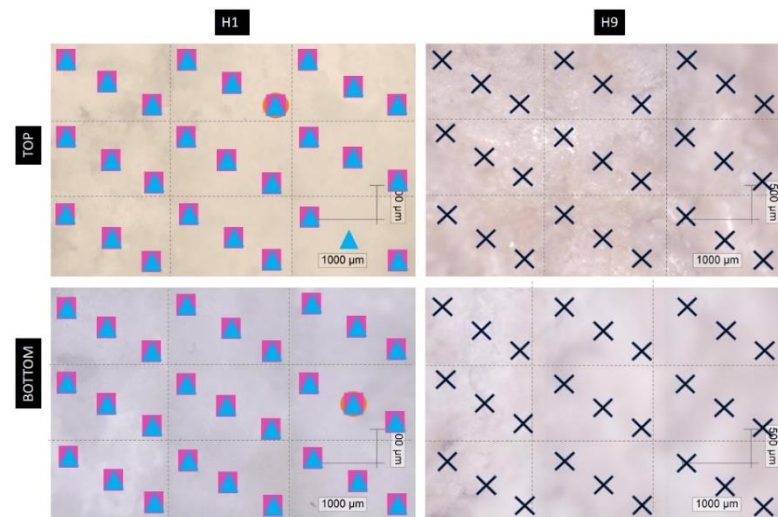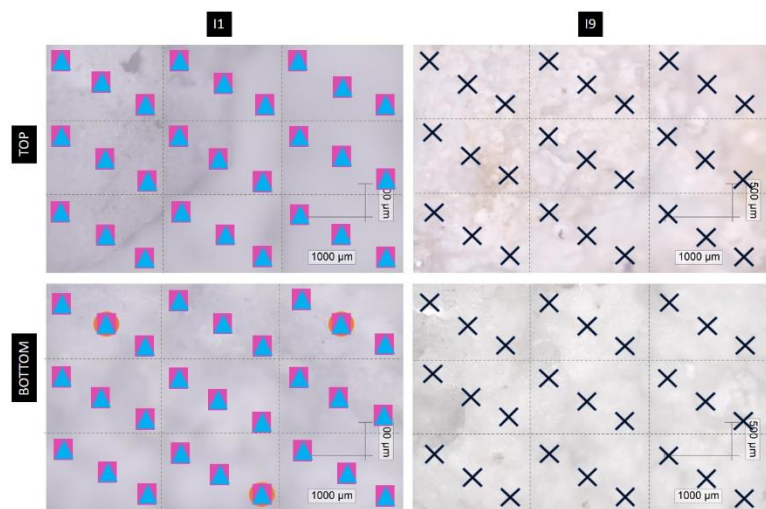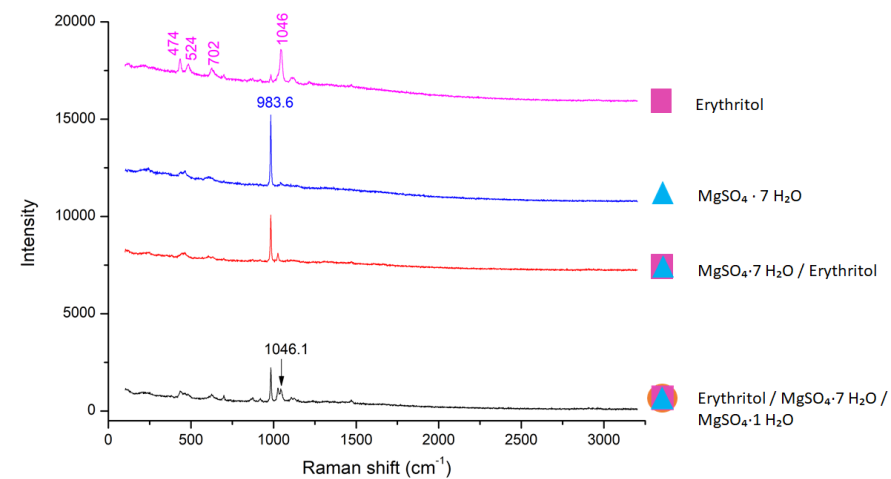
Figure 100. Raman 3x3 mapping images (bottom and top) with scanned points identified, following legend on the graph (D); (A) G1 and G9 samples, (B) H1 and H9 samples, (C) I1 and I9 samples.

(3.4) Microstructure and porosity (XRT)

The reconstruction of the microstructured images provided by X-Ray tomography is shown in Table 35, Table 36, Table 37 and Table 38. Samples containing HDPE exhibit a hole right in the middle of the tablet (see Table 35 and Table 36), this effect is even more pronounced with higher TCM content and a larger number of cycles. Whilst B1 and C1 does not show the hollow region when increasing the number of cycles (B5 and C5), this region appears to be larger and does not grow further up to 40 cycles. Both working pairs maintain the tablet physical dimensions (diameter and thickness) even after 40 cycles. This can be correlated to the porosity values obtained (see Figure 101) when at 25 cycles the porosity reaches a constant value, also reported in the proof of concept study. Thus, this phenomenon is attributed to the intrinsic thermochemical behaviour, as suggested in the proof of concept section. A higher percentage of PCM (20-25 wt.%) increases the PCM/TCM contact area, which provides a skeleton to keep the TCM in "static" positions in the composite. While a lower percentage of the polymeric PCM (10-15 wt.%) is not enough to provide enough contact area and retain the structural stability, leading to the TCM's particles agglomeration, which might be the driving force to form the hollow region.

Excess on the polymer content would reduce the porosity requirements and hence hindering the water vapour transport (due to low porosity 11-27%). As an example, the 25 wt.% of HDPE composite, which shrinks to almost a third of the initial thickness along with the thermal cycles.

$MgSO_4$-E-PA working pairs do show a more distributed porosity, also large hollow regions, but not particularly in the centre of the tablet (see Table 37 and Table 38). The porosity also increases over cycles, reaching values around 60%, which would not work at the system level as the mass and heat transfer would be hindered during hydration/dehydration, like a 40-50% bed porosity is required [25]. When 100

wt./vol.% and 90 wt./vol.% of TCM/PCM content in the gel solutions are prepared, the resulting composite eventually collapses the gel structure. The volume expansion during the hydration reaction led to confinement and, therefore, the stress generated during the growth of the hydrated crystals likely causes this collapse phenomenon. Such stress might have been the driving force for the displacement of the dried gel structure formed, which is not as flexible as the polymer one and cannot easily adapt to structural changes. Lower TCM/PCM content (80 wt./vol.%) show better results as the tablet maintains its initial dimensions even after 40 cycles (see Table 32) and the porosity is reasonable for a system-level study.
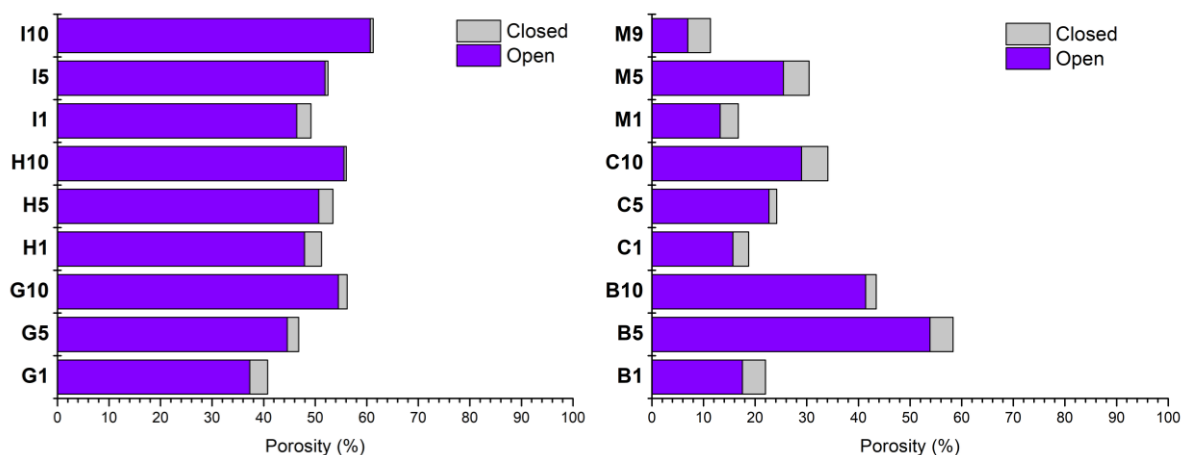
Figure 101. Open and closed porosity percentages calculated through the XRT reconstruction in the 2D model for the MgSO₄/HDPE working pairs (left) and MgSO₄/E/PA (right).

Table 35. XRT Reconstruction images of samples B1, B5, B9 and C1 from top to bottom of the tablet.
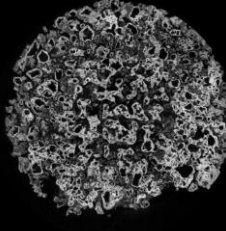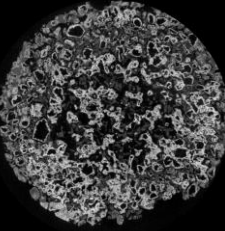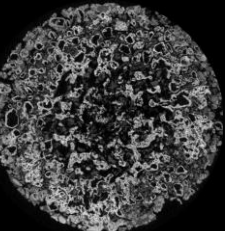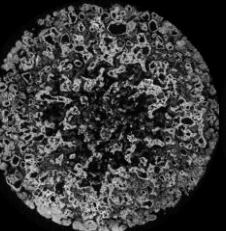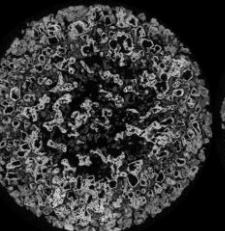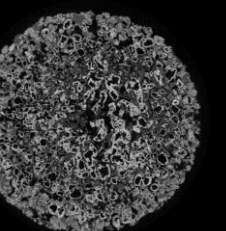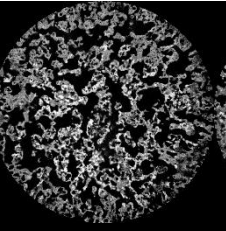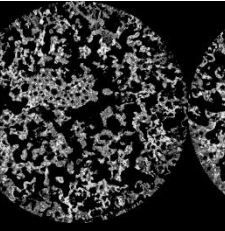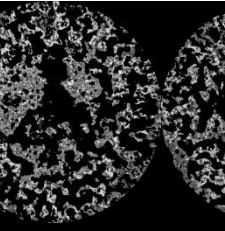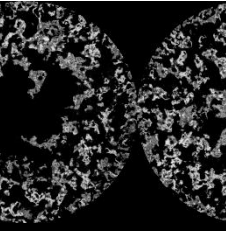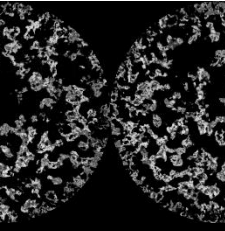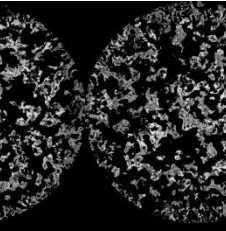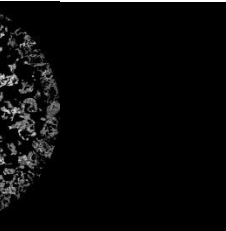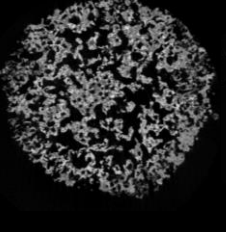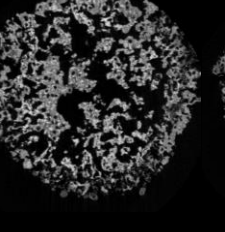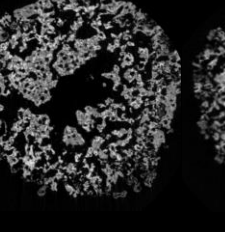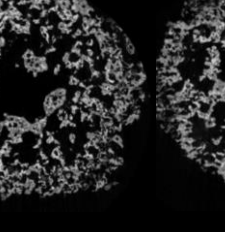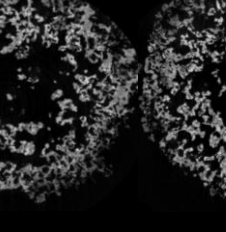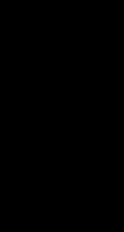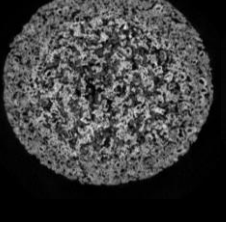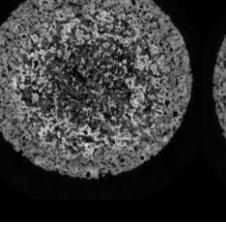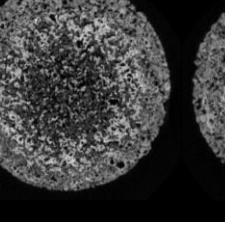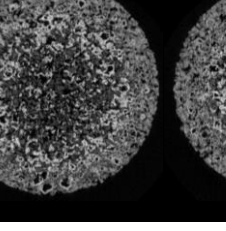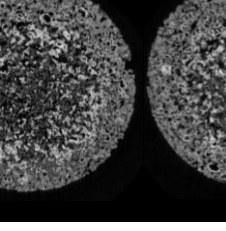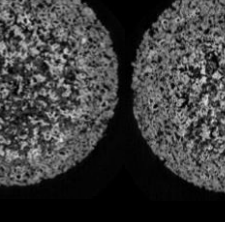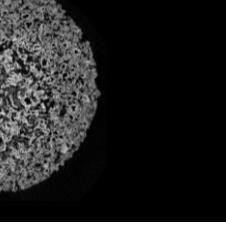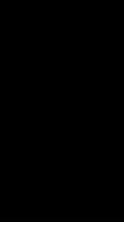
Table 36. XRT Reconstruction images of samples C5, C9, M1 and M5 from top to bottom of the tablet.
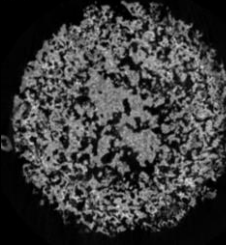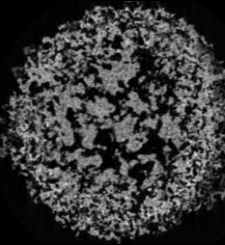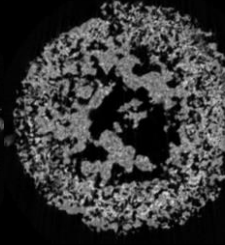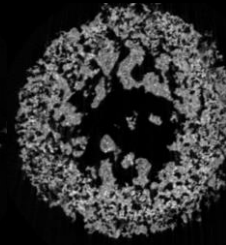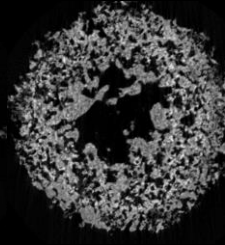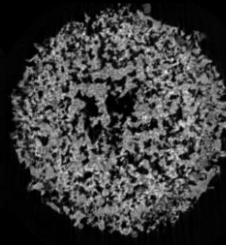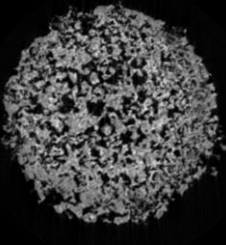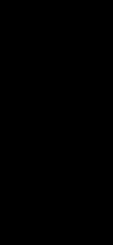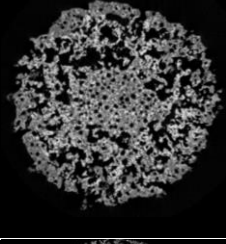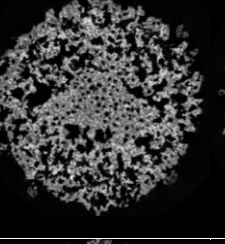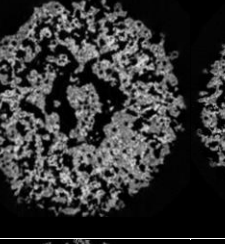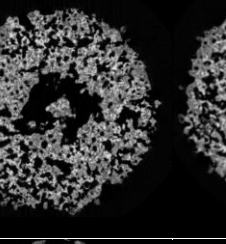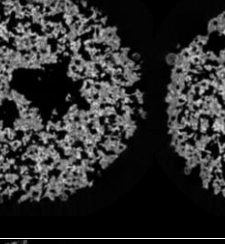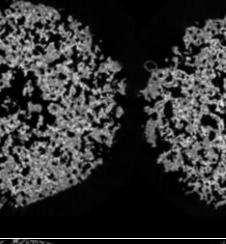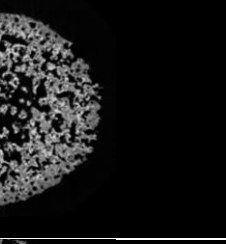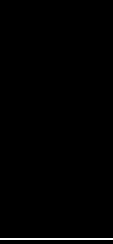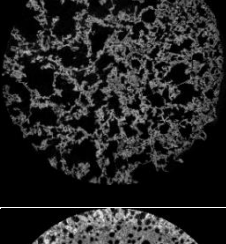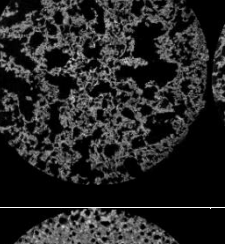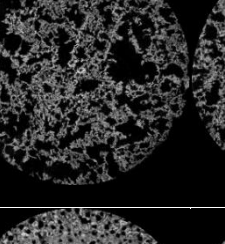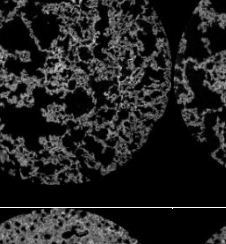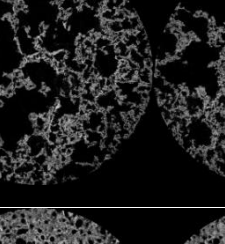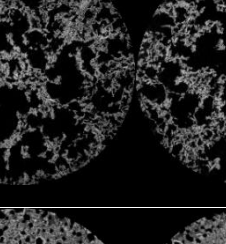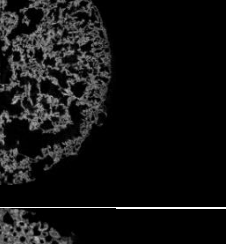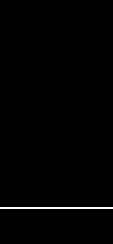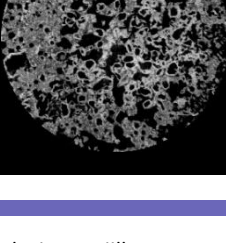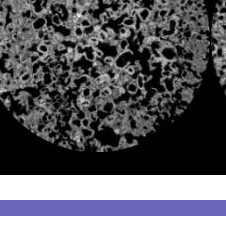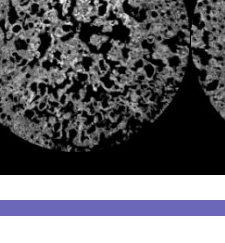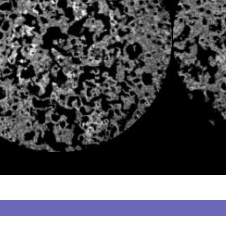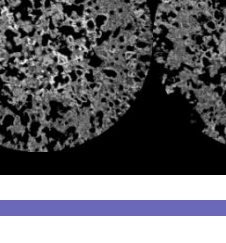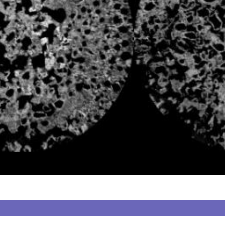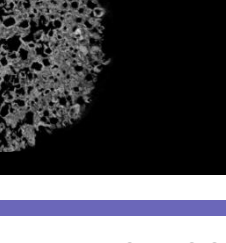
Table 37. XRT Reconstruction images of samples M9, G1, G5 and G5 from top to bottom of the tablet.
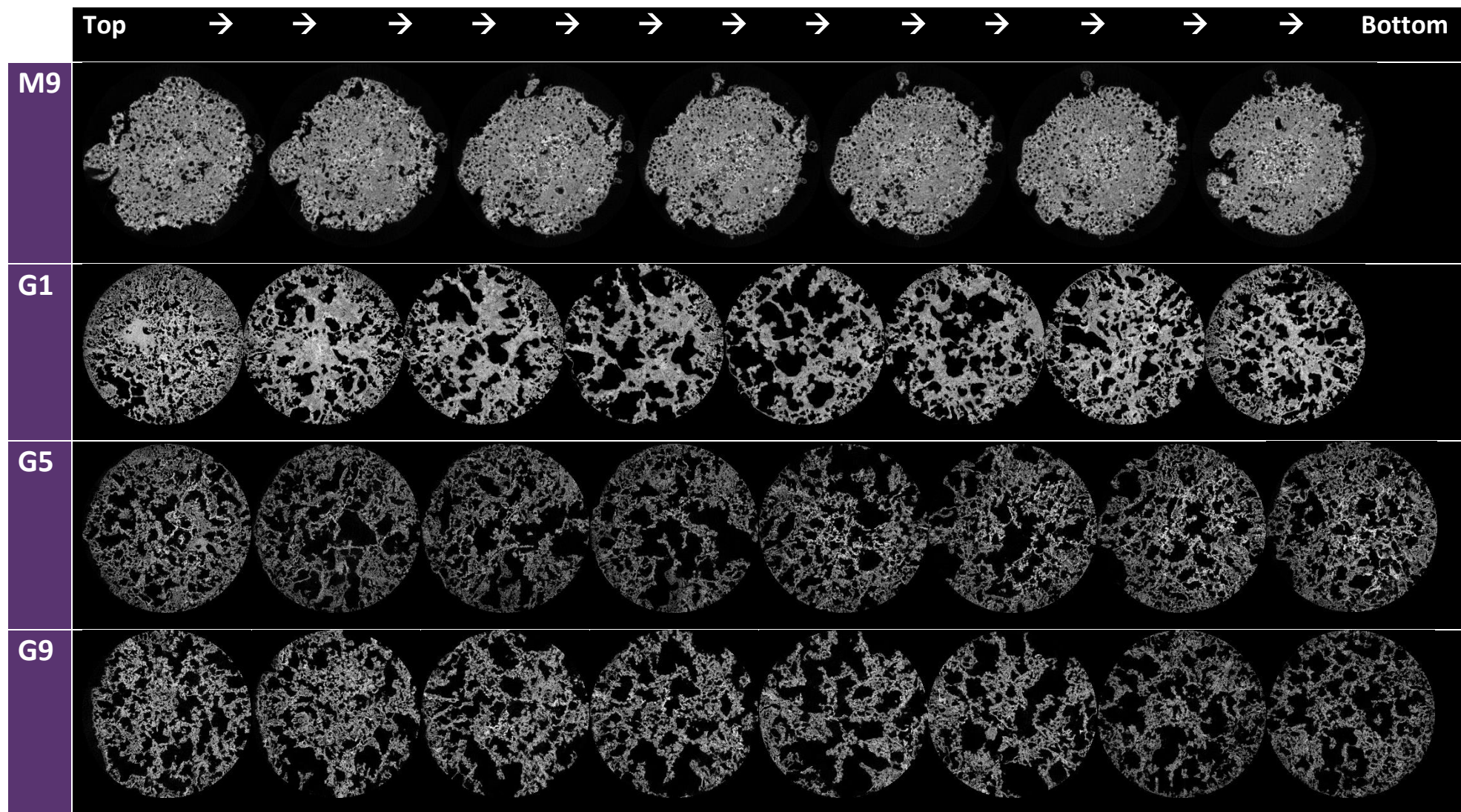
Table 38. XRT Reconstruction images of samples H1, H9, I1 and I9 from top to bottom of the tablet. Note that the set of samples H and I are just included for 1 cycle and 40 cycles.
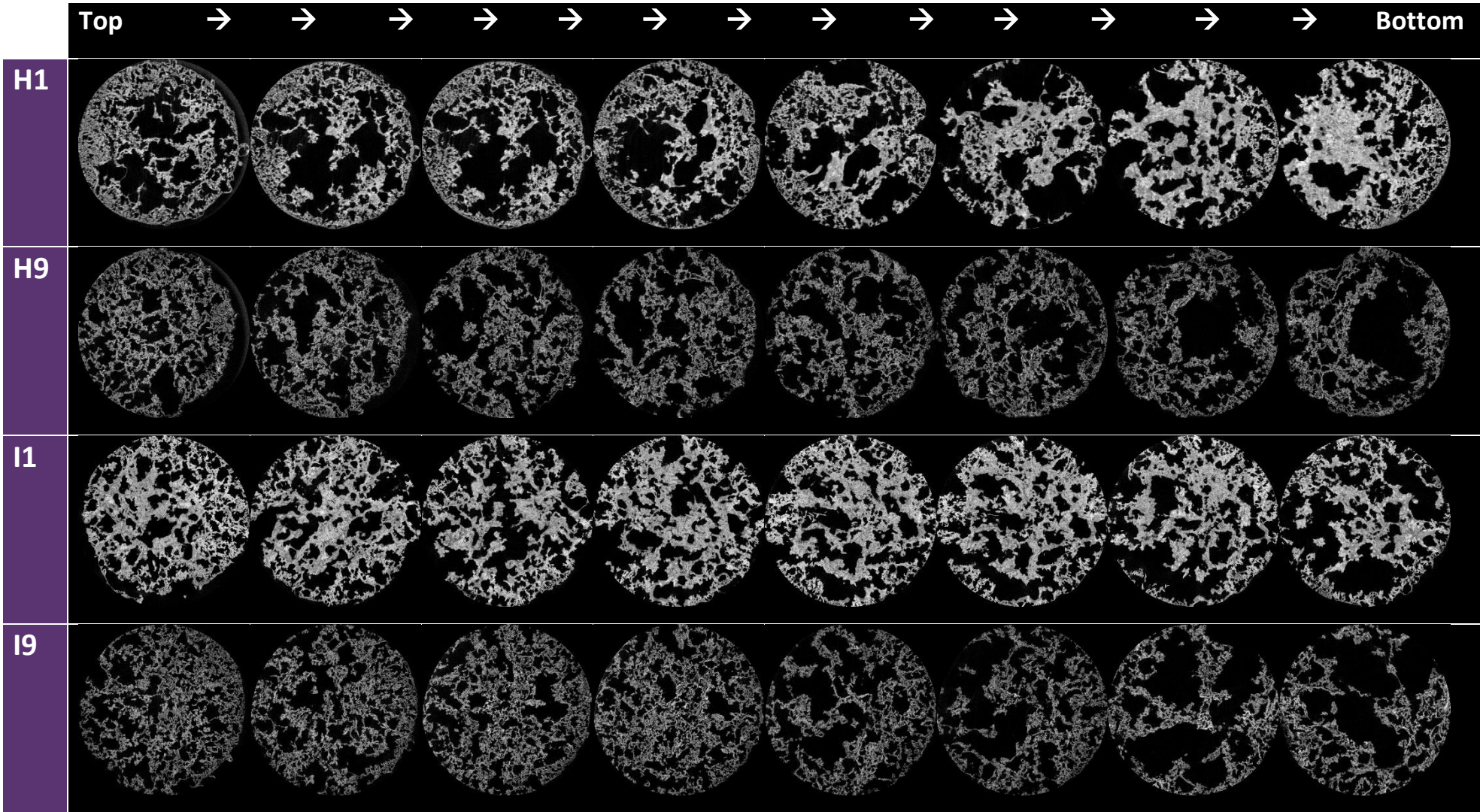
(3.4) Interaction between TCM and PCM

As reported by Seven et al. [26], during nucleation the polymer HDPE undergoes a phase change upon cooling where chains orient and align at the molecular scale into a periodic lattice. During crystal growth, polymer chains orient around the initial nucleation site, or nucleus, in a 3D pattern most often forming a spherical crystal cluster called a spherulite. Complete crystallization occurs when the crystalline and noncrystalline domains become space-filling. There are three classes of nucleation: (1) homogeneous nucleation or spontaneous nucleation; (2) self-nucleation; and (3) heterogeneous nucleation [27]. Nucleation and crystal morphology is affected by the addition of nucleating agents (NA) that promote heterogeneous nucleation. The presence of thermochemical material in the crystallisation process of HDPE could affect its crystallinity degree as well as the nucleation mechanism. The heat flow curves for the heating and cooling of HDPE in the $MgSO_4$-HDPE composite (B1, C1 and M1) are shown in Figure 102. Considering that the content of HDPE might vary within samples given the heterogeneous character of the sample, HDPE shows to crystallise even after 40 heating cycles. Comparing the heating and cooling curves non significant subcooling effect can be observed, ± 5 degrees of difference is within the error associated to the measurements of the equipment and also can be attributed to the different cooling heating rate, 1 °C/min and cooling 2.5 °C/min respectively. Besides, pure HDPE shows a melting point onset of 125-127 °C and peak at 130-132 °C, while in the 3 in 1 system the melting point of HDPE is wider and moved to lower temperatures with an onset of 110 °C. This might be attributed to chemical-physical effect of the TCM that advances the latent heat physical process.

Regarding sugar alcohols solidification mechanisms, kinetics and crystal morphologies depend on the bulk temperature. Hence, increasing the undercooling degree leads to morphological transitions [17,28]. Erythritol presents a maximum crystal growth velocity of > 400 µm/s maximum [17] and is expected to present major supercooling issues due to poor nucleation characteristic and slow crystal growth rate, although the mechanism is still not clearly understood. Besides, solidification

and crystallization phase change enthalpy differs and not all the energy stored can be retrieved [29]. The dopping of some additives (e.g. polyalcohols) and the confinement in nanopores have been reported to control of freezing and melting temperatures and reduce supercooling degree [28]. One would wonder if the addition of TCM into the sugar structure would have any effect on the supercooling degree of sugar alcohol. Looking at the DSC curves, no peaks can be identified for erythritol in none of the sample curves (G1, H1 and I1), see Figure 102. Hence, confirming that the recrystallisation is diffusion forces driven. Unfortunately, the fact that the erythritol phase transition from 150 °C to 25 °C does not involve heat, no study of the supercooling degree when adding TCM into the sugar structure has been possible by DSC. Erythritol solid-liquid phase change occurs at around 118-120 °C, however, cannot be identified in the heat flow curves, as it lies in the sample temperature range as the TCM dehydration. The presence of crystalline sugar has been confirmed by the XRD patterns, and it could be responsible for the formation of kieserite (like $MgSO_4$-HDPE). Again, the phase change is shifted at lower temperatures, which overlaps with the dehydration of magnesium sulphate and the heating peak cannot be isolated from the thermochemical process. This might be plausible as the heating peak is noticeable for MgSO4/E/PA pure samples (no cycling), see Figure 103. However, this is not observed in the cycled samples (G1, H1 or I1) not even for 40 cycles samples. Besides, erythritol has shown to crystallised under the same measurement conditions as seen in Figure 103.
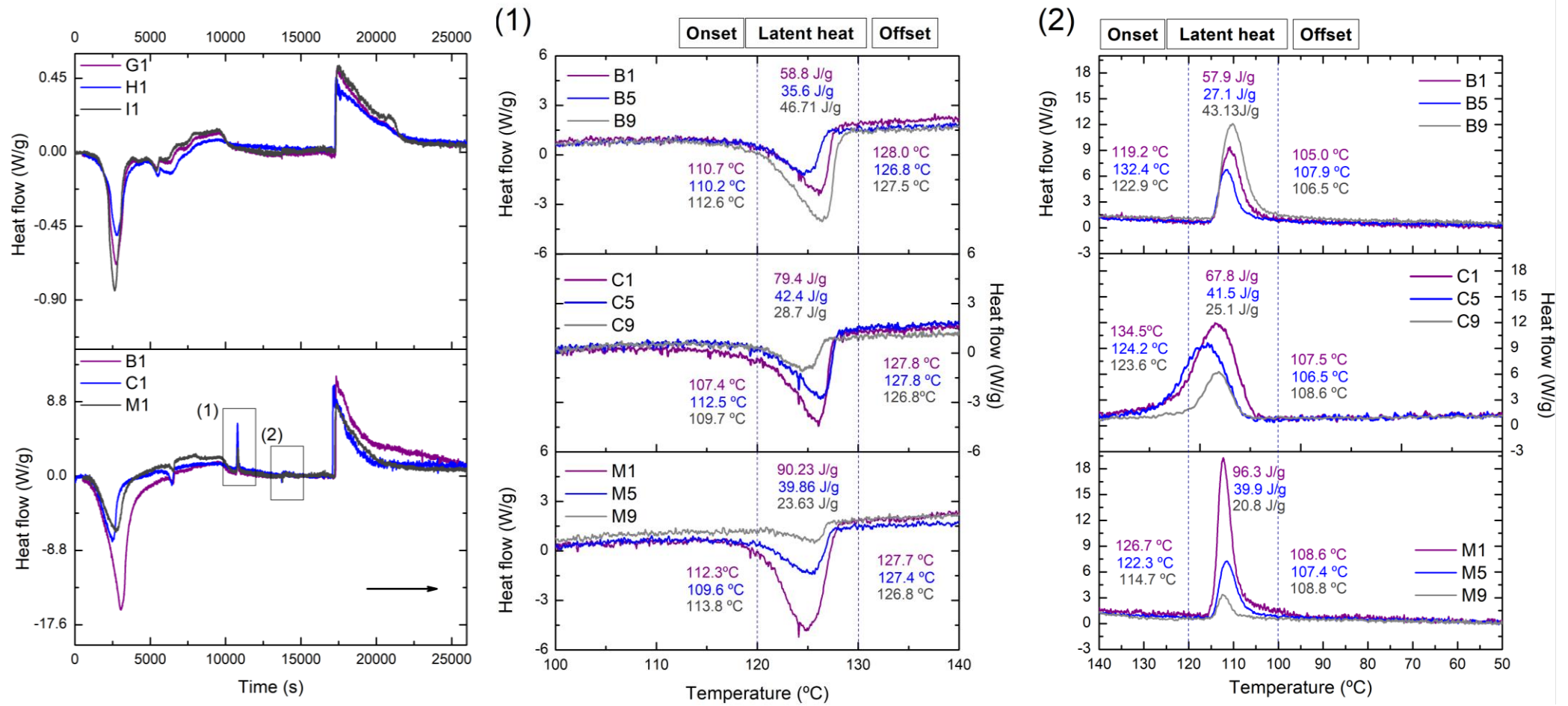
Figure 102. Heat flow vs time (left image) of the initial samples G1, H1, I1, B1, C1 and M1; and heat flow vs temperature (1) and (2) for B1, C1, M1 HDPE melting peaks. Heating from 25 °C to 150 °C 1 °C/min-hold 30 min, cooling from 150 °C to 25 °C at 2.5 °C/min.
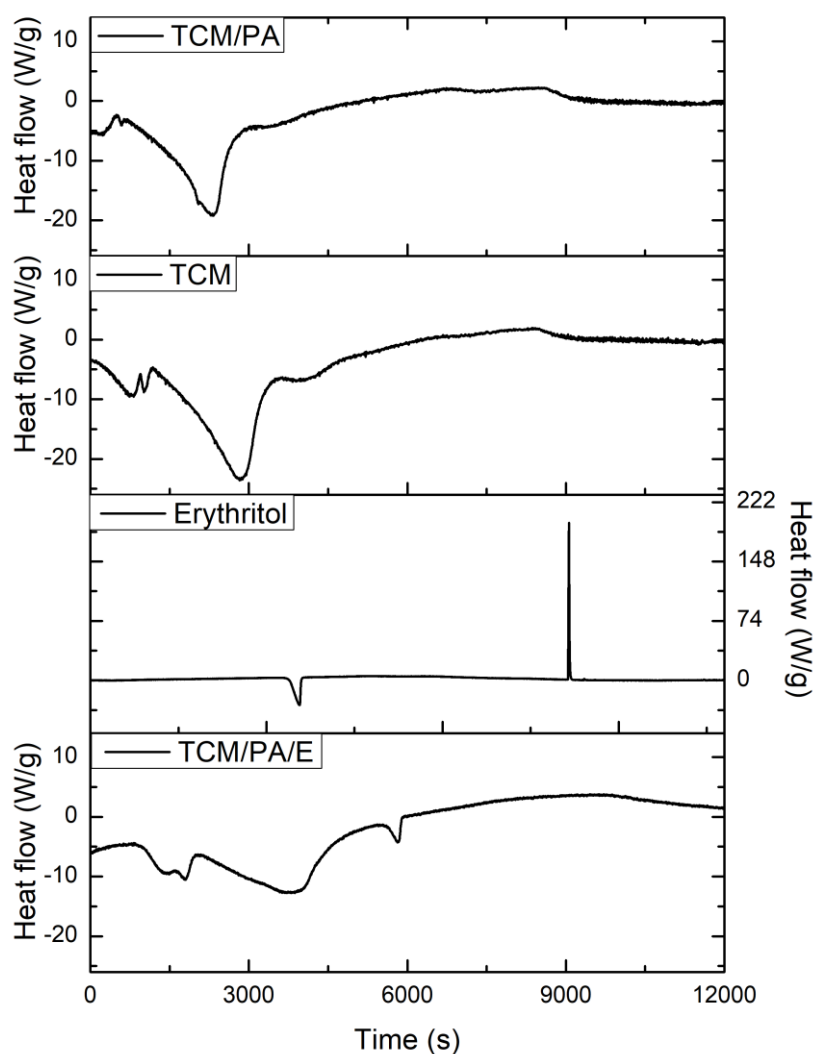
Figure 103. DSC curves of MgSO₄/PA (4 wt./vol.%), MgSO₄ pure, Erythritol and MgSO₄/E 80 wt./vol.%.

(4) Outputs

Magnesium sulphate stands up as the best TCM candidate to study at scale up-level the feasibility of the 3 in the system proposed. Magnesium chloride working pairs showed major leakage and breakage issues just after 5 cycles. The magnesium sulphate configurations experimentally validated serves as a scale-up study from 1 g to 20 g to consolidate the potential of the 3 in 1 system. Both gel and polymer working pairs

showed high energy storage capacity up to 2 GJ·m^{-3} and 2.4 GJ·m^{-3}, respectively. Besides, high dehydration (70-95%) and hydration conversions (90%) were reached even after 40 thermal cycles while maintaining structural integrity. A 25-20 wt.% of HDPE was set as optimal for the MgSO$_4$-HDPE working pair, providing a compromise between energy stored, porosity and physical integrity. Whilst the content of MgSO$_4$/E was set to 80 wt./vol.%, due to higher content leads to structural deformation of the composite. The phase change material, both polymer and sugar alcohol were found to act as nucleating agents in the magnesium sulphate crystallisation process forming a monohydrate crystalline phase (Kieserite) instead of the monohydrate amorphous phase reported in the literature.

10.3 REFERENCES

[1]   Xu C, Yu Z, Xie Y, Ren Y, Ye F, Ju X. Study of the hydration behavior of zeolite-MgSO4 composites for long-term heat storage. Appl Therm Eng 2017;129:250–9. doi:10.1016/j.applthermaleng.2017.10.031.

[2]   Donkers PAJ, Beckert S, Pel L, Stallmach F, Steiger M, Adan OCG. Water Transport in MgSO4·7H2O during Dehydration in View of Thermal Storage. J Phys Chem C 2015;119:28711–20. doi:10.1021/acs.jpcc.5b08730.

[3]   Donkers PAJ, Pel L, Adan OCG. Experimental studies for the cyclability of salt hydrates for thermochemical heat storage. J Energy Storage 2016;5:25–32. doi:10.1016/j.est.2015.11.005.

[4]   Ferchaud CJ, Zondag HA, Veldhuis JBJ, De Boer R. Study of the reversible water vapour sorption process of MgSO4.7H2O and MgCl2.6H2O under the conditions of seasonal solar heat storage. J Phys Conf Ser 2012;395. doi:10.1088/1742-6596/395/1/012069.

[5]   Gu J, Xu H, Wu C. Thermal and crystallization properties of HDPE and HDPE/PP blends modified with DCP. Adv Polym Technol 2014;33:1–5. doi:10.1002/adv.21384.

[6]   Li WD, Ding EY. Preparation and characterization of cross-linking PEG/MDI/PE copolymer as solid-

solid phase change heat storage material. Sol Energy Mater Sol Cells 2007;91:764–8. doi:10.1016/j.solmat.2007.01.011.

[7]   Xi P, Gu X, Cheng B, Wang Y. Preparation and characterization of a novel polymeric based solid-solid phase change heat storage material. Energy Convers Manag 2009. doi:10.1016/j.enconman.2009.02.013.

[8]   Ruiz-Agudo E, Martín-Ramos JD, Rodriguez-Navarro C. Mechanism and kinetics of dehydration of epsomite crystals formed in the presence of organic additives. J Phys Chem B 2007;111:41–52. doi:10.1021/jp064460b.

[9]   Steiger M, Linnow K, Juling H, Gülker G, Jarad A El, Brüggerhoff S, et al. Hydration of MgSO 4 · H 2 O and Generation of Stress in Porous Materials. Cryst Growth &Design 2008;8:336–43. doi:10.1021/cg060688c.

[10]   Grevel KD, Majzlan J. Internally consistent thermodynamic data for magnesium sulfate hydrates. Geochim Cosmochim Acta 2009;73:6805–15. doi:10.1016/j.gca.2009.08.005.

[11]   Grindrod PM, Heap MJ, Fortes AD, Meredith PG, Wood IG, Trippetta F, et al. Experimental investigation of the mechanical properties of synthetic magnesium sulfate hydrates: Implications for the strength of hydrated deposits on Mars. J Geophys Res E Planets 2010;115. doi:10.1029/2009JE003552.

[12]   U.W. Gedde and Mikael S Hedenqvist. Fundamental Polymer Science. Chapter 6. Morphology of semicrystalline polymers 201;251-326. doi:10.1007/978-3-030-29794-7_7

[13]   Liu Z, Bando Y, Drennan J, Spargo AEC. HRTEM study of orthorhombic zirconia in MgO-PSZ. J Appl Crystallogr 2003. doi:10.1107/S0021889803009075.

[14]   Zhang C, Li L, Yang X, Shi J, Gui L, Liu J. Study on the nucleating agents for gallium to reduce its supercooling. Int J Heat Mass Transf 2020;148. doi:10.1016/j.ijheatmasstransfer.2019.119055.

[15]   Styles BT. Encyclopedia of Food Sciences and Nutrition. Encycl Food Sci Nutr 2003. doi:10.1016/B0-12-227055-X/00927-5.

[16]   Crystal structure of i -erythritol and its relationship to some derived d and l and racemic substances . Proc R Soc London Ser A Math Phys Sci 1959. doi:10.1098/rspa.1959.0065.

[17]   Nakano K, Masuda Y, Daiguji H. Crystallization and melting behavior of erythritol in and around two-dimensional hexagonal mesoporous silica. J Phys Chem C 2015. doi:10.1021/jp510048g.

[18]   Lopes Jesus AJ, Nunes SCC, Ramos Silva M, Matos Beja A, Redinha JS. Erythritol: Crystal growth from the melt. Int J Pharm 2010. doi:10.1016/j.ijpharm.2009.12.043.

[19]   Wang A, Freeman JJ, Jolliff BL, Chou IM. Sulfates on Mars: A systematic Raman spectroscopic study of hydration states of magnesium sulfates. Geochim Cosmochim Acta 2006. doi:10.1016/j.gca.2006.05.022.

[20]   Mignani AG, Ciaccheri L, Mencaglia AA, Verschooten T, Ottevaere H, Thienpont H. Raman spectroscopy for distinguishing the composition of table-top artificial sweeteners. Procedia Eng., 2014. doi:10.1016/j.proeng.2014.11.634.

[21]   Ibrahim M, Ph D, He H, Ph D. Classification of polyethylene by Raman spectroscopy Author. Thermo Fish Sci 2017;792:AN52301.

[22]   Malinovsky VK, Sokolov AP. The nature of boson peak in Raman scattering in glasses. Solid State Commun 1986. doi:10.1016/0038-1098(86)90854-9.

[23]   Ando MF, Benzine O, Pan Z, Garden JL, Wondraczek K, Grimm S, et al. Boson peak, heterogeneity and intermediate-range order in binary SiO2-Al2O3 glasses. Sci Rep 2018. doi:10.1038/s41598-018-23574-1.

[24]   Gómez DA, Coello J, Maspoch S. The influence of particle size on the intensity and reproducibility of Raman spectra of compacted samples. Vib Spectrosc 2019;100:48–56. doi:10.1016/j.vibspec.2018.10.011.

[25]   Scapino L, Zondag HA, Van Bael J, Diriken J, Rindt CCM. Energy density and storage capacity cost comparison of conceptual solid and liquid sorption seasonal heat storage systems for low-temperature space heating. Renew Sustain Energy Rev 2017;76:1314–31.

doi:10.1016/j.rser.2017.03.101.

[26]   Seven KM, Cogen JM, Gilchrist JF. Nucleating agents for high-density polyethylene - A review. Polym Eng Sci 2016. doi:10.1002/pen.24278.

[27]   Polymer chemistry: properties and applications. Choice Rev Online 2007. doi:10.5860/choice.44-3878.

[28]   Duquesne M, Godin A, Del Barrio EP, Achchaq F. Crystal growth kinetics of sugar alcohols as phase change materials for thermal energy storage. Energy Procedia, 2017. doi:10.1016/j.egypro.2017.11.214.

[29]   Wang Y, Li S, Zhang T, Zhang D, Ji H. Supercooling suppression and thermal behavior improvement of erythritol as phase change material for thermal energy storage. Sol Energy Mater Sol Cells 2017;171:60–71. doi:10.1016/j.solmat.2017.06.027.

11 POTENTIAL APPLICATION AND PROSPECTIVES

6. Hybrid TES system:

3 in 1 concept

5. Targets and structure of the thesis

4. TCS Outlook

3. Introduction

2. Scientific contributions

1. Thesis timeline

Once the feasibility of the 3 in 1 system has been proved and experimentally validated at lab and scale-up level, it is time to frame all this information into the TCS field to assess the future hybrid system pathways. This section is aimed to show the 3 in 1 system's prospectives and its potential applications by comparing it to traditional TES technologies and the current commercial TES status. The current TCS systems are also considered and shaped to the 3 in 1 system.

12. Conclusions and achievements

11. Potential applications and prospective

10. Proof of concept and scale-up

9. Working pairs

8. Material screening and selection

7. Bench study specifications

11. POTENTIAL APPLICATIONS AND PROSPECTIVES
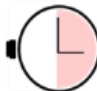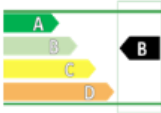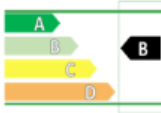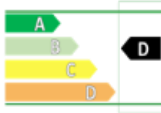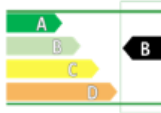
11.1 HYBRID SYSTEM POTENTIAL

The great potential of this novel TES technology is discussed in this section. We comprehensively compare the performance of the 3 in 1 with conventional systems, at the sight of capacity (the energy stored in the system), power (how fast the energy stored in the system can be charged/discharged), efficiency (the ratio of the energy provided to the user to the energy needed to charge the storage system), storage period (how long the energy is stored) and cost (to either capacity (€/kWh) or power (€/kW)). We also present possible applications where this new system can be implemented and discuss its influence in the TES development pathway. In Table 39 we show a vast comparative between sensible, latent and thermochemical heat systems to stress the potential of this technology.

(1) The capacity, which is related to the **energy density** of the system, is one of the most important attributes when selecting TES media for a specific application and determines the size of the system. The size of equal energy stored TES systems will be decreasing from sensible > latent > thermochemical. By using the 3 in 1 it is possible to get the intrinsic capacity from a thermochemical system but also includes sensible and latent capacities. The 3 in 1 allows higher TCM content than other alternatives proposed in the literature; vermiculite impregnation (up to 40 wt.% of TCM) [1–3], zeolite impregnation (up to 20 wt.% of TCM) [2,4–6] and silica gel (up to 60 wt.% of TCM) [7–11]. Despite the above-mentioned matrices also uptake water in a chemical adsorption process [12] and they can add sorption capacity, the energy that they can store cannot offset the energy taken by the addition of the matrix. The 3 in 1 system shows that an addition of up to 20% in weight of PCM can overcome this, enough to support the TCM acting as a matrix, and a surplus of stored energy that balances the energy taken from the TCM replaced. We have done some theoretical calculations to

stress this point, as shown in Figure 104 and Figure 105. The energy stored by the 3 in 1 system is very similar to the one achieved with the solely thermochemical media (see Figure 104), which is three times higher than the one stored by conventional TCM composites such as zeolite + TCM (the most studied in the literature).

Table 39. Technical key attributes of the traditional TES technologies and the 3 in 1 proposed. [13–15]

(2) TES power and capacity to determine the **storage period**. While latent heat is preferably used for short term applications (from hours to days) given its high power, high capacity and affordable heat losses, sensible and thermochemical heat have a better ability to store heat for long term application such as seasonal/interseasonal storage (from days to months). Once again, 3 in 1 can

provide a promising combination, the thermochemical heat can be stored for months while the latent and sensible heat can be discharged when needed for the end-user. In that manner, the system can either work as a short term and long-term storage.
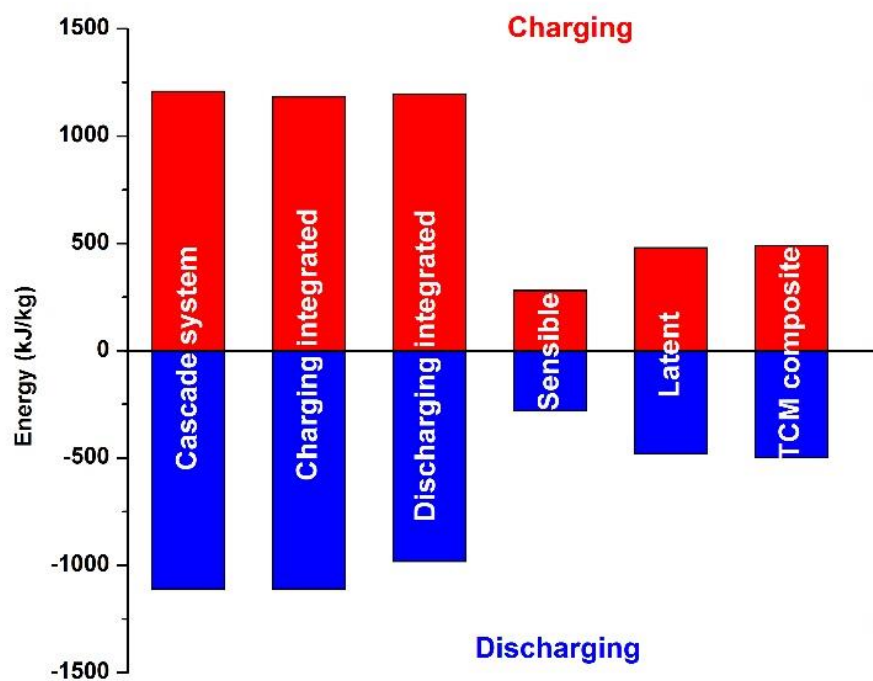
Figure 104. Energy charged and discharged for conventional TES media and 3 in 1 alternative configurations proposed in this paper (see more details in the methodology section).

.
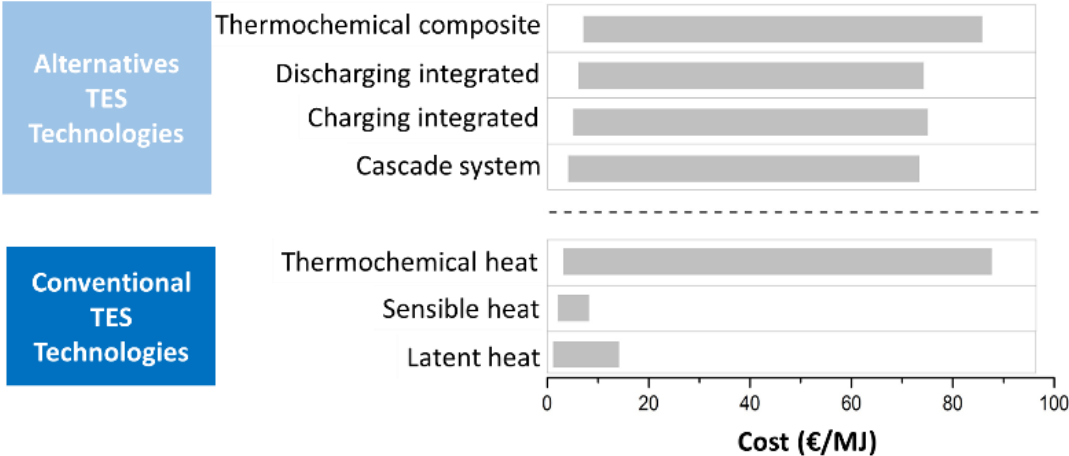
Figure 105. Cost comparison between alternative and conventional TES media, energy stored taken from calculations and averaged cost. The system has an inlet temperature of 25°C and an outlet temperature of 165°C. An average value for the latent heat has been assumed by averaging

commonly used organic phase change materials in the working temperature range [16], latent heat 200 J/kg. Likewise, an average value from the most used sorption materials, heat of reaction 1200 kJ/kg. The same latent heat and heat of reaction is used for the 3 in 1 system (cascade, charging, discharging). The thermochemical material is dehydrated from 60-150°C while it hydrates at 30°C, the melting point of the phase change material was tuned to obtain the three different 3 in 1 system. The same was applied to the sensible heat, taken different values for liquid/solid PCM and hydrated/dehydrated TCM. The TCM/PCM ratio was 80/20 wt.%. For comparison purposes, the sensible heat of the PCM was used to calculate the sensible heat material energy and the latent heat solely from the 3 in 1 system was used to calculate the latent heat energy. The TCM composite was assumed to be a zeolite matrix and the same averaged TCM used for the 3 in 1 calculation, the ratio zeolite/TCM was the typical 85/15 wt.%. The energy stored by the zeolite was taken from [17], while the price was averaged from [18] just considering a pore diameter around 0.18−0.47 cm³/cm³.

(3) Thermochemical **lifetime** media is still a challenge as it cannot maintain its physical integrity during a large number of cycles, which hinders its application. Just seasonal storage systems are suitable given the low number of cycles (two per year, one in winter and another one in summer) [19–22]. TCM lifetime can be greatly improved by the addition of PCM as the matrix, which could solve agglomeration problems and minimize the microstructural changes that lead to mass and heat transfer reduction [23].

(4) **Efficiency** here refers to thermal cycle efficiency. Considering the aforementioned and given the poor conversion of the thermochemical system after certain cycles [24–26], thermochemical has the lowest efficiency level (level D from A, B, C, and D). The round trip efficiency of thermochemical systems is potentially very high reaching values close to 95-100 % [15]. However, under working conditions, the efficiency can drop down to 50-60 % depending on the TCM considered [27]. The latent heat component of the 3 in 1 can overcome this, besides increasing the lifetime of the material, it can lessen the efficiency drop over cycles.

(5) When selecting a storage media, the **cost** is a key attribute that can shift the balance towards a specific TES technology. Thermochemical is particularly disadvantaged when considering the capital and operational storage device cost and lifetime. According to some economic application studies, the cost of the active material and the matrix can be significantly high; also the complexity of the system components and the installation [19]. The storage material strongly affects the performance and cost of such a heat storage system (typically, about 30 % of the total investment

cost) [28]. Despite TCM potential, at the current state of research, it is cost-intensive and not ready for commercialisation. The use of a less expensive matrix (polymer or other kinds of low priced PCMs) can lower the cost and offset the current imbalance between capacity and cost that tilts the scales towards a non-profitable system. 3 in 1 provides a supporting skeleton that can reduce the final cost by adding a lower-priced matrix to the overall storage media composition (<80 wt.%); even lower than the common matrices used in the field [3,19,28]. This cost reduction can be seen in Figure 18, where the 3 in 1 system, 80/20 wt.% of TCM/PCM, is also more profitable than the pure thermochemical or the thermochemical composite.

(6) **Applications**, where the new concept can be used to store and deliver heat, are industrial processes (waste heat), solar energy, district heating and cooling, and residential and commercial sectors. It allows tailoring systems where different output and input temperatures heat sources are involved. It also provides different discharging/charging strategies enabling a flexible energy storage system for coupling with renewables (especially solar power).

(7) The 3 in 1 system has the potential to open a **new TES technology pathway**, which will change the conventional TES classification. Normally, systems are designed prior to the storage media selection, and subjected to the application's requirements, making sometimes the material selection a cost extensive limiting step. In this case, the storage media and system will be design retroactively, aiming to maximize the performance and minimise the cost. The wide range of PCM matrices and TCM material combinations opens a whole range of possible applications and novel material's manufacturing routes. The tuneable system will be shaped around the application's needs (input and output temperature, charging/discharging rate, system size, cost and lifetime). The possible manufacturing routes are described in Figure 106; tabletting, extrusion and 3D printing. Tabletting is the simplest one and has already been used for TCS composites, as both PCM and TCM can be mixed in powder form, which eases the process. Besides, given that in the 3 in 1 system polymeric matrices are considered, extrusion could be taken into account as a novel manufacturing route by using

recycled PCM (e.g. HDPE). Extrusion of polymers is a mature industrial process that can bring its know-how to TCM/PCM extrusion. Recently, gels 3D printing in the food industry has been published with successful results [29]. These manufacturing methods, in a further maturation state of the 3 in 1 technology, could be used by combining a gel into the materials components and using the expertise gained on the food science field.
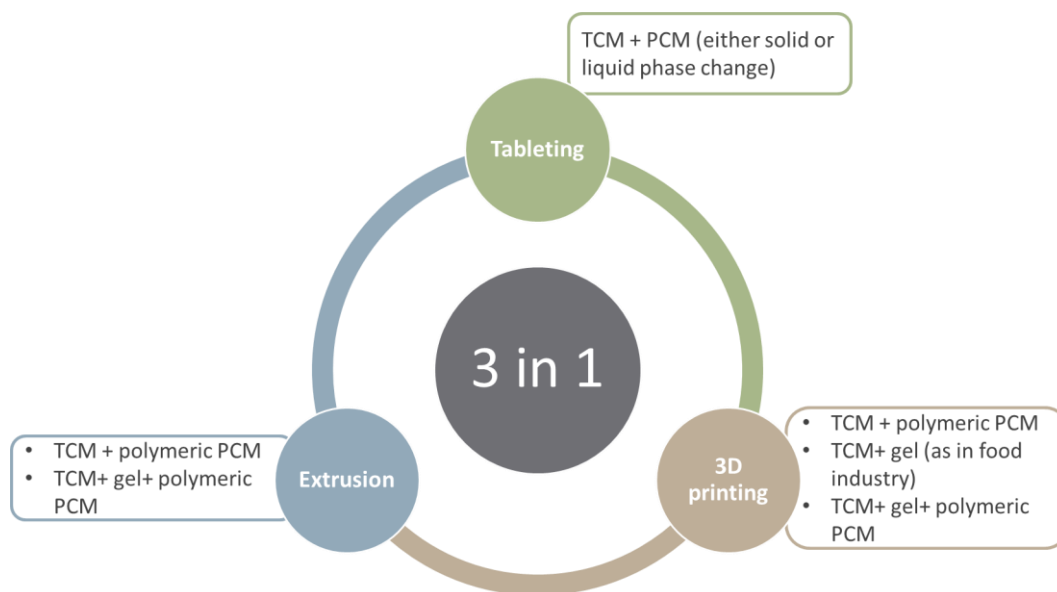
Figure 106. Manufacturing pathways for the 3 in 1 system.

11.2 APPLICATIONS

As described in the TCS Outlook section (Chapter 4), thermochemical storage can be implemented in closed or open systems, either in separated or integrated reactors. Briefly explained; open systems exchange mass and energy with the environment, typically at ambient pressure between a working fluid (air) and a thermochemical material. Thermal energy is transferred to a transport medium (air), which provides the necessary energy for the thermochemical material desorption. After the storing period, the discharging process occurs when the sorbate (e.g. water vapour) is transported into the airflow to the sorbent, and the energy stored is released. Closed systems exchange only energy with

the environment, sorbent and sorbate are stored separately and a working fluid (e.g. water) and a

TCM (e.g. salt hydrate). In both cases, thermal energy from an external energy source provides the

necessary energy for the TCM dissociation, which is transferred to the working fluid. Conventional

open and closed adsorption systems are shown in Figure 107 and Figure 108.
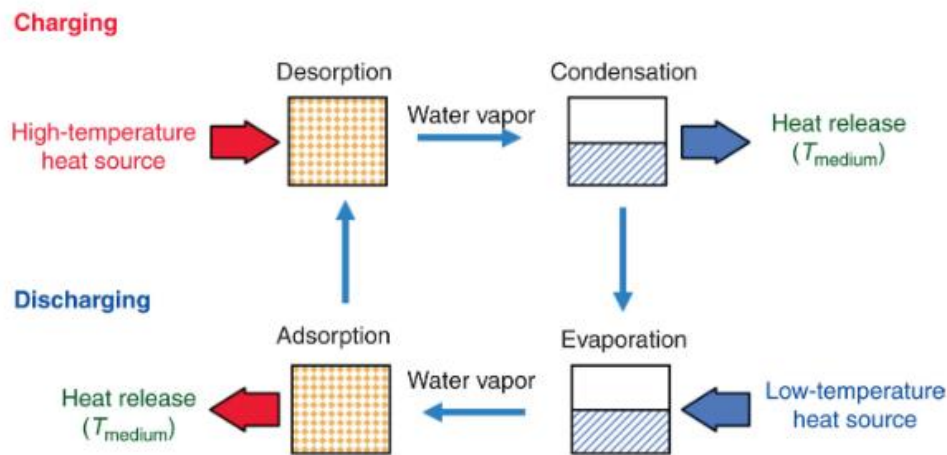
Figure 107. Conventional closed adsorption system [7].
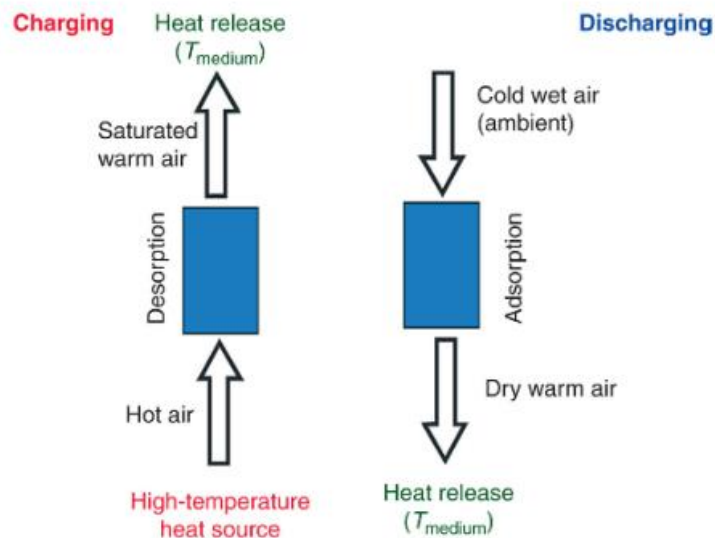
Figure 108. Conventional open adsorption system [7].

The incorporation of latent heat into the system can potentially bring an added value to the current

systems but also supposes interesting challenges to the system configuration. A sketch of the new

system's configuration for water sorption systems is shown in Figure 109, Figure 110 and Figure 111, where the three different configurations (cascade, charging and discharging) are presented for both open and closed systems. In closed systems, where additional units are required (condenser and evaporator), the 3 in 1 technology could transfer the latent heat to the evaporator (see Figure 109), reducing the energy consumption and increasing the overall efficiency. Similarly, open systems, which need a fan and a humidifier (water sorption), could provide the thermal energy stored in latent heat form to the humidifier. The fact that the material maintains its physical integrity over cycles allowing good mass and heat transfer, can potentially be translated as an enhanced mass transfer and a pressure drop reduction, compared to conventional TCM systems. Since the system has been just studied at materials/lab-scale level (see late), the configurations here presented show part of the 3 in 1 potential and future challenges.

Table 40. Comparison between open and closed systems. Adapted from [12,19].

Type	Advantages	Disadvantages	Potential 3 in 1 added value
Closed system	• Small and compact design. • Low pressure. • Higher reaction power. • Higher output temperatures than an open system. • No safety requirements. • No mass transfer with the environment.	• Presence of non-condensable gases. • Heat transfer limiting step; larger heat transfer area. • Condenser and evaporator are needed. • Complex system. Periodical evacuation required.	• Enhanced mass transfer. • Heat transferred to the evaporator. • Multiple inputs and output temperatures.
Open systems	• Simple system. • Fewer components than a closed system. • Atmospheric pressure. • Increased heat transfer • Non-compact design.	• Low reaction power. • Safety requirements • Mass transfer limiting step. • Limitation of pressure drop. • Need for additional fan and humidifier.	• Enhanced mass transfer. • Reduction of pressure drop; minimize permeability change. • Heat transferred to the humidifier. • Multiple inputs and output temperatures.

In this section, we explore how the 3 in 1 can fit into the current side TES spectrum. As explained in Table 41, TES has been mainly deployed in the building sector (e.g. domestic hot water, air conditioning, space heating) [30,31] and industrial processes [32]. TES could be empowered when coupled with renewable energies (PV, solar thermal, geothermal and wind), while renewable sources charge the TES systems, the latter one provides variable supply generation, sector coupling, demand shifting and network management. Either centralised or distributed, TES systems can help to decentralize the network across users, increasing the share of renewables and reducing their curtailment.

TES sensible heat storage systems and at some extent latent heat storage are the only technologies relevant to commercial TES applications. Different integration schemes have been proposed according to the storage media, system and application. However, there are still unsolved key issues that prevent this energy transition towards a renewable energy TES coupling scenario: mismatch between renewable energy output source and demand loads, the inability of tailoring the TES media to coupling conditions, high Levelized cost of electricity (LCOE) and poor conversion after loading/unloading the system several times.

Given the attributes of the 3 in 1 system, the main applications to be considered are district heating and cooling, residential and commercial building, waste heat and industrial processes and solar energy. How TES can be integrated into those sectors is explained in Table 41, where we will go backwards, matching the system working conditions with its potential application. Hence, discussing its suitability and potential integration.
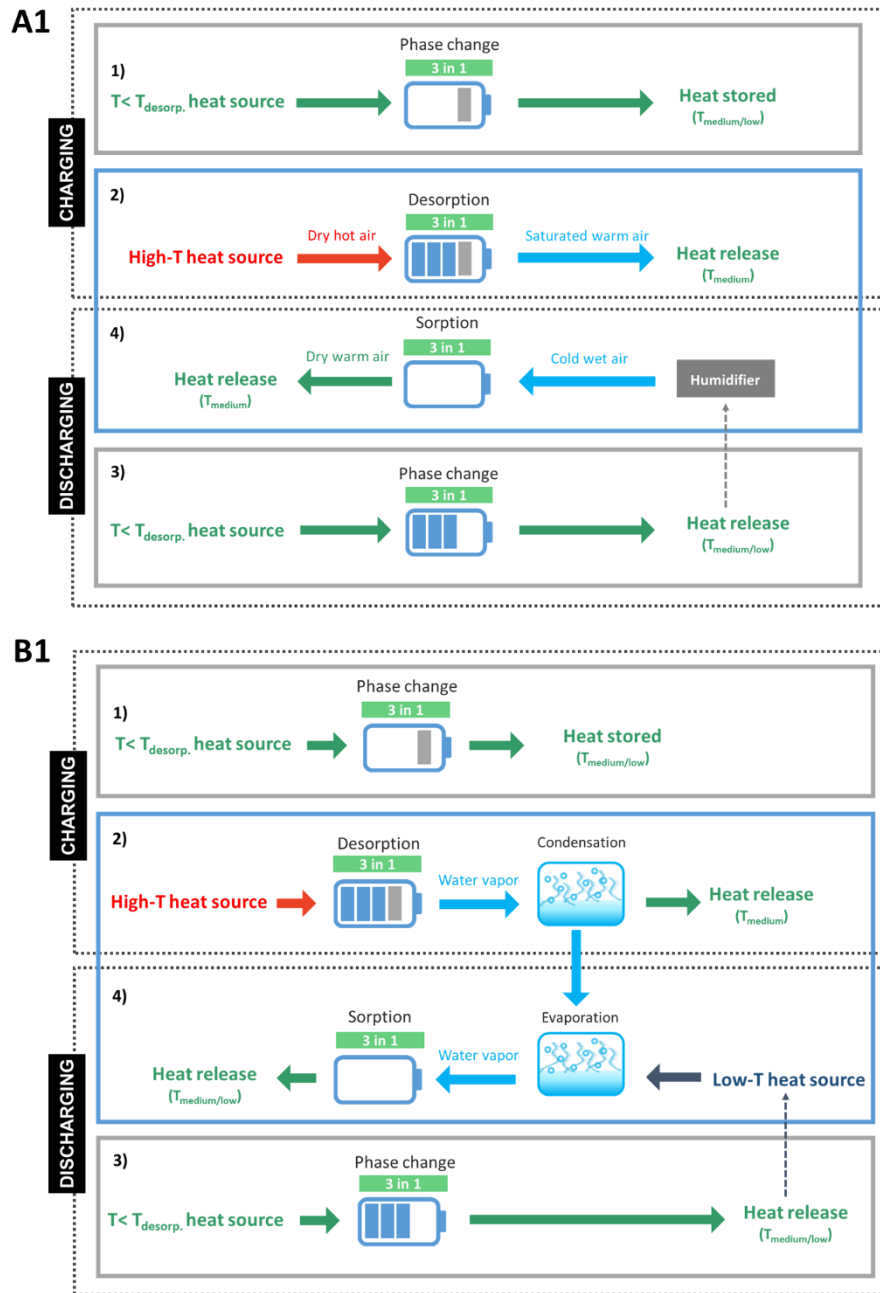
Figure 109. Schematic sketch of open (A) and closed (B) system for the three 3 in 1 system configurations where (1) is the cascade system. 1), 2), 3) and 4) in the diagram are the sequential steps of the charging and discharging processes. Figure adapted from [7].
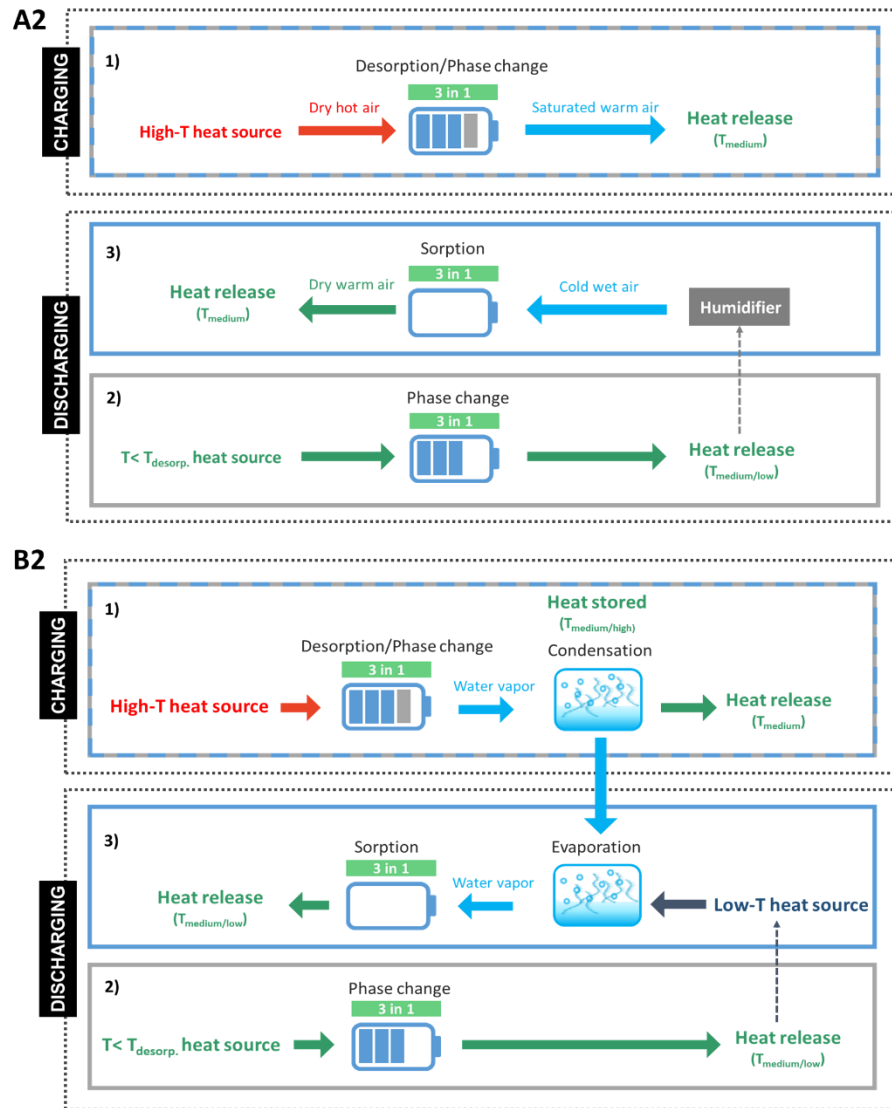
Figure 110. Schematic sketch of open (A) and closed (B) system for the three 3 in 1 system configurations were (2) the charging integrated. 1), 2), 3) and 4) in the diagram are the sequential steps of the charging and discharging processes. Figure adapted from [7].
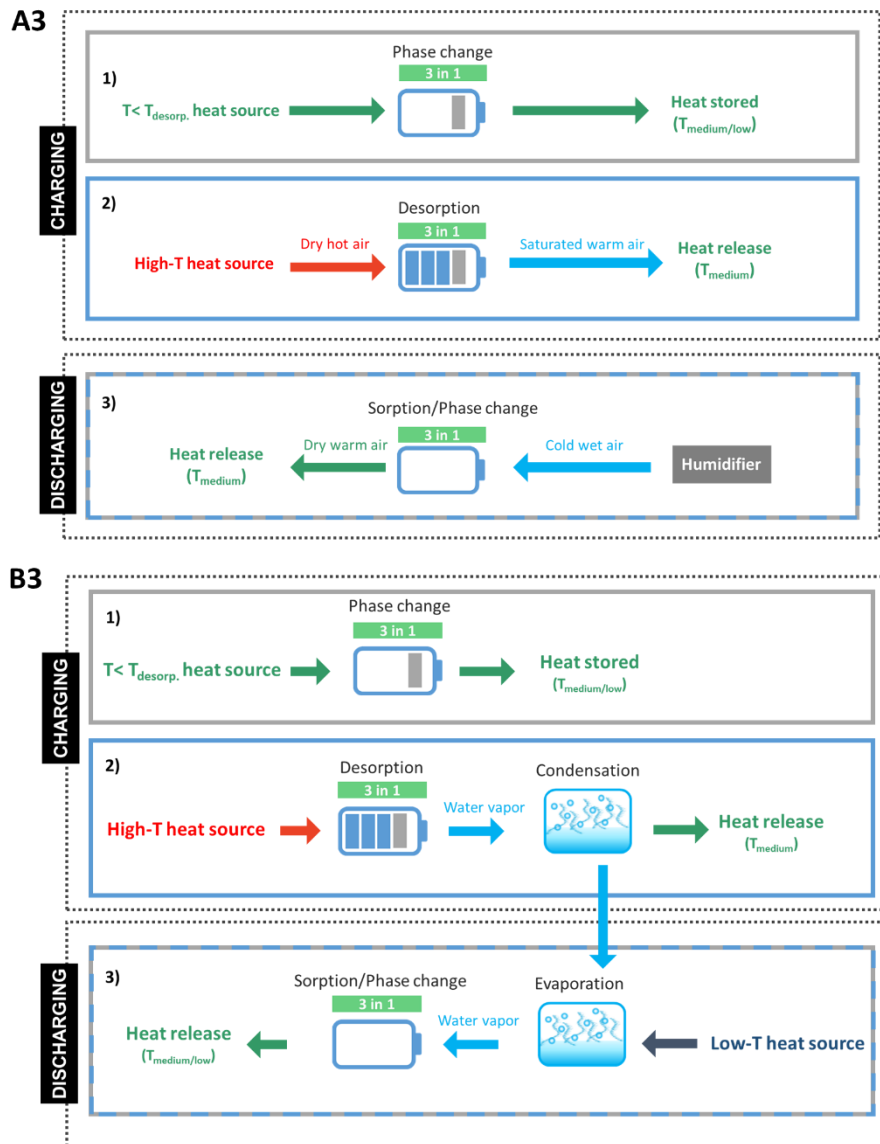
Figure 111. Schematic sketch of open (A) and closed (B) system for the three 3 in 1 system configurations were (3) the discharging integrated. 1), 2), 3) and 4) in the diagram are the sequential steps of the charging and discharging processes. Figure adapted from [7].

Table 41. The current state-of-the-art of thermal energy storage applications

Waste heat

Thermal energy storage for industrial applications can be utilised in a wide temperature range: low-temperature heat (below 150 °C), medium-temperature heat (150 °C to 400 °C), and high-temperature heat (above 400 °C) [39]. Several energy-intensive industrial sectors and processes (e.g. cement, iron and steel, glass) and manufacturing industry (e.g. automobile industry) can benefit from TES systems [40]. In this application, sensible, latent and thermochemical can be selected depending on the system constrains. However, just sensible systems for medium to high-temperature and water tanks for low-temperature processes are commercial.

Solar energy

Thermal energy storage can help alleviate the variability of solar energy systems balancing variable supply integration and network management. The excess of energy generated can be stored when renewable resources are available and re-used when the renewable source is not available [41]. Therefore, integrating variable solar heat into the energy system. Thermochemical storage, sensible heat and some high-temperature latent heat systems can be integrated into this application for either short- or long-term storage periods. The heat stored can be used to produce electricity (heat to power) or provide hot water and space heating into the building sector.

Residential and commercial buildings

Thermal energy storage can be applied for short-term storage, based on daily heat buffers or long-term heat storage for residential and commercial buildings, based on distributed heat storage systems. Ceramic bricks and water tanks (both sensible) have been used to store heat at temperatures up to 70 °C in residential storage heaters since the mid-20th century. Interseasonal storage would play a key role in the building sector for which thermochemical storage will be crucial.

District heating and cooling

TES for solar district heating/cooling schemes can help to store any surplus of heat/cold after meeting the demand, which can be delivered to multiple buildings from a centralised generation. Thermal energy storage allows the modulation of the heat/cold output to meet varying demand and better balance the scheme for short-term (daily heat buffers) or long-term (centralised system). Once again, sensible TES is the only deployed technology in this application (Underground TES and water tanks). Such systems can store heat up to 100 °C or cold at lower temperatures, with heat being upgraded with heat pumps.

(1) Cascade system

The cascade system allows two different input and output temperatures, which provides a wide operational temperature range. It also enables to discharge one component of the system while the other one it is still charged. For those reasons, this system would suit applications where the mismatch between the renewable output/input source and the coupling conditions is critical, such as the solar energy and building sector. Solar collectors, solar panels or CHP plants can be used to charge the 3 in 1. The PCM component of the system could be used for low energy demanding utilities such as water heating for daily supply, and the TCM component could be used for a higher temperature supply such as space heating in winter (long-term storage). This system is also suited for low-medium temperature industrial processes or waste heat, where different output energy sources are released at different stages of the production. That will increase renewable integration in the industry sector (only 14% of the final energy consumption is generated by renewables). That could fit into applications such as industry or hot water in commercial or residential buildings when the PCM discharging temperature is above 60 °C and an existing hot water tank can be charged. The remaining heat from the TCM can be discharged later for other purposes.

(2) Charging integrated

The charging integrated system would be specially indicated for ultra-low-grade heat recovery (<200 °C). Since the system charges at the same temperature for both components (TCM and PCM), the system could be fully charged at a temperature near 100-200 °C, with the potential utilization of waste or ultra-low-

grade heat recovery source. The system will be able to discharge at two different temperatures, which allows upgrading the heat recovered to ultra-low temperatures <65 °C (from the TCM) while providing output energy at low-medium grade near the input conditions (from the PCM). Space heating and domestic hot water (SH&DHW) usually requires 30 °C and 65 °C, which makes this system ideal for both sectors. The input heat source unit must deliver the energy required at a constant rate to make possible the charging process of both components, which makes solar collector or CHP plants suitable applications. Such systems have already been proved feasible for thermochemical sorption processes driven by waste or ultra-low grade heat in the building sector [34–37], using air from ventilation and hot wastewater/sewage evacuated from dwellings as the heating source [38].

(3) Discharging integrated

The discharging integrated system can work to an extent contrary to the charging integrated. Two heating sources will charge the system while the discharge occurs at one constant output temperature. Those attributes make this system specially indicated for district heating and the building sector, where a constant output temperature is required for either space heating or domestic hot water. The system could recover heat from the building or the network at different temperatures to reintegrate it for later discharge. Moreover, it can be integrated into industrial processes, using two different heat sources and reinserting the heat again in the manufacturing process at a constant temperature. Again, the PCM latent heat could be used to charge existing hot water tanks for commercial or residential buildings or different industrial processes.

11.4 CONCLUDING REMARKS

Thermal energy storage (TES) needs a breakthrough concept to enable its rapid deployment and contribute to achieving a net zero-carbon energy system. 3 in 1 TES system looks beyond the three traditional TES technologies to propose a novel, integrated concept where TES is brought to its ultimate level. We store thermal energy within one storage media in three forms: sensible, latent and thermochemical by addressing the fundamental challenges of each technology. Thus, opening a new vision of storing thermal energy, where the components are not acting individually but co-working synergistically to maximise the operational energy density while maintaining the controllability of the charge/ discharge processes; and at the same time, enhance the efficiency and lifetime at the system level. In this 3 in 1 system, the main fundamental challenges of each technology are surpassed: more compact systems (sensible), accommodation of volume change (latent heat), higher energy conversion and life span (thermochemical). We envision a novel technology that a) conceives a unique and revolutionary way to store thermal energy that can overpass the other TES technologies, b) follows a top-down approach to match the current energy requirements with the technology potential and c) constitutes the vehicle that suppresses the gap between TES technologies and applications that can potentially reuse a surplus of heat energy.

11.5 REFERENCES

[1]   Aydin D, Casey SP, Riffat S. The latest advancements on thermochemical heat storage systems. Renew Sustain Energy Rev 2015;41:356–67. doi:10.1016/j.rser.2014.08.054.

[2]   Casey SP, Elvins J, Riffat S, Robinson A. Salt impregnated desiccant matrices for "open" thermochemical energy storage - Selection, synthesis and characterisation of candidate materials. Energy Build 2014;84:412–25. doi:10.1016/j.enbuild.2014.08.028.

[3]   Casey SP, Aydin D, Riffat S, Elvins J. Salt impregnated desiccant matrices for "open" thermochemical energy storage - Hygrothermal cyclic behaviour and energetic analysis by physical experimentation. Energy Build 2015;92:128–39. doi:10.1016/j.enbuild.2015.01.048.

[4]   Xu C, Yu Z, Xie Y, Ren Y, Ye F, Ju X. Study of the hydration behavior of zeolite-MgSO4 composites for long-term heat storage. Appl Therm Eng 2017;129:250–9. doi:10.1016/j.applthermaleng.2017.10.031.

[5]   Hongois S, Kuznik F, Stevens P, Roux JJ. Development and characterisation of a new MgSO4-zeolite composite for long-term thermal energy storage. Sol Energy Mater Sol Cells 2011;95:1831–7. doi:10.1016/j.solmat.2011.01.050.

[6]   Dawoud B, Amer E, Gross D. Experimental investigation of an adsorptive thermal energy storage. Int J Energy Res 2007;31:135–47. doi:10.1002/er.

[7]   Jarimi H, Devrim A, Zhang Y, Ding Y, Ramadan O, Chen X, et al. Materials characterization of innovative composite materials for solar-driven thermochemical heat storage (THS) suitable for building application. Int J Low-Carbon Technol 2018;13:30–42. doi:10.1093/ijlct/ctx017.

[8]   Courbon E, D'Ans P, Permyakova A, Skrylnyk O, Steunou N, Degrez M, et al. A new composite sorbent based on SrBr2and silica gel for solar energy storage application with high energy storage density and stability. Appl Energy 2017;190:1184–94. doi:10.1016/j.apenergy.2017.01.041.

[9]   Yu N, Wang RZ, Lu ZS, Wang LW. Development and characterization of silica gel-LiCl composite sorbents for thermal energy storage. Chem Eng Sci 2014;111:73–84. doi:10.1016/j.ces.2014.02.012.

[10]   Yu N, Wang RZ, Lu ZS, Wang LW. Study on consolidated composite sorbents impregnated with LiCl for thermal energy storage. Int J Heat Mass Transf 2015;84:660–70. doi:10.1016/j.ijheatmasstransfer.2015.01.065.

[11]   Zhu D, Wu H, Wang S. Experimental study on composite silica gel supported CaCl2 sorbent for low grade heat storage. Int J Therm Sci 2006;45:804–13. doi:10.1016/j.ijthermalsci.2005.10.009.

[12]   Lele AF. State-of-Art of Thermochemical Heat Storage Systems. 2016. doi:10.1007/978-3-319-41228-3.

[13]   Renewable Energy Agency I. IRENA-IEA-ETSAP Technology Brief 4: Thermal Storage n.d.

[14]   Sarbu I, Sebarchievici C. A comprehensive review of thermal energy storage. Sustain 2018;10. doi:10.3390/su10010191.

[15]   Delta Energy & Environment Ltd. Evidence Gathering: Thermal Energy Storage (TES) Technologies 2016:1–85.

[16]   Bland A, Khzouz M, Statheros T, Gkanas E. PCMs for Residential Building Applications: A Short Review Focused on Disadvantages and Proposals for Future Development. Buildings 2017;7:78. doi:10.3390/buildings7030078.

[17]   Shere L, Trivedi S, Roberts S, Sciacovelli A, Ding Y. Synthesis and Characterization of Thermochemical Storage Material Combining Porous Zeolite and Inorganic Salts. Heat Transf Eng 2018:1–6. doi:10.1080/01457632.2018.1457266.

[18]   Jarimi H, Aydin D, Yanan Z, Ozankaya G, Chen X, Riffat S. Review on the recent progress of thermochemical materials and processes for solar thermal energy storage and industrial waste heat recovery. Int J Low-Carbon Technol 2019;14:44–69. doi:10.1093/ijlct/cty052.

[19]   Scapino L, Zondag HA, Van Bael J, Diriken J, Rindt CCM. Energy density and storage capacity cost comparison of conceptual solid and liquid sorption seasonal heat storage systems for low-temperature space heating. Renew Sustain Energy Rev 2017;76:1314–31. doi:10.1016/j.rser.2017.03.101.

[20]   van Essen VM, Zondag H a., Gores JC, Bleijendaal LPJ, Bakker M, Schuitema R, et al. Characterization of MgSO4 Hydrate for Thermochemical Seasonal Heat Storage. J Sol Energy Eng 2009;131:041014. doi:10.1115/1.4000275.

[21]   M. Gaeini,Thermochemical seasonal heat storage for the built environment:a multi-scale investigation, 2017.

[22]   Kallenberger PA, Brieler FJ, Posern K, Fröba M. Magnesium Sulfate/Polymer Composites for Seasonal, Thermochemical Energy Storage. Chemie-Ingenieur-Technik 2016;88:379–84. doi:10.1002/cite.201500095.

[23]   Version D, Eindhoven TU. Experimental study of salt hydrates for thermochemical seasonal heat storage Experimental study of salt hydrates for thermochemical seasonal heat storage. 2016.

[24]   Abedin A, Rosen M, Choi JC, Kim SD, Eindhoven TU, Habashy GM, et al. A Critical Review of Thermochemical Energy Storage Systems. Open Renew Energy J 2011;4:42–6. doi:10.2174/1876387101004010042.

[25]   Donkers PAJ, Pel L, Adan OCG. Experimental studies for the cyclability of salt hydrates for thermochemical heat storage. J Energy Storage 2016;5:25–32. doi:10.1016/j.est.2015.11.005.

[26]   Fopah-Lele A, Tamba JG. A review on the use of SrBr2·6H2O as a potential material for low temperature energy storage systems and building applications. Sol Energy Mater Sol Cells 2017;164:175–87. doi:10.1016/j.solmat.2017.02.018.

[27]   Casey SP, Aydin D, Elvins J, Riffat S. Salt impregnated desiccant matrices for 'open' thermochemical energy conversion and storage – Improving energy density utilisation through hygrodynamic & thermodynamic reactor design. Energy Convers Manag 2017;142:426–40. doi:10.1016/j.enconman.2017.03.066.

[28]   Aydin D, Casey SP, Riffat S. The latest advancements on thermochemical heat storage systems. Renew Sustain Energy Rev 2015;41:356–67. doi:10.1016/j.rser.2014.08.054.

[29]   Diañez I, Gallegos C, Brito-de la Fuente E, Martínez I, Valencia C, Sánchez MC, et al. 3D printing in situ gelification of κ-carrageenan solutions: Effect of printing variables on the rheological response. Food Hydrocoll 2019;87:321–30. doi:10.1016/j.foodhyd.2018.08.010.

[30]   Griffiths P, Colclough S, Navarro L, McCormack SJ, de Gracia A, Browne M, et al. Thermal energy storage in building integrated thermal systems: A review. Part 1. active storage systems. Renew Energy 2015;88:526–47. doi:10.1016/j.renene.2015.11.040.

[31]   Khadiran T, Hussein MZ, Zainal Z, Rusli R. Advanced energy storage materials for building applications and their thermal performance characterization: A review. Renew Sustain Energy Rev 2016;57:916–28. doi:10.1016/j.rser.2015.12.081.

[32]   Miró L, Gasia J, Cabeza LF. Thermal energy storage (TES) for industrial waste heat (IWH) recovery: A review. Appl Energy 2016;179:284–301. doi:10.1016/j.apenergy.2016.06.147.

[33]   Kerskes H. Thermochemical Energy Storage. Storing Energy With Spec. Ref. to Renew. Energy Sources, 2016. doi:10.1016/B978-0-12-803440-8.00017-8.

[34]   Bao H, Ma Z, Roskilly AP. Integrated chemisorption cycles for ultra-low grade heat recovery and thermo-electric energy storage and exploitation. Appl Energy 2016;164:228–36. doi:10.1016/j.apenergy.2015.11.052.

[35]   Zhao YJ, Wang RZ, Li TX, Nomura Y. Investigation of a 10 kWh sorption heat storage device for effective utilization of low-grade thermal energy. Energy 2016;113:739–47. doi:10.1016/j.energy.2016.07.100.

[36]   Liu H, Nagano K, Sugiyama D, Togawa J, Nakamura M. Honeycomb filters made from mesoporous composite material for an open sorption thermal energy storage system to store low-temperature industrial waste heat. Int J Heat Mass Transf 2013;65:471–80. doi:10.1016/j.ijheatmasstransfer.2013.06.021.

[37]   N'Tsoukpoe KE, Osterland T, Opel O, Ruck WKL. Cascade thermochemical storage with internal condensation heat recovery for better energy and exergy efficiencies. Appl Energy 2016;181:562–74. doi:10.1016/j.apenergy.2016.08.089.

[38]   Skrylnyk O, Courbon E, Heymans N, Frère M, Bougard J, Descy G. Energy Performances of Open Sorption Reactor with Ultra-Low Grade Heat Upgrading for Thermochemical Energy Storage Applications. Energy Procedia, vol. 135, 2017, p. 304–16. doi:10.1016/j.egypro.2017.09.522.

[39]   IRENA reports. A Renewable Energy Roadmap Report- Remap 2030. 2014.

[40]   Miró L, Gasia J, isa Cabeza LF. Th erm al en ergy storage (TES) for industrial w aste h eat (IWH)

recovery: A review n.d. doi:10.1016/j.apen.

[41]   Aneke M, Wang M. Energy storage technologies and real life applications – A state of the art review. Appl Energy 2016;179:350–77. doi:10.1016/J.APENERGY.2016.06.097.

12 CONCLUSIONS AND ACHIEVEMENTS
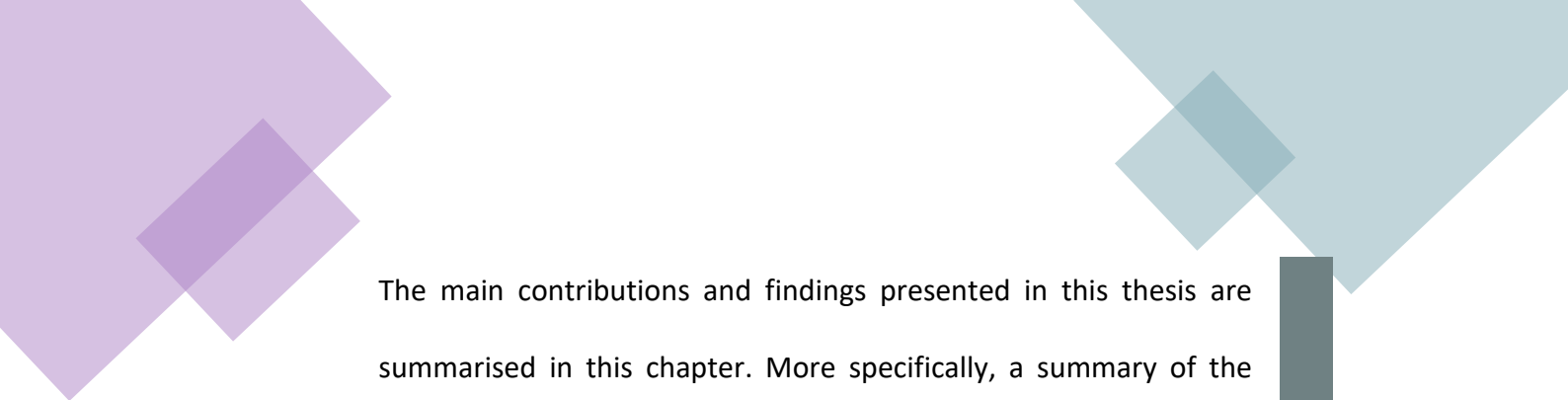
1. Thesis timeline

2. Scientific contributions

3. Introduction
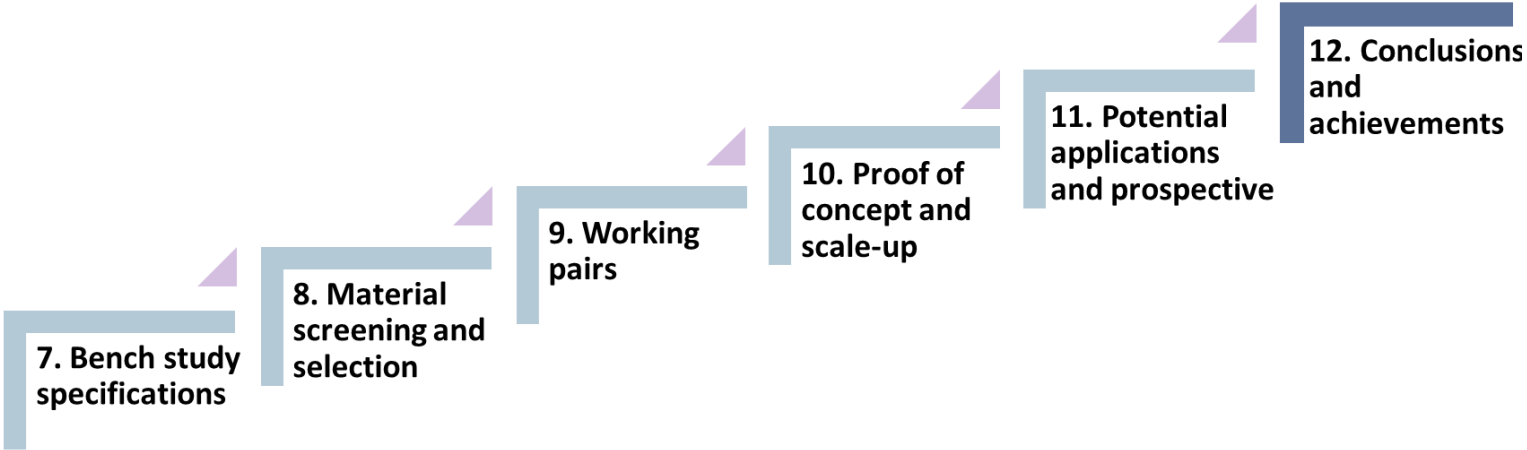
4. TCS Outlook

5. Targets and structure of the thesis

6. Hybrid TES system:

3 in 1 concept

The main contributions and findings presented in this thesis are summarised in this chapter. More specifically, a summary of the thesis contents along with a brief description of the proposed solutions and a discussion of the most relevant results are presented in Section 12.1. The achievements linked to the main objectives of the thesis are listed in Section 12.2. Then, open lines of research related to the topics addressed in this thesis are described in Section 12.3.

7. Bench study specifications

8. Material screening and selection

9. Working pairs

10. Proof of concept and scale-up

11. Potential applications and prospective

12. Conclusions and achievements

12. CONCLUSIONS AND ACHIEVEMENTS

12.1 CONCLUSIONS

This thesis is aimed at contributing to the global goal of thermal energy storage deployment, focusing on the conceptualisation of a novel hybrid TES system from laboratory to the scale-up level. The thesis has been divided into two main blocks;

(1) Thermal Energy Storage background: Chapter 3 and Chapter 4.

(2) 3 in 1 system proposal and prospectives, proof of concept and scale-up: Chapter 6, Chapter 7, Chapter 8, Chapter 9, Chapter 10 and Chapter 11.

Chapter 3 has been devoted to introducing the related topics and to review the state of the art of energy storage the 3 in 1 system in the current energy scenario. All energy storage technologies are briefly listed and defined to then focused on thermal energy storage, their classification, limitations/challenges and future pathways such as hybrid systems. Chapter 4 defines the framework of the thesis, discusses the main research challenges and presents a comprehensive overview of the material side from conceptualisation to manufacturing level has been described. This was aimed to position the reader in the current development stage of TCS systems and understand the innovation and opportunities that the 3 in 1 system allow. The main outputs from this section are; TCS materials are still at a low development level, while problems at the material level are still to be faced, novel manufacturing routes must be found to ease the commerciality way of these materials.

Chapter 6 describes the operating conditions and processes involved in the 3 in 1 hybrid system. Firstly, the three systems obtained from the tactical combination of the thermochemical and phase change material technologies are described: cascade system,

charging integrated and discharging integrated. Energy diagrams, as well as the working mechanism, are provided. Then, the processes involved, and the thermodynamic equations of the storage are detailed. To wrap up, a section on the theoretical potential of selected materials is provided at the end of this chapter, which includes low-medium temperature thermochemical materials and solid-solid/ solid-liquid phase change materials.

Chapter 7 describes the methods and experimental methodology followed in Chapter 8, 9 and 10. Chapter 8 selects the main components of the 3 in 1 system; the thermochemical material, the phase change material and when necessary, a gelling agent as an additive. The materials are first theoretically selected from a comprehensive literature review on the area. The theoretical candidates are then experimentally studied, including relevant properties unmeasured in the literature. The main outcomes of this chapter concern the thermochemical material screening process flow and the importance of considering a set of theoretical candidates when selecting a TCM for a specific application. Besides, other relevant properties such as thermal diffusivity and specific heat capacity, not often characterized in the TCM research studies found in the literature, have been also measured providing more experimental data for further comparison between studies. The outputs from the overall selection process are a narrowed down list of 9 thermochemical materials candidates; $MgSO_4·7H_2O$, $MgCl_2·6\ H_2O$, $CaCl_2·6H_2O$, $SrBr_2·6\ H_2O$ and $K_2CO_3·1.5\ H_2O$, eight-phase change materials; High-density polyethylene (HDPE), 4,40-diphenylmethane diisocyanate (MDI), polyethylene oxide (PEO), polyethylene glycols (PEG) (1,000 MW, 600 MW and 35,000 MW), erythritol (E), one matrix cellulose (CLU) and two gelling agents (polyacrylamide (PA) and guar gum (GG)). The combined materials achieve different working pairs, thus, different working temperature combinations.

Finally, the compatibility study of TCM/gel working pair in Chapter 8 has proved that gelling agents have a great potential in TCS technology, not just for the 3 in 1 system but for

pure TCMs, as they provide a skeleton structure. This has opened a new way to TCM manufacturing and fabrication. The research here presented can be used as a guide for future studies as a layout of gel/TCM compatibility is provided.

The 3 in 1 working pairs selected in Chapter 8 are experimentally validated in Chapter 9. The working pairs are studied in two main blocks; SSPCM and SLPCM-gel. The energy stored and the chemical stability of SSPCMs are studied, while the compatibility/synergies between TCM/PCM-gel working pairs (SLPCMs) are investigated.

Regarding the experimental results of the SSPCM/TCM working pair selected, interesting and novel results have been obtained as such combinations have not been yet studied elsewhere. Thus, the full understanding of the characterisation performed is a challenge at this stage as there are not enough shreds of evidence in the literature to compare with and further experimental investigation should be performed. For that reason, the behaviour of the 3 in 1 working pair have been mainly compared to the pure TCM, and the following outputs were drawn from that study. The 3 in 1 system is feasible when SSPCMs are used, while SLPCMs has proved to need an additional component (gelling agents) to prevent leakage and breakage of the composite.

SSPCM experimental data show that PCM can affect reaction times, can work as a matrix and can change the dehydrated species of the TCM stabilising or changing the dehydration steps reported in the literature. In this sense, the working pairs containing higher PCM content show higher conversion rates, but lower energy stored given there is a lower TCM content in the composite. Calcium chloride is not experimentally validated as showed very similar behaviour to magnesium chloride. Potassium carbonate is discarded for material incompatibility with all the PCM tested. A maximum 80/20 TCM/PCM ratio is obtained for magnesium chloride while a 90/10 ratio works for magnesium sulphate and strontium bromide. Among all the working pairs experimentally validated magnesium chloride is the one

that shows higher energy density while magnesium sulphate composites suppose a compromise between energy stored and structural stability. Strontium bromide performs very well under cycling conditions, although shows the lowest energy stored.

The main outputs from the SLPCM compatibility test are that, as a general trend, all the main issues exhibited by the gel formulations are related to material compatibility besides leakage. Thus, the gel can work as a complementary component to hold the phase change and allow the sorption reaction. Looking at the three 3 in 1 system proposed; discharging integrated has shown to be the most complex as it is challenging to find a solid-liquid PCM that can hold the composite together through hydration/dehydration. In this case, TCM integrity is crucial for successful working pairs, e.g. strontium bromide is the only TCM that works with PEG 600/PEG 1,000. Charging integrated system can be achieved by combining magnesium sulphate and erythritol, which has shown very good stability while providing high temperature stored given that sugar alcohols possess a high latent heat (see later). Cascade system could have been designed by the combination of PEG 35,000 with either magnesium sulphate or magnesium chloride. The use of gels proofs to have the potential for thermochemical synthesis as it reduces the leakage and enhances the cycling stability even of pure TCMs. The final working pairs for proof of concept and scale-up validation are selected as the main outputs of Chapter 9; $MgSO_4$/E/PA and $MgSO_4$/HDPE for charging integrated system, $MgSO_4$/MDI, $MgSO_4$/CLU, MgCl2/PEO and $MgCl_2$/MDI for cascade system and $MgCl_2$/HDPE for charging integrated.

In chapter 10, the 3 in 1 system has been brought to the ultimate level in the thesis, with the proof of concept and the scale-up study. In the proof of concept, the $MgSO_4$/HDPE working pair (charging integrated system) is studied in a temperature range between 30 °C and 150 °C, which working conditions are suitable for space heating and domestic hot water supply. In this chapter, we prove that the PCMs help to maintain the physical integrity of the composite by

accommodating the volume change and holding the structure together during cycles. Besides, the combination of a polymer and a thermochemical material allows for a cost-effective storage media that can store up to 2 GJ·m^{-3}, with hydration and dehydration conversions up to 90%.

Regarding the scale-up study, the final working pair candidates from Chapter 9 are experimentally validated through a complete set of characterisation techniques. Magnesium sulphate stands up as the best TCM candidate of the scale up-level study (1 g to 20 g). Magnesium chloride working pairs showed major leakage and breakage issues just after 5 cycles. Magnesium sulphate, both gel and polymer working pairs, showed high energy storage capacity up to 2 GJ·m^{-3} and 2.4 GJ·m^{-3}, respectively. Besides, high dehydration (70-95%) and hydration conversions (90%) were reached even after 40 thermal cycles while maintaining structural integrity. A 25-20 wt.% of HDPE was set as optimal MgSO$_4$-HDPE working pair, as they provide a compromise between energy stored, porosity and physical integrity. Whilst the content of MgSO$_4$/E was set to 80 wt./vol.%, due to higher content leads to structural deformation of the composite. The phase change material, both polymer and sugar alcohol were found to act as nucleating agents in the magnesium sulphate crystallisation process forming a synthetic monohydrate crystalline phase (Kieserite) instead of the reported in the literature monohydrate amorphous phase.

Chapter 11 states the 3 in 1 system's prospectives and its potential applications by comparing it to traditional TES technologies and the current commercial TES status. The 3 in 1 system is comprehensively compared to the performance of conventional systems, at the sight of capacity (the energy stored in the system), power (how fast the energy stored in the system can be charged/discharged), efficiency (the ratio of the energy provided to the user to the energy needed to charge the storage system), storage period (how long the energy is stored) and cost (to either capacity (€/kWh) or power (€/kW)). Possible applications where

this new system can be implemented are presented and its influence in the TES development pathway is discussed.

The 3 in 1 system shows that an addition of up to 20 wt.% of PCM can overcome the current challenges, providing a TCM/PCM combination enough to support the TCM acting as a co-matrix, and a surplus of stored energy that balances the energy taken from the TCM replaced. The energy stored by the 3 in 1 system is very similar to the one achieved with the solely thermochemical media, which is three times higher than the one stored by conventional TCM composites such as zeolite + TCM (the most studied in the literature). Besides, the 3 in 1 can provide a promising combination, the thermochemical heat can be stored for months while the latent and sensible heat can be discharged when needed for the end-user. In that manner, the system can either work as a short term and long-term storage. TCM lifetime can be greatly improved by the addition of PCM as the co-matrix, which has the potential to solve the agglomeration problems and minimize the microstructural changes that lead to mass and heat transfer reduction. Moreover, the 3 in 1 provides a supporting skeleton that can reduce the final cost by adding a lower-priced matrix to the overall storage media composition (<80 wt.%). Finally, the novel hybrid system can be used to store and deliver heat in industrial processes (waste heat), solar energy, district heating and cooling, and residential and commercial sectors. It also allows tailoring systems where different output and input temperatures heat sources are involved. It also provides different discharging/charging strategies enabling a flexible energy storage system for coupling with renewables (especially solar power).

412 Chapter 12. Conclusions and achievements

12.2. SUMMARY AND ACHIEVEMENTS

The main achievements are listed below in correlation with the objectives described in Chapter 5.

(1) **C1: Open a new TES technology pathway, where the new system changes the conventional TES classification.** The 3 in 1 system has been presented in Chapter 6 (cascade, charging integrated and discharging integrated). As proofed in Chapter 9 and 10, in the 3 in 1 system, the main fundamental challenges of each technology are surpassed: more compact systems (sensible), accommodation of volume change (latent heat), higher energy conversion and life span (thermochemical).

(2) **C2: The selection and screening of PCM and TCM candidates as 3 in 1 working pairs.** In Chapter 8 a throughout material selection is conducted were to 9 thermochemical materials; $MgSO_4·7H_2O$, $MgCl_2·6 H_2O$, $CaCl_2·6H_2O$, $SrBr_2·6 H_2O$ and $K_2CO_3·1.5 H_2O$, eight-phase change materials; High-density polyethylene (HDPE), 4,40-diphenylmethane diisocyanate (MDI), polyethylene oxide (PEO), polyethylene glycols (PEG) (1,000 MW, 600 MW and 35,000 MW), erythritol (E), plus one matrix cellulose (CLU) and two gels (polyacrylamide (PA) and guar gum (GG)).

(3) **C3: The optimization and experimental validation of various TCM/PCM pairs for different applications.** In Chapter 9 the working pairs resulting from the combinations between TCM, PCM matrix and gel selected in Chapter 9 are experimentally validated. The final working pairs for proof of concept and scale-up validation are selected as the main outputs of Chapter 9; $MgSO_4$/E/PA and $MgSO_4$/HDPE for charging integrated system, $MgSO_4$/MDI, $MgSO_4$/CLU, $MgCl_2$/PEO and $MgCl_2$/MDI for cascade system and $MgCl_2$/HDPE for charging integrated.

(4) **C4: The study of proof of concept and validation.** In Chapter 10 a proof of concept study is provided. In the proof of concept, 1 g- tablet of the $MgSO_4$-HDPE working pair in

formulations from 90/10 to 80/20 are studied over 15 thermal cycles. The composites are proved to ensure physical stability over cycles and allow for a cost-effective storage media that can store up to 2 GJ·m^{-3}.

(5) **C5: The study of material scale-up and validation.** In Chapter 10 a scale-up study is provided. In the scale-up study, 20 g- tablet of working pairs selected in Chapter 9 are studied over 40 thermal cycles. Magnesium sulphate stands up as the best TCM candidate to study at scale-up level, whereas magnesium chloride working pairs showed major leakage and breakage issues just after 5 cycles. Both gel and polymer working pair showed high energy storage capacity up to 2 GJ·m^{-3} and 2.4 GJ·m^{-3}, respectively. Besides, high dehydration (70-95%) and hydration conversions (90%) were reached even after 40 thermal cycles while maintaining structural integrity.

(6) **C6: Explore how the 3 in 1 system can change the TES portrait by studying its integration into different applications and potential.** In Chapter 11 the 3 in 1 system has been studied in comparison to the conventional TES categories in terms of energy stored, lifetime, efficiency, applications, cost, manufacturing routes and storage time. Besides, sketches of the open and the closed system including the 3 in 1 system added value have been also included in the section.

12.3 FUTURE WORK

This thesis has aimed at proving that the new 3 in 1 technology is effective and can pave the future TES hybrid systems not only with the main contributions summarized in the previous section but also opening new research topics that this thesis has not been able to cover.

Regarding this, the main open research lines are mainly based on the outputs given in Chapter 8, 9, 10 and 11:

(1) Chapter 8:

- From the TCM screening selection, there is further work regarding a higher grade of understanding of TCMs reactions under different conditions. A more extensive TCM database properties should be provided on the rest of the outstanding candidates. Conditions for closed and open systems should be considered and compared to determine the best performance for each TCM working pair. Along this line, thermal conductivity and specific heat capacity (through dynamic and areas method) should be studied at different temperatures providing a wider range of values over the working temperature. Reaction kinetics (reaction rate, conversion, etc) should be also studied under different conditions and other possible TCM candidates in the TCS field.

- From the PCM selection, the material selection should include other phases change materials such as other organic PCMs (e.g. paraffin) and mixtures (e.g. polymer blends with soft and hard segments). Microencapsulated PCMs could also be an option for the 3 in 1 system. Binary and ternary mixtures of polyalcohols should also be studied. Polymer with different structures and crystallinity rates could be further considered. Deeper study on specific heat and thermal conductivity methods in a wider temperature range should also be provided. Specifically, for the 3 in 1 system, the degradability and interaction with water vapour conditions should be studied further.

- From the gelling agent, further action could involve extending the gel compatibility study to other thickenings/gelling agents and mixtures of them. Preparation parameters and conditions (sharing rate, drying temperature, resting time, concentration, pH modifiers, etc) should be studied further and specifically designed for each TCM/gel combination requirements. The study of lower TCM percentages (<80 wt./vol.%) would be interesting to understand the underlying mechanism for the gel formation in each TCM media. Upgraded studies could involve tailoring the parameters for gel microstructure formation control (e.g. porosity, particle size etc), different geometries could be also considered (e.g. squared tablet). Further, the study of reaction rate and conversions at different heating rates and conditions.

- Other supporting matrices similar to cellulose, such as magnesium oxide could be studied with TCM or in combination with the TCM/PCM working pair.

(2) Chapter 9

- From the SSPCM, further study of the polymer crystallinity effect on different TCMs, a study of the crystallisation of the TCM, interaction (nucleating) of PCM nucleation. Extend the ratios for each TCM/PCM working pair and study intermediates formulations. To conduct further and thoroughly characterisation of all TCM working pairs like the one presented in Chapter 10. To study different preparation methods (pressure, tablet dimensions, etc) and particle size of the TCM/PCM combinations to correlate with the properties measured.

- From SLPCMs, the content of TCM/PCM could be extended (from 90/10 to 80/20), to study higher gel content when adding the PCM into the preparation parameters. The sole combination of TCM and gel exhibits promising results, thus the study of TCM/gel with different percentages of the gelling agent over cycles (microstructure etc) could bring improved performance into the system. Besides, the same

methodology has been used for all the TCM/PCM-gel working pairs to reduce the number of parameters affecting the composites comparison. However, further study is required to understand the effect of such parameters in the performance of the composite (drying temperature, compressing pressure, shape, particle size, agitation speed, etc). To further study the reason for the incompatibilities between TCM/PCM and TCM/PCM/gel.

- The thermal conductivity of the working pairs should also be considered as a key property for selection. Unfortunetly, due to covid this was not possible to perform during the time-being of the thesis.

(3) Chapter 10

- From the proof of concept, further studies could conduct the proof of concept study with different working pairs to observe how the scaling up affects the TCM/PCM attributes. The 1 g tablet could be further cycled up to lager number of cycles. The preparation conditions such as pressure, tablet geometry and particle size should be considered. Further study of the reaction rate with increasing water vapour pressure and how PCM addition affects the TCM attributes (such as deliquescence, permeability, etc.) to compare to scale-up outputs. Microstructure studies aside from SEM should be performed (XRT) as well as the study of open and closed porosity for scale-up study. To further evaluate thermal conductivity, specific heat capacity, BET surface energy, and the study of the heating rate variation effect on the reaction kinetics (reaction rate, conversion, etc).

- From the scale-up, higher tablets sizes should be considered to fully reach the scale-up stage. To extend the study to more tablets (for higher sampling) and a larger number of cycles. Interactions between TCM/PCM should be further

studied to bring more experimental evidence of the effects between the phase change material and the thermochemical storage. Among those interactions; how does crystallinity of PCM affect the TCM, what is the energy-involved in the crystallization process of the monohydrate instead of the amorphization of the phase or to study a supercooling degree at different heating rates. As for the proof of concept, the study of conversion and reaction rates at different reaction conditions is relevant to understand the 3 in 1 system. Other techniques such as polarised light could be of interest to see how does the PCM recrystallize, and TEM, FT-IR microscopy and Raman microscopy at high temperature to study the topology of the tablet and the hydration/dehydration mechanism beyond the TCM ones. Other burning questions such as does the PCM affects the TCM-water phase diagram?; Does the PCM (e.g. sugar alcohol) solidifies or remains in a liquid state? , etc are still to be answered. Further knowledge should bring more clarity to the underlying mechanisms of TCM/PCM storage technology.